

**PREPARATION AND CHARACTERIZATION OF HIGH DENSITY
POLYETHYLENE / CHITOSAN / HYDROXYAPATITE
POLYMER COMPOSITES**

Thesis Submitted to the **University of Calicut** for the Award of
DOCTOR OF PHILOSOPHY IN CHEMISTRY

by
MERIL SHELLY

Under the supervision of
Dr. Tania Francis (Guide)
Dr. Meril Mathew (Co-Guide)



**DEPARTMENT OF CHEMISTRY
ST. JOSEPH'S COLLEGE (AUTONOMOUS), DEVAGIRI
CALICUT, KERALA-673008
MAY 2022**

DECLARATION

I hereby declare that the thesis entitled “**Preparation and Characterization of High Density Polyethylene / Chitosan / Hydroxyapatite Polymer Composites**” submitted to the University of Calicut in partial fulfillment of the requirements for the award of the Degree of Doctor of Philosophy in Chemistry is a bonafide record of the research work carried out by me under the guidance of **Dr. Tania Francis**, Assistant Professor and Head, Department of Chemistry, St. Joseph’s College (Autonomous), Devagiri, Calicut and **Dr. Meril Mathew**, Assistant Professor and Head, Department of Physics, St. Joseph’s College (Autonomous), Devagiri, Calicut and the same has not been submitted elsewhere for any other degree.

Kozhikode



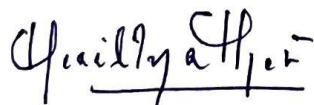
Meril Shelly

CERTIFICATE

This is to certify that the work embodied in the thesis entitled **“Preparation and Characterization of High Density Polyethylene / Chitosan / Hydroxyapatite Polymer Composites”** submitted by Meril Shelly to the University of Calicut for the award of the degree of Doctorate of Philosophy in Chemistry under the Faculty of Science, is an authentic record of precise research work carried out at the Department of Chemistry, St. Joseph’s College (Autonomous) Devagiri, Calicut, under our supervision and guidance. The contents of the thesis have been checked for plagiarism using the software ‘Ouriginal’ and the similarity index falls under permissible limit. We further certify that the contents of this thesis have not been submitted elsewhere for any degree or diploma.

We also certify that the corrections suggested by the adjudicators have been incorporated in the corrected thesis.

Research Guides



Dr. Meril Mathew

(Co-guide)

Dr. Meril Mathew
Head of the Department
Department of Physics
St. Joseph's College, Devagiri
Kerala- 673008



Dr. Tania Francis

(Guide)

Dr. TANIA FRANCIS
Assistant Professor & Head
Post Graduate & Research Department of Chemistry
St. Joseph's College (Autonomous) Devagiri
Calicut - 673 008

ACKNOWLEDGEMENT

The satisfaction and euphoria that accompany the successful completion of any task would be incomplete without mentioning the people who made it possible, whose constant guidance and encouragement crowned out effort with success.

A profound sense of gratitude binds me to my guide and path-finder **Dr. Tania Francis**, Assistant Professor and Head, Department of Chemistry, St. Joseph's College (Autonomous), Devagiri, Calicut. She has been the backbone in moulding me throughout the academic life from my under graduation course to research supervision. I shall be forever obliged to her for her guidance, valuable suggestions and constructive criticism throughout the course of my research life. I would also like to express my sincere thanks to my Co-guide, **Dr. Meril Mathew**, Assistant Professor and Head, Department of Physics, St. Joseph's College (Autonomous), Devagiri, Calicut for providing her warm motivations, insightful and critical suggestions and patient guidance. Apart from the academic, both my supervisors have taken a keen interest in my personal success. I also extend my thanks to their families too.

I wish to express a special note of gratitude to the Manager, Fr. Dr. Biju Joseph CMI and to the Principal, Dr. Bobby Jose. I also record my gratitude and respect to the former Manager, Late Fr. Joseph Paikada CMI, Former Principals, Sabu K Thomas, Dr. Sibichen M Thomas and Dr. Jose John Mallikasseri and former Heads of the Department of Chemistry, Dr. Joy Joseph and Dr. Babu I Maliakkal for their support and help throughout these time.

I acknowledge Kerala State Council for Science Technology and Environment (KSCSTE) for the financial assistance in the form of research fellowships.

I owe my special thanks to

- Dr. Abraham Joseph and Dr. Renuka N, members of the research advisory committee for providing me suggestions and encouragement throughout the research work.
- Dr. H.B. Ravikumar, Associate Professor, Department of Physics, University of Mysore, for helping me to carry out Positron Annihilation lifetime spectroscopic (PALS) analysis.
- Dr. Aswini Prabhu, Assistant Professor, Yenepoya Research Centre, Mangalore for cell proliferation analysis.

- Research scholars and staffs at National Institute of Technology, Karnataka, Department of Polymer Science and Rubber Technology, Cochin University of Science and Technology (CUSAT) and Department of Physics, University of Mysore, for helping me from the sample preparation to sample analysis.
- Mr. Renjith R, Assistant Professor, Department of Mechanical Engineering, Federal Institute of Science and Technology (FISAT), Angamaly, Kerala and Mr. Dony Dominic, Assistant Professor, Department of Mechanical Engineering, Christ College of Engineering, Irinjalakuda, Thrissur, Kerala for helping me with the computational modelling studies.
- Library and other supporting staff at St. Joseph's College (Autonomous), Devagiri.
- All my friends and research scholars at St. Joseph's College (Autonomous), Devagiri especially Ms. Annie Stephy and Ms. Bashpa P for providing a wonderful experience in research life.

I owe my special thanks to all teaching and non-teaching staffs of Department of Chemistry, St. Joseph's College (Autonomous), Devagiri, for the constant support and encouragement given to me during the entire time of research works.

I would also like to express my heartfelt gratitude to all my family, friends and well-wishers for their support and encouragement during my entire research work. I thank all those who directly / indirectly helped me to complete the research work.

Last but not the least I am grateful to my grandparents, parents, in – laws, brother, husband and to my loving son for their patience and moral support shown to me which enabled me to complete this task.

KOZHIKODE

MERIL SHELLY

MAY, 2022

TABLE OF CONTENTS

	Contents	Page No
	List of Figures	i
	List of Tables	v
	Nomenclature	vii
	Preface	ix
Chapter 1	Introduction	
1.1	Introduction	1
1.2	Background of composite technology development	1
1.3	Classification of Composites	3
1.4	Bio-composites	4
1.5	Applications of bio-composites	7
1.6	Matrices in bio-composites for tissue engineering applications	12
1.7	HDPE as matrix in bio-composites	12
1.8	Fillers in thermoplastic based composite materials for medical applications	15
1.8.1	Chitosan	16
1.8.2	Hydroxyapatite	18
1.9	HDPE based composites	19
1.10	Chitosan based composites	21
1.11	Hydroxyapatite based ternary composites	23
1.12	Characterization of thermoplastic (polyethylene) based composites	24
1.12.1	Mechanical analysis of thermoplastic / natural polymer / ceramic - based composites	25

1.12.1.1	Computational Modelling of mechanical properties of thermoplastic / natural polymer / ceramic - based composites	27
1.12.1.2	Finite Elemental Analysis (FEA)	28
1.12.2	Morphological and structural analysis of thermoplastic / natural polymer / ceramic - based composites	33
1.12.3	Microstructural analysis of thermoplastic / natural polymer / ceramic - based composites	36
1.12.4	Thermal analysis of thermoplastic / natural polymer / ceramic-based composites	43
1.12.4.1	Thermal oxidative degradation kinetics - using Coats Redfern model	45
1.12.5	Dielectric Properties of thermoplastic / natural polymer / ceramic - based composites	50
1.12.6	Bio-degradability and Bio-compatibility analysis of thermoplastic / natural polymer / ceramic - based composites	53
1.13	Research Gaps	56
1.14	Objectives and scope of the work	56
1.15	Scope of the work	57
Chapter 2	Materials and Methodology	
	Summary	59
2.1	Materials	59
2.1.1	High density polyethylene (HDPE)	59
2.1.2	Chitosan	60
2.1.3	Hydroxyapatite	61
2.1.4	Maleic Anhydride	61
2.1.5	Dicumyl Peroxide	62
2.1.6	Palm Oil	63
2.1.7	Cell lines	64
2.2	Preparation of composites through melt mixing process	65

2.3	Characterization Techniques	68
2.3.1	Mechanical characterizations	68
2.3.1.1	Impact strength analysis	68
2.3.1.2	Stress-Strain analysis	69
2.3.1.3	Computational Modelling using Finite Element Analysis	71
2.3.2	Microstructural characterizations	74
2.3.2.1	Scanning Electron Microscopy (SEM)	74
2.3.2.2	Fourier Transform Infrared spectroscopy – Attenuated Total Reflectance (FTIR - ATR)	74
2.3.2.3	X-ray diffractometry (XRD)	75
2.3.2.4	Positron Annihilation lifetime spectroscopy (PALS)	75
2.3.3	Thermal characterizations	77
2.3.3.1	Thermogravimetric Analysis (TGA)	78
2.3.3.2	Thermal modelling studies - Coats Redfern Model	78
2.3.3.3	Dynamic mechanical analysis (DMA)	79
2.3.4	Dielectric characterizations	80
2.3.4.1	Dielectric characterizations – LCR Meter	80
2.3.4.2	Broadband Dielectric Spectroscopy	81
2.3.5	Biocompatibility and bio-degradable characterizations	82
2.3.5.1	Water Sorption analysis	83
2.3.5.2	Soil Burial Analysis	83
2.3.5.3	Water contact angle measurements	84
2.3.5.4	Cell proliferation analysis	84

Chapter 3 **Investigation of the Mechanical Properties of High Density Polyethylene / Chitosan Composites and High Density Polyethylene / Chitosan / Hydroxyapatite Composites**

Summary	85
---------	----

3.1	Introduction	86
3.2	Results and discussion	88
3.2.1	Impact strength analysis of HC composite series	88
3.2.2	Stress-strain analysis of HC composite series	89
3.2.3	Impact strength analysis of HP composite series	92
3.2.4	Stress-strain analysis of HP composite series	93
3.2.5	Computational modelling of HC composite series and HP composite series using Finite Element Analysis	94
3.2.6	Morphological analysis of the tensile fractured surfaces of HC composite series and HP composite series	97
3.2.7	Impact strength analysis of HA composite series	98
3.2.8	Stress-strain analysis of HA composite series	100
3.2.9	Impact strength analysis of HAW composite series	102
3.2.10	Stress-strain analysis of HAW composite series	103
3.2.11	Computational modelling of HA composite series and HAW composite series using Finite Element Analysis	105
3.2.12	Morphological analysis of HA composite series and HAW composite series	106
Chapter 4	Microstructural investigation of High Density Polyethylene / Chitosan Composites and High Density Polyethylene / Chitosan / Hydroxyapatite Composites	
	Summary	109
4.1	Introduction	110
4.2	Results and discussion	112
4.2.1	Fourier Transform Infrared spectroscopy – Attenuated Total Reflectance (FTIR-ATR) analysis	112
4.2.1.1	FTIR-ATR analysis of matrix: HDPE and filler: chitosan	112
4.2.1.2	FTIR-ATR analysis of HC composite series	114

4.2.1.3	FTIR-ATR analysis of HP composite series	116
4.2.1.4	FTIR-ATR analysis of HA composite series	117
4.2.1.5	FTIR-ATR analysis of HAW composite series	120
4.2.2	X-ray Diffractometry (XRD)	122
4.2.2.1	XRD analysis of HC composite series	122
4.2.2.2	XRD analysis of HP composite series	123
4.2.2.3	XRD analysis of HA composite series	124
4.2.2.4	XRD analysis of HAW composite series	125
4.2.3	Positron Annihilation Lifetime Spectroscopic (PALS) analysis	127
4.2.3.1	PALS analysis of HC composite series and HP composite series	127
4.2.3.2	PALS analysis of HA composite series and HAW composite series	129

Chapter 5 Thermal Analysis of High Density Polyethylene / Chitosan Composites and High Density Polyethylene / Chitosan / Hydroxyapatite Composites

	Summary	131
5.1	Introduction	132
5.2	Results and discussion	134
5.2.1	Thermogravimetric analysis (TGA)	134
5.2.1.1	Thermogravimetric analysis of HC composite series	134
5.2.1.2	Thermogravimetric analysis of HP composite series	137
5.2.1.3	Activation energy analysis of HC composite series and HP composite series	138
5.2.1.4	Thermogravimetric analysis of HA composite series	139
5.2.1.5	Thermogravimetric analysis of HA composite series	141
5.2.1.6	Activation energy analysis of HA composite series and HAW composite series	142

5.2.2	Dynamic mechanical analysis (DMA)	144
5.2.2.1	Dynamic mechanical analysis of HC and HP composite series	144
5.2.2.2	Dynamic mechanical analysis of HA and HAW composite series	148
Chapter 6	Electrical Properties of High density polyethylene / Chitosan composites and High density polyethylene / Chitosan / Hydroxyapatite composites	
	Summary	153
6.1	Introduction	154
6.2	Results and Discussion	155
6.2.1	Surface study of HC and HA composite series – Scanning electron microscope (SEM)	155
6.2.2	Dielectric properties of HC composite series	156
6.2.3	Dielectric properties of HP composite series	159
6.2.4	Dielectric properties of HA and HAW composite series	162
6.2.5	Broadband dielectric spectroscopic analysis of HA composite series	164
Chapter 7	Biodegradable and Biocompatibility Studies of High Density Polyethylene / Chitosan Composites and High Density Polyethylene / Chitosan / Hydroxyapatite Composites	
	Summary	169
7.1	Introduction	170
7.2	Results and Discussions	171
7.2.1	Water sorption studies	171
7.2.1.1	Water sorption studies of HC composite series and HP composite series	171
7.2.1.2	Water sorption studies of HA composite series	172

7.2.1.3	Water sorption studies of HAW composite series	173
7.2.2	Soil burial tests	174
7.2.2.1	Soil burial analysis of HC composite series	174
7.2.2.2	Soil burial analysis of HA composite series and HAW composite series	177
7.2.2.3	Mechanical strength analysis of HC, HP and HA composite series – before and after soil burial analysis	179
7.2.3	Contact angle analysis of High density polyethylene / Chitosan / Hydroxyapatite Polymer composites	183
7.2.4	Cell Proliferation analysis of the optimized High density polyethylene / Chitosan / Hydroxyapatite Polymer composites	185
	Conclusions	189
	Recommendations	197
	References	199
	List of Publications based on PhD research work	
	Biodata	

LIST OF FIGURES

Figure No.	Figure Caption	Page No.
1.1	General classification of composites	4
1.2	Classification of biocomposites	6
1.3	Global production capacity of bioplastics: 2019- 2025	7
1.4	Applications of bio-composites	8
1.5	Structure of High density polyethylene (HDPE)	13
1.6	Structure of Chitosan	17
1.7	Structure of Hydroxyapatite	18
1.8	Factors for designing bio-composites	25
1.9	(a) Stress-strain graph and (b) un-notched Izod impact strength of various thermoplastics	27
1.10	An overview of Finite Element Analysis	28
1.11	SEM image of tensile fractured surface of HDPE	33
1.12	(a) TGA and (b) DMA graphs of thermoplastic composites	45
2.1	(a) Brabender Plasticoder Model PL 3S and (b) Roller type rotors for melt mixing	65
2.2	Test specimen for impact strength analysis	69
2.3	Test specimen for tensile strength analysis	69
2.4	(a) Stress-strain graph (b) Young's Modulus from the expanded portion of graph 2.4 (a)	71
2.5	(a) CAD and (b) FEA design of the tensile test specimen	71
2.6	Boundary conditions and Mesh size of the test specimen	73
2.7	Applied load on the tensile test specimen	73
2.8	Schematic representation of α , β and γ transitions in polyethylenes	80
3.1	Impact strength analysis of HC composite series	89
3.2	Stress-strain graphs of HC composite series	90
3.3	Young's Modulus of HC composite series	91
3.4	Impact strength analysis of HP composite series	92
3.5	Stress-strain graphs of HP composite series	93

3.6	Young's modulus of HP composite series	94
3.7	Total deformation (a) HC0, (c) HC2, (e) HC4 and (g) HP2 and Equivalent stress of (b) HC0, (d) HC2, (f) HC4 and (h) HP2	95
3.8	SEM images of the tensile fractured surface of (a) HC0 (b) HC2 (c) HC4 and (d) HP2	98
3.9	Impact strength analysis of HA composite series	99
3.10	Stress-strain graphs of HA composite series	100
3.11	Young's modulus of HA composite series	102
3.12	Impact strength analysis of HAW composite series	103
3.13	Stress-strain graphs of HAW composite series	104
3.14	Young's Modulus of HAW composite series	104
3.15	Total deformation of (a) HA1, (c) HA4, (d) HAW4, (f) HAW5 and equivalent stress analysis of (b) HA1, (d) HA4, (e) HAW4 and (g) HAW5	105
3.16	SEM images of the tensile fractured surfaces of (a) HA1, (b) HA2, (c) HA4, (d) HA5, (e) HAW4 and (f) HAW5	107
4.1	FTIR-ATR spectra of (a) HC0 and (b) neat HDPE	112
4.2	FTIR-ATR spectra of Chitosan	114
4.3	FTIR-ATR spectra of HC composite series	115
4.4	FTIR-ATR spectra of HP composite series	117
4.5	FTIR-ATR spectrum of hydroxyapatite	118
4.6	FTIR-ATR spectra of HA composite series	119
4.7	FTIR-ATR spectra of HAW composite series	120
4.8	XRD spectra of HC composite series	122
4.9	XRD spectra of HP composite series	123
4.10	XRD spectra of HA composite series	124
4.11	XRD spectra of HAW composite series	125
5.1	TGA of HDPE, HC0 and chitosan	135
5.2	TGA and DTG (inset) analysis of HC composite series	136
5.3	TGA and DTG (inset) analysis of HP composite series	137
5.4	TGA and DTG (inset) analysis of HA composite series	139
5.5	TGA and DTG (inset) analysis of HAW composite series	141
5.6	Storage modulus of (a) HC composite series and (b) HP composite series	144
5.7	Loss modulus of (a) HC composite series and (b) HP composite series	146

5.8	Tan delta of (a) HC composite series and (b) HP composite series	147
5.9	Storage modulus of (a) HA composite series and (b) HAW composite system	148
5.10	Loss modulus of (a) HA composite series and (b) HAW composite series	150
5.11	Tan delta of (a) HA composite series and (b) HAW composite series	151
6.1	SEM images of the surfaces of (a) HC0, (b) HC2, (c) HC4, (d) HP2, (e) HA3 and (f) HA4	156
6.2	Dielectric constant of HC composite series	157
6.3	Tan δ of HC composite series	158
6.4	ac conductivity of HC composite series	159
6.5	Dielectric constant of HP composite series	160
6.6	Tan δ of HP composite series	161
6.7	ac conductivity of HP composite series	161
6.8	Dielectric constant of (a) HA composite series and (b) HP composite series	162
6.9	Dielectric loss of (a) HA composite series and (b) HAW composite series	163
6.10	ac conductivity of (a) HA composite series and (b) HAW composite series	164
6.11	Frequency dependence of ϵ'' imaginary part of dielectric constant of HA composite series	165
6.12	Frequency dependence of M'' imaginary part of electric modulus of HC composite series and HA composite series	167
6.13	Frequency dependence of ac conductivity of HA composite series	168
7.1	Water sorption studies of HC composite series and HP2	171
7.2	Water sorption studies of HA composite series	173
7.3	Water sorption studies of HAW composite series	173
7.4	Soil burial analysis of HC0, HC2 and HP2 (<i>The solid lines shown to understand the degradation rate</i>)	175
7.5	Images of composites before degradation (HC0, HC2, HC4 and HP2) and after 30 days of degradation (HC0', HC2', HC4' and HP2')	176
7.6	Soil burial analysis of HA composite systems and HAW composite systems	177

7.7	Images of composites before degradation (HA4, HA5, HAW4 and HAW5) and after 30 days of degradation (HA4', HA5', HAW4' and HAW5')	178
7.8	The stress-strain analysis of the composite systems (a) HC0 (b) HC2 (c) HP2 (d) HA4 (e) HA5 (f) HAW4 and (g) HAW5 before and after 30 days of soil burial analysis	181
7.9	Contact angle measurements of the High density polyethylene / Chitosan / Hydroxyapatite polymer composites	184
7.10	Fluorescence images of (a) HC0, (b) HC2, (c) HP2, (d) HA4 and (e) HAW4	187

LIST OF TABLES

Table No.	Table Caption	Page No.
1.1	Patents on thermoplastic / ceramic - based systems for bone-tissue engineering applications	9
1.2	Mechanical properties of thermoplastic / natural polymer / ceramic - based composites	30
1.3	SEM studies of thermoplastic / natural polymer / ceramic - based composites	34
1.4	FTIR studies of thermoplastic / natural polymer / ceramic - based composites	38
1.5	XRD studies of thermoplastic / natural polymer / ceramic - based composites	40
1.6	PALS studies of thermoplastic / natural polymer / ceramic - based composites	41
1.7	TGA studies of thermoplastic / natural polymer / ceramic - based composites	46
1.8	DMA studies of thermoplastic / natural polymer / ceramic - based composites	48
1.9	Electrical studies of thermoplastic / natural polymer / ceramic - based composites	51
1.10	Biocompatibility of thermoplastic / natural polymer / ceramic - based composites	54
2.1	Properties of HDPE from technical data sheet	59
2.2	Properties of Chitosan	60
2.3	Physical properties of hydroxyapatite from material safety data sheet	61
2.4	Physical properties of maleic anhydride from material safety data sheet	62
2.5	Physical properties of Dicumyl peroxide from material safety data sheet	63

2.6	Physical properties of Palm oil from Lab experiments (obtained from KINFRA)	64
2.7	Specifications of MC3T3-CE1 cell lines	64
2.8	Formulations of HDPE / Chitosan (HC) composite series	66
2.9	Formulations of HDPE / Chitosan composites with palm oil as plasticizer (HP composite series)	66
2.10	Formulations of HDPE / Chitosan / Hydroxyapatite (HA) composite series and HDPE / Chitosan / Hydroxyapatite composite series unplasticized with palm oil (HAW)	67
2.11	Material properties of HDPE, chitosan and hydroxyapatite	72
3.1	Comparison of tensile strength analysis of experimental data with theoretical data for HC composite series and HP composite series	96
3.2	Comparison of tensile strength analysis of experimental data with theoretical data for HA composite series and HAW composite series	106
4.1	FTIR –ATR peaks of hydroxyapatite	118
4.2	% crystallinity of HC composite series and HP composite series	126
4.3	% crystallinity of HA composite series and HAW composite series	127
4.4	PALS studies of HC composite series and HP composite series	128
4.5	PALS studies of HA composite series	129
4.6	PALS analysis of HAW composite series	130
5.1	Activation energy analysis of HC composite series and HP composite series	138
5.2	Activation energy analysis of HA composite series and HAW composite series	143
7.1	Contact angle values of HDPE / Chitosan / Hydroxyapatite composites	183
7.2	Graph representing the cell proliferative efficacy of the test composites on mouse pre-osteoblast MC3T3-E1 cells. Values are represented as relative mean % \pm SD (n=3)	185

NOMENCLATURE

FRP	Fibre Reinforced Polymer
FDA	Food and Drug Administration
MA	Maleic anhydride
HA	Hydroxyapatite
CS	Chitosan
PEO	Polyethylene oxide
FEA	Finite Elemental Analysis
CAD	Computer Aided Design
POSS	Polyhedral oligomeric silsesquioxanes
VFM	Video Force Microscopy
FE	Finite element
UHMWPE	Ultrahigh molecular weight polyethylene
PEGMA	Poly-Ethylene- <i>co</i> -Glycidyl Methacrylate
DCP	Dicumyl peroxide
HDPE	High density polyethylene
PP	Polyethylene
PE	Polyethylene
BC	Benzoyl chloride
PTFE	Polytetrafluoroethylene
PS	Polystyrene
PLGA	Poly(lactic glycolic acid)
PVA	Poly vinyl alcohol
PVC	Polyvinyl chloride
PAN	Polyacrylonitrile
Ca/P	Calcium/Phosphorous
Mg – PS2	Magnesium
MDPE	Medium-density polyethylene
PLA	Poly(lactic acid)

FEA	Finite element analysis
CaCO ₃	Calcium Carbonate
LLDPE	Linear low-density polyethylene
LDPE	Low-density polyethylene
OMMT	Organic montmorillonite
HC	HDPE / Chitosan composites series
HP	HDPE / Chitosan composites series with palm oil as plasticizer
HA	HDPE / Chitosan / Hydroxyapatite composite series
HAW	HDPE / Chitosan / Hydroxyapatite composite series un-plasticized with palm oil

PREFACE

The thesis entitled “**Preparation and Characterization of High Density Polyethylene / Chitosan / Hydroxyapatite Polymer Composites**” comprise the development of a bio-based hybrid composite system that can be used as potential bone implant materials.

The introductory chapter highlights the significance of bio-based composites over commercially available synthetic and metal-based bone implants. Recent research on the mechanical, microstructural, thermal, electrical and biocompatible analysis of thermoplastics / Chitosan / ceramic-based polymer composites are discussed in detail.

Chapter 2 covers the details about the materials used for the preparation of composites, methodology and experimental techniques utilized for the preparation of HDPE / Chitosan composites and HDPE / Chitosan / Hydroxyapatite composites.

Chapter 3 focuses on the mechanical and morphological analysis of the binary composites and ternary composites system. The main objective of this chapter was to choose the optimized composite systems, which has superior mechanical strength for applications in bone implant material. The morphological analysis was studied from the tensile fractured images of the composites. The experimental values were compared with the theoretical data to ensure the compatibility of the results and mechanical stability of the system. Chapter 4 covers the details of the microstructural properties of the composites using FTIR-ATR, XRD and PALS techniques. The miscibility of filler and matrix, crystallinity, phase formation and extent of crosslinking were studied in this chapter. Chapter 5 provides an outline of the thermal properties and viscoelastic properties of the prepared binary and ternary composite systems using TGA and DMA analysis. The thermal stability was analysed from the Coats - Redfern Method, obtained from the thermal data from TGA.

Chapter 6 covers the electrical properties such as dielectric constant, electric modulus and ac conductivity analysis of the prepared composites. The studies were further compared with the dielectric properties of natural bone. Chapter 7 describes the biocompatibility and biodegradable properties of the composites under study. The water sorption analysis was correlated with the biodegradation results obtained from soil burial analysis. The hydrophilicity of the composites was analyzed using water contact angle measurements and was correlated with the cell proliferation studies using MC3T3- E1 cell lines.

The conclusions of the work, recommendations for future scope and relevant references are provided towards the end of the thesis.

Chapter 1

Introduction

1.1 Introduction

The current era is witnessing an explosion in material development by trying to synthesize composites that form a bridge between synthetic polymers and natural fillers. This development can be witnessed in all sectors including transportation, health, food industry, infrastructure, sports, electricity, etc. The rapid increase in technology creates a growing concern for environmental sustainability owing to an unprecedented increase in environmental pollution. To overcome this catastrophe, modification/replacement of synthetic materials with renewable as well as natural polymers/materials is a much-explored methodology these days. In an advancing society, most materials used are made of composite materials. The combination of different materials tends to create a more versatile product that can be tuned depending upon the requirement. The use of composite materials in health sector is becoming more notable in the present scenario. The combination of synthetic materials with biomaterials leads to hybrid systems – bio-based composites, which have higher mechanical performance and bio-compatible properties.

1.2 Background of composite technology development

The history of composites starts from 1500 BC when Egyptians and Mesopotamians started utilizing a combination of mud and straw to create durable buildings. Later, straw was used as reinforcement in composites to prepare pottery and boats. By 1200 AD, Mongols developed bows using a combination of wood, bone and animal glue. It continued to be the most powerful weapon on earth until the discovery of gunpowder.

The use of modern composites started with the development of Bakelite (formaldehyde + phenol), followed by polyvinyl chloride, polystyrene, phenolics and polyesters since 1900. These synthetic products outnumbered the use and development of natural composites in all fields of development. 1935 saw the beginning of the Fibre Reinforced Polymer (FRP) industry, with the development of strong-structured fibre glass by Owens Corning. World War II brought many great advancements in the field of composites. The FRP industry brought into the limelight more light-weight material production in military aircrafts. Soon, the properties of bio-glass and other developed composites were studied and were adapted for sheltering electronic radar equipment (Radomes). Later, in 1940, the first commercial boat hull was developed. During this time, Brandt Goldsworthy, known as the “Grandfather of composites”, further improved the processing and experimentation in the composite industry. His most famous discovery is the manufacturing process known as “pultrusion”. Fiberglass developed in late 1940 was the first modern composite and is still the most common composite used in sporting goods, swimming pool linings, surfboards, etc (P. Sharma et al. 2013). In the 1970s, better plastic resins and fibers were developed *viz-a-viz* Carbon fibers, Kevlar, etc. The increased use of non-renewable resources and environmental pollution during the course of plastic production has shifted the focus to green composite preparation.

Composite engineering is still growing and is concentrating on modifying material development based on renewable sources of energy (Nagavally 2017). Composite materials (or “composites” for short) are engineered materials made from two or more constituent materials with significantly different physical or chemical properties, which remain separate and distinct on a macroscopic level within the finished structure (Dorozhkin 2011). Wood and long fiber of cellulose are some examples of

natural composites. In a composite, one material binds to another leading to binary composite systems, ternary composite, quaternary composite, and so on. Materials like polymers, ceramics and metals are mainly employed as well as reinforcement depending upon the required application. Often, a binary composite consists of a single matrix phase and a reinforcement phase. But during the preparation of higher levels of composites, more than one filler is seen added to the matrix system. Compounding with two or more fillers can be accompanied with the simultaneous improvement of mechanical properties of the composites. This introduces the concept of hybrid systems. The incorporation of a maximum of two fillers is found to be more appropriate when designing a hybrid composite that requires higher mechanical performance. Hybrid composites show improvement in all properties (balanced tensile strength, thermal stability, biocompatibility, maintaining pore size etc.), especially in impact strength. In addition to the enhancement in structural and mechanical properties, greater control over the final composite is also achieved (Banerjee et al. 2014). Composites exhibit better strength, and good electrical and magnetic properties when compared with the properties of the individual components that were employed to prepare them. Hence the combined properties of the material can be applied for various applications including bio-implants, coating technology, food industry, automobile industry and sports (Soo Jin 2011).

1.3 Classification of Composites

A composite is formed from the combination of materials namely polymers, metals, inorganic/organic substances at the micro/macro meter level. They can be classified based on its processing techniques, microstructure, properties and applications (Pechanul and Valdez 2015). Based on the type of materials used, properties, and

applications, composites can be classified as given in Figure 1.1.

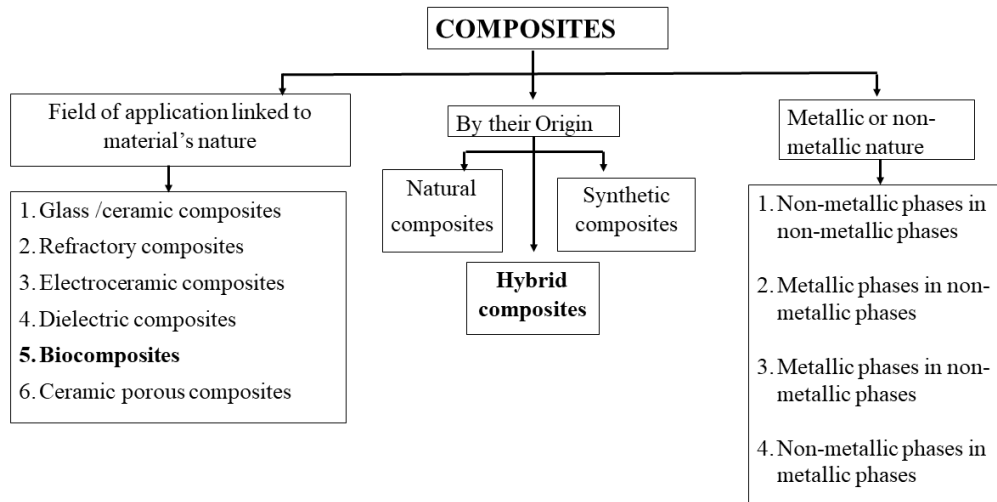


Figure 1.1 General classification of composites (Pech-canul and Valdez 2015)

1.4 Bio-composites

The dependence on petroleum-based polymers like polypropylene (PP), polyethylene (PE), polytetrafluoroethylene (PTFE), and polystyrene (PS), in composite fabrication, has increased extensively over the years. The chemical inertness, flexibility, reusability and strength of the product have helped them gain tremendous use in day-to-day life (Nagalakshmaiah et al. 2019). However, the use of these polymers leads to various challenges such as the decline of fossil fuels and environmental concerns such as their slow degradation, global warming, recycling factors (such as cross-contamination) and toxicity. To overcome these concerns and to reduce the use of petroleum-based products, research focusing on materials of bio-origin has been introduced. Studies are progressing on the syntheses of composites possessing both matrix and filler from plant and animal origin. Recent studies show that bio-filler reinforced composites have a direct effect on product properties (Reichert et al. 2020).

Composites reinforced with degradable polymers are termed “Bio-composites/ Green composites”. The idea of bio-composites originated early from the use of agricultural waste and products for the production of green materials. Bio-based composites are generally obtained from renewable sources (Singh et al. 2017). They were the first composites originated and developed. Ancient Egyptians have been using natural fibre reinforced composites. Clay reinforced with straw was the first known bio-composite used by them in ancient times for the construction of houses. But the notable invention in the field of bio-composites was carried out by Henry Ford in 1930, when he designed his first prototype car made of hemp fibres. During World War II, aircrafts had fuselage made of unidirectional, unbleached flax yarn impregnated with phenolic resin. The rising concerns of the impact of petroleum-based products on the environment and the non-biodegradability of such products have revolutionized the production of the bio-synthetic duo during the past 50 years. At the same time, biodegradable composites can also be obtained from petroleum-based products. Bio-composites can be prepared by the combination of the following (a) natural fiber reinforced with petroleum derived polymers, which are non – biodegradable, (b) Bio-polymers reinforced with natural fibres (c) Bio-polymers reinforced with synthetic fibres. Hence, the general definition of bio-composite can be given as “Composite materials in which at least one of the constituents is derived from a natural source ". They prove to be environmentally compatible materials with minimum volume of carbon dioxide emissions (Kalia et al. 2009). The classification of bio-composites is given in Figure 1.2.

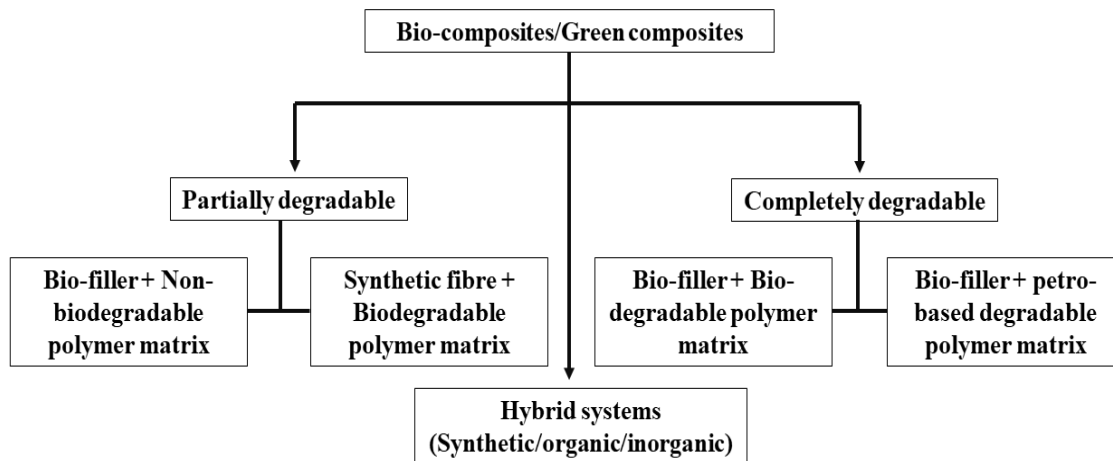


Figure 1.2 Classification of bio-composites (Bahrami et al. 2020)

Modern technologies and industries have been challenged to develop more sustainable products with regard to environmental protection laws by minimizing the use of petroleum based plastics and related products. Among the developed bio-plastics, bio-composites based on thermoplastic materials are widely used (Sharma et al. 2013, Cleetus et al. 2013). A composite material formed through combining a natural polymer with synthetic polymers, polysaccharides, ceramics, or metals makes them environmental friendly and biocompatible (Kalia et al. 2009). They can be obtained as membranes, mouldings, coatings, particles, fibres and foams. Numerous studies have been conducted to develop eco-friendly composites for their use in the field of sensors, tissue engineering, scaffolds, packaging sector and many more (Haraguchi 2014). The high manufacturing speed and enhanced environmental compatibility has increased the demand of bio-composites (Mantia and Morreale 2011, Riedel and Gmbh 2012). Bio-composites have also been used in the medical field, and the automobile industry due to their excellent mechanical, electronic, flame retardancy and wear resistance properties. According to the Bio-plastic market update 2020, in the 15th European bio-plastic conference, global bio-plastic production capacity is

estimated to increase from 2.11 million tonnes in 2020 to 2.87 million tonnes in 2025, as is shown in Figure 1.3. (15 European Bio-plastic Conference, Bio-plastics market development update 2020).

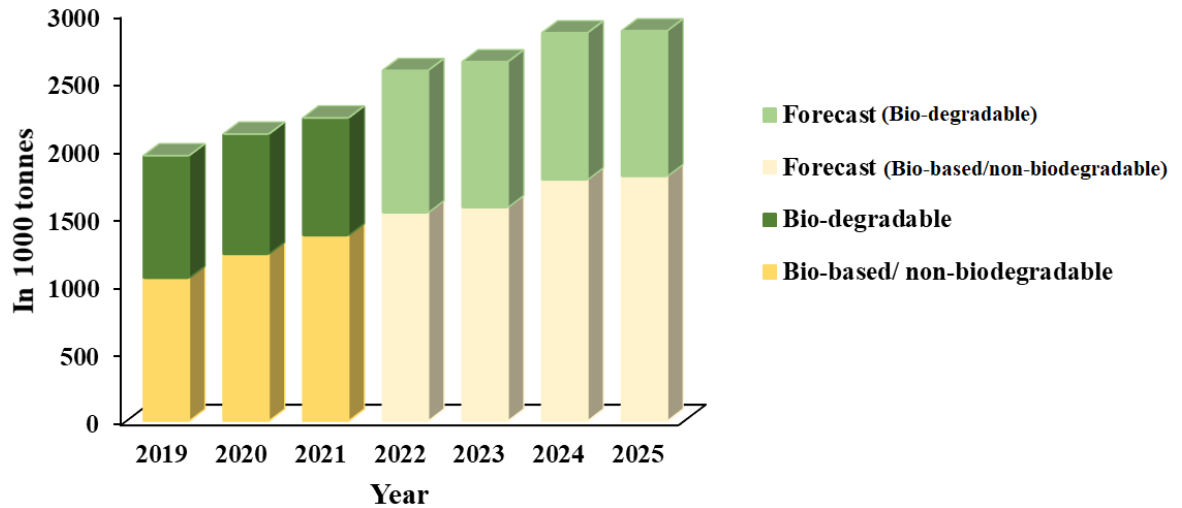


Figure 1.3 Global production capacity of bio-plastics: 2019- 2025

Bio-composites with polyethylene as matrix and natural polymers and ceramics as fillers have notable applications in the modern world. The nature and origin of the bio-fillers also help in designing the properties of the composite for specific applications. The fillers from natural origin are anisotropic and their properties depend upon their isolation. Natural fillers are more advantageous over inorganic filler; but in addition to this, their particle size has to be considered. The particle size of the filler plays a major role in determining the strength, stability and durability of the composite. Some of the notable bio-fillers used in the composite material are cellulose, starch, chitosan etc. (Nikola et al. 2019, Mohammed et al. 2015).

1.5 Applications of bio-composites

Surface treatment of the natural fibres with highly chemical resistant as well as water

resistant thermoplastic can be utilized for the development of bio-based thermoplastic composites (Ali et al. 2021). They not only provide mechanical stability but also economic viability. The thermal properties and electrical properties like dc conductivity, dielectric constant, dielectric loss, etc., can be tuned with the help of bio-polymers. The role of bio-composites in the medical field are also notable (Müller et al. 2017). They have also been used in high voltage applications, sports, (surfboards) etc. Some of the applications of bio-based thermoplastic composites (based on Scopus data from 1997-2022) and patents are given below in Figure 1.4 and Table 1.1 respectively.

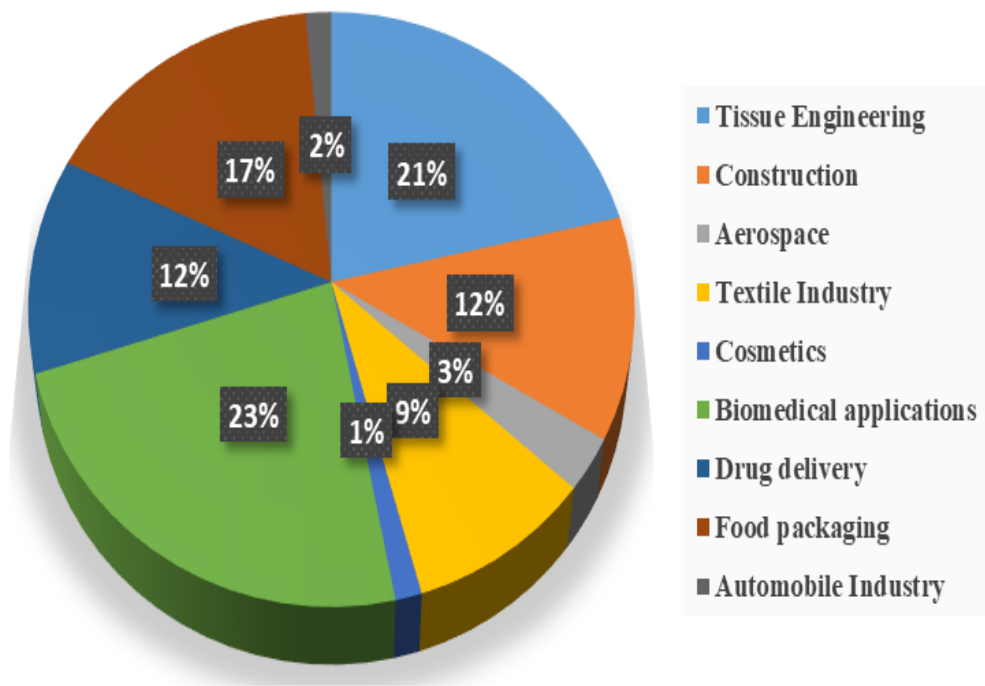


Figure 1.4 Applications of bio-composites

Table 1.1 Patents on thermoplastic / natural polymer / ceramic - based composites for bone-tissue engineering applications

Sl.No	Patent No and Year	Material	Novelty
1.	US3662405A (1972)	Blend of alumina and phosphoric acid	Reinforced porous ceramic bone prosthesis (Seymour et al. 1972)
2.	GB2085461B (1984)	HDPE-hydroxyapatite composites	Composite material for use in orthopaedics (Bonfield et al. 1984)
3.	US5017627A (1991)	Polyolefin + Inorganic particulate (CaCO ₃ , hydroxyapatite)	Applications in endoprosthesis (Bonfield et al. 1991)
4.	US5338772A (1994)	Hydroxyapatite and D/L polylactide	A three-dimensional open-pore structure with growing-in and healing-in properties (Bauer et al. 1994)
5.	US5431652A (1995)	Powdered Poly-(lactic acid) were pelletized and subjected to hydrostatic extrusion	Biodegradable polymer for fixing fractured bones (Shimamoto et al. 1995)
6.	US5679723A (1997)	Mixtures of poly(lactide), poly(glycolide), poly(trimethylene carbonate), poly(p-dioxanone) and poly(ε-caprolactone) with calcium phosphate	Improved absorption characteristics and other physical properties. (Cooper et al. 1997)
7.	US5766618A (1998)	poly(lactide-co-glycolide) (PLGA) – hydroxyapatite (50:50) – Casting	A three-dimensional macroporous polymer matrices (100-250 microns) for use as bone graft or implant material was developed. (Cato et al. 1998)

8.	WO1998024483A2 (1998)	Mixture of polylactic acid (PLA), polyglycolic acid (PGA) with N-methyl-pyrrolidone (NMP) as plasticizer	Biocompatible therapeutic implants for insertion into a patient's body (<u>Leatherbury</u> et al. 1998)
9.	US6071530A (2000)	poly(DL-lactide) and about 63% N-methyl-2-pyrrolidone (NMP) polymer mixture	Enhanced cell growth and tissue regeneration, wound and organ repair, nerve regeneration, soft and hard tissue regeneration. (Polson et al. 2000)
10.	US6296667B1 (2001)	Zirconia-hydroxyapatite composites	Strong porous bone substitute material (Johnson et al. 2001)
11.	US6281257B1 (2001)	Poly(methyl methacrylate) (PMMA) – hydroxyapatite composites	A 3D porous matrices as structural templates for cells having good mechanical performance which can be used as platforms for in vitro cell cultivation, implants for tissue and organ engineering (Peter et al. 2001)
12.	WO2003026714A1 (2003)	PLGA + Highly substituted calcium phosphate (CaP) apatite	A porous ceramic composite implant for connective tissue replacement with high mechanical performance (Timothy et al. 2003)
13.	US7211266B2 (2007)	calcium sulfate hemihydrate + stearic acid + calcium sulfate dihydrate, and/or an ionic salt such as potassium sulfate, or sodium sulfate (accelerant) + saline solution.	Bone graft substitute compositions, containing calcium sulfate and can be used as filler for voids or defects in bone. They can also promote bone growth. (Cole et al. 2007)

14.	EP2542187B1 (2011)	Bioactive glass/collagen	A bone regenerative implant for bone fractures (David et al. 2011).
15.	WO2014152113A2 (2014)	Polyethylene glycol and bioactive glass fibres	Bioactive porous composite bone graft implants for tissue regeneration (Bagga et al. 2014).
16.	JP2014506506A (2014)	An electrospun polycaprolactone (PCL) fiber scaffold functionalized with phosphonic acid polymer dispersed in the dissolved PCL	An injectable composite material comprising a fibrous material (Daunzu et al. 2014).
17.	WO2018117266A1 (2017)	Production of PEEK fibres by irradiating belt shaped laser beam	Bone implantable material with no reduction in mechanical properties (Takashi et al. 2017).
18.	US11103620B2 (2021)	Hybrid implant (Polymers like PDLLA, PLGA, PCL, HDPE, PE, UHMWPE, PEAK, PEEK, PP, and PUR+ CaCO ₃ + metallic component)	A completely or partially degradable composite with pore size between 300 μm - 450 μm that have active interaction with the tissue environment. (Daniel et al. 2021).

1.6 Matrices in bio-composites for tissue engineering applications

The most commonly used synthetic materials in tissue engineering are polylactic glycolic acid (PLGA), poly vinyl alcohol (PVA), polyvinyl chloride (PVC), polyacrylonitrile (PAN), and thermoplastics (HDPE, LDPE, UHMWPE), and commonly used natural polymers are chitosan, collagen, etc. Ceramic matrices like calcium phosphates are also employed for the development of the bone-tissue engineering applications to improve strength, porosity and cell proliferation.

According to Langer and Vacanti, tissue engineering can be defined as an interdisciplinary field where life science and engineering are combined for the development of substitutes that could replace/restore, maintain, or improve the function of tissues (Langer and Vacanti, 1999). The immense development in tissue engineering can be attributed to the increased use of hybrid composite produced from the combination of synthetic materials, biomaterials and ceramics. The latest report released amongst the COVID-19 crisis on the global market for Tissue Engineering is estimated at US\$11 Billion in the year 2020 and can reach to \$26. 8 Billion by 2027. Among them, in Orthopaedics, Musculoskeletal & Spine is estimated to achieve 12.1% Compound Annual Growth Rate (CAGR) and reach US \$6.9 Billion by 2027. The Tissue Engineering market in the U.S. is estimated at US \$3.3 Billion in the year 2020. China is predicted to reach the market size of US\$4.7 Billion by the year 2027. Countries like Australia, India, and South Korea, are forecasted to reach US\$3.2 Billion by the year 2027.

1.7 HDPE as matrix in bio-composites

Polyolefins are generally selected as candidates for making composites with the bio-fillers due to their chemical resistance, water resistance, thermal stability, film

forming ability, toughness, and flexibility. The good barrier properties exhibited by the polyethylenes can be used as good packaging material (Cooper et al. 2007). Depending upon the density and mode of branching, polyethylenes can be classified as low-density polyethylene (LDPE), high-density polyethylene (HDPE), linear low-density polyethylene (LLDPE), and medium-density polyethylene (MDPE). Polyethylenes are polymeric materials which have ethene (C₂H₂) as their basic fragment. Among polyethylenes, HDPE has strong intermolecular force due to its linear nature and finds wide applications in the medical field (Figure 1.5).

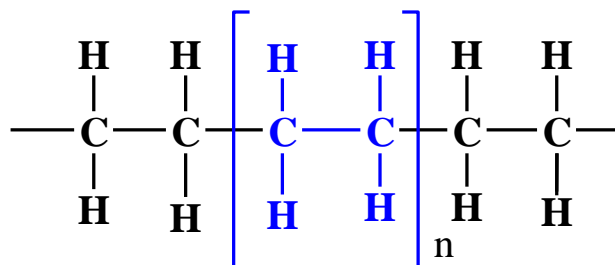


Figure 1.5 Structure of High density polyethylene (HDPE)

HDPE is a semi-crystalline polymer which can withstand temperature till 120 °C, making it a candidate for “hot fill” and pasteurisation applications (Cooper et al. 2007). On considering the physical properties, HDPE has a tensile strength of 30.5 ± 5 MPa, impact strength (un-notched), 46 kJ/m², and tensile modulus at 28 °C: 900 - 1550 MPa. The monomers and additives used in HDPE are close to that of LDPE. The comparatively high mechanical strength in HDPE when compared with LDPE can be employed for making composites with natural polymers like chitosan and ceramics for bone tissue applications. In addition to the mechanical performance, the biodegradability and biocompatibility of polyethylenes are also considered to get a better understanding about the surface analysis and cell proliferation on the prepared systems. Besides the thermo-UV pre-treatment methods, photo catalysis and treatment

with pre-oxidants, the biodegradation of polyethylenes (PE) is possible with the help of bacteria and fungi. It has been noted that fungal degradation is more effective than bacterial degradation due to its ability to adhere to the hydrophobic surface of polyethylenes. The biodegradation process involves abiotic and biotic factors that leads to the breakage of the polyethylene backbone. (Hersztek and Kopeć 2019) Reports shows that certain microbes like cyanobacteria and algae can degrade PE. The algae species *oscillatoria subbrevis*, *scenedesmus dimorphus*, *navicula pupula* are found to form colonies on the surface of PE by utilizing the polymeric carbon causing effective degradation (Sarmah and Rout 2020). Alk B family alkane hydroxylases has helped in converting 20 % low molecular weight PE into CO₂ in 80 days at 37 °C. It was also noticed that pre-treating the samples with thermo UV radiation or addition of oxidising agents stimulates the degradation of polymer matrix (Ghatge et al. 2020, Albertsson 2004)

HDPE has also proved to be highly biocompatible and extremely stable for long term applications. The use of polyethylene as implant materials for bone or cartilage in humans has been an emerging field of research for the past 60 years. Polyethylenes with molecular weight (M_w) 20,000 g/mol have limited biocompatible properties and M_w above 300000 g/mol have processing difficulties for the preparation of the composites. HDPE and LDPE have M_w between this range with HDPE exhibiting more strength and high biocompatibility. Studies have reported HDPE as medical grade and can be sintered to form a framework of interconnecting pores (Khorasani et al. 2018). They also have minimal surrounding soft tissue reaction. HDPE based implants are easy to shape depending upon the nature of the bone defect. HDPE has also played a major role in the development of implants in the field of maxillofacial defects. It can easily integrate bones with tissue and can become stable against bones.

When compared with other thermoplastics like polytetrafluoroethylene (PTFE), HDPE has more flexibility. The large and stable pores of porous HDPE promote rapid bone and fibrous in-growth into the implant. It can anchor the implant and maintain the local host immune response. Some of the features of HDPE that makes it suitable for bio-applications are: a) their biocompatible nature; b) they can be moulded to the shape required; (c) flexible yet firm; (d) the pore size in polyethylene can be engineered depending upon the implant; (e) the chain mobility of the polyethylene can help in changing the pore volume; (f) the structure of the final implant is stable as well as inert and (g) light weight (Ranjan et al. 2015, Deshpande and Munoli 2020). The HDPE implants are generally available as MEDPOR (1985) and later BIOPOR and OMNIPOR since 2006.

1.8 Fillers in thermoplastic based composite materials for medical applications

The need for bio-active materials as reinforcement in thermoplastic matrices for bone-tissue engineering applications has led to the replacement of the currently available bone replacement materials such as steel, titanium-based alloys, silicones etc. Due to the increased incompatibility due to allergic conditions, degradation within the body, tissue reaction, cytotoxicity, strength, and stability, substitution of these materials with bio-ceramics and natural polymers having structural similarity with the bone is widely studied. Natural polymers such as chitosan, collagen, gelatin, cellulose, starch, alginate and bio-inert ceramics such as sintered hydroxyapatite, alumina, zirconia (TZP, Mg- PS2) are widely used in bio-based composites for implant materials. Numerous reports show that chitosan-based scaffolds have been used in tissue engineering applications due to their role in promoting adhesion, improved

functionality and non-toxic nature. To improve the mechanical stability of bio-based composites, an inorganic component namely hydroxyapatite has been extensively used in chitosan-based and thermoplastic-based materials for implant fixation and for establishing a bonding between the implant and the site (Ong et al. 2015, Liu et al. 2014). The plasticizers and compatibilizers in composites that induces segmental mobility and miscibility in the system also contribute to the bio-implant applications. Palm oil based polyols has been used in dentistry for dental restoration materials (Tajau et al. 2021). Maleic anhydride based PLA/CNC bio-composites exhibiting superior mechanical strength and biocompatibility have also been used for medical applications (Cai et al. 2009). Based on the fillers and additives used, the properties of chitosan and hydroxyapatite in medical applications are discussed briefly.

1.8.1 Chitosan

Chitosan is the deacetylated derivative of chitin, which is the second most abundant biomaterial found on earth. They are mainly found in the exoskeleton of crustaceans. Chitin is structurally identical to cellulose, where the secondary hydroxyl on the second carbon of the hexose repeat unit in cellulose is replaced by acetamide group (Rinaudo 2006). Chitosan, a copolymer consisting of β -(1,4)-2-acetimido-D-glucose and β -(1,4)-2-amino-D-glucose units is derived by the deacetylation of chitin in an alkaline medium (Figure 1.6). It is a linear poly-cationic polysaccharide that is non-toxic, biodegradable, and biocompatible. The degree of deacetylation, molecular mass, temperature and concentration of the alkali affects the properties of the formed chitosan. Due to the presence of positive charges on the amino groups, chitosan is the only commercially available water-soluble cationic polymer making it suitable for a variety of applications in cosmetics, food and pharmaceuticals.

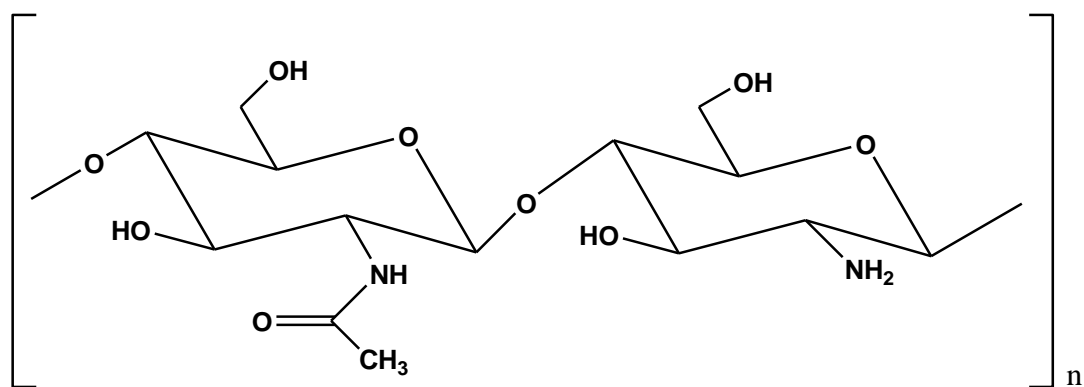


Figure 1.6 Structure of Chitosan

The processing of chitin is difficult owing to its limited solubility in water thus making it less feasible for use in laboratories and industries. Chitosan, though insoluble in water, has been found to be soluble in mildly acidic solution. Among the pH responsive polymers, low molecular weight chitosan is widely employed for biomedical applications (Rinaudo 2006) (Elieh-Ali-Komi and Hamblin 2016). It is also soluble in dilute acids and this solubility facilitates the biocompatibility and biodegradable properties when mixed with a non-degradable polymer matrix. Chitosan has also been considered in tissue engineering due to its biocompatibility, non-toxicity, non-antigenicity and adsorption properties. The structural similarity of chitosan to glycosaminoglycans, which is the primary component of extracellular matrix of bone and cartilage, makes it a suitable for bone - tissue engineering applications too. Studies also reveal the osteo-conductivity and the ability of bone formation of chitosan in-vitro and in-vivo. To enhance the strength and biocompatibility of chitosan, various studies have been conducted by incorporating bioactive materials like hydroxyapatite, collagen, alginate, gelatin silk fibrin and glycosaminoglycans (Thein Han and Misra 2009).

1.8.2 Hydroxyapatite

Hydroxyapatite (HA) is an inorganic ceramic having the chemical formula $\text{Ca}_5(\text{PO}_4)_3\text{OH}$, which is structurally similar to the inorganic component of the bone (Figure 1.7).

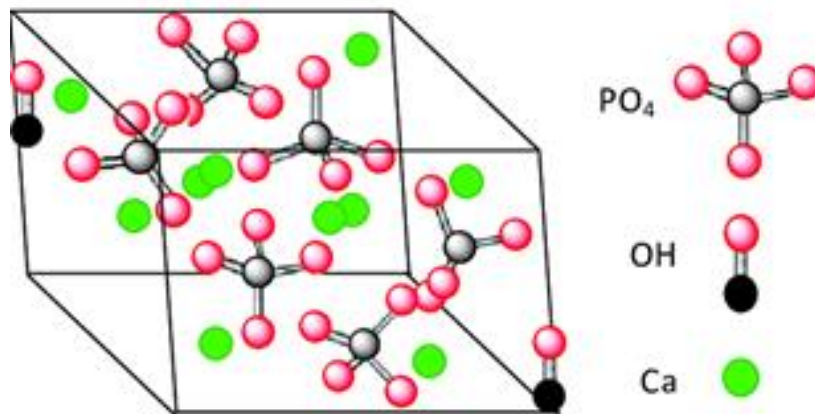


Figure 1.7 Structure of Hydroxyapatite (Sawittree et al. 2014)

Nano-hydroxyapatite is the major component of bone constituting 70% of bone weight. It generally has a molecular weight of 502.31 g/mol. Hydroxyapatite being the unique form of calcium phosphate, also depends upon its Ca/P ratio of 1.6. It is generally hexagonal in shape and is biocompatible. The properties of nano-hydroxyapatite can be enhanced by modifying and doping with polymers. Hydroxyapatite can be synthetically obtained from natural sources like mammalian bone, aquatic sources like fish bone and fish scale, shells (egg shell, sea shell), plants, algae, and minerals. It can form strong chemical bond with the host bone and can be considered as a good bone graft material. HA can be obtained as powders, granules, and porous blocks. The synthesis process includes sol-gel synthesis, wet chemical precipitation method, etc. Hydroxyapatite is non-toxic, non-immunogenic and its structure is crystallographically similar to the bone mineral (Dorozhkin 2011). Nano-

hydroxyapatite has greater surface area and hence uniformly distribute in polymer matrices. They have structural similarities to the inorganic mineral component in bone (Kalambettu et al. 2012). As a result, they can mimic the bone like properties and have been used extensively in bone implants. The shape of HA in natural bone is needle like/rod like with a length of 40-60 nm and width of 10-20 nm. The chemical similarity of hydroxyapatite with bone has been extensively used in hard tissue replacement in addition to their biocompatibility and osteoconductivity. The physical and chemical properties like size of the particle, shape, and purity also depend upon the crystallinity and mechanical strength of the composite. The addition of hydroxyapatite to polymers may increase the modulus of the whole composite system and make it comparable with the strength of bone. The implantable materials based on polymer - orthophosphate bio-composite and hybrid composites have been introduced since 1981. The HDPE/HA composite has been approved by FDA at 1994 and is commercially available as HAPEX since 1995 (Mohamed et al. 2014). Besides medical applications, hydroxyapatite has been widely used in waste water treatment and removal of various heavy metals such as cadmium, chromium, uranium etc. Iron doped HA and cobalt doped HA has been widely used for dye removal. HA can also absorb most of the emerging pollutants like cosmetics, herbicides pesticides, pharmaceutical compounds like antibiotics, drugs etc. (Pai et al. 2020).

1.9 HDPE based composites

Studies based on synthetic polymers incorporated with bio-fillers are increasing rapidly than biodegradable synthetic polymers due to the higher shelf life, cost effective production and good mechanical and structural properties of the former. High density polyethylene (HDPE) based composites usually exhibit good mechanical

and structural properties when incorporated with bio-fillers, metals and ceramics. Environment-friendly techniques such as solvent free methods like high energy beam radiation and melt mixing processes are generally used for modifying the properties of HDPE. Studies of surface functionalism of HDPE composites were conducted by having Nylon-66 interact with HDPE by modifying its surface through irradiation techniques with high mechanical strength of 120 MPa (Kim et al. 2001). HDPE composite systems melt mixed with natural polymers and ceramics are also a developing field which has its applications in bio-implants and food packaging sector. When a synthetic polymer is mixed with a bio-filler, the presence of additives as well as crosslinkers can improve its miscibility. HDPE/chitosan composite crosslinked with vinyl triethoxysilane with a dicumyl peroxide (DCP) initiated melt mixing technique showed decreased crystallinity and elongation at break. This was due to the addition of chitosan, which developed a strong interaction at the polymer interface (Mir et al. 2011). HDPE based composites have also been widely used in medical application by incorporating chitosan as well as hydroxyapatite. Sintered and non-sintered hydroxyapatite have been mixed with HDPE by using silane as crosslinker. The mechanical strength increases with the addition of hydroxyapatite due to higher particle surface area, small particle size distribution and high chemical reactivity (Sousa et al. 2003). HDPE/HA composites showed bone apposition rather than fibrous encapsulation when compared with other implant materials. The homogeneous distribution of nano-HA in the polymer matrix can be utilized for the preparation of HDPE/HA composites. Nano-HA particle can promote more contact surface area with HDPE, thereby increasing the interaction between filler and matrix. The addition of hydroxyapatite to HDPE can also affect the overall thermal, rheological, fracture behavior and viscoelastic properties. Additionally, the storage modulus of all

HDPE/HA composites have been found to increase with increase in content of HA. When 30 wt% HA is added to HDPE, high wear resistance and a storage modulus of 8.3×10^{11} MPa was observed. The aging of the composite also has significant effect on the hardness and fractional toughness of the system. A decrease in tensile strength from 43.3 MPa to 35.2 MPa was observed for 30 wt% HA added HDPE system (Fouad et al. 2013).

1.10 Chitosan based composites

The potential of chitosan in food industry, medical field, etc., has been widely explored owing to its excellent film forming ability and good mechanical and barrier properties in addition to its biocompatibility, biodegradability and antibacterial properties. A significant shortcoming of natural biopolymers like chitosan is that their industrial use is limited as compared to synthetic polymer materials produced from petrochemicals resources owing to their hydrophilic nature. The hydrophilicity makes the end product such as biodegradable films sensitive towards environmental conditions such as temperature and relative humidity. This causes the films to be susceptible to water sorption and hence thus less stable. The poor barrier and weak mechanical properties of bio-polymers have attained research attention. The addition of materials such as emulsifier, surfactants or plasticizers improved the strength, chain mobility, flexibility and shelf life of chitosan based systems (Ali et al. 2014). It is possible to obtain products of synthetic polymers with chitosan, using processing methods like melt mixing techniques which is used industrially, with acceptable properties and being more friendly to the environment. Polyolefins represent one of the most suitable matrix candidates in the fabrication of chitosan blend films as they have good flexibility, toughness and excellent barrier properties at a low cost (Z. Wu

et al. 2018). A favourable cost-performance ratio for the development of an environmentally friendly material can be achieved by combining chitosan with a commodity synthetic polymer that can achieve a balance in physical and mechanical properties of the films. The miscibility of chitosan with the synthetic polymers has been achieved by using crosslinkers and compatibilizers. Citric acid has been used as an effective green - crosslinker in chitosan / polyethylene–oxide (PEO), where the final system showed an improvement in anti-bacterial activity and thermal stability (Grkovic et al. 2017). The concentration of chitosan in the composite system also affects the mechanical strength which can be due to agglomeration formed beyond the optimized concentration and lesser compatibility between hydrophilic chitosan and hydrophobic polymer system. Despite these conditions, PLA/chitosan films have shown an accepted shelf life of 15 days for packing Indian white prawns (*Fenneropenaeusindicus*) (Fathima et al. 2018). The presence of plasticizer also showed considerable effect on the chitosan/PLA composites by achieving a Young's Modulus value of 324 ± 14.5 MPa. Chitosan has acted as a nucleating agent in the spherulitic growth of the PLA crystals. A reduction in oxygen permeability was also noted for the prepared films (Pal and Katiyar 2016). The presence of crosslinker also affects the mechanical properties, surface characteristics, and anti-microbial properties. When glycerol borate and tripolyphosphate were added as crosslinkers to chitosan/cellulose composite systems, the glycerol crosslinked system showed superior mechanical properties with a tensile value of 20.4 ± 30.4 MPa. However, the borate crosslinked system showed good wetting properties. In addition to this, the presence of crosslinkers has caused a decrease in the anti-microbial properties of the system (Liang et al. 2019). The combined property of polyethylene and bio-filler can also affect the permeation properties as well as the mechanical characteristics of the

composite. LDPE matrix coated with chitosan shows permeation rate less than 100 to 1000 times than that of PE films, which follows the order $P_{CO_2} > P_{O_2} > P_{air}$ in the dry state than in wet state (Kurek et al. 2012).

1.11 Hydroxyapatite based ternary composites

The efficiency of a composite depends upon the filler as well as the matrix that is being selected. The mechanical performance of composites is seen to increase from binary composite to ternary system. Present day research is equally concentrated on binary systems as well as ternary systems. Ternary composite based on chitosan and hydroxyapatite coated on ultra high molecular weight polyethylene (UHMWPE) was prepared through an immersion method. The adhesive nature of chitosan as well as the inter-molecular hydrogen bonding and chelate interaction between chitosan and hydroxyapatite is involved in the formation of the composite. The composite attained a maximum compressive strength of 120 MPa. The possibility of application of this material in dentistry, orthopedics, surgical procedures and ophthalmology has been studied (Arizmendi-morquecho et al. 2013). The presence of chlorotrimethyl silane on nano-hydroxyapatite/chitosan/polyacrylamide system also shows an increase in the mechanical properties of the system. The SEM studies shows a wavy pattern indicating a well dispersed pattern. Nano-hydroxyapatite can occupy the free holes formed in the system which can further enhance the potential to induce HA crystal formation on the surface of the composite. This can increase the stability of the composite at the implanted site and can easily bond to hard tissue like bone (Kalambettu et al. 2012). Hydrophilicity is an important parameter that helps to know the transfer of cell nutrients and metabolites. The presence of citric acid on HA/Chitosan/gelatin composites has improved the formation of bone-like apatite

layer on the surface of the composites. 0.2 M of citric acid has been optimised for the formation of bone like apatite layer on the composite surface (Mohamed et al. 2014). Various studies have been reported for HA/chitosan system as drug carrier, bone repair scaffolds and bone implant materials. Glutaraldehyde crosslinked chitosan/ HA scaffolds have been used as bone repair materials as well as drug carriers for icariin - a bone density conservation agent. The mechanical property of the tissues repaired through employing HA/CS composite showed properties similar to that of bone due to its differentiation capacity of bone precursor cells. They show compression strength of 685 MPa, which is closer to the strength of the cancellous bone. Porosity of the scaffolds, the molecular weight of the chitosan (5.75×10^4) and size of the filler also determines the flexural strength and mechanical strength of the composite (Li et al. 2013). The bioactivity of hydroxyapatite and Al_2O_3 with the combination of HDPE has resulted in a ternary composite which can be used as an alternative for bone - tissue engineering applications. The HDPE/HA/ Al_2O_3 composites have promoted a direct biological contact between viable bone and the composite surface. The histological observations also showed a strong tendency for bone formation at the composite interface when compared with the LDPE implants. The HDPE/20 wt% HA/20 wt% Al_2O_3 composite has been optimized and has contributed more to neo-bone deposition at the interface (Tripathi et al. 2012).

1.12 Characterization of thermoplastic (polyethylene) based composites

The structural characteristics of a composite depend mainly on the miscibility achieved by the matrix with the filler. The miscibility determines the pore formation and free-hole volume, interaction existing between fillers and matrix, stability of the

system, crystallinity, structural properties, mechanical strength, and biocompatibility in the composite system. For the preparation of bio-materials, the following aspects given in Figure 1.8 are considered.

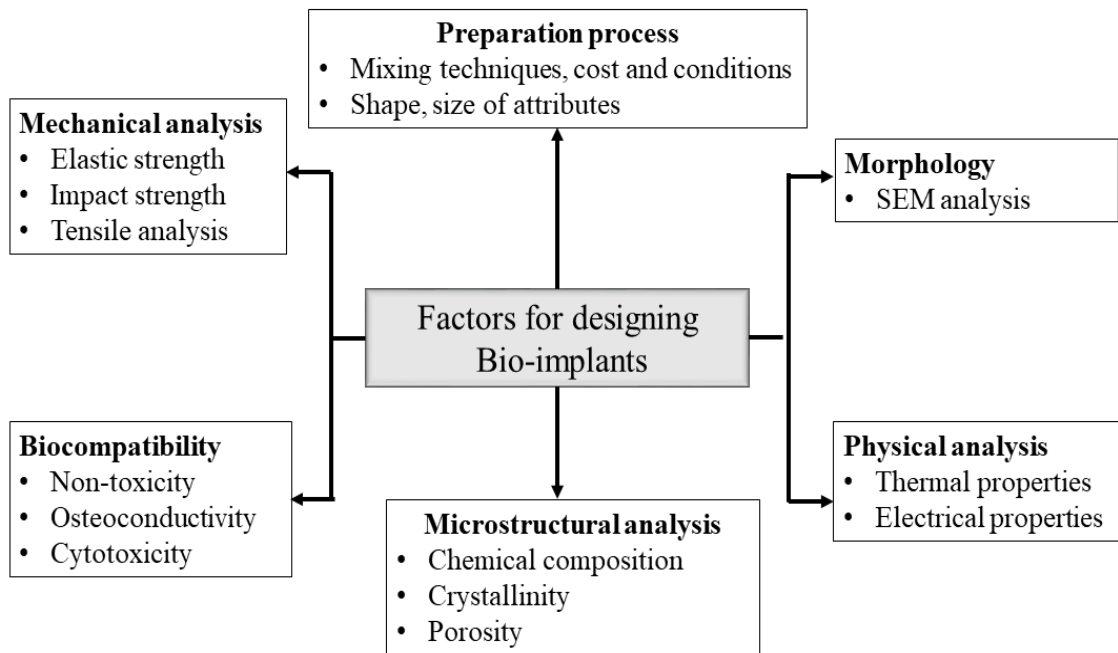


Figure 1.8 Factors for designing bio-composites (A. K. Sharma and Gupta 2020)

1.12.1 Mechanical analysis of thermoplastic / natural polymer / ceramic - based composites

Deformation mechanisms in composite materials are important in understanding the mechanical characteristics of the prepared system. It occurs when an external load/stress falls on the system under investigation. Hence, the deformation in polymer composites, especially in thermoplastic - based systems, depend on various parameters such as stress-strain, speed and magnitude of applied load, miscibility of fillers with the matrix, effect of crosslinking and morphology of the system. Plastic deformation determines the energy absorbed by the system. More the energy absorbed

by the composite, greater is the ability to preserve its stiffness by maintaining the plasticity in the system. This makes the system suitable for load bearing applications (Pundhir et al. 2021). Mechanical properties are one of the most informative characterizations that give information about the interactions between the filler and the matrix. The strength of a composite depends on three factors: (a) interfacial adhesion between the components in a matrix; (b) interaction between the filler and the matrix and (c) miscibility during mixing. The amount and molecular size of additives such as plasticizers, compatibilizers, crosslinkers and free radical initiators also affect its strength to a certain extent. For instance, plasticizer improves the flexibility of the composite system by enabling the segmental mobility in the composite system. It has been reported that they also reduce the rigidity of the final composite system by increasing the chain mobility. Palm oil as plasticizer in LDPE/chitosan films has acted as a separator of agglomeration (Sunilkumar et al. 2012).

Stress-strain analysis, impact strength analysis, compression tests, fracture tests and hardness are some of the mechanical analyses widely used in material strength characterization (Mohan et al. 2019). The molecular structure, polymer chain branching, bond strength, physical and chemical interaction between the components determine the strength of the material under study. The stress-strain behavior of a material explains the tension and degree of deformation based on the stress applied on it. It can provide data regarding tensile strength, Young's Modulus and elongation of the material before fracture. The impact strength analysis provide valuable data about the formation of micro-cracks, brittle/ductile nature of the composite and the amount of energy it can hold when subjected to an external load. The tensile strength and

impact strength of various thermoplastics are shown in Figure 1.9 (a) and 1.9 (b) respectively.

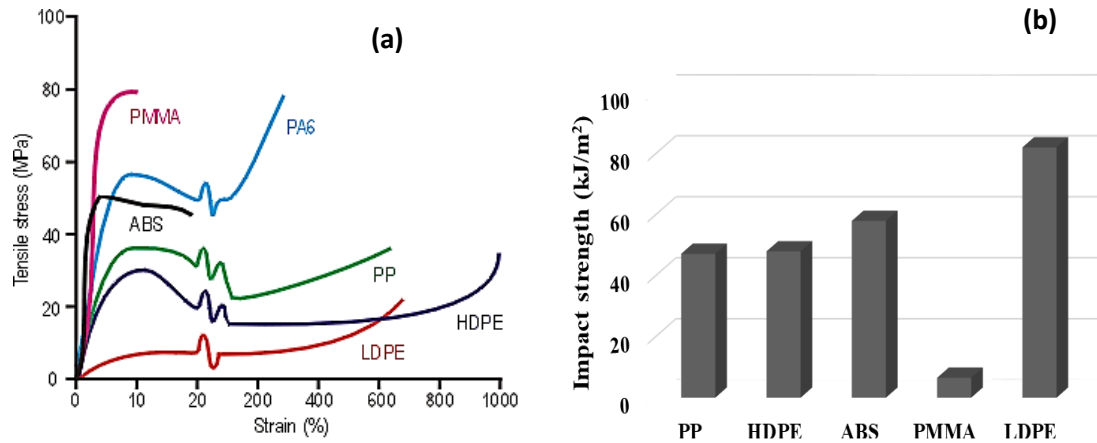


Figure 1.9 (a) Stress-strain graph and (b) un-notched Izod impact strength of various thermoplastics

1.12.1.1 Computational Modelling of mechanical properties of thermoplastic / natural polymer / ceramic - based composites

Theoretical modelling studies in mechanical characterization of composite materials help in predicting the stress-strain phenomena which helps establish data for design purpose. But the process is quite not easy for anisotropic materials. Micromechanical models using a combination of Mori-Tanaka method and Generalized Methods of Cells were used to predict the properties of composites based on polypropylene (PP) and polystyrene (PS). In this case, the approximation of experimental data was quite difficult. To overcome these limitations, Finite Element (FE) model based on mathematical equations and mechanics was suggested. It helped in consolidating the quasi-static and long-term response of material. Few models implemented in FE packages include: (a) The Polynomial Node: used for elastic materials; (b) Ogden

Model: used for describing stress-strain relationship in elastomers and thermoplastics. This model can also be used for describing the hyper-elasticity in biological tissues; (c) The Yeoh Model: This model simulates the mechanical behavior of elastomers by understanding the stiffening effect in large strain domain in thermoplastics like HDPE; (d) Marlow Model: used for uniaxial tests (tensile strengths & compression tests) of polymers. In addition to these models, SIMPLE, SIMPLEC, PISO models are also widely used for the mechanical simulation of data (Rodri'guez-Sa'nchez et al. 2019).

1.12.1.2 Finite Elemental Analysis (FEA)

For the easy comparison and analysis of experimental results with the theoretical data, computational modelling studies arising from the numerical results using Finite Element analysis is widely used in industry as well as academia. Virtual analysis of experiment conducted with accurate and optimized results help in the prediction of lifetime and product development. An overview of FEA is shown in Figure 1.10. (Alhijazi et al. 2020).

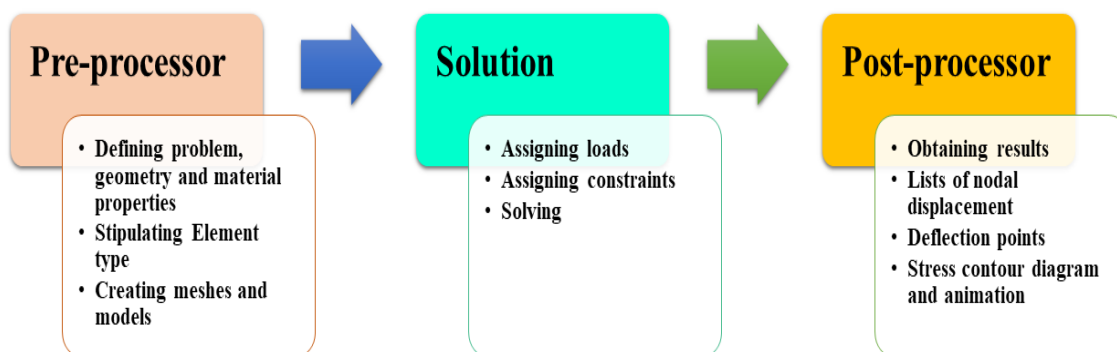


Figure 1.10 An overview of Finite Element Analysis (Alhijazi et al. 2020)

Some of the commercially available FEA software's are ANSYS, IDEAS, PATRAN, ABAQUS, NISA, and COMSOL. ANSYS workbench is the most flexible software for the stress analysis in thermoplastic based composites (Alhijazi et al. 2020). Here the 3-D model of the developed material can be generated through Computer Aided Design (CAD) software. This method is used mainly in clinical applications especially for studying the mechanical performance of bio-implants. The analysis can predict the stress distribution around the implant material. It focuses on the quantitative evaluation of stress on the surrounding bone and the implants. The mathematical equations in the software help in solving complex structural problems through integrating and dividing into simpler structures. Hence, ANSYS is more reliable and easier than Video Force Microscopy (VFM) and CellFIT which depends only on equilibrium alone (Crowley et al. 2008, Brodland 2015). The tensile strength and Young's modulus of HDPE/fly ash composites compatibilised with HDPE-g-MA has been studied and compared with FE analysis. FEA has been employed to simulate and calculate the ring stiffness. The study also showed that the composites could be used for the preparation of large diameter rings (Wu et al. 2021). Few of the important data on mechanical properties of thermoplastic / natural polymer / ceramic-based materials are shown in Table 1.2.

Table 1.2 Mechanical properties of thermoplastic / natural polymer / ceramic - based composites

Sl.No	Composite	Mechanical Properties	Observations	Applications
1.	Polyvinyl chloride/wood flour (WPVC) composites	<p>Tensile strength- PVC/DOP:16.7MPa</p> <p>Impact strength (vertical) WPVC/EFAME :15.4 kJ/m²</p> <p>Elongation at break WPVC/EFAME: 69%</p>	High tensile strength is attributed to the plasticization in the system. Small molecular structures of plasticizers enabled high better interaction promoting high elongation at break. Easier lubrication and relaxation of smaller molecules in the PVC matrix promotes high impact strength.	Characterizations (Xie et al. 2014)
2	HDPE/chitosan composites	<p>Tensile strength: 23.14 MPa</p> <p>Impact strength (horizontal): 229.20 kJ/m²</p> <p>Modulus of elasticity: 828.38 MPa</p>	HDPE/2 wt% chitosan is optimized. Chitosan is evenly distributed in the system and the energy is evenly distributed throughout the system resulting in good mechanical properties. Chitosan acted as resistance to plastic deformation.	Biomedical applications (Daramola et al. 2020)
3	HDPE/chitosan composites using	<p>Tensile strength: 19.7 ± 2.4 MPa for HDPE/CM95/5</p>	Immiscibility between chitosan and HDPE resulted in low mechanical	Biomedical applications (Maro et al. 2020)

	High viscosity chitosan and medium (CM) and low viscosity chitosan (CN)	15.7± 1.5 MPa for HDPE/CN95/5 Young's modulus: 19.7 ± 2.4 MPa for HDPE/CM95/5 15.7± 1.5 MPa for HDPE/CN95/5	properties. The presence of chitosan is restricting the flow behavior of the system.	
4	HDPE-hydroxyapatite (HAPEX™)	Tensile strength: 20.67± 1.56 MPa Young's Modulus: 4.29± 0.17 GPa	40wt% hydroxyapatite in HDPE has been optimized. Smaller the size of hydroxyapatite, greater is the tensile strength obtained.	Bone implants (Wang et al. 1998)
5	HDPE-chitosan composite with MA-g-PE as compatibilizer	Tensile strength: 21.6± 0.2 MPa Young's Modulus: 1499± 94 MPa Impact Strength: 41± 2.5 J/m	HDPE/C10/Q10 has been optimized. The presence of compatibilizer have improved the compatibility in the system. Chitosan acts as tension concentrators and propagates cracks with low energy consumption.	Characterization (Lima et al. 2019)
6	HDPE-hydroxyapatite composites (HA)	Tensile strength (Maleated HDPE grafted composite): 25± 1.5 MPa Tensile Modulus (HDPE-HA): 1460± 36 MPa Impact Strength (HDPE-HA): 14±	Composite with 10 phr HA is optimized for both systems. Reduction in impact strength for grafted systems is due to poor interfacial bond between HDPE and HA particles.	Bone replacement materials. (Balakrishnan et al. 2013)

		2.0 kJ/m ²		
7	Polyethylene modified with crude palm oil (CPO)	Tensile strength: ~ 32MPa Impact strength: 55 J/m	5 wt% CPO optimized with high mechanical values on HDPE.	Characterization (Ratnam et al. 2006)
8.	Chitosan/polylactic acid/hydroxyapatite nanocomposite	Elastic Modulus: 880 MPa Compressive strength: 266.477 MPa	CS/PLA-HA3 has been optimized. Good interfacial interaction between HA and the organic phase.	Bone tissue engineering applications (Cai et al. 2009)
10.	HDPE/hydroxyapatite composite	Tensile strength: ~ 17MPa Impact strength: Decreased with HA loading till ~150 J/m	Lack of chemical interaction. Possibility of mechanical interlocking from FTIR studies. Poor energy absorption ability	Characterizations (Jaggi et al. 2012)
11.	UHMWPE/hydroxyapatite	ANSYS analysis of dynamic compression characterization	The simulation is numerically valid. Accurate predictions were obtained.	Medical applications (Crowley et al. 2008)
12.	HDPE/wood fibre (Pine, cherry tree, walnut tree)	Tensile strength: ~ 8 MPa to 10 MPa	Experimental results and FEA methods were in good agreement.	Structural applications (Rodríguez-Sánchez et al. 2019)
13.	Chitosan/gelatin/fluoro-hydroxyapatite	Elastic modulus: 182 MPa	FEA was in agreement with the experimental values	Cartilage scaffold (Cheng et al. 2021)

1.12.2 Morphological and structural analysis of thermoplastic / natural polymer / ceramic - based composites

The morphological analysis using scanning electron microscopic (SEM) analysis explains the miscibility and interaction of the components in a composite. The strength of filler-matrix bonding and the further interactions leading to extensive interfacial failure or adhesion are studied. In all reported thermoplastic composites, a ductile or a brittle fracture is commonly observed. Polyethylenes possess an anisotropic nature due to the individual crystalline lamellar stacks and partial amorphous phase in them. Palm oil plasticized HDPE shows highest anisotropic properties with ductile morphology when compared with palm oil plasticized LLDPE and LDPE as shown in Figure 1.11. The addition of additives can alter the orientation of linear long chain of olefinic groups in HDPE thereby reducing its anisotropic nature. This can create defects in HDPE as well as alter its crystallinity. Studies show that plasticizers usually concentrate on the amorphous phase of polyethylenes (Sander et al. 2012). Even a small amount of plasticizer can impart the segmental mobility enabling the movement of macromolecules. Hence, the polymer chains can reorganize themselves parallel to the direction of applied stress showing a wave like morphology.

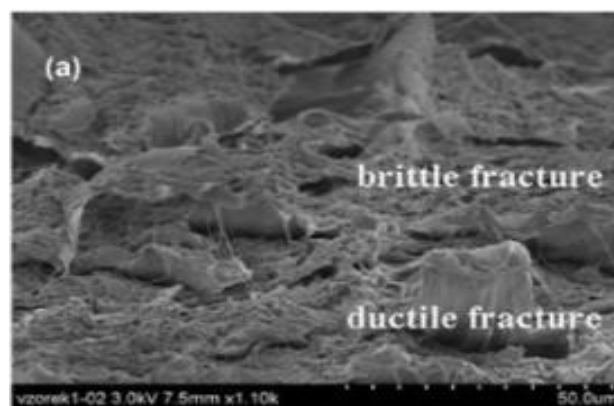


Figure 1.11 SEM image of tensile fractured surface of HDPE (Ratnam et al. 2016)

Table 1.3 SEM studies of thermoplastic / natural polymer / ceramic - based composites

Sl.No.	Composite	Morphology (Optimized)	Properties and Observations
1	Chitosan/polyacrylamide/nanohydroxyapatite	A definite wavy pattern	Well dispersion of polymers in the composite. This results in smooth surface indicating small pore size and minimum agglomeration. The stability is increased and hydroxyapatite in the pores can form an interlock between the implant and the hard tissues (Kalambettu et al. 2012).
2	Polyvinyl chloride/wood flour (WPVC) composites	WPVC-DBP and WPVC-EFAME shows homogeneous surface	The tensile fracture surface shows better plasticizing effect, good plastic fracture and tough characteristics, improved elongation at break (Xie et al. 2014)
3	HDPE/modified calcium silicate composites	Crazing was observed at the surface and the tensile fractured composite surface showed interior imperfection, deboned calcium silicate particles, elongated voids and fine filaments	Crazing is the characteristics of semi-crystalline polymers. This is followed by the formation of microscopic voids. The vinyltriethoxysilane modified calcium silicate showed miscibility in HDPE matrix (Kusuktham et al. 2014)
4	HDPE/ wood fibre composites with Poly-Ethylene-co-Glycidyl	Poor intercalated/exfoliated surface for uncompatibilized (97.5% HDPE + 2.5% Clay) composite.	Presence of EGMA increased the interfacial adhesion between the components. Density and aggregation is decreased. Spherulites acts as nucleating agent in the

	Methacrylate (PEGMA) and clay	HDPE/PEGMA composite- Smooth clean surface HDPE/Wood/PEGMA/Clay-spherulites	composites and this property is used by the composites where wood is used as the filler (Badji et al. 2016).
5	HDPE/curaua/EVA blends	Co-continuous morphology	Uniform distribution of EVA in HDPE was obtained. On extracting acetone from the EVA, the empty spaces developed were also homogeneously distributed (Morais et al. 2016).
6	HDPE/chitosan	Rough fracture surface for pure HDPE Smooth fracture surface for HDPE/chitosan composites	HDPE shows a ductile mode of fracture. Voids present in the composite acts as stress raisers due to the presence of chitosan makes brittle mode of fracture (Daramola et al. 2020).
7	HDPE/chitosan	Extended phase separation	No interaction between chitosan and HDPE, but absence of voids are noted. Improved interfacial strength are also observed (Maro et al. 2020).
8	HDPE/hydroxyapatite (HAPEX™)	Fibrous appearance	Homogeneous distribution of hydroxyapatite in HDPE (Wang et al. 1998)
10.	HDPE/hydroxyapatite composites (HA)	Uniform surface	Impact fractured surface are studied. Mechanical bonding between HDPE and HA (Balakrishnan et al. 2013)

1.12.3 Microstructural analysis of thermoplastic / natural polymer / ceramic - based composites

Microstructural analysis of composites provides relevant information about the bonding, interaction and orientation planes of the prepared composites which is required for determining the bulk properties and performance during service. The mechanical stability, thermal resistance, electrical properties, and biocompatibility depend on the interfacial adhesion between the matrix and reinforcement phase in a composite. The physical as well as chemical bonding at the interface can be evaluated using FTIR techniques, XRD analysis and PALS measurements (Cecen et al. 2008). The surface of the composites gives valuable information about the presence of chemical components, its miscibility and phase formation. The extent of crosslinking and bonding can be further analysed by calculating the holes and size of free holes formed. The interaction of the filler with matrix as observed from FTIR spectra is analysed from the peak shift and variation in the intensity of peaks (Morais et al. 2016). The FTIR analysis of thermoplastic based composites are given in Table 1.4.

XRD enables us in evaluating the crystallinity as well as the amorphous nature of composites. In hydroxyapatite/chitosan/polyacrylamide system, the presence of crosslinker, methylene bisacrylamide (MBA) has improved the crystallinity of the composite. The absence of peak of the individual components of a composite also indicates the interaction between the components. The diffraction pattern of HDPE is not affected by the plasticizer or filler as they usually occupy the pores in the matrix and have little or no interaction with the matrix (Kalambettu et al. 2012). The XRD of thermoplastic based composites are given in Table 1.5.

Positron annihilation lifetime spectroscopy (PALS) has been reported as a unique method to analyse and correlate the free holes within the composite system. The size of free holes plays a major role in determining o-Ps lifetime whose intensity is found to be proportional to the fraction of free hole volume. In grafted composites, the probability of o-Ps formation decreases. The formation of broader o-Ps lifetime distribution is generally observed in immiscible composite systems. The microstructural properties like compactness of the system, miscibility and filler-matrix interfacial interaction can be analysed from PALS measurements. In the work reported by Zeng et al, the compactness of chitosan system increased with the addition of glutaraldehyde (GA), as observed with the formation of higher concentration of free holes with smaller size. Furthermore, when GA crosslinked chitosan was mixed with PVP, an increase in I_3 occurred due to the migration of PVP segments into the free holes formed during GA/chitosan crosslinking. The nature of free holes formed can also be related to the amorphous and crystalline nature of the polymer chains (Zeng et al. 2011). The free hole volume analysis can also be correlated with the electrical, mechanical and thermal properties of the system. A composite system consisting of polyvinyl alcohol:polypyrrole blend with bismuth sulphide as filler has been analysed for its free hole volume properties and was correlated with the electrical properties of the system. At optimum concentration of bismuth sulphide, the particles are uniformly dispersed causing a reduction in the free hole volume of the system. But at higher concentration, the formation of agglomeration interrupts the arrangement of polymer chains in the interface of filler. This affects the interaction of and miscibility of the system (Hebbar et al. 2018). Some of the important data on PALS analysis of thermoplastic/natural polymer/ceramic materials is shown in Table 1.6.

Table 1.4 FTIR studies of thermoplastic / natural polymer / ceramic - based composites

Sl.No	Composite	Peak position (cm ⁻¹)	Shift in peak position/New peaks	Observations
1	Chitosan/polyacrylamide/ nano Hydroxyapatite (CS– PAAm–nHA)	<ul style="list-style-type: none"> • N-H vibration of acrylamide (3400 cm⁻¹ and 3500 cm⁻¹) • 1230 – 1300 cm⁻¹ • Si-O (900-870) • Si-N(830-750) 	<ul style="list-style-type: none"> • 3181 cm⁻¹ followed by overlapping with O-H stretching. • 1313 cm⁻¹ • 894 and 800 cm⁻¹ due to Si-O and Si-N vibrations. 	<ul style="list-style-type: none"> • Peak broadening at O-H indicates the interaction of chitosan and hydroxyapatite. • Shift in phosphate group of nHA. • Presence of CTMS (chlorotrimethylsilane) in interaction of hydroxyl group of hydroxyapatite and NH₂ groups of chitosan (Kalambettu et al. 2012).
2	HDPE / chitosan		<ul style="list-style-type: none"> • 1055 and 1105 cm⁻¹ 	<ul style="list-style-type: none"> • Vibrations of phosphate group of HA • Peak intensity increased with concentration of chitosan (Fouad et al. 2013).
3	Chitosan/hydroxyapatite composite crosslinked with glutaraldehyde	<ul style="list-style-type: none"> • 1644 cm⁻¹ (amide 1, C=O of chitosan) 1550 cm⁻¹ (NH deformation of primary 	<ul style="list-style-type: none"> • 1630 cm⁻¹ • Peak intensity is decreased 	<ul style="list-style-type: none"> • Hydrogen bond interaction between Oh of hydroxyapatite and NH₂ of chitosan. Interaction of GA and

		amine)		chitosan (Li et al. 2013).
4	Hydroxyapatite/alginate/ chitosan composites	<ul style="list-style-type: none"> • 1022 cm^{-1} (C-O-C of alginate) • 1645, 1548, 1403 cm^{-1} (amide 1, amide11 and CH_2 bending of chitosan) 	<ul style="list-style-type: none"> • 1009 cm^{-1} • 1637,1548 and 1403 cm^{-1} 	<ul style="list-style-type: none"> • Ionic interaction between C-O-C of alginate between Ca^{2+} of HA. • Electrostatic repulsion and formation of ionic complex. Interaction of chitosan with HA (Kim et al. 2015).
5	LDPE/chitosan		<ul style="list-style-type: none"> • 3419 cm^{-1} 	<ul style="list-style-type: none"> • Intermolecular interaction between chitosan and PE-g-MA (Quiroz-castillo et al. 2014)
6	Chitosan grafted silk fibre / PVA films	<ul style="list-style-type: none"> • 3300 cm^{-1} (O-H stretching band of PVA) 	<ul style="list-style-type: none"> • Peak is broadened 	<ul style="list-style-type: none"> • Hydrogen bonding between hydroxyl and NH/C=O groups of PVA and chitosan grafted silk fibres • No functional group alteration (Sheik et al. 2018)
7	Hydroxyapatite/chitosan films	<ul style="list-style-type: none"> • 1654 cm^{-1}(carbonyl, C=O stretching of chitosan) • 1654 and 1595 cm^{-1} 	<ul style="list-style-type: none"> • Enhancement of peak intensity at 1654 cm^{-1} • 1648 and 1590 cm^{-1} 	<ul style="list-style-type: none"> • Reaction of carboxymethyl group of genipin with amino groups of chitosan • Good miscibility between CS and HA (Teng et al. 2009)

Table 1.5 XRD studies of thermoplastic / natural polymer / ceramic - based composites

Sl.No	Composite	Peaks formed /Shift	Properties and Observations
1	Chitosan/hydroxyapatite composite crosslinked with glutaraldehyde	Peaks of HA (2θ): 25.8° (002), 32.9° (300), 34.0° (202), 39.9° (130), 46.7° (222), 49.4° (213) Peaks of chitosan (2θ): 19.8°, 21.9°	Typical crystalline peaks indicates no structural change in hydroxyapatite (HA) and chitosan (CS). Increase in concentration of HA decreases the peak intensity of CS (Li et al. 2013).
2	HDPE/chitosan composite with MA-g-PE as compatibilizer	Peaks of HDPE (2θ): 21.6°, 24.2° Peaks of chitosan (2θ): 20.1°	<ul style="list-style-type: none"> • Crystalline nature of composites are revealed • Orthorhombic crystalline structure of HDPE (Lima et al. 2019).
3	3D hydroxyapatite-chitosan nanocomposite rods	Peaks of chitosan at (2θ): 10.8°, 20.1° Shift in peaks from (2θ): 20.1° to 20.5°/ 21.8° / 19.9°	Peak intensity of chitosan is decreased. Shift in peaks indicates: a) crosslinking reaction b) crystal plane space of chitosan is reduced after crosslinking with HA (Wang et al. 2010)
4	Chitosan/polylactic acid/hydroxyapatite nanocomposite	<ul style="list-style-type: none"> • Peaks of HA (2θ): 26° (002), 32° (211) • Peak broadening at $2\theta = 32^\circ$ 	Peak broadening indicates low crystallinity, Depends on crystallinity and overall particle size of HA (Cai et al. 2009)..
5	Chitosan/nanohydroxyapatite	<ul style="list-style-type: none"> • Peaks of chitosan at (2θ): 10°, 18°, 25° • Peaks of HA(2θ): 25.8°, 32.2°, 33°, 34.1° 	Peak at 18° can be due to genipin. Crystallinity of chitosan is weakened due to the introduction of hydroxyapatite in chitosan (Li et al. 2013).

Table 1.6 PALS studies of thermoplastic / natural polymer / ceramic - based composites

Sl.No	Composite	Values	Observations	Properties
1	Acrylic modified chitosan	$\sim 130 \text{ \AA}^3$ for grafted medium molecular weight chitosan, (DD~78.2%). $\sim 150 \text{ \AA}^3$ for grafted chitosan (DD~95.2%)	τ_{0-Ps} and V_h is higher in grafted films than pure chitosan films	τ_{0-Ps} is increased with higher grafting ratio. Grafting enabled breaking of chitosan chains and increased interaction between chitosan and acrylic polymer (Pablo et al. 2016).
2	HDPE/carbon black	$\tau_3 = 2.50 \text{ nm}$	Composite with 20 phr carbon black is studied	τ_3 is constant below T_g due to lack of polymer chain movement and increases above T_g . Conductivity and free volume is correlated (Shaojin et al. 2002).
3	Dental composites Based on dimethacrylate Resins	$\tau_3 = 0.893 \pm 0.090 \text{ nm}$ $I_3 (\%) = 12 \pm 1.1$	Matrix: Bis-GMA, TEGDMA, Filler: SiO ₂ , HA(5wt.% Si as dopant)	Decrease of micro-pores Highest concentration of free hole volume similar to commercial composites (Kleczewskaa et al. 2010)
4	Nanohydroxyapatite agglomerates	$\tau_3 = 3.7 \pm 0.03 \text{ nm}$ $I_3 (\%) = 4.4 \pm 0.03$	2 hours of heating is given for preparation (reaction time)	Accurate in closed-pore systems than gas absorption methods. Highly nanoporous structure (Morsy et al. 2010).

5	Electron irradiated HDPE	$\tau_3 = 1.8 \text{ nm}$ $I_3 (\%) = 8 \pm 1.5$	Decrease in τ_3 and I_3	Formation of new bonds leads to the decrease. Reduction of mean free hole volume (Zaydouri and Grivet 2009)
6	Polyvinyl Pyrrolidone/chitosan	$\tau_3 = 1.778 \pm 0.011 \text{ nm}$ $I_3 (\%) = 16.9 \pm 0.5$	Reduction in τ_3 and I_3 with the addition of glutaraldehyde (GA) as crosslinker	Smaller mean free volume size and higher free volume concentration with the addition of GA. Partition effect created higher free hole volume concentration (Zeng et al. 2011).
7	Starch based composite (STM) coated with chitosan	$\tau_3 = 219 \text{ ps to } 13 \text{ ps}$	Non-coated STM has more lifetime than coated STM	Free hole volume is related to water sorption (Lin et al. 2010).
8.	HDPE/polystyrene(P S)/clay and HDPE grafted with acrylic acid/PS (PEAA/PS) with clay	For grafted Samples $\tau_3 \sim 2.14 \text{ nm}$ $I_3 (\%) \sim 24$ For un grafted samples $\tau_3 \sim 2.14 \text{ nm}$ $I_3 (\%) \sim 20$	τ_3 is really unchanged and I_3 is increased for non-grafted samples. I_3 is lower for grafted systems.	For HDPE/PS the increasing presence of clay causes Ps inhibition. The inhibition of Ps formation decreases with clay concentration in grafted systems due to increase in segmental mobility (Wang et al. 2009).

1.12.4 Thermal analysis of thermoplastic / natural polymer / ceramic - based composites

Thermal analysis is a sophisticated material analysis technique that provides information about the processing conditions which finally help in the optimisation of composite materials. The rate of change of weight and molecular mobility with respect to temperature confirms the thermal stability, amorphous / crystallinity acquired by the system. The size of the filler, chemical structure, crosslinking, incorporation of fillers, matrix and their orientation contribute to the thermal properties of the system (Neto et al. 2021). The thermal properties of the composites can be easily analysed using thermogravimetric analysis (TGA) and dynamic mechanical analysis (DMA). The molecular deterioration of the composite system occurs due to heating at various temperatures (Arda et al. 2017, Pryde et al. 1990). The action of heat at lower temperatures to elevated temperatures helps in understanding the properties of composites from movement of small segments or groups to decomposition / degradation of systems (Aboulkas et al. 2008). DMA analysis provides the temperature dependent viscoelastic behavior of composite materials. It provides the following thermal data (a) storage Modulus (E'); (b) Loss Modulus (E''); and (c) tan delta. Physical adhesion, crosslinking and structural arrangement of molecules determine the viscoelastic properties of the system. Fillers and additives can either restrict the movement of polymer chains or improve the flexibility within the system and can improve interaction between the components of the system. DMA is also helpful in understanding the crystalline nature of the composite. A shift in alpha transition temperature explains the restriction of the movement of HDPE chains in the inter-crystalline regions due to the presence of polyhedral oligomeric silsesquioxanes (POSS) around the crystalline boundaries

(Joshi et al. 2006). Temperature and frequency play a major role in the dynamic mechanical properties of the composite. When temperature is increased, the segments of HDPE side chain move easily resulting in decreased stiffness of the system. This in turn reduces the storage modulus of the composites. Increased amorphization also affect the storage modulus as well as the loss modulus of the system. In addition to the storage modulus, the loss modulus which is the energy dissipated as heat due to internal friction between the two phases can also be determined. The HDPE/teak wood flour (TWF) composites have higher energy loss due to the fact that the energy dissipated can be absorbed by the filler and the voids between the phases (Sewda et al. 2013). The presence of hydroxyapatite also shows an increase in storage modulus from 1.16 to 1.55 till 10 wt% HA loading at a frequency of 1 Hz for HDPE/HA composites. This increase in storage modulus with increase in concentration of hydroxyapatite can also be related to the decrease in free volume and restriction of mobility of the polymer chains. The gamma irradiated HDPE/HA samples showed a further increase in storage and loss modulus due to the increased crosslinking between the matrix and the filler (Alothman et al. 2014). Greater the modulus, less easily the samples deform, giving greater rigidity to the material. This can increase the crystallinity and crosslinking between the filler and matrix. Furthermore, the glass transition temperature, T_g , of the composites are determined from the intermolecular and intramolecular interactions taking place in the composite system. The transitions occurring during the movement of polymer chains in the amorphous and crystalline regions influences the T_g . The T_g obtained from the loss modulus data helps in evaluating the transition from glass state to rubbery state. This is due to the movement of polymer chains that results in the formation of more free holes in the system with increase in temperature. The shift in T_g to higher temperature in a composite system

indicates the formation of lower free hole volume in the composite system (Baatti et al. 2019). The TGA and DMA graphs of thermoplastic materials are shown in Figure 1.12 (a) and Figure 1.12 (b) respectively.

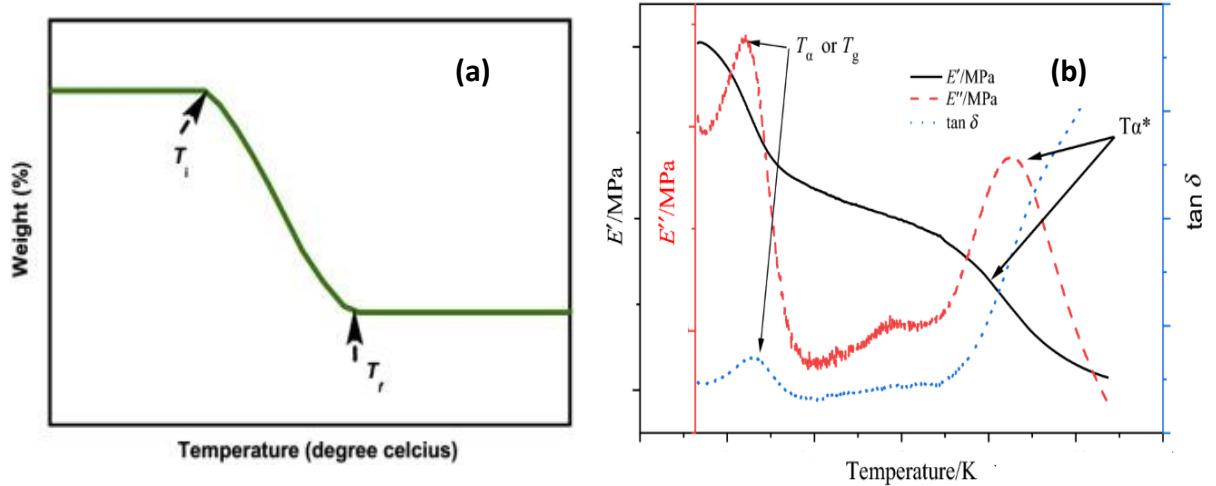


Figure 1.12 (a) TGA and (b) DMA graphs of thermoplastic composites (Baatti et al. 2019, Loganathan et al. 2017)

Some of the important data on TGA and DMA analysis of thermoplastic / natural polymer / ceramic materials is shown in Table 1.7 and Table 1.8 respectively.

1.12.4.1 Thermal oxidative degradation kinetics - using Coats Redfern model

Thermal degradation studies are mainly employed in examining the degradation behavior and kinetics of composites, blends and materials. It identifies the thermal stability and maximum usage temperature of the specific substance. Numerous theoretical modelling techniques (Kissinger Model, Flynn - Wall-Ozawa Model, Coats Redfern Model) have been employed to understand the thermal stability and activation energy of composites (Aboulkas et al. 2008). Coats - Redfern model is the most versatile method in evaluating the kinetic parameter of degradation behavior of composites

Table 1.7 TGA studies of thermoplastic / natural polymer / ceramic - based composites

Sl.No	Composite	Degradation steps		Properties
1	HDPE/chitosan	50 – 100 °C	Weight loss %	<ul style="list-style-type: none"> • Good thermal stability • Process able at HDPE processing temperature (190 °C) (Maro et al. 2020).
			CM : 7.9% CN : 8.9%	
		Starts at 260 °C	Decomposition of saccharide backbone	
		T _{max}	302 °C and 270 °C for CM at N ₂ and O ₂ atmosphere resp. 296 °C and 273 °C for CN at N ₂ and O ₂ atmosphere resp.	
2	HDPE/chitosan composite with MA-g-PE as compatibilizer	120 °C	Loss of water trapped	<ul style="list-style-type: none"> • HDPE/C20/Q20 exhibits more thermal stability with maximum residue (Lima et al. 2019).
		294.7 ± 4.3 °C	Decomposition of chitosan backbone	
		470.8 ± 2.8 °C	Final decomposition	
3	LDPE/chitosan with PE-g-MA as compatibilizer	~230 °C	Thermal degradation of composites	<ul style="list-style-type: none"> • Compatibiliser improved thermal stability. Resistance of weight loss till processing temperature (Quiroz-castillo et
		Starts at 125 °C	Addition of glycerol as plasticizer	

				al. 2014).
4	Nano- HA/chitosan/polyethylene glycol (PEG)	50-200 °C	Loss of adsorbed water	<ul style="list-style-type: none"> • PEG improved the thermal stability of the system. Ternary composites are stable till 800 °C and HA-CS systems are stable at 225-600 °C (Shakir et al. 2014).
		225-375 °C	Decomposition of chitosan, CS	
		Total weight loss	HAP-CS: 72-75% HAP-CS-PEG: 30-30%	
5	Hydroxyapatite filled chitosan/polyacrylic acid	60–128°C 130–240 °C 300–600 °C	Three stage degradation	<ul style="list-style-type: none"> • Degradation temperature increased with hydroxyapatite concentration (Sailaja et al. 2003).
6.	HDPE polymer systems	Pyrolysis reaction was studied using Coats-Redfern model. Reaction mechanism of thermal degradation of plastics were studied.		<ul style="list-style-type: none"> • Activation energy in the range of 238-247 kJ/mol was obtained (Aboulkas et al. 2008).
7.	HDPE/surface treated hydroxyapatite	Activation energy of HDPE/HA composites was obtained at 330 kJ/mol.		<ul style="list-style-type: none"> • Kinetic information about the optimisation and development of composites (Albano et al. 2010).
8.	cellulose acetate/niobium & chitosan/niobium composites	Thermodynamic parameters shows non-spontaneous process of degradation. Chitosan based composites were more stable		<ul style="list-style-type: none"> • Activation energy confirmed the thermal stability of the systems (Faria et al. 2007)

Table 1.8 DMA studies of thermoplastic / natural polymer / ceramic - based composites

Sl.No	Composite	DMA analysis			Properties and Observations
1	HDPE/chitosan	Storage Modulus, E'	Loss Modulus, E''	Tan δ	High crystallinity and high reinforcing effect of CM than CN is observed. Chitosan have no effect on the T_g of HDPE composites due to difference in polarity (Maro et al. 2020).
		Increase at 40 °C	-	T_g of HDPE at - 113 °C	
2.	Rice Husk Biochar/HDPE Composites	Increased with increase in frequency (10 Hz)	Curves shifted to higher temperature (10 Hz)	Decreased with increase in frequency (10 Hz)	Viscoelastic properties were studied in a range of different frequency (1,2,5,10 Hz). Biochar being a rigid filler improved storage modulus (Zhang et al. 2017).
3.	HDPE/nanohydroxyapatite	Increased with concentration of hydroxyapatite	Decreased with increase of temperature	-	E' and E'' decreased at higher temperature with mobility of polymer chains. High E' indicates stiffness, restriction of mobility of polymer chain, decrease of free hole volume. Increase in crystallinity (Fouad et al. 2013)
4.	HDPE/hydroxyapatite	Increased with HA ~3500 to	Two peaks at 0 °C and 50 °C		Change in E' is attributed to the free hole volume changes with temperature. Two peaks of E'' indicates bimodal distribution of

		4100 MPa			polymer chains due to segmental mobility (Jaggi et al. 2012).
5.	Fe ₃ O ₄ /GO/CS composites	E' of Fe ₃ O ₄ /GO/CS is higher than Fe ₃ O ₄		T _g of Fe ₃ O ₄ /GO/CS : 264 °C T _g of GO/CS: 267 °C	High storage modulus in ternary composite is due to the strong interactions between the components. Decrease in Tg due to increase in mechanical stiffening (Yadav et al. 2014).
6.	Chitosan/graphene oxide (CS/GO)			T _g for CS: 173 °C T _g for CS/GO: 165 °C	GO aggregates and weaken the interactions of bonding within chitosan by forming bonding with the polymer. This increases α relaxation and hence Tg decreases (Nath et al. 2018).

1.12.5 Dielectric Properties of thermoplastic / natural polymer / ceramic - based composites

The higher dielectric properties of inorganic substances compared to polymeric materials can be utilized in tuning the dielectric properties of polymer/inorganic based composites. Moisture content, temperature, amount of crosslinking, free -hole volume, polar groups, and ions present in the composite are some of the factors that affect its dielectric property. The additives added to improve the miscibility of the system also plays a major role in tuning the dielectric properties of the system. Palm oil as plasticizer in LDPE/chitosan systems has improved the electrical properties which can be attributed to the segmental mobility achieved due to the availability of polar groups in the system (Sunilkumar et al. 2014). Compatibilizer provides physical and chemical interaction in the interfacial zones of the composite system and can play a major role in defining the segmental mobility of the system. This can affect the relaxation peaks in $\tan \delta$ of the prepared composites (Ali et al. 2020). Broadband dielectric spectroscopy also helps in understanding the dielectric properties of the material over a frequency range of 10^{-2} to 10^7 . HDPE/alumina composites show a reduction in relative permittivity at low frequency regions due to electrode interfacial polarisation and are stabilized over frequency of 10^3 Hz, making it a good dielectric material (Saleh et al. 2020). The electrical properties of bio-based ceramics showed that the surface of polarised hydroxyapatite due to negatively charged OH^- ions could enhance osteobonding in bone tissues and facilitate bone growth (Das et al. 2019). Some of the important data on dielectric properties of thermoplastic/natural polymer/ceramic materials is shown in Table 1.9.

Table 1.9 Electrical studies of thermoplastic / natural polymer / ceramic - based composites

Sl.No	Composite system	Observations	Applications
1.	Chitosan/ZnO composite films (LCR meter)	The increasing concentration of ZnO have increased the dielectric properties due to space charge polarization developed in the composites. As the frequency is increased the dielectric constant was decreasing in all the composites which can be attributed to the lag in polarization with application of electric field. The presence of nanoparticles have also contributed to the smooth conductivity in the composite material.	Food packaging applications as well as dielectric materials (Rahman et al. 2018).
2.	High density polyethylene (HDPE)/calcium carbonate nanocomposites (NCC) (LCR meter)	The studies were conducted from 1 kHz to 1MHz. The presence of 1 wt% HDPE-g-MA as compatibilizer has provided homogeneous distribution of NCC on the matrix surface thereby improving the dielectric properties of the composite. Two small peaks were observed for $\tan \delta$ due to the interfacial	They can be used in the insulation of high-voltage cables (Ali et al. 2020).

		polarisation mechanism of the heterogeneous system.	
3.	Low density polyethylene (LDPE)/chitosan composites (LCR meter)	Deacetylated low molecular weight chitosan with 2.5 wt% palm oil was optimised. The dielectric constant of palm oil plasticized LDPE-chitosan composites was higher than its un-plasticized samples. The conductivity of the composites increased with the increase in concentration of chitosan.	Dielectric properties have been correlated with the antimicrobial properties (Sunilkumar et al. 2014).
4.	HDPE/cellulose, HDPE/kraft composites (Broadband dielectric spectroscopy)	Dielectric constant increased from 1.36 to 2.15 and 2.53 for cellulose based and kraft based composites respectively. Structural modification and high polarizability is indicated by change in dielectric constant. High dielectric loss indicates heterogeneity. Crystallinity also influences the dielectric loss.	Material characterization (Khouaja et al. 2021).
5.	Chitosan and nitrile-modified cellulose nanocrystals	Size, presence of polar groups contributes to the dielectric constant of the material. Low dielectric loss at lower frequency was observed.	Energy storage device (Bonardd et al. 2018).

1.12.6 Biodegradability and biocompatibility analysis of thermoplastic / natural polymer / ceramic - based composites

The bone-tissue interface responsible for the reduction of stress can be classified into three transition forms namely: (a) bone cartilage; (b) bone tendon and (c) bone ligament. The biocompatibility of the prepared implant is mainly studied using cell proliferation studies. Bio-composite containing natural fillers along with the bone mineral hydroxyapatite can promote high biocompatibility as well as mechanical strength to the bone-implants. Hydroxyapatite can promote cell attachment and differentiation. The cell proliferation studies mainly employ osteoblastic cell line models and primary osteoblast cells. *In-vitro* cell studies using MG-63 and SW-1353 cell lines on zein/chitosan/hydroxyapatite composite scaffolds showed faster differentiation of osteoblastic like cell on it. POSS incorporated scaffolds have shown good cell proliferation making it a suitable material for bone regeneration. The biocompatibility of a system can be correlated to its contact angle analysis. Surface wettability is the best factor for cell - biomaterial interaction. More hydrophilic or more hydrophobic surface has a negative impact on cell proliferation. A neutral condition where the contact angle lies between 70 - 90° is considered appropriate for protein absorption and cell adhesion. The wettability of the system can be altered with the concentration and presence of the filler that is reinforced. (Tamburaci et al. 2019). Here, the presence of bio-glass and hydroxyapatite in polyethylene has increased the cell proliferation and bioactivity of MC3T3-E1 cell lines. This further explains that hybrid systems like ternary composites are capable of neutral wettability and good cell proliferation. Some of the important data on biocompatibility studies of thermoplastic / natural polymer / ceramic materials is shown in Table 1.10.

Table 1.10 Biocompatibility analysis of thermoplastic / natural polymer / ceramic - based composites

Sl.No	Composite	Biocompatibility studies		Properties and observations
		Name of study	Values	
1	HDPE / chitosan	Water contact angle	81.6 ± 3.6° (HDPE/CM 95/5)	Cytostatic effect High adhesion of cell lines on composite Spindle shaped fibroblasts on composite High wettability ,Contact angle properties have no effect on surface roughness (Maro et al. 2020).
		Cell studies(fibroblastic cell line NHDF)	Increased cell growth with chitosan	
2	Nanohydroxyapatite/chitosan composites	Cell proliferation	MC3T3-E1 cell lines were used	Cell proliferated and clusters were formed. Uniform distribution of cells (Kong et al. 2005).
3	Hydroxyapatite/alginate/ chitosan composites	Cell proliferation	MC3T3-E1 cell lines were used	ALP activity measured over 14 and 21 days. Mineralisation of osteoblasts were enhanced over time on HA containing scaffolds (Kim et al. 2015).
4	Chitosan/Si-nHA and Zein/POSS	Water contact angle	Chitosan: 83° Chitosan/40% Si-nHA: 85°	Protein adsorption and subsequent cell adhesion Depends on surface alterations at microscale (Tamburaci et al. 2019).
5	Chitosan grafted silk fibre /	Cell studies	Highest activity observed for	Rapid proliferation and grew into small

	PVA films	(NIH3T3 cells)	3wt% film (103.25 ±13.23)	colonies. Films supported cell growth and is non-toxic (Sheik et al. 2018).
6	Chitosan/nanohydroxyapatite	Cell studies (MC3T3 E1 cells)	Spherical/triangular/elongated structure for cells	Active cell growth with flattened, polygonal morphology. Adhesive to rough film surface (Teng et al. 2009).
7	Chitosan/nanohydroxyapatite	Cell studies (L929 cell)	Composite with 30% HA was studied	Membranes were non-toxic The increasing concentration of HA reduced pore size, hence water sorption was less at higher values of HA. Interaction of chitosan with HA reduced the free amine group of chitosan (Li et al. 2012).
		Water sorption	Decreased from 1800% to 830% with increase in concentration of HA	

1.13 Research Gaps

The literature on bio-composites comprising of thermoplastic-based ceramics and natural fibre report numerous possibilities for replacing the presently available bone implant materials. But, it was observed that, metal based implants as well as synthetic polymers has superior mechanical properties when compared with the bio-based composites. A bio-composite – hybrid system with enhanced mechanical strength closer to natural bone has not been developed. Reviews shows that porosity of the material can promote cell-proliferation in the developed systems. Even though plasticizer has been employed to improve the segmental mobility of polymer chains to improve the flexibility, the action of plasticizer in modifying the porosity of the systems has not been studied. The effect of green plasticizer – palm oil has also not been studied in detail to study the microstructural properties of the systems. The modification of HDPE/Hydroxyapatite (HAPEX™) composite system, a notable commercially available bone implant has not been developed for the aim of improving the mechanical stability and bio-compatible properties. Hence, palm oil plasticized HDPE / Chitosan binary systems and palm oil plasticized HDPE / Chitosan / Hydroxyapatite ternary systems has been developed and the effect of palm oil on the prepared composites has not been studied till now.

1.14 Objectives and scope of the work

The objectives of the current studies are given below:

1. To develop a binary bio-composite system, with palm oil plasticized HDPE / chitosan composites compatibilized with maleic anhydride.

2. To prepare ternary composite system: HDPE / Chitosan / Hydroxyapatite polymer composites.
3. To investigate the effect of chitosan and hydroxyapatite on the properties of the newly developed composites.
4. To study the mechanical behavior of the composites and comparison of the results with theoretical predictions.
5. To analyse the extent of interfacial adhesion between the filler and the matrix by FTIR, XRD, PALS and DMA and by theoretical modelling studies.
6. To investigate the dielectric properties of the composites and to correlate it with the bio-compatibility of the system.

1.15 Scope of the work

The scope of the present studies can be divided as follows:

- The commercially available bone implant materials are generally petroleum based materials or metallic based materials. Hence, while undergoing the surgical process for bone traumas or injuries, the cyto-toxicity and allergic conditions caused by these materials are a major concern. Hence, the need for a non-toxic, non-allergic material with superior mechanical strength having improved bio-compatibility is required to overcome this situation. So, modifying the existing systems or designing a new system comprising of thermoplastic / bio-polymer / ceramic based hybrid composite can solve these problems to a certain extent.
- The incorporation of bio-based materials like chitosan and palm oil can be used in enhancing the biodegradability of the systems. The environmental

concerns produced by these bio-materials can be reduced by incorporating them in the development of hybrid composites.

- Besides the chemical modification of the systems by employing additives, the role of plasticizers and compatibilizers in tuning the porosity of the systems can be used in tuning the properties of a material. The comparison of binary composite series with ternary composite series are not explored in detail. The present work, provides a better understanding about the role of additives and fillers in the development of a hybrid composite system.

Chapter 2

Materials and Methodology

Summary

The materials, equipment and methodologies used in the preparation and characterization of High density polyethylene / Chitosan binary composites followed by plasticization using palm oil to the optimized binary system and the ternary system, HDPE / Chitosan / Hydroxyapatite composites is presented in the current chapter.

2.1 Materials

2.1.1 High density polyethylene (HDPE)

High density polyethylene homopolymer with a melt flow index of 20 g/10 min was supplied by Reliance Industries Limited, Mumbai, India. Properties of HDPE grade HD50MA180 from the technical data sheet is given in Table 2.1.

Table 2.1 Properties of HDPE from technical data sheet

Property	Test Method	Unit	Typical Value
Melt flow index	ASTM D1238	gm/10 min	20.0
Density	ASTM D1505	gm/cm ³	0.950
Tensile strength at yield	ASTM D638	MPa	22
Elongation at Yield	ASTM D638	%	12
Flexural modulus	ASTM D790	MPa	900
Notched Izod Impact Test	ASTM D256	J/m	30
Vicat softening point	ASTM D1525	°C	123

2.1.2 Chitosan

Low density chitosan (0.15 - 0.3 g/cm³) was obtained from Matsyafed, the Kerala State Co-operative Federation for Fisheries Development Ltd., Kollam, Kerala, India. The properties of chitosan are tabulated in Table 2.2. The viscosity average molecular weight of chitosan in 1% acetic acid has been measured using Ubbelohde viscometer. The degree of deacetylation of chitosan was calculated from FTIR-ATR analysis. The UV absorbance and compression strength was also calculated based on the reported procedures (Kasaai et al. 2000, Kasaai 2009). The particle size has been calculated using ImageJ software from SEM images of the chitosan particles.

Table 2.2 Properties of Chitosan

Property	Approximate Value
Appearance	
Form	Solid, Powder
Color	Off-white powder
Degree of deacetylation	>85 %
Viscosity average molecular weight	570 kDa
Compression strength	60 MPa
Modulus	0.3 GPa
UV absorbance	310 nm
Particle size	133.07 μ m
Solubility	1% acetic acid

2.1.3 Hydroxyapatite

Hydroxyapatite in the form of nanopowder (< 200 nm) was procured from Sigma – Aldrich, India. The physical properties of hydroxyapatite from the material data sheet are given in Table 2.3.

Table 2.3 Physical properties of hydroxyapatite from material safety data sheet

Property	Approximate Value
Appearance	
Form	Solid, Powder
Colour	White, Off white
Molecular weight	502.31 gmol ⁻¹
Melting point/range	1,100 °C-lit (MSDS)
Relative density	3.140 g/cm ³
Water solubility	Insoluble

2.1.4 Maleic Anhydride

Maleic anhydride was used as the compatibilizer to improve the miscibility of the composites. They were procured from Sigma-Aldrich, India. The physical properties of maleic anhydride from the material data sheet are given in Table 2.4.

Table 2.4 Physical properties of maleic anhydride from material safety data sheet

Property	Approximate Value
Appearance	
Form	Solid
Colour	White
Molecular weight	98.06 gmol ⁻¹
Melting point/range	51 - 56 °C
Initial boiling point and boiling range	200 °C
Relative Density	1.48 g/cm ³ at 20 °C
Partition coefficient: n-octanol/water	log Pow: -2.61 at 20 °C - OECD Test Guideline 107

2.1.5 Dicumyl Peroxide

Dicumyl peroxide was used as the free radical initiator in all mixes during the preparation of the composites. It was procured from Sigma - Aldrich, India. The physical properties from the data sheet are given in Table 2.5.

Table 2.5 Physical properties of Dicumyl peroxide from material safety data sheet

Property	Approximate Value
Appearance	
Form	Crystalline
Colour	Beige
Molecular weight	270.37 gmol ⁻¹
Melting point/range	39-41 °C – lit
Flash Point	110 °C – closed cup
Relative Density	1.56 g/cm ³ at 20 °C
Decomposition Temperature	90 °C and above
Water solubility	0.00046 g/l at 25 °C - slightly soluble
Partition coefficient: n-octanol/water	log Pow: 5.6 at 25 °C

2.1.6 Palm Oil

Palm Oil was used as the plasticizer and it was procured from Kerala Industrial Infrastructure Development Corporation (KINFRA) Techno Industrial Park, Malappuram, Kerala, India. The properties of palm oil are given in Table 2.6.

Table 2.6 Physical properties of Palm oil from Lab experiments (obtained from KINFRA)

Parameter	Lab results
FFA (in oleic acid)	0.13%
Iodine value	53.31
Refractive Index	1.4590
Saponification value	202
Specific Gravity	0.910

2.1.7 Cell lines

Mouse osteoblastic cell lines, MC3T3-E1 were procured from National Centre for Cell Science (NCCS), Pune (India). They were used to study the cell proliferation and MTT assay in the prepared composites. The specifications of MC3T3-E1 cell lines are given in Table 2.7.

Table 2.7 Specifications of MC3T3-E1 cell lines

Properties	Description
Organism	Mus musculus, mouse
Cell Type	Preosteoblast
Tissue: Bone	Calvaria
Age	Neonate
Morphology	Fibroblast
Growth properties	Adherent

2.2 Preparation of composites through melt mixing process

The melt mixing of polymers with fillers or particles is a simple and feasible method of preparing new composites. Due to its solvent-free and least by-products, this process is a very economic technique. Melt mixing was done in Brabender Plasticoder Model PL 3S (Figure 2.1) with a volumetric capacity of 40 cm³ at 160 °C and 60 rpm for 20 minutes. Mixing or shearing of material is done in a mixing chamber with the help of a roller-type rotor. The rotors rotate in the opposite direction producing a shearing force on the material. Here, the material is sheared against the walls of the mixing chamber. The melt mixer was preheated to the desired temperature. Mechanical dissipation heat is developed in the small gap between rotors and chambers and when the temperature goes beyond the limit it is automatically cut off.

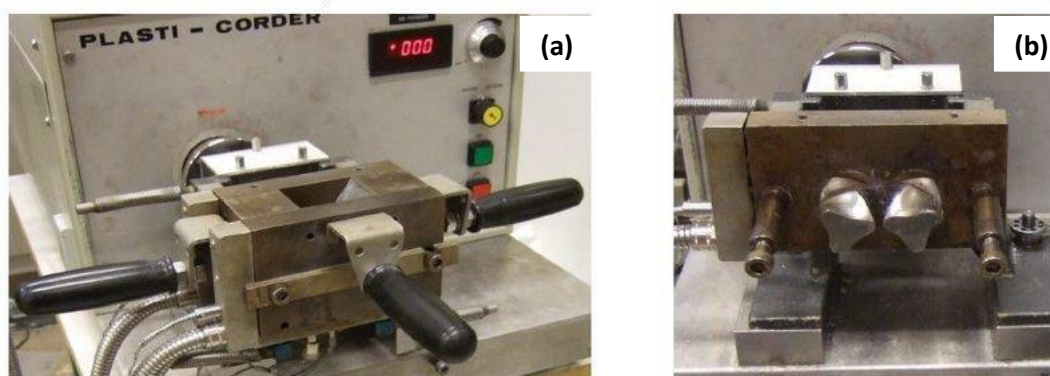


Figure 2.1 (a) Brabender Plasticoder Model PL 3S and (b) Roller type rotors for melt mixing

The constituent components of the composite were preheated at 80 °C overnight to get rid of the moisture before melt compounding. Initially HDPE pellets are introduced into the previously temperature set heating chamber. After the complete melting various concentration of chitosan is added to the chamber. Fixed concentrations of dicumyl peroxide (0.5 wt%) and maleic anhydride (2 wt%) was added to the system

to enable the miscibility between HDPE and chitosan. The formulations are given in Table 2.8.

Table 2.8 Formulations of HDPE / Chitosan (HC) composite series

Sample Code	HDPE (g)	Chitosan (wt %)
HC0	30	0
HC1	30	2.5
HC2	30	5
HC3	30	7.5
HC4	30	10

**Maleic anhydride : 2 wt% and Dicumyl peroxide : 0.5 wt%*

To the mechanically optimized HDPE / Chitosan composites with good mechanical properties, the varying concentration of palm oil as plasticizer has been added as given in Table 2.9.

Table 2.9 Formulations of HDPE / Chitosan composites series with palm oil as plasticizer (HP composite series)

Sample Code	HDPE (g)	Chitosan (wt%)	Palm Oil (wt%)
HP1	30	5	2.5
HP2	30	5	5

**Maleic anhydride : 2 wt% and Dicumyl peroxide : 0.5 wt%*

The HP composite series was further optimized and varying concentration of hydroxyapatite was added to the optimized plasticized HDPE / Chitosan composite as given in Table 2.10.

Table 2.10 Formulations of HDPE / Chitosan / Hydroxyapatite (HA) composite series and HDPE / Chitosan / Hydroxyapatite composite series un-plasticized with palm oil (HAW)

Sample Code	HDPE (g)	Chitosan (wt%)	Palm Oil (wt%)	Hydroxyapatite (wt%)
HA1	30	5	5	2
HA2	30	5	5	4
HA3	30	5	5	6
HA4	30	5	5	8
HA5	30	5	5	10
HAW4	30	5	0	8
HAW5	30	5	0	10

The well mixed composites from the Brabender mixer were compression moulded to 0.1 mm thick sheet at 160 °C and at a pressure of 200 kg/cm³. Here the sample is first pre-heated followed by pressing the die for four minutes to get the required sheet. Also at the same time, the hot mix from the mixing chamber was immediately pressed using a hydraulic press at a pressure of 100 kg/cm³ and the resulting sheets were cut down to small pieces. The test specimens for mechanical characterizations were prepared using a plunger type semi automatic – Texstar Injection Moulding Machine (Model Jim 1H small series, 4508) with a barrel temperature suitable for each composite. The molten mix is injected into the corresponding mould at a pressure of 1000 kg/cm³ to get specimens of required shape.

2.3 Characterization Techniques

2.3.1 Mechanical characterizations

The mechanical characterization of the composites were studied using impact strength analysis and stress-strain measurements. The mechanical modelling of the tensile strength analysis were conducted using Finite Element Analysis using ANSYS software.

2.3.1.1 Impact strength analysis

The Izod Impact strength (un-notched) of the rectangular samples was characterized by using Resil Impactor Junior (CEAST) as shown in Figure 2.2. The impact test of the samples comes under ASTM D256.

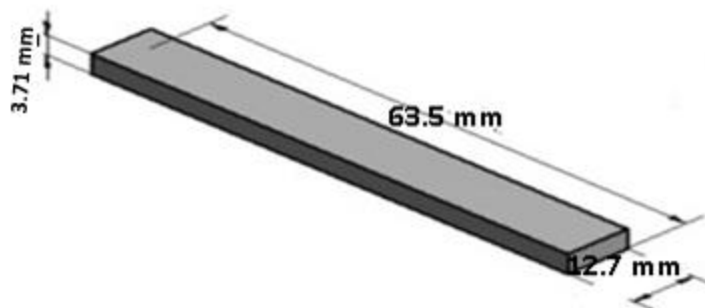


Figure 2.2 Test specimen for impact strength analysis

Impact strength is defined as the capacity of the specimen to absorb or resist shock energy before it fractures. It is given by the difference between the potential energy of the hammer or striker before and after the impact. The impact properties of the polymeric materials are directly related to the overall toughness of the material. Here, toughness is related to the ability of the composite to absorb applied energy.

The specimens were tested on the impact tester having 4 J capacity and striking velocity of 3.6 m/s. The un-notched specimen is held as a vertical cantilevered beam and is broken by a pendulum. The impact resistance has been evaluated from the impact values which are obtained directly from the tester. Impact strength is expressed in kJ/m^2 .

2.3.1.2 Stress-Strain analysis

The tensile properties of the samples were determined according to ASTM D638 using dumb shell shaped specimens (Figure 2.3) on a 'Shimadzu Autograph AG-X series' Universal Testing Machine (UTM) at a cross head speed of 50 mm/min. The length between the jaws at the start of each test was fixed to 40 mm. An average of 5-6 concordant measurements done for each composition were taken to represent each data. The thickness of the narrow portion was measured using a digital thickness gauge. The standard test piece is gripped at both ends in the jaws of UTM, which slowly exerts an axial pull so that the sample is stretched and finally it breaks. The tensile strength, elongation at break and Young's modulus were determined from the stress-strain analysis.

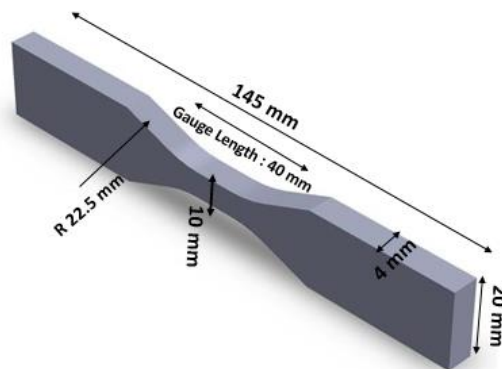


Figure 2.3 Test specimen for tensile strength analysis

The tensile strength, Young's Modulus and elongation at break can be obtained from the stress-strain analysis. Tensile strength (σ) is defined as a stress, that can be described as force per unit area. Generally, a change in cross-sectional area is observed after the stress-strain analysis, hence the area used in the calculation is the un-deformed cross sectional area, A.

$$\sigma = \frac{\text{Force}}{A} \quad (2.1)$$

Strain is measured as the change in length (L) to the initial length (L_0) of the sample.

$$\text{Strain } (\varepsilon) = \frac{L}{L_0} \quad (2.2)$$

The deformation of the material depends upon the magnitude of the external stress imposed on it. At a lower stress level, strain is directly proportional to stress (Hooke's Law). The majority of the specimen undergoes a linear stress- strain relationship, where the material shows an elastic behavior. Beyond the linear region, the deformations are not elastic and do not return to the original length.

Young's Modulus / Modulus of elasticity/ tensile modulus (E) is the linear portion of the stress – strain curve. It measures the stiffness of the material.

$$E = \frac{\sigma}{\varepsilon} \quad (2.3)$$

The stress-strain changes and Young's Modulus of the HDPE / Chitosan composite system are shown in Figure 2.4.

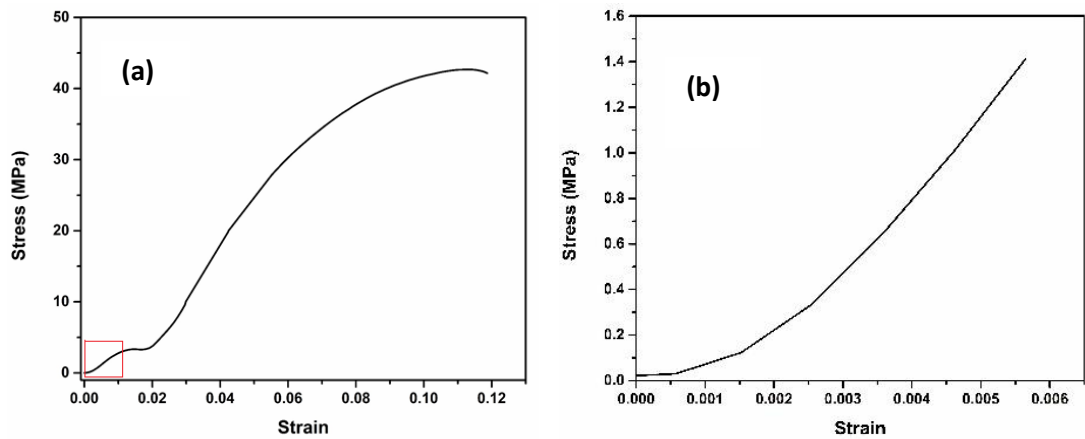


Figure 2.4 (a) Stress-strain graph (b) Young’s Modulus from the expanded portion of the marked region in Figure 2.4 (a)

2.3.1.3 Computational Modelling using Finite Element Analysis

The ASTM D638 uniaxial tests were simulated using a computer aided design (CAD) model. The Finite element analysis (FEA) was chosen for the modelling studies as shown in Figure 2.5.

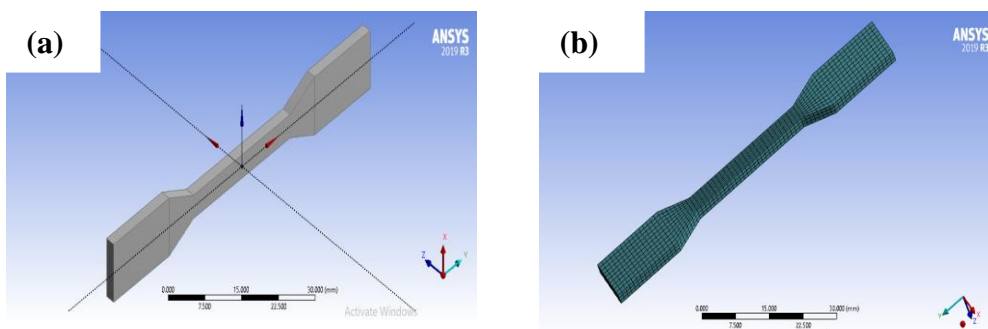


Figure 2.5 (a) CAD and (b) FEA design of the tensile test specimen

The following parameters have been considered during the analysis:

- a) The material is assumed to be homogeneous and isotropic in nature.
- b) A three dimensional modelling is chosen and the material is considered to be deformable.
- c) The mechanical parameters, such as tensile strength, Young's Modulus is obtained from the stress-strain graphs.

The boundary conditions were similar to that of the experimental conditions. The material properties of HDPE, chitosan and hydroxyapatite are given in Table 2.11.

Table 2.11 Material properties of HDPE, chitosan and hydroxyapatite

Properties	Input values		
	HDPE	Chitosan	Hydroxyapatite
Young's modulus (GPa)	0.950	0.3	6
Poisson's ratio	0.46	0.3	0.27
Density (g/cm ³)	0.950	0.15	3.140

Mesh controlling decides the accuracy of the results. A high quality mesh is required for better numerical results. The number of nodes and elements are restricted to 15402 and 12000 respectively with a mesh size of 0.5 mm. The meshing used for the FEA analysis using ANSYS software is shown in Figure 2.6.

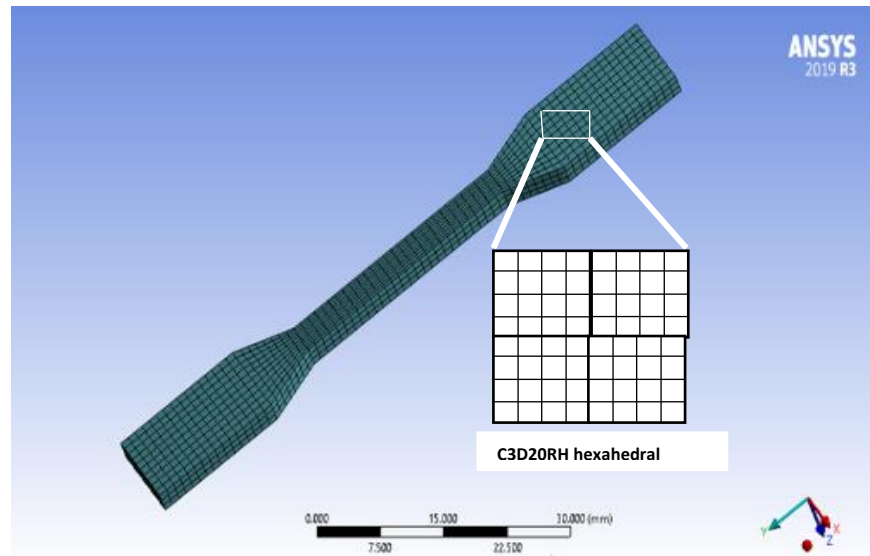


Figure 2.6 Boundary conditions and Mesh size of the test specimen

The linear static stress analysis was conducted using Mechanical APDL solver target in ANSYS Workbench Design software (The static structure analysis was performed using the Mechanical APDL solver in (ANSYS 2019 R3). All samples were subjected to the same boundary conditions. As shown in Figure 2.7, a displacement load was applied to one end and the other end was fixed to a support. The total displacement and equivalent stress are obtained from the data.

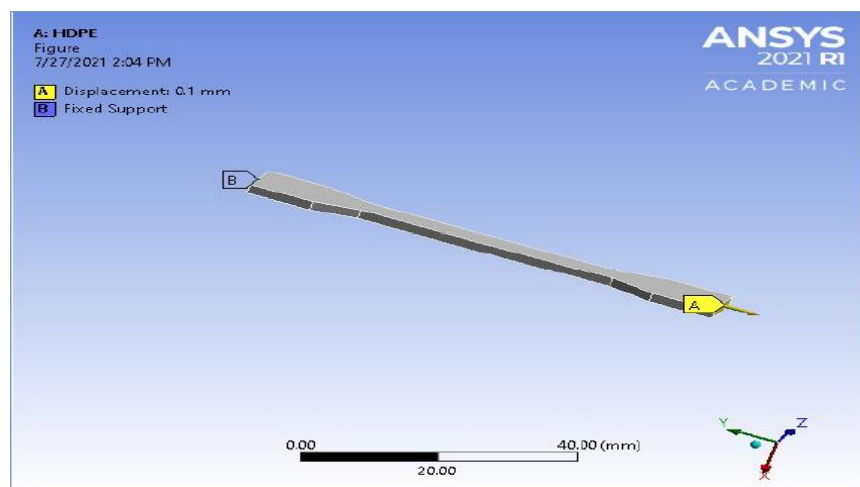


Figure 2.7 Applied load on the tensile test specimen

2.3.2 Microstructural characterizations

The microstructural characteristics of the prepared binary and ternary composite series were studied using SEM, FTIR-ATR, XRD and PALS measurements. They were conducted for analyzing the interaction of filler and matrix, extent of mixing and homogeneous distribution during the preparation of HDPE / Chitosan / Hydroxyapatite polymer composites.

2.3.2.1 Scanning Electron Microscopy (SEM)

The morphology of the tensile fractured surfaces used in tensile strength and the surface image of the composites were studied using SEM (EVO MA18 with Oxford EDS(X-act)). The specimens from the tensile fractured surface were mounted on a metallic stub with the help of silver tape and conducting paint in the upright position. The sample is then kept in an ion-sputtering unit for the gold coating of the sample to make it conduct.

2.3.2.2 Fourier Transform Infrared spectroscopy – Attenuated Total Reflectance (FTIR - ATR)

Thermo Scientific Nicolet™ iS5 was used to obtain the FTIR spectra of the prepared composites. The FTIR is equipped with Attenuated Total Reflectance (ATR) sample accessory with a resolution of 4 cm^{-1} with a total of 32 scans in the range of $400\text{-}4000\text{ cm}^{-1}$. In traditional FTIR, the beam penetrates the sample entirely so the samples have to be prepared with very little thickness to facilitate the beam penetration. In ATR, the beam penetrates only on the surface of the sample such that the IR beam from the beam splitter approaches the sample and passes through the crystal and reflects

internally within the crystal (Zn-Se crystal) and the sample above it. The reflected IR beam is attenuated based on the chemical composition of the test specimen.

2.3.2.3 X-ray diffractometry (XRD)

The information about phase formation and crystallinity of the prepared polymer composites has been studied using Rigaku Miniflex 600 (5th gen) employing Cu-K α radiation and Ni filter operating at 40 kV and 15 mA. The relative intensities were recorded within the range of 5 – 80 (2θ) at a scanning rate of 0.5 $^\circ$ /min.

Polymers are generally crystalline, semi-crystalline, microcrystalline or amorphous in nature. The incorporation of chitosan and hydroxyapatite into semi-crystalline HDPE can influence the crystallinity of the final system (Pal and Katiyar 2016). The % crystallinity of the composite was calculated as follows:

$$\% \text{ crystallinity} = \frac{\text{Area of crystalline peaks}}{\text{Area of crystalline peaks} + \text{Area of amorphous peaks}} * 100 \quad (2.4)$$

2.3.2.4 Positron Annihilation lifetime spectroscopy (PALS)

Positron annihilation spectroscopy is the most suitable method for free hole volume analysis as it can detect free holes down to atomic scale and is highly sensitive to changes up to 1 ppm. It is based on the principle of annihilation of positrons (e^+) or positronium (Ps) the hydrogen like bound state of an electron and positron. The shortest lifetime, τ_1 (100 - 200 ps) reported for the annihilation of para –positronium (p-Ps) can be ascribed to the annihilation of free or trapped positrons. The second lifetime, τ_2 (200-500 ps) is ascribed to the lifetime of positrons in the interphase region of crystalline/amorphous phases. The third lifetime τ_3 is confined to ortho (o-Ps) which consists of a positron bound to an electron having the same spin. o-Ps give significant data on the structure of polymeric composites. The lifetime o-Ps (τ_3)

reduces, when it is found in an environment containing electrons of opposite spin, giving valuable information about the free volume size and number density of free volume. In some cases, the materials have a longer life time τ_4 , due to the smaller and larger free hole size.

According to the model developed by Tao and Eldrup, positronium is assumed to be localized in a spherical potential well having an infinite potential barrier of radius R_0 with an electron layer in the region $R < r < R_0$. The mathematical relation between o-Ps lifetime, τ_3 and the radius of the free volume cavity R in polymers is given by the equation (5),

$$\tau_3 = \frac{1}{2} \left[1 - \frac{R}{R_0} + \frac{1}{2\pi} \sin \left(\frac{2\pi R}{R_0} \right) \right]^{-1} \quad (2.5)$$

Where, $R_0 = R + \delta R$, where δR is given a value of 0.167 nm, which indicates an adjustable fitting parameter obtained from the electron layer thickness obtained from the o-Ps lifetime of molecular solids. Substituting this value for δR , free volume radius R can be calculated from Equation 5. The average size of free hole volume V_f is given as:

$$V_f = \frac{4}{3} \pi R^3 \quad (2.6)$$

From the average free hole size obtained from Equation (6), the fractional free hole volume can be obtained as follows:

$$F_v = AV_f I_3 \quad (2.7)$$

Where, A is a structural constant and is an arbitrarily chosen scaling factor for spherical cavity. It is estimated as 0.0018 \AA^3 from different experiments (Hebbar et al. 2018).

The positron lifetime analysis were taken at room temperature by a conventional fast–fast coincidence lifetime spectrometer having a time resolution of 230 ps. The instrument was equipped with a pair of conically shaped BaF₂ scintillators coupled to photomultiplier tubes of type XP2020/Q with quartz window as detectors. On each side, samples with 1 mm thickness, were stacked together and were placed on either side of a ²²Na positron source with 10 μ Ci strength, deposited on a pure Kapton foil of 0.0127 mm thickness. The lifetime spectrum is obtained by placing the source and sample between the two detectors. Two to three positron lifetime spectra, each with more than a million counts, were acquired in a period of 4–6 hours. Consistently, reproducible spectra were analysed and resolved into three lifetime components with the help of computer program PATFIT- 88 with proper source and background corrections. The source correction term and resolution function were estimated from the lifetime of well-annealed aluminium using the program RESOLUTION. The three Gaussian resolution functions were used in the analysis of positron lifetime spectra of the prepared composites.

2.3.3 Thermal characterizations

The thermal analysis of the composites was done with thermogravimetric analysis and dynamic mechanical analysis. The thermal stability of the composites was analyzed using Coats Redfern Model.

2.3.3.1 Thermogravimetric Analysis (TGA)

Thermogravimetric analysis (TGA) has been employed to investigate the thermal stability as well as the calculation of activation energy of the polymeric composites prepared. The analyses were carried out using TG/DTA, STA7200 (Hitachi) at a heating rate of 10 °C/min from room temperature to 1000 °C with 6-7 mg of the sample in platinum pans under nitrogen environment. The chamber was continuously swept with nitrogen at a rate of 100 mL/min. The corresponding weight changes were noted with the help of ultrasensitive microbalance. The data of weight loss versus temperature and time was recorded online using Measure software. Differential thermal gravimetric (DTG) curves was also obtained from the software.

2.3.3.2 Thermal modelling studies - Coats Redfern Model

The thermal behavior of thermoplastics enables to understand the decomposition kinetics and degradation behavior of plastics. A model fitting method – Coats Redfern Method, has been reported as the most versatile method for estimating the kinetic parameters for degradation. The whole degradation process of HC composite series and HA composite series were considered as one single step. The kinetic data was calculated from the formal kinetic equation, such that the rate function, $f(\alpha)$ including the volatilization / pyrolysis process can be expressed as,

$$f(\alpha) = (1 - \alpha)^n \quad (2.8)$$

$$\alpha = \frac{W_0 - W_t}{W_0 - W_\infty} \quad (2.9)$$

Where, α = volatilization / pyrolysis conversion rate, n = reaction order, W_0 = weight of sample at start time (mg), W_t = weight of sample at time, t (mg), W_∞ = weight of

sample at end time (mg). On combining with Arrhenius equation, and assuming $n = 1$, $2RT/E < 1$, then the final equation is given by,

$$\ln \left[\frac{g(x)}{T^2} \right] = \ln \left[\frac{AR}{\beta E} \right] - \frac{E}{RT} \quad (2.10)$$

Where, $g(x) = -\ln(1 - \alpha)$, A = pre-exponential factor (min^{-1}), E = activation energy (Jmol^{-1}), β = heating rate (Kmin^{-1}). The kinetic parameters were obtained from TG/DTG data. The plot of $\ln \left(\frac{-\ln(1-\alpha)}{T^2} \right)$ versus $\frac{1}{T}$, a straight line with slope $\frac{E}{R}$ and intercept $\ln \left(\frac{AR}{\beta E} \right)$ has been obtained (Li and Suzuki 2009). The pre-exponential factor can be determined from the slope of the graph. Based on $g(x)$ and $f(x)$, the solid state degradation follows chemical reaction mechanism coming under F1 model (chemical reaction order 1) (Naqvi et al. 2018).

2.3.3.3 Dynamic mechanical analysis (DMA)

DMA analysis are mainly concentrated on the interphase studies such that the changes in molecular level like glass transition temperature T_g and crystallinity are clearly detected. An oscillating force is applied to the samples and the deformations occurring are measured as modulus or stiffness. According to the reports, polyethylene exhibits three relaxation process prior to melting, namely: α , β and γ transitions (Sewda and Maiti 2013). A schematic representation of α , β and γ transitions in polyethylenes are shown in Figure 2.8.

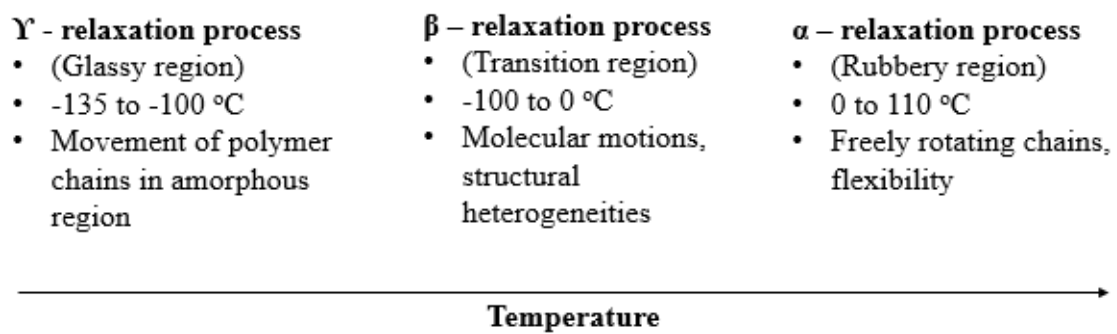


Figure 2.8 Schematic representation of α , β and γ transitions in polyethylenes

The dynamic mechanical properties of the prepared composites were determined using Mechanical Thermal Analyzer (DMTA; Model 2980, supplied by TA Instrument (USA). Rectangular torsion bars of 80 mm x 10 mm x 4 mm were prepared. The dual cantilever mode of deformation was used under the test temperature range from -135 to 110 °C with a heating rate of 2 °C/min and angular frequency of 1 rad/s under liquid nitrogen flow. The Storage modulus (E') loss modulus (E'') and loss tangent ($\tan \delta$) of each sample were recorded.

2.3.4 Dielectric characterizations

The electrical properties of the composites were conducted using dielectric broadband spectroscopy and LCR meter. The effect of electrical properties on the bone healing properties were analyzed.

2.3.4.1 Dielectric characterizations – LCR Meter

The dielectric properties were measured using LCR Hi TESTER 3532 - 50 impedance meter. The test frequency was set from 100 Hz to 5 MHz at high resolution. The instrument was used to measure the parameters such as impedance, phase angle, inductance L, capacitance C, resistance R and dielectric loss (D), out of the fourteen

parameters within the scope of the machine. The electrical conductivity was obtained using the equation given below

$$\epsilon_r = \frac{C.d}{\epsilon_0.A} \quad (2.11)$$

Here, d = thickness of the sample in mm , C = capacitance (F), A = area of cross section of the sample in mm^2 , ϵ_0 = permittivity of free space

The ac conductivity is calculated as:

$$\sigma_{ac} = \epsilon_r . \epsilon_0 . \omega . \tan \delta \quad (2.12)$$

Where, ϵ_r = relative permittivity of the material which is a dimensionless quantity,

ω = angular frequency and $\tan \delta$ = dissipation factor.

2.3.4.2 Broadband Dielectric Spectroscopy

It has been well known fact that BDS is a powerful tool to study the electrical and dielectric responses to reveal the molecular fluctuation and charge transport of samples with squat electric field evolved as a marvelous technique to explore the information from the complex dielectric function over a broad frequency. From the applied voltage and measured current, the value of complex impedance can be calculated using the equation.

$$Z^*(\omega) = Z'(\omega) + jZ''(\omega) = \frac{V^*(\omega)}{I^*(\omega)} \quad (2.13)$$

It evaluates the molecular and the collective response of the sample to the applied field and measures complex impedance function $Z^*(\omega)$, where ω is the angular frequency, from which the complex dielectric function can be derived using the formula,

$$\varepsilon^*(\omega) = \varepsilon'(\omega) - i\varepsilon''(\omega) = \frac{1}{j\omega\varepsilon_0 Z^*(\omega)} \quad (2.14)$$

Consequently, a number of parameters can be derived from the complex dielectric function like conductivity by the equation

$$\sigma^*(\omega) = \sigma'(\omega) + j\sigma''(\omega) = j\omega\varepsilon_0\varepsilon^*(\omega) \quad (2.15)$$

Modulus can also be derived using the following equation (16),

$$M^*(\omega) = M'(\omega) + jM''(\omega) = \frac{1}{\varepsilon^*(\omega)} \quad (2.16)$$

Isobaric dielectric measurements were carried out using a GmBH Alpha impedance analyzer by Novo-Control Technologies. The sample was kept between two stainless cylindrical electrodes with diameter 30 mm forming a capacitor with a gap of 0.1 mm using two narrow teflon spacers. Temperature control was achieved by Novo-Control Quattro system using Nitrogen gas cryostat having a temperature stability of ± 0.1 K. Before the dielectric measurements, the sample cell capacitor was calibrated with empty cell and standard load of 100 Ω . The dielectric measurements were collected from a wide frequency range (10^{-2} to 10^7 Hz).

2.3.5 Biocompatibility and biodegradable characterizations

The biodegradability of the prepared composites were conducted using water sorption analysis and soil burial tests. The biocompatibility of the system were studied using water contact analysis and cell proliferation studies.

2.3.5.1 Water Sorption analysis

HC composite series and HA composite series with an approximate size of 25 mm x 20 mm x 1mm were prepared as per ASTM D570-81. Initially, the samples were preheated at 60 °C and were dried overnight. The initial weight of the sample (W_0) was taken and was immersed in distilled water. The composites were taken out periodically and wiped immediately with a filter paper and the weight was noted (W_n). The experiment was conducted for 35 days and the average value of 3 samples were obtained for further calculations. The water sorption ability (%) is calculated as:

$$\text{Water sorption (\%)} = \left(\frac{W_n - W_d}{W_d} \right) * 100 \quad (2.17)$$

2.3.5.2 Soil Burial Analysis

The soil burial analysis has been conducted on HC composite series and HA composite series to study the biodegradability of the system. Composites with ASTM D638 specification were used for the analysis. Wet compost soil with pH – 8 was placed in plastic covers with tiny holes perforated at the bottom to ensure air and water circulation. The dumb bell shaped specimens were buried in the soil at a depth of ~ 10 cm and were subjected to the action of micro-organisms in it. The samples were taken periodically and carefully washed with water to remove the soil and was dried in oven. The weight of the dried samples was taken and analysis continued for 4 weeks. The mechanical strength of the samples after soil burial analysis were taken and compared with the initial strength of the samples. The % weight loss of the samples after the analysis were calculated as follows:

$$\% \text{ weight loss} = \frac{W_0 - W_t}{W_0} * 100 \quad (2.18)$$

2.3.5.3 Water contact angle measurements

Water contact angle measurements were conducted on the prepared composites to study the surface wettability as well as hydrophilicity of the samples. Using a micro syringe, 7 μ L volume of water were used by sessile drop method at 27 °C using Digidrop–MCAT goniometer (GBX). The measurements were repeated for three samples and the images were recorded.

2.3.5.4 Cell proliferation analysis

Proliferative efficacy of the test compounds was studied using Methyl Thiazolyl Tetrazolium (MTT) Assay. The test compounds were sterilized using ethanol and dried and was kept in desiccator for further studies. Mouse Osteoblast cells (MC3T3) were cultured in minimal essential medium with alpha modifications (alpha-MEM) supplemented with 10% FBS, 1% antibiotic-antimycotic solution and 1% L-glutamine. Cells were maintained at 37 °C and 5% CO₂ in a humidified atmosphere. The cell proliferative efficacy were assessed as follows: Cells were seeded onto the test films in 96 well microtiter plates at a seeding density of 5000 cells/well. 24 hours post-incubation with test materials, MTT reagent was added to the wells and incubated at 37 °C for 4 hours. Formazan crystals were solubilized using DMSO and absorbance was recorded at 570 nm using multimode microplate reader (FluoSTAR Omega, BMG Labtech). Percentage proliferation of the cells was calculated with respect to untreated cell control. Photomicrographs of the cells treated with different test materials were captured using an axiocam attached to an inverted microscope (PrimoVert, Carl Zeiss).

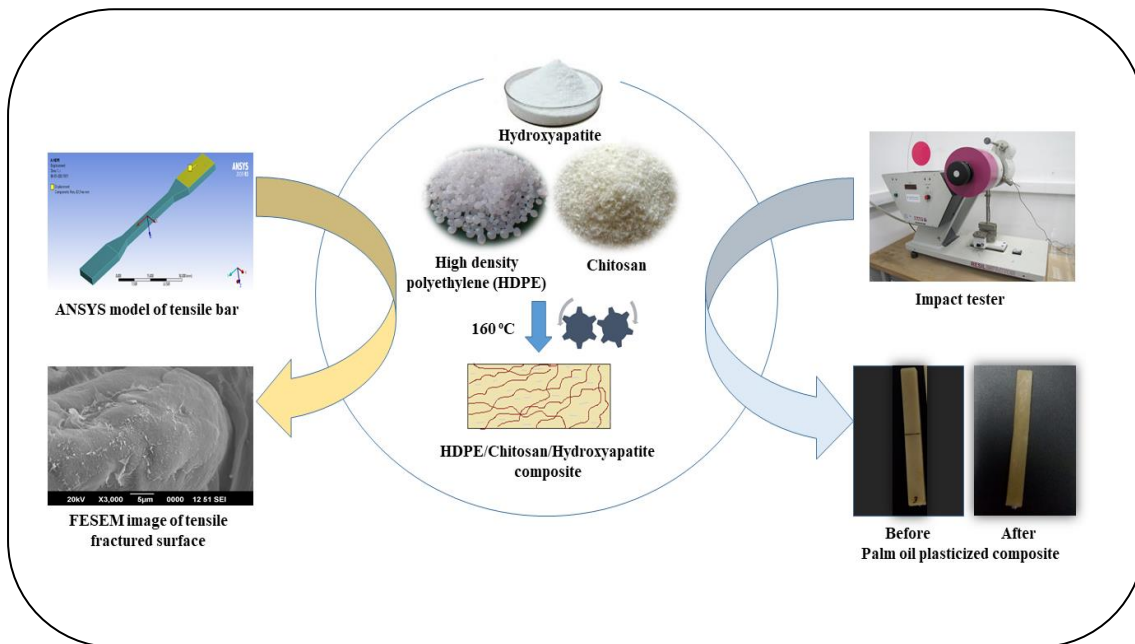
Chapter 3

Investigation of the Mechanical Properties of HDPE / Chitosan Composites and HDPE / Chitosan / Hydroxyapatite Composites

Summary

HC composite series and HA composite series were successfully prepared via melt mixing technique. The mechanical properties of the composites such as impact strength, tensile strength and Young's Modulus of the binary and ternary systems were analyzed. The effect of palm oil on the mechanical properties of the prepared composites was also studied. Moreover, the experimental data have been compared with the theoretical modelling studies using Finite Element Analysis (FEA) using ANSYS. The tensile fractured surface of the composites was analyzed using Scanning Electron Microscope (SEM) to understand the extent of crosslinking and interaction formed in the composite system. A hybrid bio-composite with a tensile strength of 36.88 ± 0.30 MPa and impact strength of 115 ± 3 kJ/m² was developed, that showed better mechanical performance showing good potential as bio-implant material.

Graphical Abstract



3.1 Introduction

The enhanced mechanical characteristics and structural modifications of a composite are greatly influenced by the compatibility between filler and matrix. Numerous methods have been proposed to improve the miscibility of matrix and fillers through the addition of various additives like compatibilizers, plasticizers, crosslinkers etc. (Rzayev 2011). They improve the mechanical stability of the composites effectively, especially, the tensile properties, impact strength, stiffness and many more (Tong et al. 2014). Palm oil has proved to be an effective plasticizer in polyethylene composites due to the homogeneity formed in the system, improved flexibility and good mechanical performance (Zulkifli 2009). The brittle nature, stiffness and toughness of a composite can be evaluated from the stress-strain graphs. According to the work reported by Gracia *et al*, the elongation at break is decreased for high concentration of filler in HDPE/peanut shell composites due to the rigid interface

formed between the filler and the matrix (Gracia et al. 2021). In addition to the stress-strain analysis, the tensile strength increases with improved interaction in the filler-matrix interface as observed in cross-linked HDPE/Chitosan composites. During an effective stress transfer, the optimization of a composite is accomplished from the mechanical analysis where the stress transfer at the filler-polymer interface is sufficient. The addition of natural polymers can also be shown to affect the stiffness of the composites which results in a reduction in elongation at break (Kusuktham et al. 2014). The ability to absorb external energy is studied from un-notched impact strength as the sample undergoes crack initiation and crack propagation, unlike the notched tests. The additives used in the composites change the conformation of the molecules and enable effective interaction in the system resulting in better impact strength as observed in HDPE/wood composites (Huang and Zhang 2008). The morphological analysis of the fractured surfaces provides information about the strength at which the fillers interact better in the composite. Big voids/holes show low bonding strength as observed in benzoyl chloride (BC) treated SPF/GF/PLA hybrid composites (Crespo et al. 2007). The surface morphology of a composite is governed by the adhesion, interaction, mechanical interlocking, and distribution of small voids over the surface. This property can also affect the surface energy as well as the surface property of the composite (Sanyang et al. 2015). The proper composite ratio, preparation process and optimum loading conditions can provide an economic and environmentally benign hybrid composite for diverse applications. The success of experimental data can be analyzed using theoretical modelling methods including numerical modelling methods as well as computational modelling methods (Xie et al. 2014, Sherwani et al. 2021). To be more precise on the quasi-static and long-term

response of the composites prepared, the present work has utilized Finite Element Analysis (FEA) to predict the success of the composite processing.

In the present study, the mechanical performance of HC composite series with varying concentrations of chitosan was initially studied. The composite was optimized based on its impact strength and later varying concentration of palm oil was added to the optimized binary system. The effect of palm oil on mechanical and morphological analysis was carried out on the prepared composites. Finally, a novel hybrid system was developed by the incremental addition of hydroxyapatite as the inorganic filler to the optimized HP composite system. The studies were oriented to contribute to the formulation of a bio-compatible bone implant material consisting of hydroxyapatite in palm oil plasticized HDPE / Chitosan composite system. The results were correlated with the computational modelling technique using Finite Element Analysis (FEA) using ANSYS software.

3.2 Results and discussion

3.2.1 Impact strength analysis of HC composite series

The impact strength measures the ability of a material to absorb energy when it is subjected to a sudden load. Figure 3.1. show the variation in the impact strength of HC composite series on adding an increasing amount of chitosan as filler. The impact strength is found to increase with the addition of chitosan till HC2, and decreased with higher concentration of chitosan. When chitosan is added, the interaction between the reactive groups of maleic anhydride occurs, causing an increase in the crosslinking in the system. HC2 with 5 wt% of chitosan shows the highest impact strength value of 105.1 kJ/m^2 , among the prepared HC composite series.

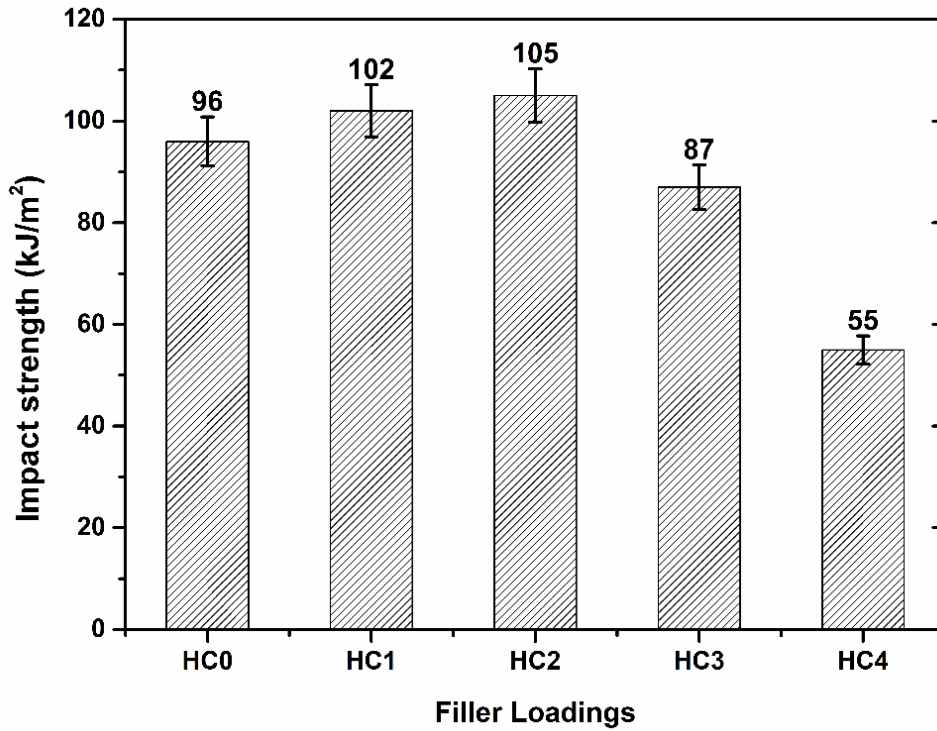


Figure 3.1 Impact strength analysis of HC composite series

The effective crosslinking and uniform distribution of chitosan in the HDPE matrix provides enough energy to withstand the external force. At higher concentration of chitosan, beyond 5 wt%, the filler - filler interaction dominates over filler - matrix interaction. This causes the formation of agglomerates in the system, forming more stress concentration regions such that they require only less energy to initiate or propagate a crack. This reduces the efficiency of the composite in holding external force (Huang and Zhang 2008).

3.2.2 Stress-strain analysis of HC composite series

The tensile strength analysis of HC composite series are studied from the stress-strain graphs given in Figure 3.2.

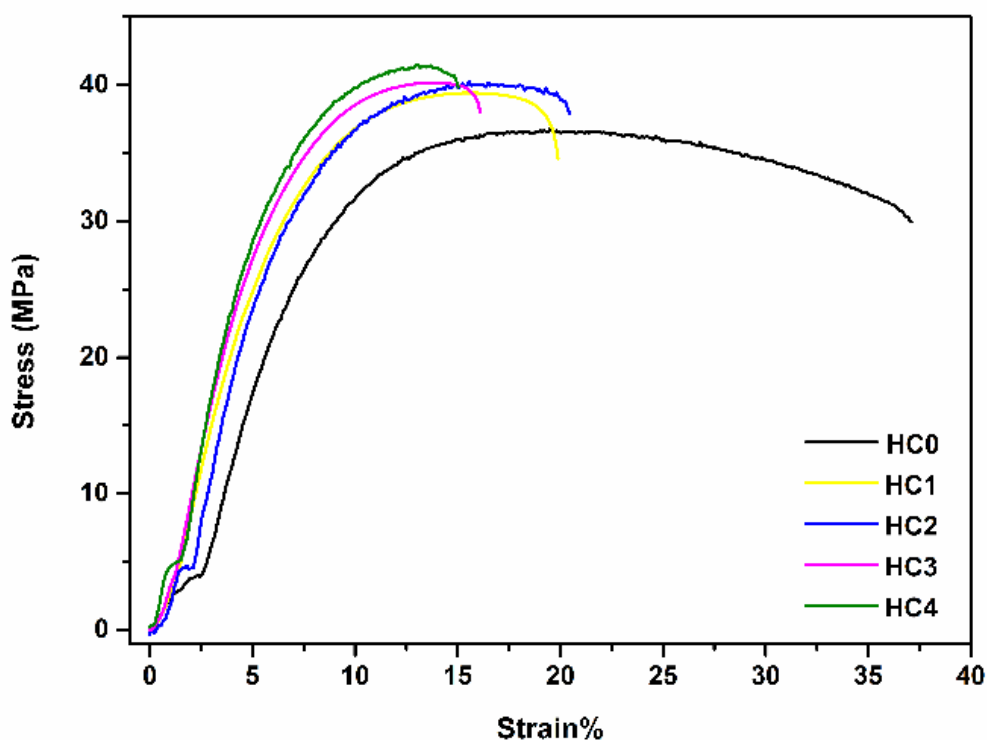


Figure 3.2 Stress-strain graphs of HC composite series

The tensile strength of the prepared composites are gradually increasing with increase in concentration of chitosan as observed from the stress-strain graphs. A maximum tensile strength of 41.5 ± 0.25 MPa is obtained for HC4 composite system, while HC2 and HC3 showed strength at 40.30 ± 0.10 MPa and 40.2 ± 0.1 MPa respectively. The increase in tensile strength with the addition of chitosan can be ascribed to the improvement in interfacial bonding between HDPE and chitosan leading to good mechanical interlocking in the system. With higher concentration of chitosan a rough surface is formed which can be observed with reduced elongation for the composites (Sherwani et al. 2021). At optimum concentration, when the load is distributed equally, the fillers are held together due to better interaction and inter-bonding between the components in the system. The elongation at break is found to be increased at lower concentration of chitosan (2.5 wt%) when compared with the other HDPE / Chitosan series observed from the stress-strain graphs. This is due to the

insufficient interaction of chitosan with compatibilized HDPE that lead to the formation of voids such that when an external load is applied, coalescence of voids occurs, leading to more elongation. The lower elongation at break for higher concentration of chitosan beyond 5 wt% shows a brittle nature, which can be attributed to the formation of agglomerates that are dominating over filler-matrix interaction.(Huang and Zhang 2008). The findings are supported by the morphological examination of the composites studied using scanning electron microscopy (SEM). The same trend in tensile strength is noted for Young's Modulus of HC composite series as shown in Figure 3.3. When a stress is applied to the material, partially separated microspaces initially occurs due to the detachment of fillers from the matrix or breakage of bonds. This impedes the stress propagation between the filler and matrix. When, the filler is tightly adhered to the matrix, the composite can withstand the external force without change in deformation. This further increases the stiffness of the material (Tong et al. 2014).

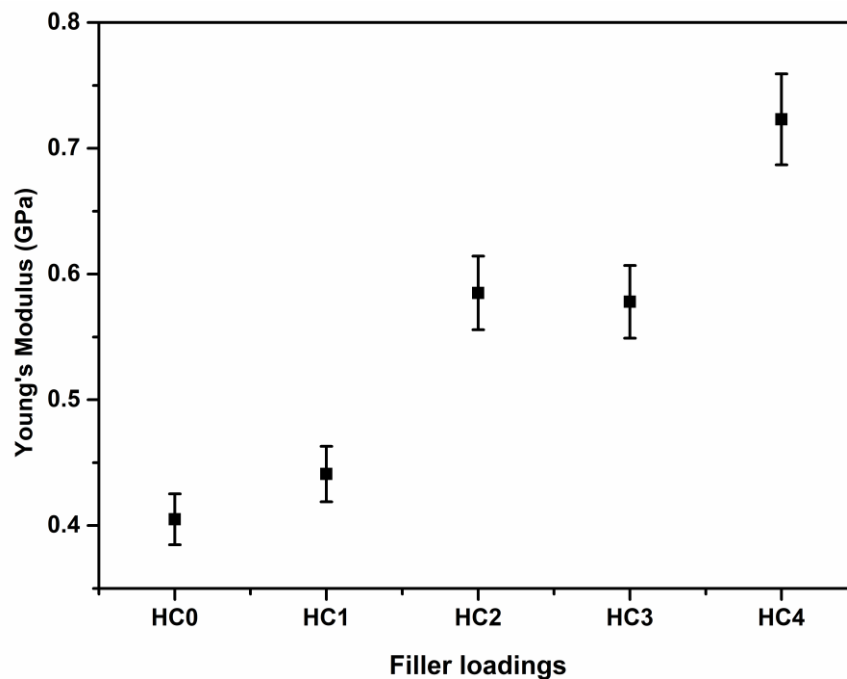


Figure 3.3 Young's Modulus of HC composite series

3.2.3 Impact strength analysis of HP composite series

Figure 3.4. shows the variation of impact strength of HP composite series on addition of varying concentration of palm oil as plasticizer. A slight decrease in impact strength is obtained for HP1 and HP2, which is due to the plasticization occurring on addition of palm oil. With the increase in concentration of palm oil from 2.5 wt% to 5 wt%, the impact strength is increased from 85 kJ/m² to 102.1 kJ/m².

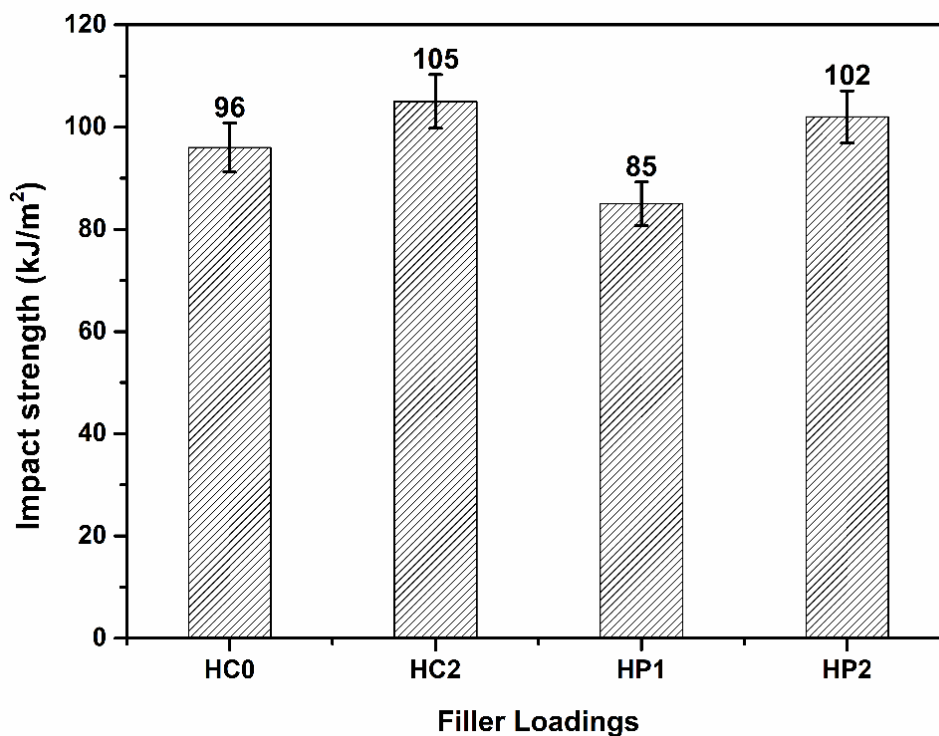


Figure 3.4 Impact strength analysis of HP composite series

The long-chain bulky groups of palm oil find it difficult to penetrate into the system when a lower concentration of palm oil is used. It has the possibility to form small clusters with chitosan, rather than improving the segmental mobility for further crosslinking and interaction. With higher concentration of palm oil, the long alkyl groups of palm oil penetrate into the matrix system providing easier relaxation of the HDPE polymer chains. This increases the interaction between HDPE and chitosan. As

a result, the impact energy could quickly disperse into the composites leading to comparable impact strength with HC2 (Shinoj et al. 2011).

3.2.4 Stress-strain analysis of HP composite series

The stress-strain analysis of HP composite series are given in Figure 3.5.

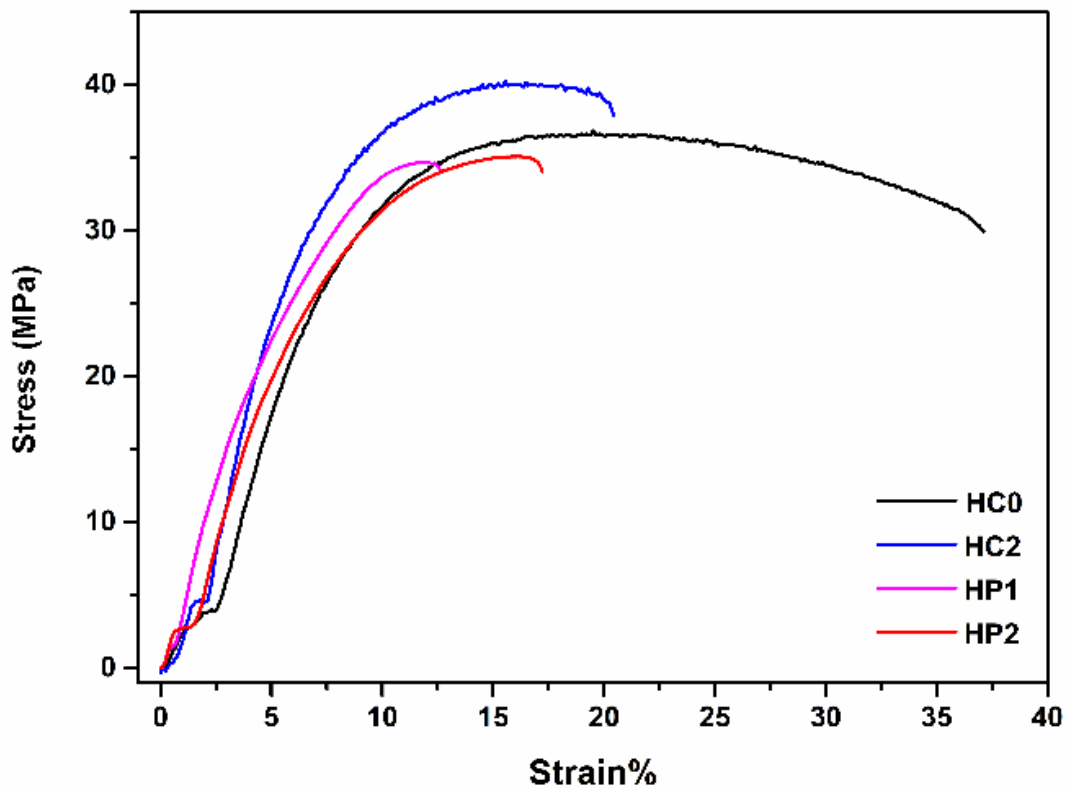


Figure 3.5 Stress-strain graphs of HP composite series

A remarkable decrease in tensile strength is observed with the addition of palm oil to the composite systems as previously reported (Crespo et al. 2007). The unsaturated centers of palm oil consume dicumyl peroxide during the initial mixing process, resulting in a slight reduction in the tensile strength of the system. With the increase in concentration of palm oil, easier relaxation of polymer chain occurs, thereby

increasing the segmental mobility. In such cases, the filler - matrix interaction dominates over filler – filler interaction and hence increases the tensile strength of the system. This creates more interaction between chitosan and compatibilized HDPE at higher concentration of palm oil (Sanyang et al. 2015). It was also reported that, beyond 5 wt% of palm oil, the tensile strength of thermoplastic based systems are decreased drastically. Hence, the composition – HP2 has been optimized for further studies. The similar trend is observed in the Young's Modulus of HP composite series as observed from Figure 3.6.

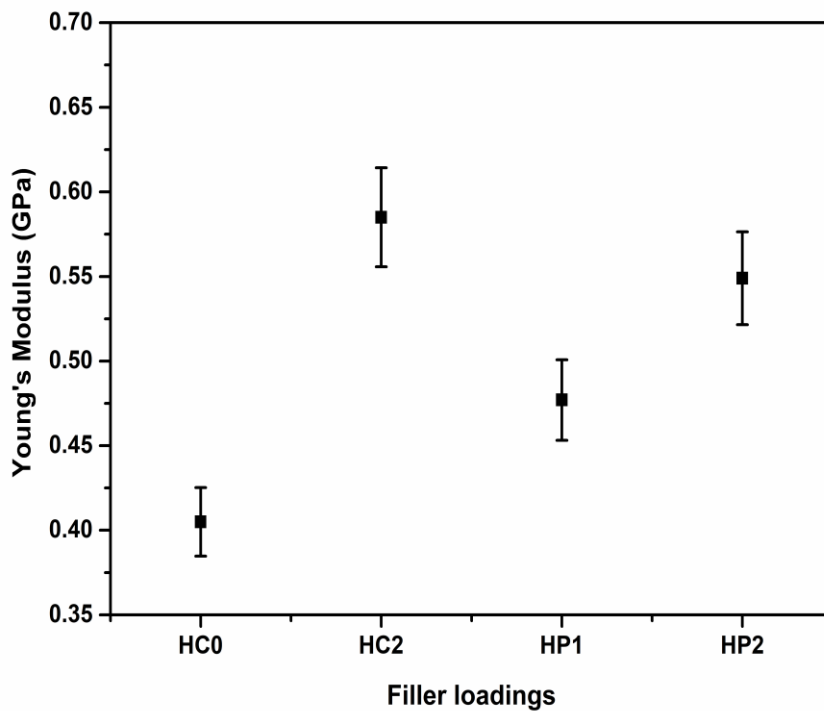


Figure 3.6 Young's modulus of HP composite series

3.2.5 Computational modelling of HC composite series and HP composite series using Finite Element Analysis

A comparison between the experimental results and theoretical models is compared using the ANSYS software. Figure 3.7. shows the equivalent stress and total deformation from the finite element analysis.

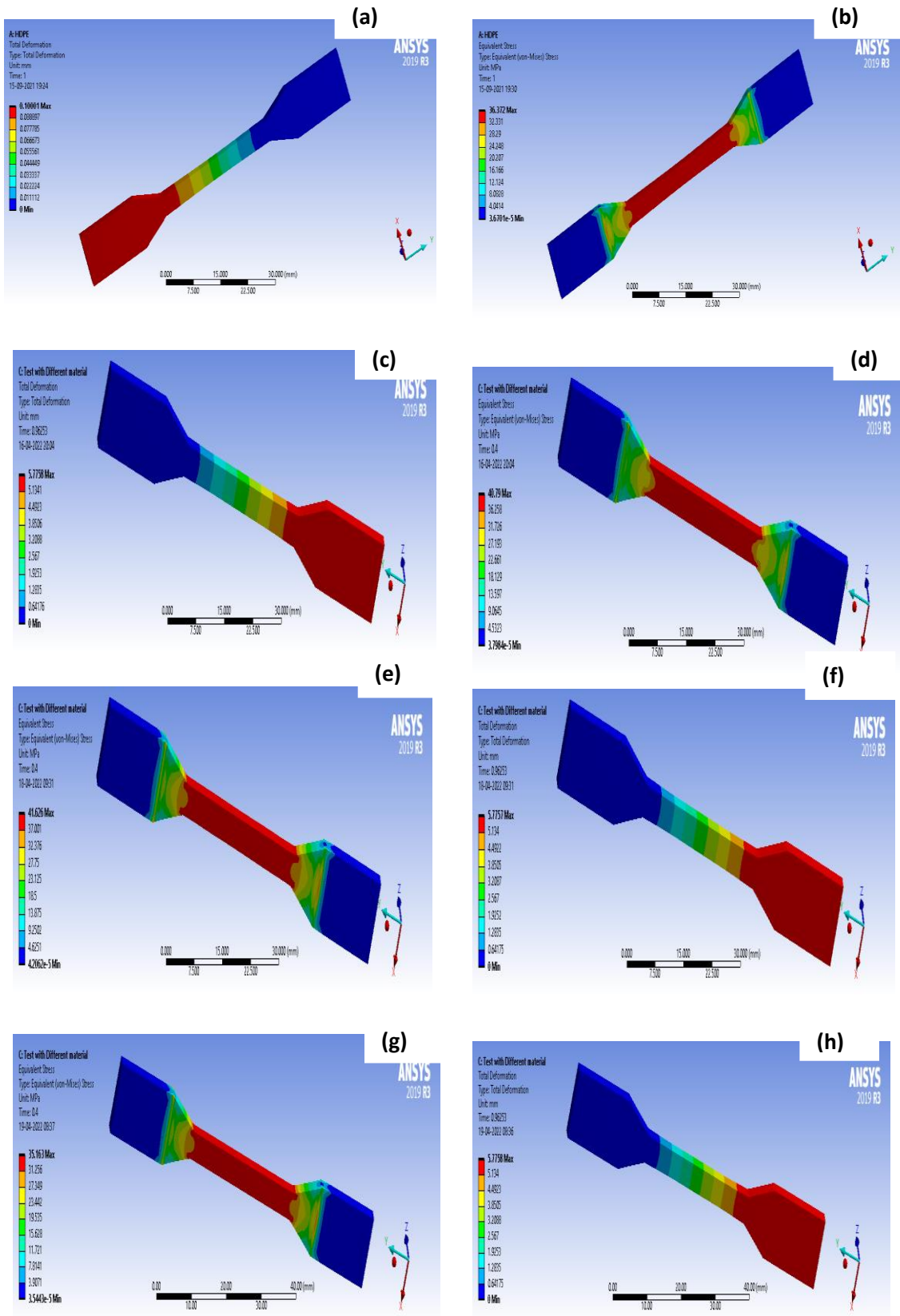


Figure 3.7 Total deformation (a) HC0, (c) HC2, (e) HC4 and (g) HP2 and Equivalent stress of (b) HC0, (d) HC2, (f) HC4 and (h) HP2

Different color zones indicate the stress concentration point during the analysis. Red color zone indicates the maximum stress zone indicating the failure starting point where the load is applied and blue color zone shows the minimum stress zones formed in the composites. The comparison of FEA analysis values with the experimental data is closely related to each other as shown in Table 3.1.

Table 3.1 Comparison of tensile strength analysis of experimental data with theoretical data for HC composite series and HP composite series

Sample	Experiment Value (MPa)	ANSYS data (MPa)	Error (%)
HC0	36.2	36.4	0.55
HC1	39.4	37.7	4.5
HC2	40.3	40.8	1.2
HC3	40.2	40.6	1.0
HC4	41.5	41.6	0.24
HP1	32.8	33.2	1.2
HP2	35.1	35.2	0.28

The error limits are between 1% to 10%, which is considered to be in the acceptable error range for model validation (Leong et al. 2015). The values of tensile strength obtained for the finite element analysis are slightly higher than the experimental values for almost all composites. This is due to the assumptions adopted for finite element analysis such as perfect fiber orientation and interface properties. During the experimental processing of composites, the fillers are randomly oriented at different stress concentrations. This creates difficulty in achieving the isotropic nature for the synthesized composites. Due to the closeness of the results, it can be concluded that

the synthesized systems have been close to isotropic behavior indicating the uniform mixing achieved in the system (Wang et al. 1998).

3.2.6 Morphological analysis of the tensile fractured surfaces of HC composite series and HP composite series

The SEM images of the tensile fractured surface of the prepared composites are shown in Figure 3.8. HC0 shows a wavy nature for the fractured composites indicating a ductile morphology. The long linear chain of HDPE is distorted with the addition of maleic anhydride and palm oil. This affects the anisotropic nature of HDPE further promoting irregularities in the system (Ratnam et al. 2006). The irregularities in the fractured surface as observed from the images also explain the extent of miscibility of chitosan with compatibilized HDPE. A disruption in the ductile structure is observed in all composites with the addition of chitosan which is observed more in HC1 than HC2 and HC4. The limited compatibility of the filler and matrix leads to low tensile strength and this is observed from the pulling out of the fibril like structure from the composite system. The increased elongation of HDPE polymer chain as obtained from stress-strain graph in Figure 3.2 further supports this. Furthermore, the surface of the composite becomes more homogeneous with the addition of palm oil when compared with the un-plasticized samples. The fractured surface shows that the composites have undergone wedging, which is one of the characteristics of ductile morphology. This can be due to the micro-cracks or free hole formed in the composite during the mixing process. At higher loading of chitosan, the dispersion of chitosan is continuous and it results in the improved interfacial interaction of filler and the matrix. At higher concentration of chitosan, agglomeration occurs in the system and is observed with large number of clumps pulled out from the system. Similar trend is obtained in the studies conducted by Bin Rusayyis et al (Bin

Rusayyis et al. 2018, Kalambettu et al. 2012). The presence of palm oil in HC2 has provided a more homogeneous morphology when compared with the un-plasticized system.

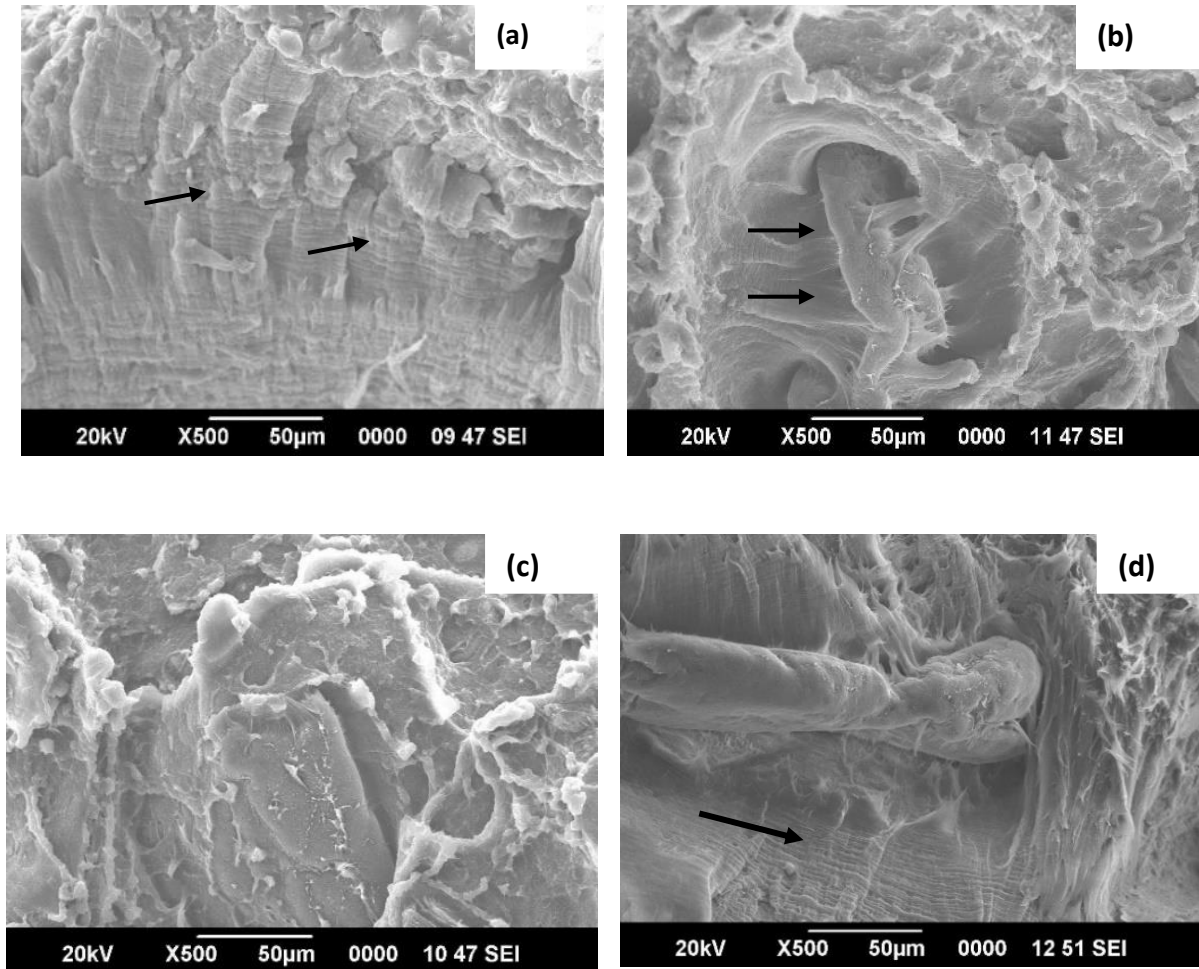


Figure 3.8 SEM images of the tensile fractured surface of (a) HC0, (b) HC2, (c) HC4 and (d) HP2

3.2.7 Impact strength analysis of HA composite series

The mechanical properties of HA composite series on adding increasing amount of hydroxyapatite was evaluated from the impact strength analysis as shown in Figure 3.9.

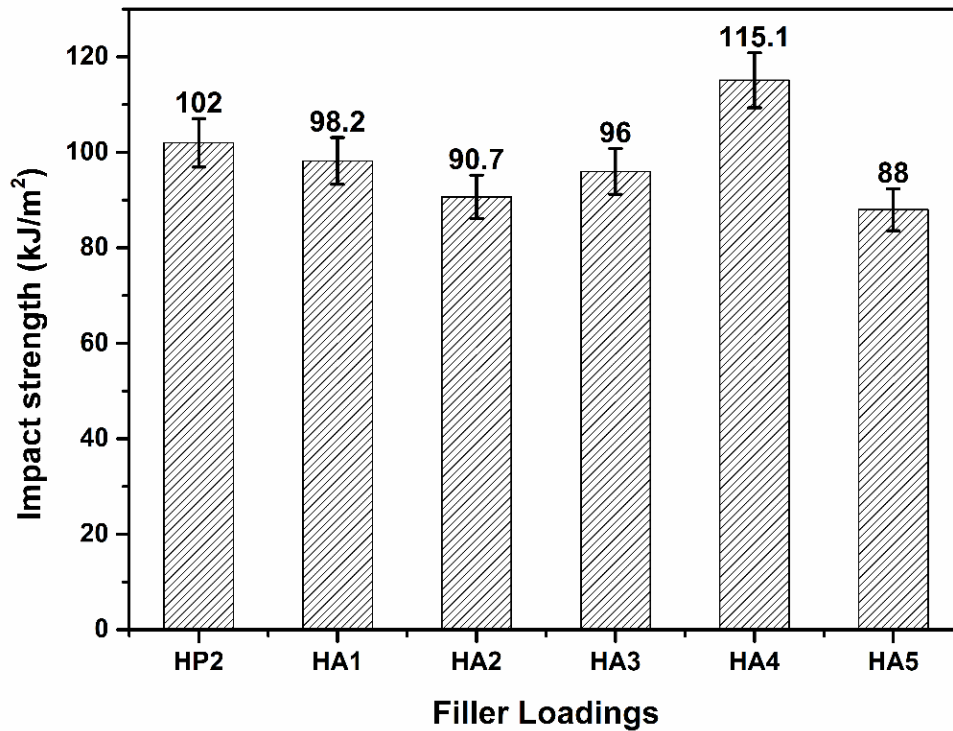


Figure 3.9 Impact strength analysis of HA composite series

As seen from the values, the impact strength of ternary composites are initially lower than HP2 system, but it is gradually increasing with the concentration of hydroxyapatite. An initial decrease in impact strength for HA composite series can be ascribed to the decreased interaction of filler with the matrix due to the formation of clusters with palm oil as observed from the SEM images in Figure 3.16. This creates more voids in the system, thereby forming more stress concentration regions. But, the impact strength starts to increase from 6 wt% addition of hydroxyapatite, indicating the onset of interaction between fillers and matrix, as evidenced from the increase in fracture initiation energy (Huang and Zhang 2008). At 8 wt% of hydroxyapatite, the impact strength of the ternary composite is outperforming all samples and a value of 115.1 kJ/m² is obtained. The increase in impact strength with the addition of hydroxyapatite can be ascribed to two major reasons: (a) the interaction of more flexible amino group of chitosan with the stiff and polar groups of hydroxyapatite. This reduces the flexibility of the HA composite system and (b) ability of the

composite to hold the impact energy due to minimum number of microcracks formed in the system, arising due to good filler-matrix interaction (Yadav et al. 2014, Sreekumar et al. 2013). At 10 wt% of hydroxyapatite, the impact strength is further decreased to 88 kJ/m², which shows the formation of agglomerates.

3.2.8 Stress-strain analysis of HA composite series

Figure 3.10 shows the stress versus strain curves HA composite series compared with the optimized plasticized binary system – HP2.

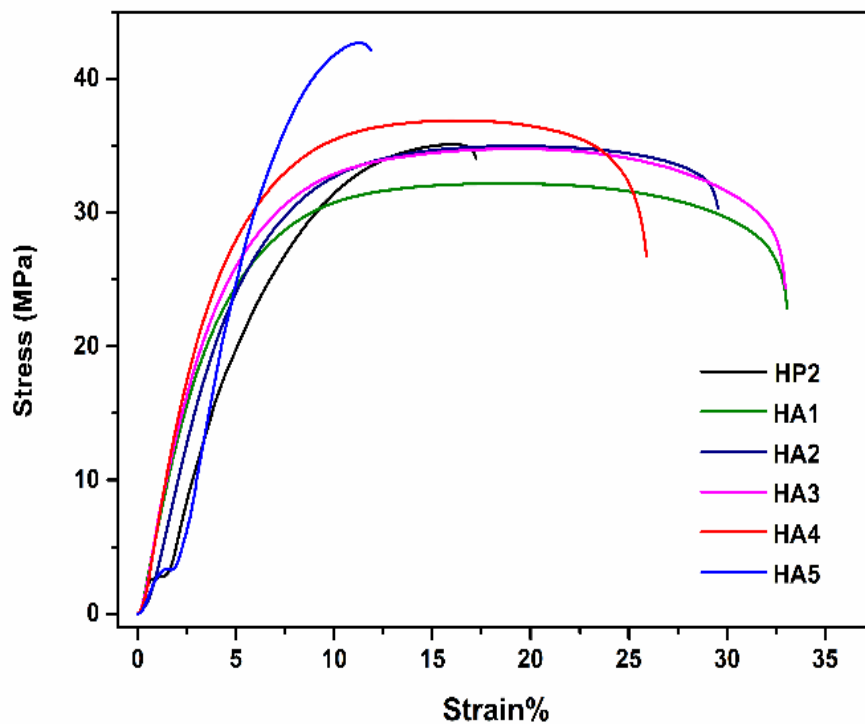


Figure 3.10 Stress-strain graphs of HA composite series

In practice, the role of plasticizer is to improve the processing properties and segmental mobility of the system. But, the results exposed a considerably lower tensile strength in HP2 when compared with HC0. At the same time elongation of HP2 was also lower when compared with the other systems under study. This can be attributed to the partial brittle nature achieved due to the penetration of long chains of palm oil in the voids providing stiffness to the system. The elongation at break under

the applied stress can be ascribed to the movement of polymer chains (Xie et al. 2014). The presence of varying concentration of hydroxyapatite in HP composite system - HP2, has initially caused a decrease in tensile strength. The palm oil may bound to the hydroxyapatite particles to form small clusters in the composite system, leading to an anti-plasticization effect (Bergquist et al. 1999, Sanyang et al. 2015). As a result, the interaction of hydroxyapatite with chitosan reduces and flexibility attained by the HDPE is retained. This causes an elongation for HA composite series at lower concentration of hydroxyapatite giving lower tensile strength. With higher concentration of hydroxyapatite, the stress-strain graph became steeper with reduced elongation. At the same time the tensile strength also reached a higher value of 36.88 MPa at 8 wt% loading of hydroxyapatite. Higher the concentration of hydroxyapatite, higher is its ability to get more mixed with HDPE matrix and lesser is its ability to get agglomerated and bonded with the plasticizer. Upon considering the tensile strength and elongation at break, it is observed that a more homogenous mixing is attained for HA4 composite system. This makes HA4 the most optimized sample among the prepared composite (Wang et al. 2016). The mechanical properties of HA composite series deteriorate beyond 8 wt% of hydroxyapatite with reduction in impact strength in the system. In HA4, a system was accomplished with higher tensile strength that retained the impact strength of the system due to the improved interaction caused due to compatibilizers and plasticizer used in the system. A similar trend of tensile strength is observed for Young's Modulus of the synthesized composite system as shown in Figure 3.11. When fillers are added to HC0, it reduces the effective cross-section in the polymeric system. At any given external loading, when compared with the unfilled matrix system, the addition of chitosan can create an internal stress in the system. Stress concentration of the chitosan around the matrix interface also

contributes to this internal stress. This facilitates a deviation in Young's Modulus with the addition of higher concentration of hydroxyapatite. The Young's Modulus of HA4 is higher than the corresponding composites, which can be attributed to the stiffening action of hydroxyapatite.

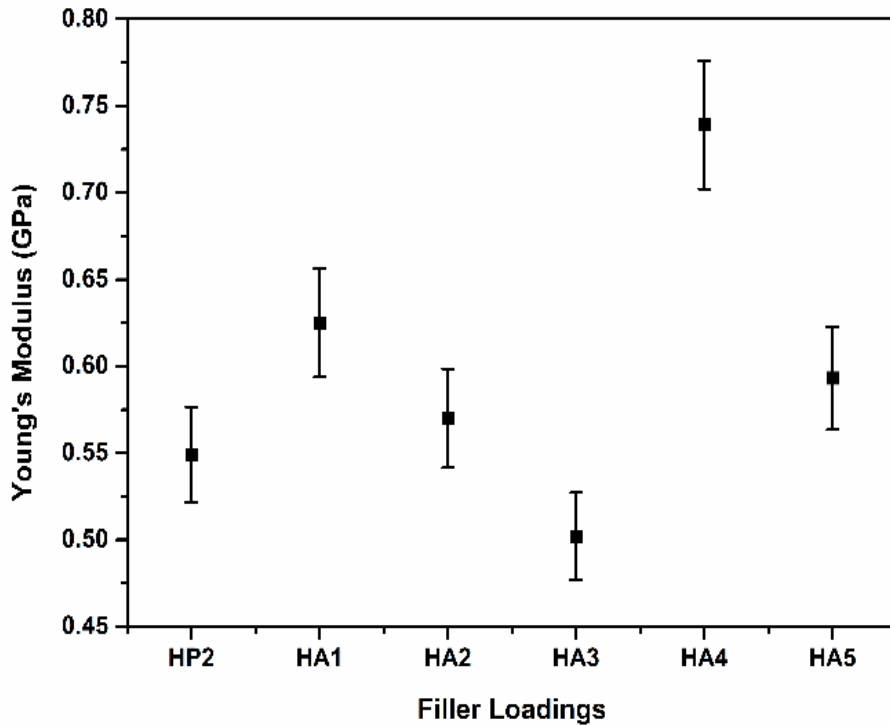


Figure 3.11 Young's Modulus of HA composite series

3.2.9 Impact strength analysis of HAW composite series

The impact strength analysis of HAW composite series is shown in Figure 3.12. The ability to resist impact force is high in plasticized composites and it is higher in ternary systems rather than in binary systems. The absence of palm oil in HA composite series has induced brittleness in the system which has resulted in reduced impact strength. Hence, the ability to absorb energy from an external sudden impact is lower in HAW composite series.

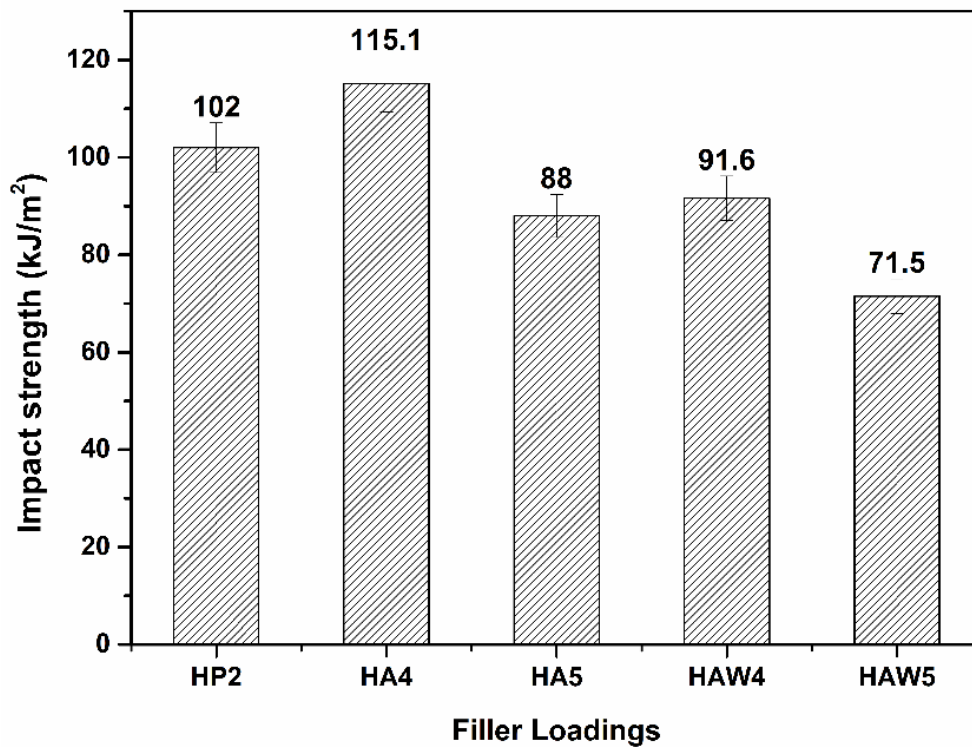


Figure 3.12 Impact strength analysis of HAW composite series

3.2.10 Stress-strain analysis of HAW composite series

The stress-strain analysis and Young's Modulus of HAW composite series are compared with HA4 and HA5 as shown in Figure 3.13. A subsequent increment in tensile strength is observed for HAW composite series when compared with HA4 and HA5. A decrease in elongation is observed from the stress-strain graph for HAW4 and HAW5. As mentioned earlier, palm oil reduces the flexibility of the system, thereby reducing the segmental mobility by reducing the interaction of the component in the system. In such cases, hydroxyapatite gets attached to the melted HDPE, rather than interacting with chitosan. This reduces the ductile nature of the system and miscibility between the components in the composites. The ability to hold the fillers to the matrix also decreases due to the minimum miscibility in the un-plasticized system. This resulted in low Young's modulus for HAW composite series as shown in Figure 3.14.

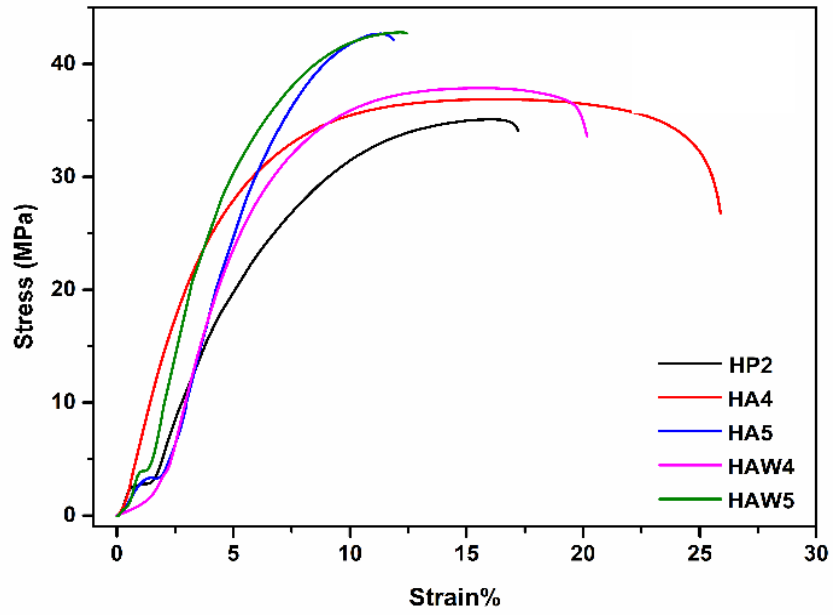


Figure 3.13 Stress-strain graphs of HAW composite series

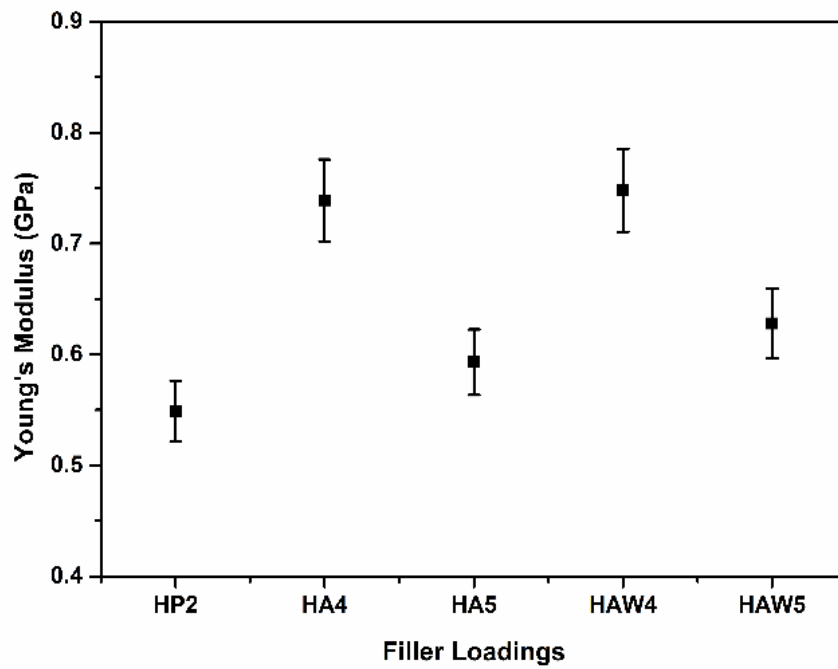


Figure 3.14 Young's Modulus of HAW composite series

3.2.11 Computational modelling of HA composite series and HAW composite series using Finite Element Analysis

Figure 3.15 shows the stress–strain responses such as total deformation and equivalent stress for HA composite series and HAW composite series.

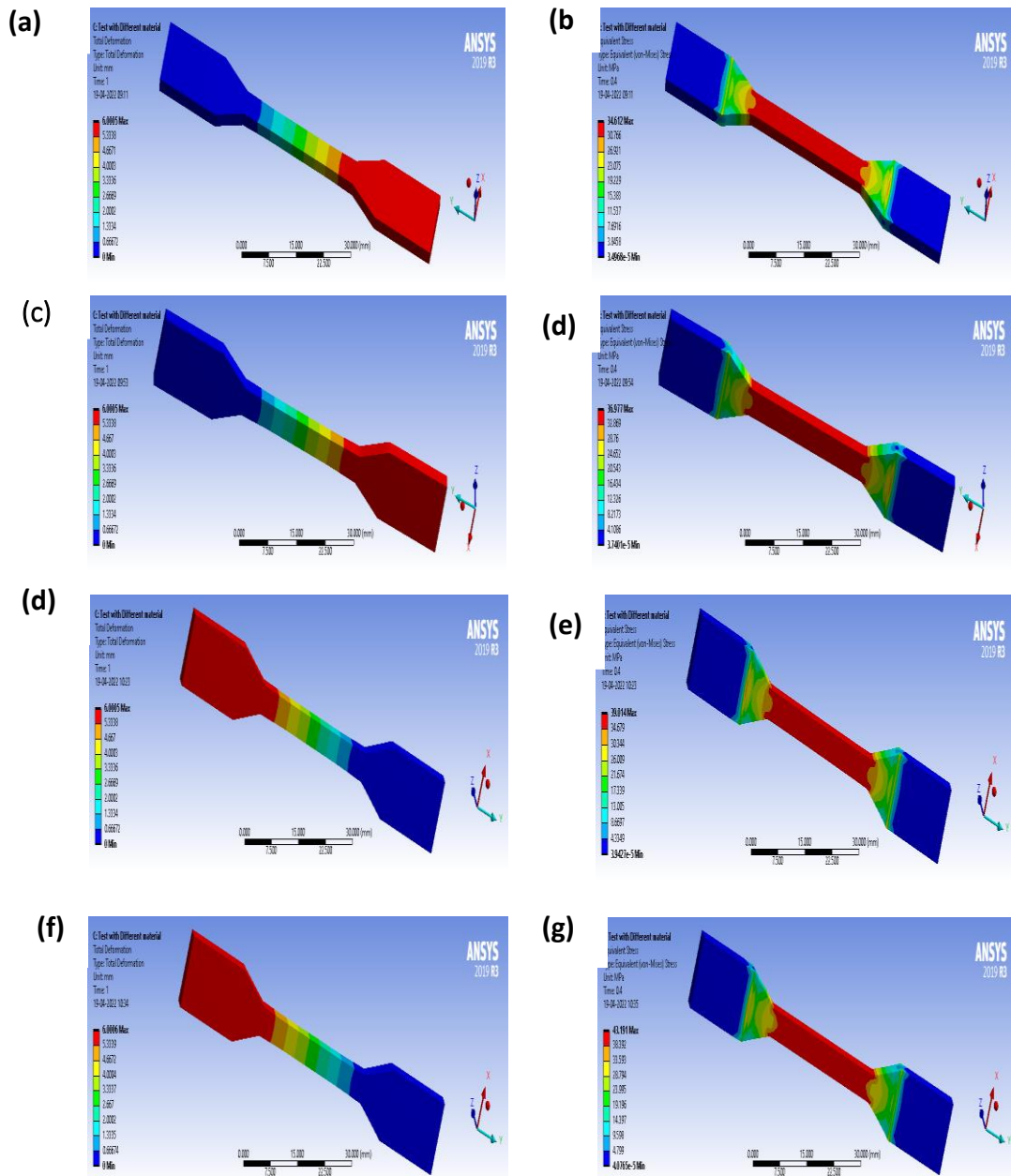


Figure 3.15 Total deformation of (a) HA1, (c) HA4, (d) HAW4, (f) HAW5 and equivalent stress analysis of (b) HA1, (d) HA4, (e) HAW4, (g) HAW5

As seen from the Figures, the simulation is predicted for the experimental value. As observed, the highest tensile value is obtained for the HA4 composite system with improved elongation than HP2. The error magnitude of the experimental values has been evaluated from theoretical analysis as shown in Table 3.2. The % error is achieved within the acceptable range.

Table 3.2 Comparison of tensile strength analysis of experimental data with theoretical data for HA composite series and HAW composite series

Sample	Experimental (MPa)	Theoretical (MPa)	% error
HA1	34.5	34.6	0.29
HA4	34.9	35	0.28
HA3	34.8	35.2	1.13
HA4	36.9	37	0.27
HA5	42.6	42.2	0.95
HAW4	38.9	39	0.26
HAW5	42.8	43.2	0.93

3.2.8 Morphological analysis of HA composite series and HAW composite series

The morphological analysis of the tensile fractured surface of a polymer composite can explain the interaction of filler – matrix system and helps analyze the miscibility of the systems. During the tensile strength analysis of a composite system, the composite undergoes formation of the cavity at the initial stage due to the breaking and detaching of filler with the matrix. It is then followed by the formation of voids leading to its coalescence. Finally, the system undergoes tearing and breakage. The morphology of the fractured surface helps to understand the deformation undergone by the system and the effectiveness of interaction in the composite (Xie et al. 2014).

As observed from the prepared ternary composites, small clusters are observed from the SEM images as shown in Figure 3.16.

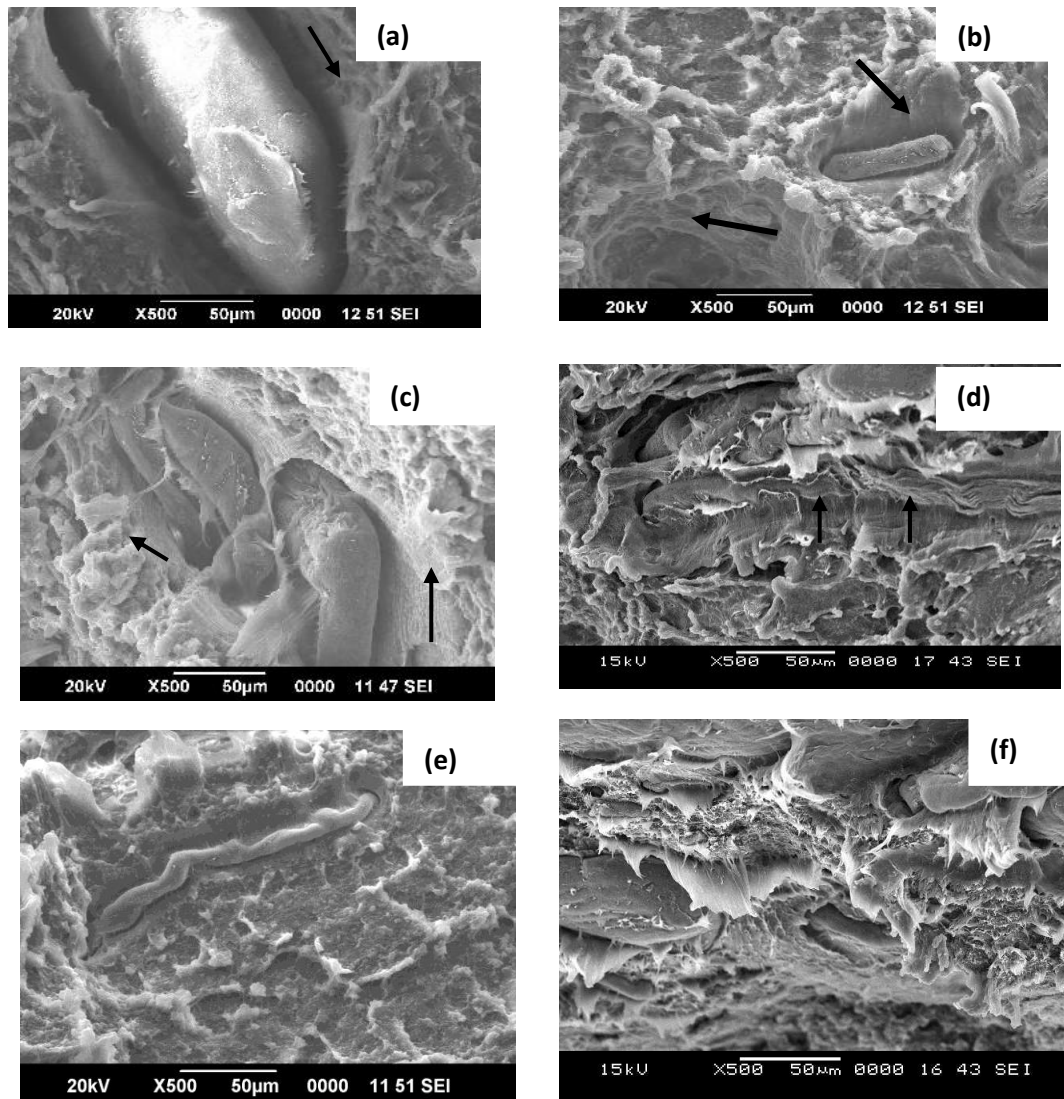


Figure 3.16 SEM images of the tensile fractured surfaces of (a) HA1, (b) HA2, (c) HA4, (d) HA5, (e) HAW4 and (f) HAW5

The formation of large number of clusters is high till 6 wt% hydroxyapatite loading, but it is gradually decreased with 8 wt% hydroxyapatite loading. The wave-like morphology was retained for the HA4 system and the formation of clusters was minimum indicating good matrix-filler interaction. The same morphological appearance was obtained for HAPEXTM systems reported by Wang *et al* (Wang et al. 1998). A fibrous-like appearance observed for HA5, was due to the de-bonding of homogenously distributed hydroxyapatite particles from the composite system. Furthermore, the presence of agglomeration in HAW composite series is observed from the SEM images obtained. The reduced interaction between matrix and fillers in the absence of palm oil has caused agglomerates that lead to the formation of voids (Huang and Zhang 2008).

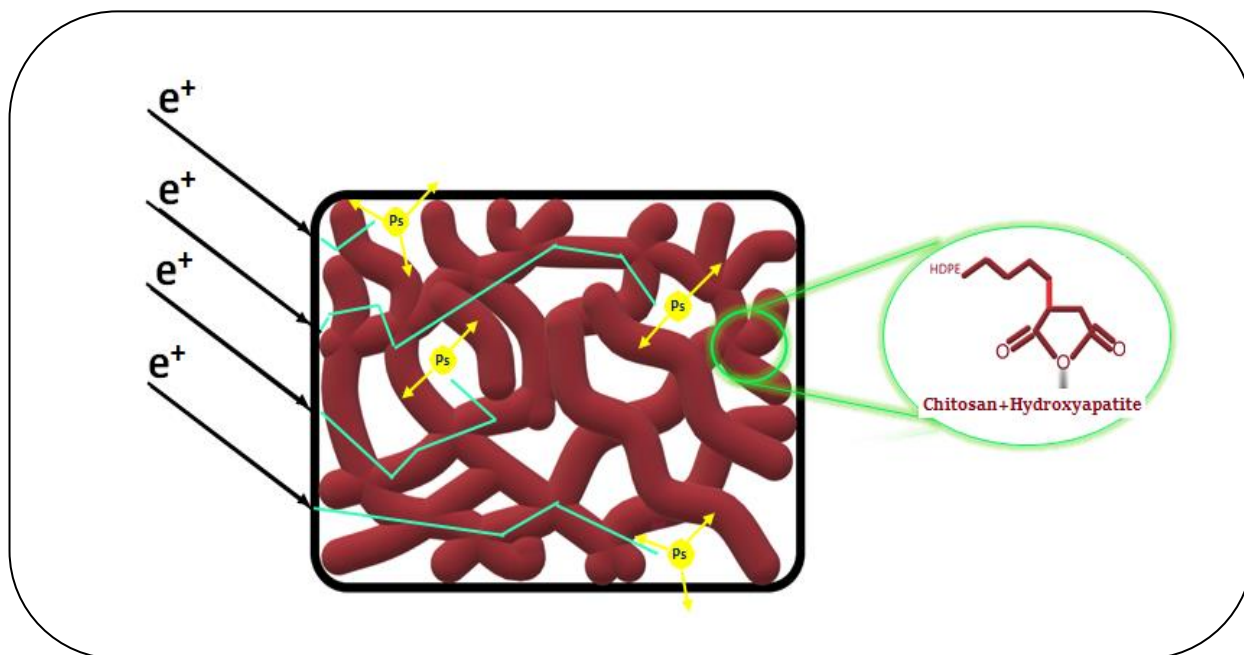
Chapter 4

Microstructural investigation of HDPE / Chitosan Composites and HDPE / Chitosan / Hydroxyapatite Composites

Summary

Microstructural analyses of composites provide a deep understanding of the orientation and interaction of fillers and matrices. The present chapter is focused on the phase identification, interaction and free hole volume formed in the composite system arising from the interaction of chitosan and hydroxyapatite with compatibilized HDPE. The interactions between the components in the composites were analyzed using FTIR-ATR spectroscopy. The phase identification and crystallinity of the prepared systems were studied using X-ray diffractometry (XRD). The formation of free-hole volume in the system formed through the interaction of fillers with the polymer matrix was analyzed using PALS. The analyses confirmed the presence of characteristic properties of the individual components in the system that helps in maintaining the stability of the composite. The microstructural analyses can be further used to investigate and confirm the mechanical, thermal and electrical properties of the system.

Graphical Abstract



4.1 Introduction

Polyolefin composites especially HDPE, LDPE, PP based systems can be compounded with a variety of natural compounds, metallic and inorganic components as fillers to produce a final material for various applications. The size, shape and concentration of the fillers used, particle size distribution, mechanical strain, mixing procedure and preparation conditions plays an enormous role in the interface and microstructural properties of the final composite. The physical properties especially mechanical, thermal, biocompatible and electrical properties of the composite mainly depend on the microstructural arrangement of the components in the composite. Besides these properties, molecular-level information about the structure of the composite can also be utilized to explain the physical characteristics. Miscibility between matrix and filler decides the final properties of the system such as structure, composition, crystallinity, stability and mechanical strength (Sheik et al. 2018). When a material is designed for biomedical applications, mechanical stability is a major

consideration. The microstructural analysis of a composite is generally performed on stressed samples as it alters the microstructural properties of the system. The reorganization of the molecules occurs and results in the improvement of the microstructural analysis of the composite. XRD is one of the most powerful methods for analyzing structural properties in semi-crystalline polymers. For instance, the peak shift to lower 2θ angles indicates a larger interlayer distance, which can be attributed to intermediate dispersion status (Jankovič et al. 2016). An increase in interlayer spacing has been noted in HDPE/CaCO₃/OMMT ternary composite due to the intercalation of HDPE into OMMT (organic montmorillonite) (Dai et al. 2010). Retaining the crystallographic orientation of the individual components after the composite preparation helps to incorporate its characteristics into the final system (Sheik et al. 2018). No shift in peak position in XRD also indicates the purity of the system as observed in oil-palm fiber/clay reinforced high-density polyethylene composites (Essabir et al. 2016). The compatibility and interaction between sisal fibers, chitosan and HDPE were observed from the peak intensity and peak position obtained from the XRD data (Agboola et al. 2021). FTIR analysis also gives information regarding the interfacial interaction between the filler and matrix. Almost all polyethylene-base composites show no considerable difference in the peaks between the pure polyethylene and its corresponding composites as studied from HDPE/graphene composites (Han et al. 2021). The spaces formed in the composite system due to crosslinking result in the formation of pores. The porosity can tune the properties of a system, especially the mechanical stability of the system. The high energy γ quanta can easily pass through the thick walls of a pressure chamber and analyze the nature and pores present in it under high pressure (Zaleski et al. 2015).

Chapter 4 is mainly focused on the microstructural analysis of the HC composite series and HA composite series. The miscibility of filler with matrix, pore formation and phase transformation is discussed in this chapter.

4.2 Results and discussion

4.2.1 Fourier Transform Infrared spectroscopy – Attenuated Total Reflectance (FTIR-ATR) analysis

4.2.1.1 FTIR-ATR analysis of matrix: HDPE and filler: chitosan

The FTIR spectra help in identifying the chemical interactions, crosslinking and identification of functional groups in a composite system. Figure 4.1 shows the spectra of neat HDPE and HC0. The spectra obtained for both the systems are similar, except with slight variations in its intensity and this helps in explaining the semi-crystalline nature to a great extent.

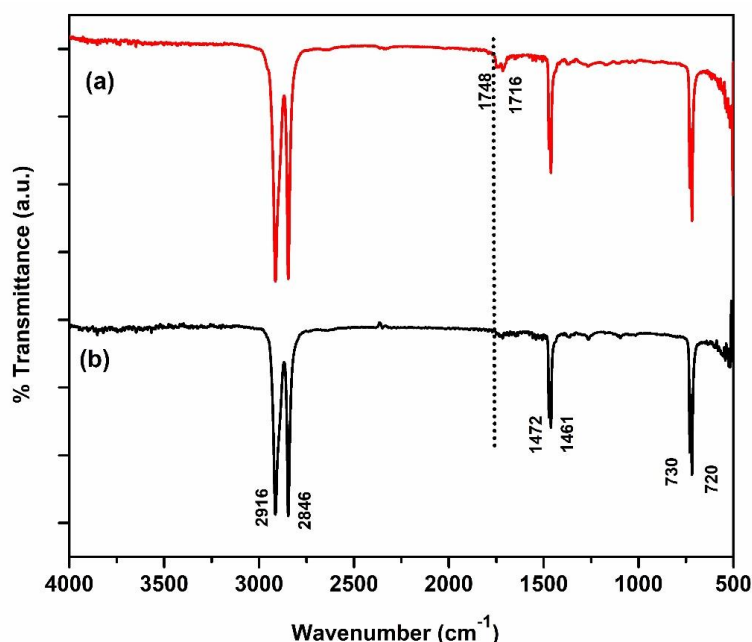


Figure 4.1 FTIR-ATR spectra of (a) HC0 and (b) neat HDPE

The strong intense peaks at 2916 and 2846 cm^{-1} observed for HDPE and HC0 correspond to the CH_2 asymmetric stretching and CH_2 symmetric stretching of the polyethylene polymer chain. The peak at 1090 cm^{-1} in the HDPE spectra can be attributed to the C-C stretching vibrations. This peak is not noticeable in HC0, which can be due to the compatibilizing action of maleic anhydride (Sunilkumar et al. 2012). A weak band at 1266 cm^{-1} observed for HDPE due to asymmetric C-CH bending is also absent in HC0. The peaks at 1472 and 1461 cm^{-1} corresponds to the asymmetric CH_2 bending and CH_2 scissoring respectively. Furthermore, the peak at 720 cm^{-1} is due to the CH_2 rocking. Due to the high crystallinity of HDPE, this peak splits and forms a less intense peak at 730 cm^{-1} . The peaks at 1472 and 730 cm^{-1} correspond to the crystalline phase and peaks at 1461 and 720 cm^{-1} corresponds to the amorphous phase of HDPE. Weak peaks observed at 1094 cm^{-1} (C-C stretching), and 1370 cm^{-1} (CH_2 wagging) in HDPE is slightly broadened for HC0. New peaks at 1716 and 1748 cm^{-1} for HC0 shows the carbonyl peak of maleic anhydride, indicating the interaction of maleic anhydride with HDPE (Ahn et al. 2016, Charles et al. 2009, Pagès 2005).

Figure 4.2. shows the FTIR-ATR spectra of the filler- low-density chitosan. The characteristics peaks are: 3332 cm^{-1} (strong and broad peak stretching peak of O-H overlapped with NH), 2925 cm^{-1} (C-H symmetric stretching), 2863 cm^{-1} (peak axial stretching of CH), 1645 cm^{-1} (C=O stretching, amide I), 1560 cm^{-1} (N-H stretching, amide II), 1419 cm^{-1} (CH_2 bending), 1371 cm^{-1} (CH_3 symmetrical deformation), 1317 cm^{-1} (C-N stretching, amide III), 1148 cm^{-1} (symmetric stretching of C-O-C), 1059 and 1027 cm^{-1} (C-O stretching) (Queiroz et al. 2014).

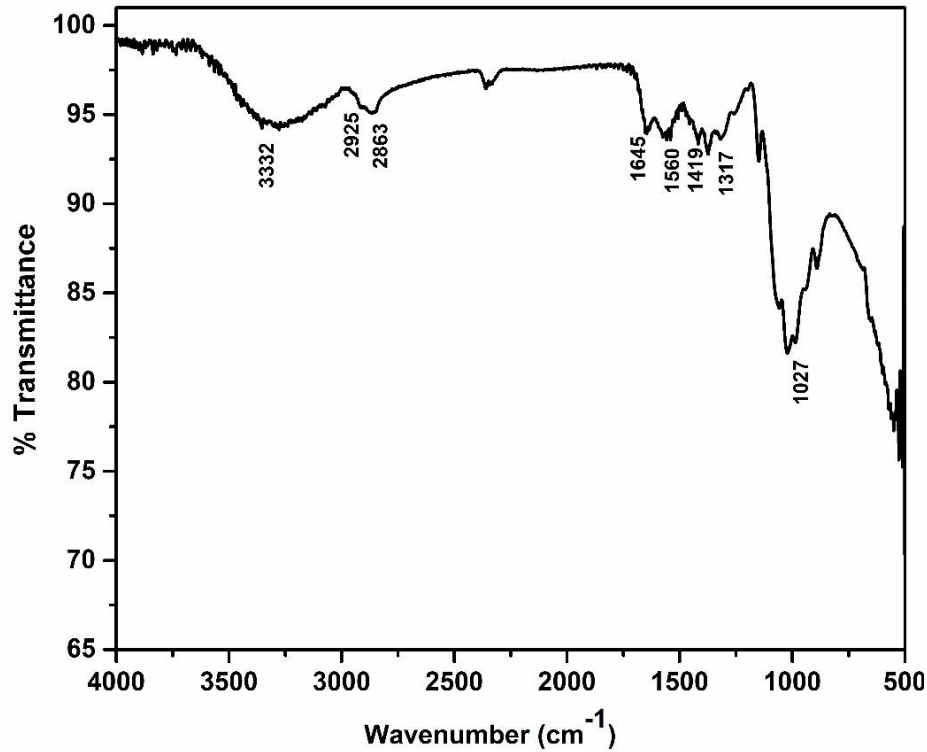


Figure 4.2 FTIR-ATR spectrum of Chitosan

4.2.1.2 FTIR-ATR analysis of HC composite series

An insight into the specific interaction of compatibilized HDPE with varying concentrations of chitosan is studied using FTIR-ATR characterization technique. Figure 4.3. depicts the FTIR-ATR spectrum of HC composite series. Apart from the characteristic peaks of HDPE explained in Figure 4.1., a reduction in peak intensity for all peaks has been observed in all chitosan added composites. On the other hand, the presence of higher concentration of chitosan in compatibilized HDPE shows a reduction in peak broadening and peaks at 1748 cm⁻¹ and 1716 cm⁻¹ indicates the interaction of C-O groups of maleic anhydride with the reactive groups of chitosan. But, for the HC composite system with 10 wt% of chitosan, the filler - filler interaction is dominant leading to agglomeration with an increase in peak intensity at

all the characteristics peaks of chitosan. The slight shift and broadening of peaks at 1371 to 1378 cm^{-1} , 1148 to 1169 cm^{-1} also indicate the interaction of chitosan with the compatibilized HDPE system (Heidari et al. 2016). Hence, no new functional groups were formed during the preparation process, but the peak shift and variation in intensity confirm the formation of HC composite series by retaining the characteristics peaks of the individual components.

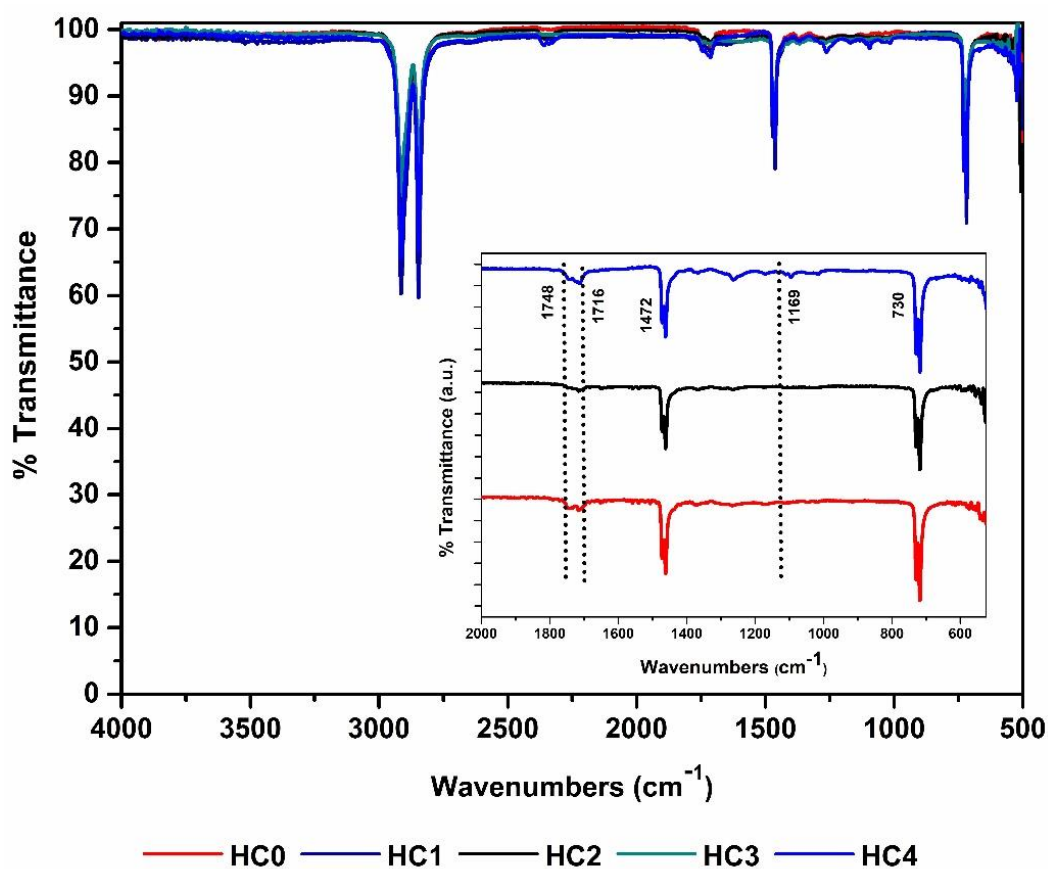
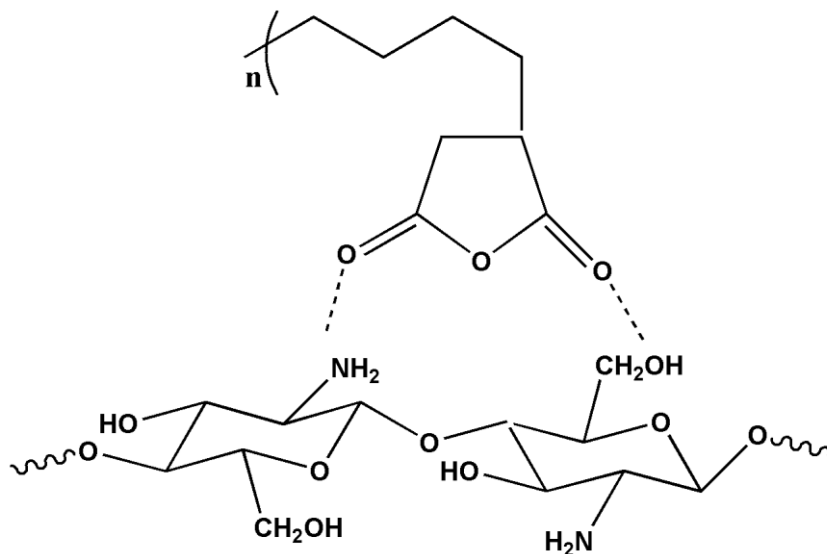


Figure 4.3 FTIR-ATR spectra of HC composite series

The schematic representation of the interaction of chitosan with compatibilized HDPE is shown in Scheme 4.1.



Scheme 4.1 Schematic representation of interaction of compatibilized HDPE with chitosan

4.2.1.3 FTIR-ATR analysis of HP composite series

The FTIR-ATR spectra of HP composite series within the range of 4000 to 400 cm^{-1} , compared with HC2 are presented in Figure 4.4. The addition of varying concentrations of palm oil to HC2 composition has reduced peak broadening which indicates the segmental mobility attained by the composites. The sharp and dominant peaks of HDPE were observed in all HP composite series. The high peak intensity at 1472 and 1461 cm^{-1} is decreased in the presence of palm oil, which shows that, palm oil has acted in the crystalline and amorphous phase of HDPE by enhancing chain relaxation, making it suitable for more interactions within the composite system. It is also notable that, HP2 has the lowest peak intensity at 720 cm^{-1} which further shows the improved interaction of $-\text{CH}_2$ of HDPE with maleic anhydride (Fouad et al. 2013). The peak at 1748 cm^{-1} is broadened in HP2, showing the less availability of reactive groups of maleic anhydride. The peak at 1066 cm^{-1} has been shifted to 1095 cm^{-1} suggesting the presence as well as interaction of chitosan in HP1. But the same peak intensity is very weak for HP2 as observed from the graphs. The characteristic

peaks of chitosan are noted in the spectrum obtained for HP1. But, its intensity is reduced and broadened with higher concentration of palm oil. Hence, the plasticizing effect of palm oil has improved the segmental mobility of the system thereby improving the interaction between chitosan and HDPE.

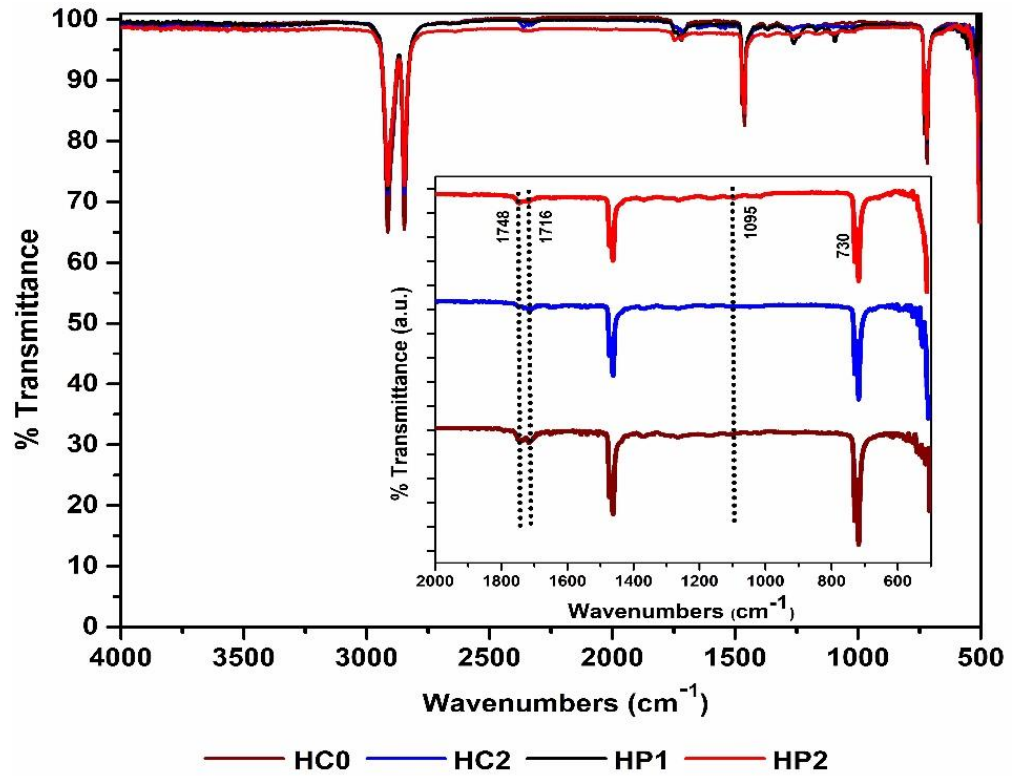


Figure 4.4 FTIR-ATR spectra of HP composite series

4.2.1.4 FTIR-ATR analysis of HA composite series

Hydroxyapatite has been used as filler for the preparation of HA composite series. The characteristics peak of hydroxyapatite is given in Table 4.1. and its corresponding FTIR-ATR spectrum is shown in Figure 4.5.

Table 4.1 FTIR – ATR peaks of hydroxyapatite

Peaks (cm ⁻¹)	Assigned to
3431 and 1640	Presence of lattice water
3578 and 636	Stretching vibration of O-H of hydroxyapatite
870 and 1414	Carbonate ions
572, 606	O-P-O bending
1105-1015	ν_3 P-O asymmetric stretching
1086, 1053	Triply degenerate asymmetric ν_3 P-O stretching modes
603, 571	Triply degenerate vibration ν_4 of O-P-O bonds

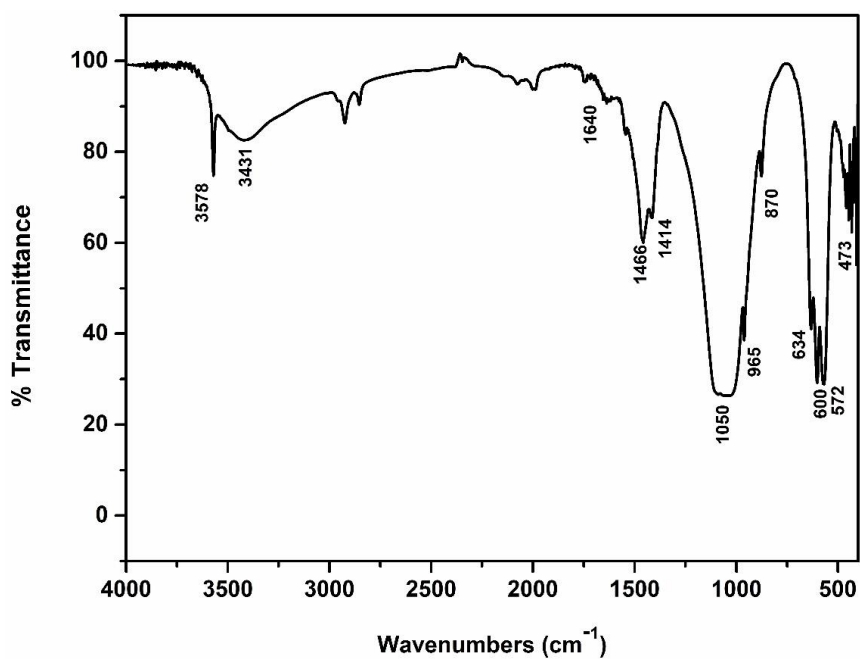


Figure 4.5 FTIR-ATR spectrum of hydroxyapatite

The FTIR-ATR spectra of the HA composite series are shown in Figure 4.6. The most intense stretching and bending vibrations of polyethylene as mentioned in the previous sections is observed in the spectra obtained for HA composite series.

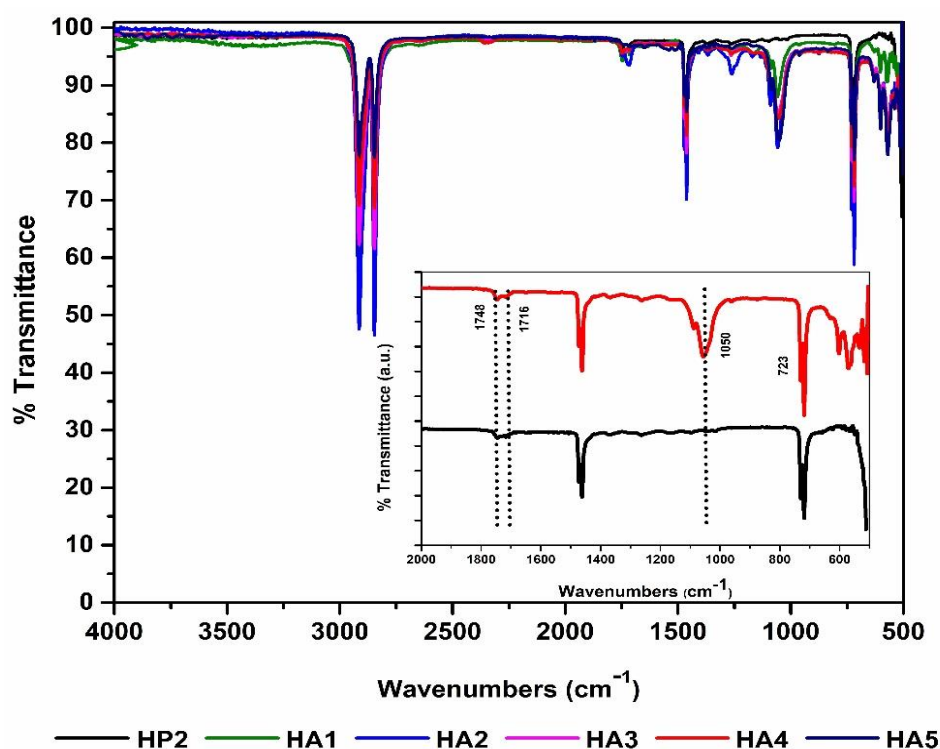


Figure 4.6 FTIR-ATR spectra of HA composite series

The IR findings indicate that HA composite system with 8 wt% of hydroxyapatite has undergone effective interaction. At lower concentrations of hydroxyapatite, the chemical bonding and interactions are not much effective due to the minimum interaction of chitosan and hydroxyapatite as observed from the peak broadening at 3332 cm^{-1} and -NH bending of primary amine obtained at 1594 cm^{-1} . The bending of the hydroxyl group is minimum in HA4 composite system attributing to the lowest peak intensity at 1264 cm^{-1} . The peaks observed in the range of $560\text{--}1100\text{ cm}^{-1}$ gives information about the interaction of the PO_4^{3-} groups of hydroxyapatite with chitosan. Moreover, the broadening of peaks in this region depicts formation of interlinked bonds between hydroxyapatite and chitosan (Dreghici et al. 2020). The broadening of band at 1050 cm^{-1} and 1170 cm^{-1} corresponds to the restrictions of the molecular vibrations of phosphate groups due to the interaction of hydroxyapatite with chitosan (Heidari et al. 2015, Kim et al. 2009). The peak intensity of HA4 is observed to be

minimum due to the improved crosslinking and reduction in unsaturated groups present in the system (Fouad et al. 2013). The peaks at 1088, 963, 630, 602 and 569 cm^{-1} are decreased / broadened, pointing to the hydroxyapatite phase and its miscibility in the composite system.

4.2.1.5 FTIR-ATR analysis of HAW composite series

FTIR-ATR spectra of HAW composite series compared with HP2, HA4 and HA5 are shown in Figure 4.7.

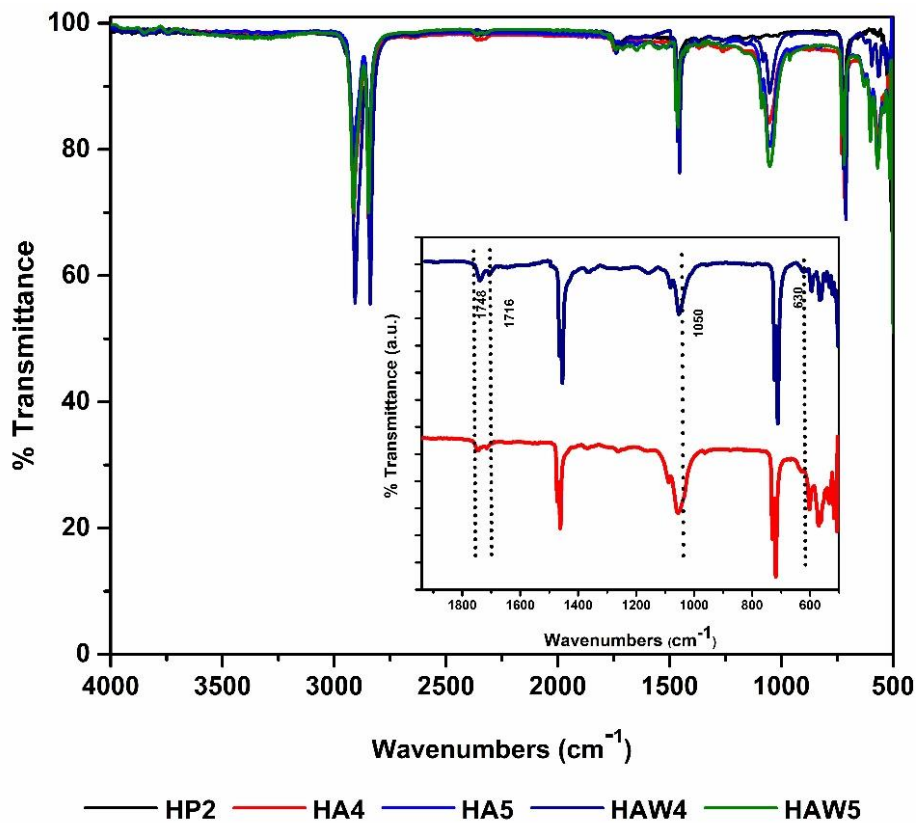
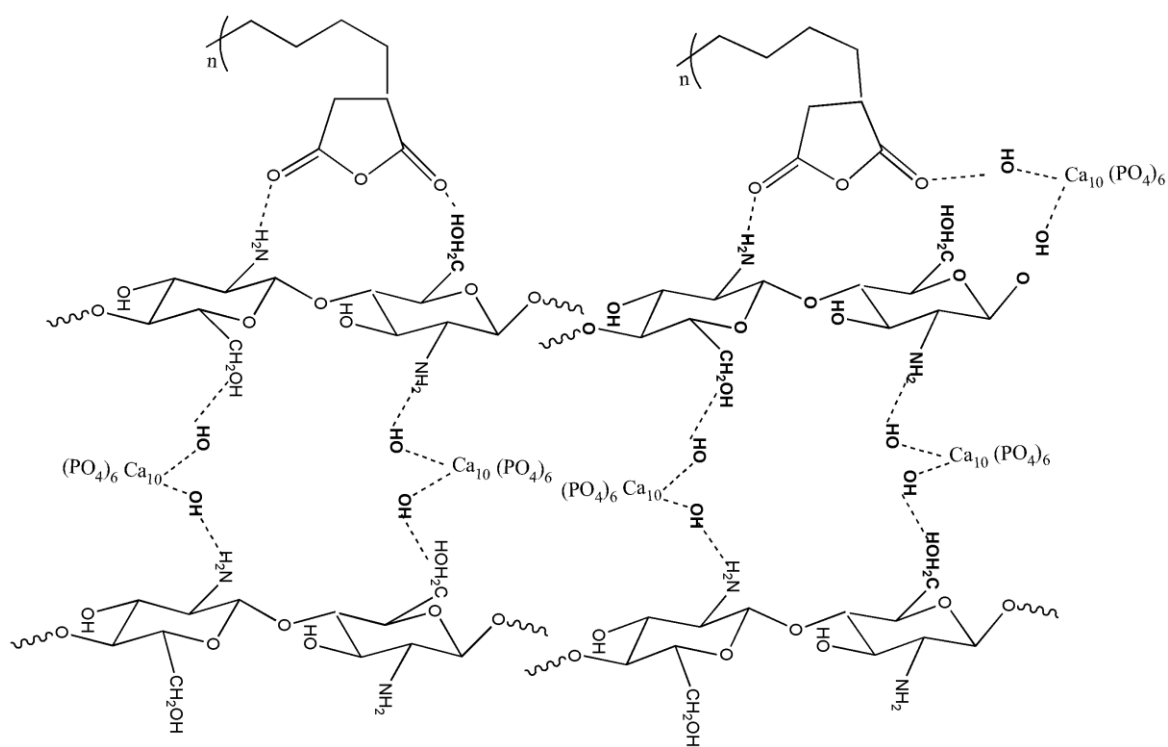


Figure 4.7 FTIR-ATR spectra of HAW composite series

All spectra exhibited similar appearance in peaks with slight broadening and variation in peak intensity but still showed the characteristic peaks of hydroxyapatite. The palm oil plasticized samples showed low peak intensity in all spectra indicating a reduction in the unsaturated groups which is due to the improved interaction. Minimum

interaction between hydroxyapatite and chitosan in un-plasticized systems was observed from the peak at 630 cm^{-1} , due to the stretching vibrations of O-H of hydroxyapatite. But, the presence of palm oil reduced the strong intermolecular interactions in the systems making the system available for more effective interactions. In the composite system, palm oil has acted as an effective catalyst as well as plasticizer by improving the flexibility within the composite. A schematic representation of the interaction of maleic anhydride compatibilized HDPE with chitosan is shown in Scheme 4.2.



Scheme 4.2 Schematic representation of interaction of chitosan and hydroxyapatite with compatibilized HDPE

4.2.2 X-ray diffractometry (XRD)

4.2.2.1 XRD analysis of HC composite series

The XRD patterns shown in Figure 4.8 revealed the characteristics peaks of HDPE polymer matrix and chitosan in all the spectra measured. The characteristic peaks of HDPE obtained at $2\theta = 21.7^\circ$, 24.1° and 36.4° scattering from (110), (200) and (020) respectively of the HDPE crystal lattice (ICDD # 53-1859) are observed in all spectra.

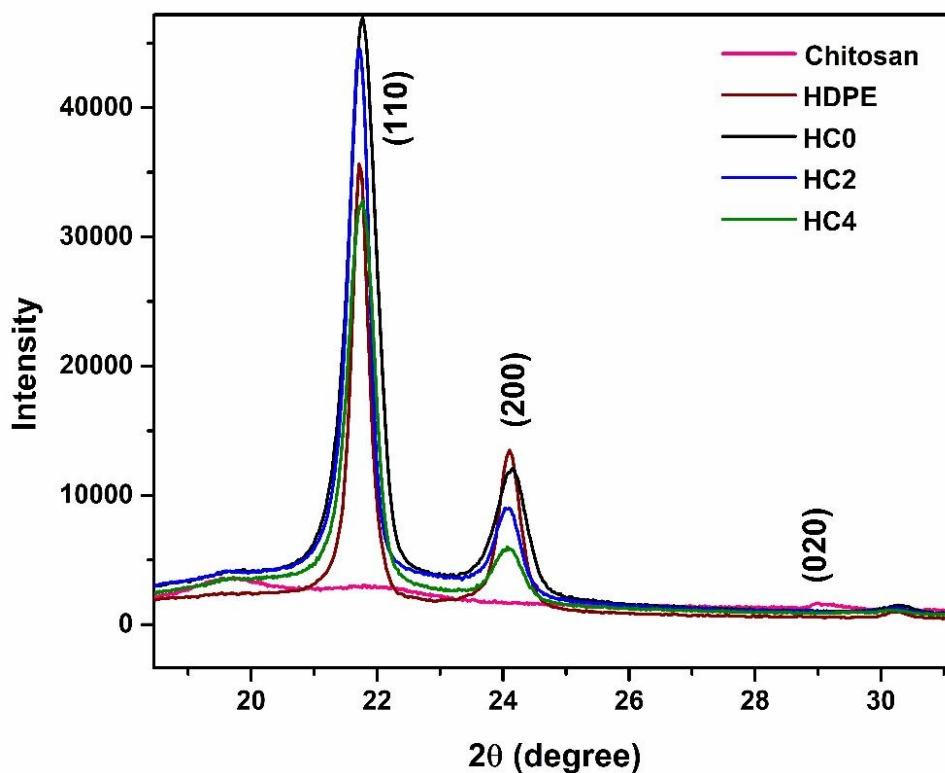


Figure 4.8 XRD spectra of HC composite series

The moderate intensity peaks appearing above 40° correspond to semi-crystalline nature of HDPE matrix. This shows that the HDPE under investigation has an orthorhombic structure (Benabid et al. 2019). However, the peaks at 19.7° and 9.3° indicate the amorphous nature of chitosan. When neat HDPE is compatibilized with maleic anhydride, the peak intensity is increased, indicating an increase in crystallinity as observed in Table 4.2. The XRD spectrum suggests a good interaction

as well as fine compatibility between chitosan and HDPE. There are no specific peaks corresponding to chitosan which shows that it is amorphous in nature. On adding chitosan, a reduction in crystallinity is observed at lower diffraction angles, indicating the amorphous nature attained by the composites. However, the sharp peaks observed from the graphs indicate the semi-crystalline nature retained by the composites with the addition of chitosan as filler.

4.2.2.2 XRD analysis of HP composite series

The basic peaks of HDPE and chitosan have not changed in the XRD spectra of HP composite series as shown in Figure 4.9. The characteristic peak of chitosan at $2\theta = 20^\circ$ has been masked by HDPE as observed from the graph. The presence of palm oil has not produced any phase transformations during the processing of the composites.

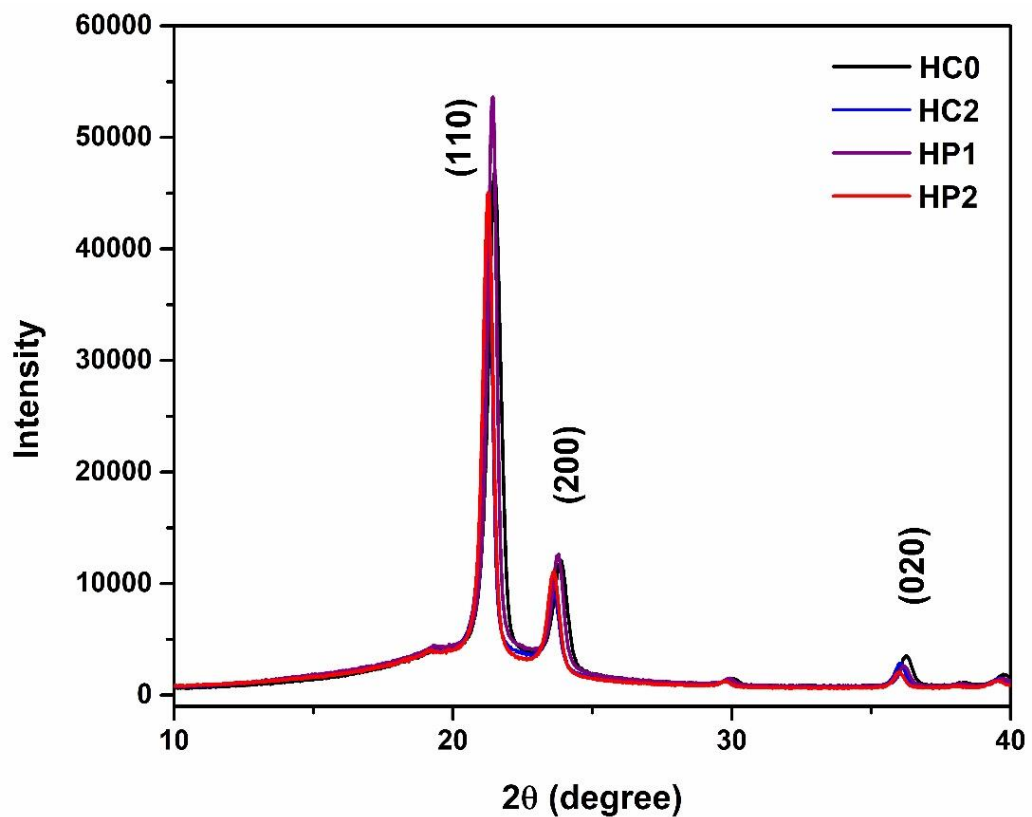


Figure 4.9 XRD spectra of HP composite series

4.2.2.3 XRD analysis of HA composite series

The XRD spectra of HA composite series are depicted in Figure 4.10. The characteristic peaks of hydroxyapatite at $2\theta = 26.1, 31.9, 32.3, 33$ and 36.4° scattering from the lattice planes (002), (221), (222), (060) and (026) respectively are observed in all spectra.

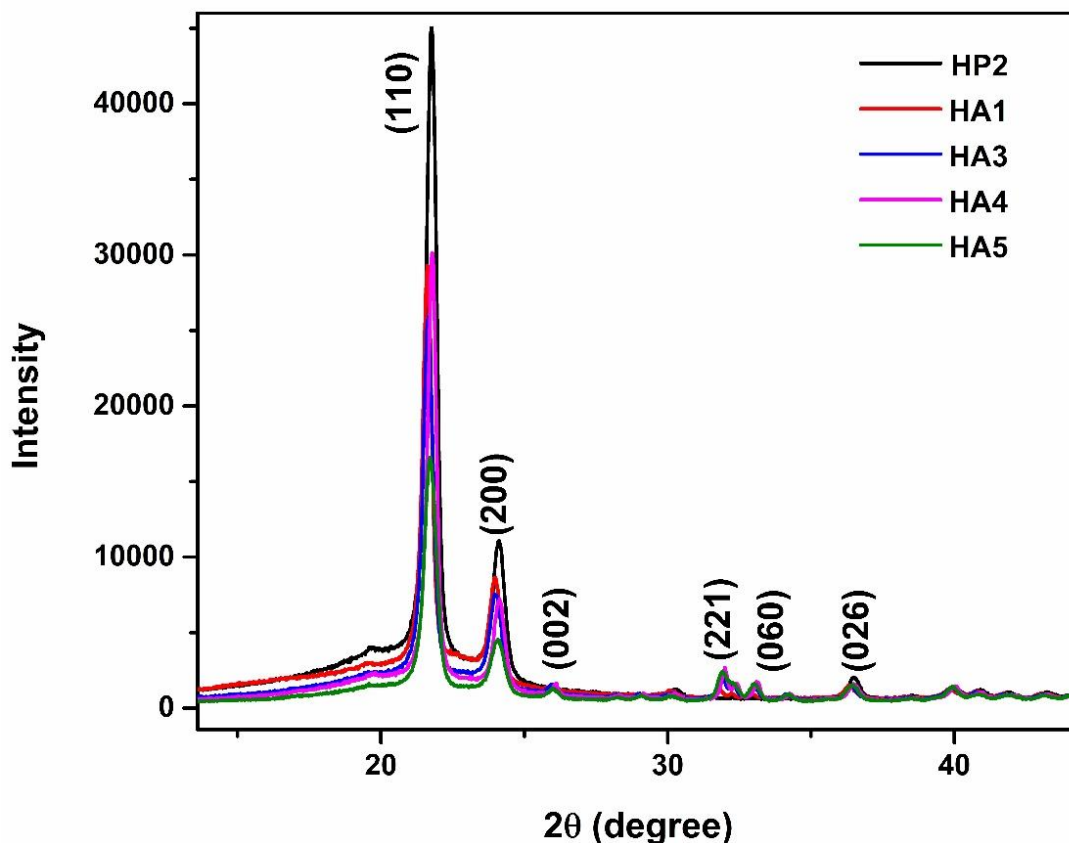


Figure 4.10 XRD spectra of HA composite series

The peaks obtained shows that the crystallographic structure of hydroxyapatite is analogous to the natural bone mineral (Shakir et al. 2015 b). Also, the presence of characteristic peaks of HDPE, chitosan and hydroxyapatite in the XRD spectrum shows the non – interference of crystal planes, which shows that, the chemical interactions are lesser when compared with the adhesions in the prepared systems

(Jaggi et al. 2012). A slight variation in peak intensity owing to the presence of hydroxyapatite can be attributed to the variation in size of the filler particles resulting in lattice strain in the system (Rahman et al. 2018). Furthermore, peak broadening at lower diffraction angles has reduced with the addition of hydroxyapatite, indicating increased crystallinity achieved by the system.

4.2.2.4 XRD analysis of HAW composite series

Some distinct differences in peak position were observed for HAW composite series when compared with HA4 and HA5 as shown in Figure 4.11.

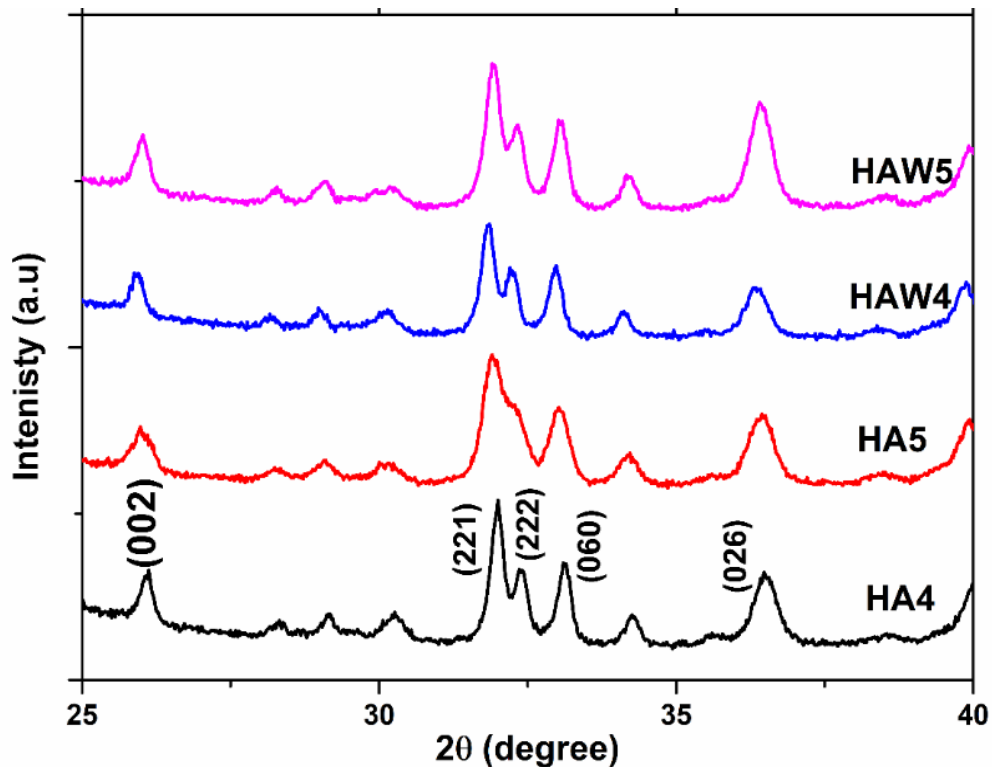


Figure 4.11 XRD spectra of HAW composite series

The pronounced peak of hydroxyapatite is observed in all spectra. The peak of HA5 corresponding to the crystal plane (222) has been broadened owing to the possibility of formation of agglomeration at higher concentration of hydroxyapatite. This can be

ascribed to the increase in particle size.(Heidari et al. 2015). The agglomeration results in lowering the crystallinity of HA5 composite system.

Table 4.2 shows the % crystallinity of the prepared HC composite series. An increase in the amorphous content in HC composite series is observed with incremental addition of chitosan. The addition of 5 wt% of chitosan to compatibilized HDPE has disrupted its hydrogen bonding resulting in reduction of crystallinity from 53.3 % to 35.7% (Agboola et al. 2021). On further addition of chitosan, the crystallinity is increased to 40.7% due to a much better packing achieved by the system. Higher crystallinity is formed due to the effective interaction of the system arising from the alignment of the fillers during the melt mixing process. This leads to enhanced interaction that provides uniform packing of fillers forming a more organized composite material (Islam et al. 2015).

Table 4.2 % crystallinity of HC composite series and HP composite series

Sample	Chitosan	HC0	HC2	HC4	HP1	HP2
% crystallinity	18.3	53.3	35.7	40.7	39.4	41.3

The addition of hydroxyapatite to the HP2 composite system improved the crystallinity of the resulting HA composite systems as shown in Table 4.3. HA4 system showed a crystallinity of 53 % indicating its closeness to HC0. The addition of 8 wt% hydroxyapatite marked a homogeneous distribution of filler in the matrix which caused an improvement in the crystallinity of the system. The interaction of highly crystalline hydroxyapatite with the optimized HP2 system gives a more crystalline material.

Table 4.3 % crystallinity of HA composite series and HAW composite series

Sample	Hydroxyapatite	HA1	HA3	HA4	HA5	HAW4	HAW5
% crystallinity	47.08	48.8	53	86.2	74.3	80	71

4.2.3 Positron Annihilation Lifetime Spectroscopic (PALS) analysis

4.2.3.1 PALS analysis of HC composite series and HP composite series

Positron Annihilation Lifetime Spectroscopy (PALS) helps in the analysis of the formation of free holes or pores at the nanometer or sub-nanometer level. The third lifetime, τ_3 of ortho-positronium o-Ps, provides wide information on the structure of solids. The lifetime and intensity (I_3) depend on the electron density as well as the size of free holes formed (Jankovič et al. 2016). Table 4.4. shows the PALS studies of the HC composite series. The lifetime of ortho-positronium, τ_3 and intensity of o-Ps signal, I_3 helps to know the mean free volume of the polymer composite under study. τ_3 is mainly associated with the size of the free hole volumes. In general, when the concentration of the filler increases, the free hole volume decreases. But, depending on the inter and intra molecular interactions and crosslinking of the components, a variation in τ_3 is observed. A reduction in τ_3 is observed for HC2, directing to the formation of holes with minimum size. When the size of free hole increases, the electron density surrounding the o-Ps decreases, and it takes time to annihilate. Due to this reason, I_3 also increases, indicating an increase in number of the free volume sites leading to higher number of o-Ps formation and trapping sites (Forsyth et al. 1995). The annihilation of o-Ps in the amorphous region results in maximum τ_3 in HC1 composite system.

Table 4.4 PALS studies of HC composite series and HP composite series

Sample	$\tau_3(\text{ns})\pm 0.010$	$I_3\pm 0.16$	$V_f(\text{\AA})^3\pm 0.96$	$F_v\pm 0.003$
HC0	2.15	16.30	111.96	0.127
HC1	2.18	16.38	114.90	0.131
HC2	2.06	16.55	103.21	0.118
HC3	2.17	14.72	113.88	0.114
HC4	2.16	15.88	112.86	0.124
HP1	1.94	25.70	91.94	0.164
HP2	1.90	25.63	88.25	0.157

The average free volume size V_f , obtained in HC2 shows a more homogeneous distribution of fillers in the HDPE matrix. Higher the value of F_v in HC0 and HC1 shows the available free space in the system after the interaction. In the presence of chitosan beyond the optimum concentration, a variation in F_v is noted. It can be used as a tool to predict the agglomeration in the system beyond the optimum concentration. Furthermore, the free volume size in HP composite series are lower than HC2 as shown in Table 4.4. HP2 shows a reduction in τ_3 which signifies the enhanced interaction between the filler and the matrix, which resulted due to the improved segmental mobility and relaxation of polymer chains. A reduction of free volume by 20 \AA^3 and I_3 by 8% in HP2 depicts the formation of free holes with smaller size and higher free volume concentration (Zeng et al. 2011). The long alkyl chains of palm oil have played a role in movement of polymer chains enabling the enhanced interaction and dispersion of chitosan in HDPE. Also, the probability of migration of palm oil into the voids created during mixing process has also contributed to the

reduction in pore size (Behzad et al. 2004). The F_v in palm oil plasticized composites are much higher that confirms the easier relaxation of polymer chain with the addition of plasticizer (Zeng et al. 2011).

4.2.3.2 PALS analysis of HA composite series and HAW composite series

The formation of a polymer composite requires specific interactions and miscibility of the components in the system. This led to the formation of free holes due to the irregular molecular packing in the amorphous phase. The effect of varying concentrations of hydroxyapatite on the HP2 composite system on the free hole volume of the composite is given in Table 4.5.

Table 4.5 PALS studies of HA composite series

Sample Code	$\tau_3(\text{ns}) \pm 0.010$	$I_3 \pm 0.16$	$V_f(\text{\AA})^3 \pm 0.96$	$F_v \pm 0.003$
HA1	1.89	26.63	87.39	0.161
HA2	2.05	21.92	102.26	0.156
HA3	1.90	27.03	88.49	0.166
HA4	2.19	15.92	115.82	0.128
HA5	2.11	15.26	108.07	0.114

As observed from Table 4.5., the free hole volume is low at a lower concentration of hydroxyapatite. Initially, a lower amount of hydroxyapatite has bound to palm oil during the mixing process, making considerable changes in the system. As a result, τ_3 of HA1 is very much closer to HP2. This is also reflected in the V_f values of HA1. When the concentration of hydroxyapatite is further increased, the free hole volume, V_f is also increased. This can be related to the miscibility of chitosan and

hydroxyapatite with compatibilized HDPE. Yet, HA4 shows the lowest F_v value, indicating the formation of a large number of pores with minimum pore size. This is an essential property for a bio-implant material, as it promotes porosity and mechanical stability to the composite material, making it suitable for cell proliferation. Beyond the optimum concentration, the filler - filler interaction exceeds filler - matrix interaction leading to agglomeration causing a reduction in V_f . The small hydroxyapatite particles occupy the pores formed during the mixing process and reduce the pore volume to a great extent (Joshi et al. 2006). The positron lifetime parameter of HA4 and HA5 composite series compared with HAW composite series are shown in Table 4.6.

Table 4.6 PALS analysis of HAW composite series

Sample Code	$\tau_3(\text{ns}) \pm 0.010$	$I_3 \pm 0.16$	$V_f(\text{\AA})^3 \pm 0.96$	$F_v \pm 0.003$
HA4	2.19	15.92	115.82	0.128
HA5	2.11	15.26	108.07	0.114
HAW4	1.88	25.40	86.44	0.152
HAW5	1.82	27.03	81.07	0.152

The o-Ps lifetime of HAW4 and HAW5 is lower than its corresponding plasticized samples. The presence of palm oil increases the segmental mobility that enables more interaction of components in the system. But, in the absence of palm oil, the hydroxyapatite particles tend to occupy the pores, rather than interacting with the components in the system. This has resulted in high intensity with a large number of voids.

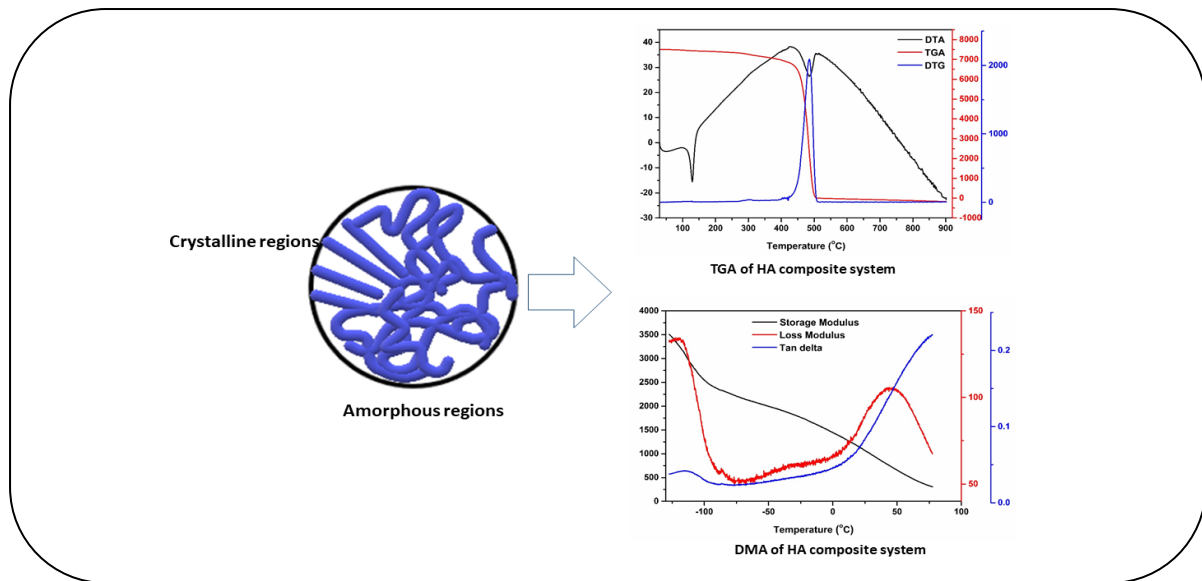
Chapter 5

Thermal Analysis of High Density Polyethylene / Chitosan Composites and High Density Polyethylene / Chitosan / Hydroxyapatite Composites

Summary

Thermal and viscoelastic properties of HC composite series and HA composite series were analyzed and compared. The effect of palm oil as a plasticizer on the thermal stability of the composites was investigated. The thermal stability of the composites was determined from the activation energy analysis obtained from the Coats Redfern model. Among the HC composite series, HC2 exhibits good thermal stability due to the homogeneous dispersion of chitosan in the matrix and effective interaction in the system. The addition of varying concentrations of hydroxyapatite to the optimized plasticized system (HP2) affected the degradation behavior of the ternary systems. The dynamic mechanical analysis (DMA) of the synthesized composites revealed the effect of chitosan and hydroxyapatite in the amorphous region of the HDPE matrix. The calculation of the glass transition temperature (T_g) from loss modulus values brought to light the homogeneity of the prepared composites. The limitation of movement in the polyethylene chains shows the effect of fillers in the amorphous region of the composite system. A thermally stable composite was established for bone-tissue engineering applications

Graphical Abstract



5.1 Introduction

Thermal analysis is one of the most effective and useful analytical techniques in material science to study the chemical and physical stability of the system. The continuous advancement in thermal analytical methods helps to know precisely the material property of a system with respect to temperature. Depending upon the material under consideration, the thermal analysis techniques are classified as: (a) Thermogravimetric analysis (TGA); (b) Differential thermal analysis (DTA); (c) Differential scanning calorimetry (DSC); (d) Dynamic mechanical analysis (DMA); (e) Evolved gas analysis; (f) Laser flash analysis (LFA); (g) Thermo – optical analysis (TOA); (h) Dielectric thermal analysis (DEA); and (i) Dilatometry (DIL).

TG-DTA is an important tool in analyzing the thermal stability of a composite system. For biomaterial systems, thermal studies beyond the normal body temperature (37 °C) are conducted using thermal analysis techniques. This helps to understand the property of the biomaterial under study at higher temperatures during the sterilization process (Shakir et al. 2015 b). Ternary composites exhibits better thermal stability

than binary composites due to the increased miscibility formed in the systems. When inorganic fillers are added for the preparation of composites, they protect the matrix phase and make the composite thermally resistive. An increase in decomposition temperature from 404 °C to 510 °C has been reported for HDPE/CaCO₃/OMMT ternary composite when compared with HDPE polymer system (Dai et al. 2010). The physical properties including interfacial interactions of the components of the composites at varying temperature/frequency can be analysed with the help of DMA (Bashir 2021). Generally, polymers and composites respond to the energy of motion especially as elastic and viscous response. DMA is also an effective method in determining the glass transition temperature (T_g) of the system. The fillers and the additives play a major role in determining the storage modulus, loss modulus and tan delta of the system. They restrict the movement of polymer chains at higher temperature by forming bonds and hence cause an effective crosslinking in the system. The storage modulus of the ternary system is generally observed to be higher than the neat polymer matrix at higher temperature as observed from the DMA analysis of HDPE/CaCO₃/OMMT composites. The improved miscibility between the matrix phase and reinforcement is observed through shift in peaks as well as the peak intensity. The intercalation effect between the components in the system has restricted the movement of polymer chains and formed better interaction within the composites (Dai et al. 2010). The effect of plasticizers in the inter-chain bond interactions can be easily evidenced from the loss modulus, storage modulus and damping parameters obtained from the DMA analysis. Higher the intermolecular interactions in the composite, higher the storage modulus obtained for the system (Sanyang et al. 2015).

The present work is focused on determining the thermal stability and viscoelastic properties of HC composite series and HA composite series composites with

temperature. The variation of decomposition temperature gives an idea about the miscibility of the fillers with compatibilized HDPE. The viscoelastic properties like storage modulus, loss modulus and damping parameters are analyzed to study the interphase properties in the crystalline and amorphous phases. The role of chitosan and hydroxyapatite on the structural orientation and thermal stability of the prepared HC composite series and HA composite series has been analyzed. The modification of composites under molecular level, crystallinity, glass transition temperature (T_g), interphase properties and stability is studied and explored using TGA and DMA analysis.

5.2. Results and discussion

5.2.1 Thermogravimetric analysis (TGA)

Thermal analysis of polymer bio-composites plays a major role in understanding the stability of the composites beyond the processing temperature. At elevated temperatures, the structural and mechanical stability of the composites decreased that led to the decomposition of the system.

5.2.1.1 Thermogravimetric analysis of HC composite series

Thermogravimetric analysis (TGA) of chitosan, un-compatibilized HDPE (HDPE) and its corresponding compatibilized sample, HC0 are shown in Figure 5.1. The interaction of maleic anhydride with HDPE is easily understood from the TGA analysis. HDPE consists of well-stacked long linear polymer chains leading to strong intermolecular hydrogen bonding interactions. This increased the thermal stability of HDPE, with its degradation temperature ranging from 390 – 505 °C. HC0 also showed a single-step degradation similar to HDPE. With the addition of maleic

anhydride to HDPE, an earlier degradation starting at 350 °C was observed for the resulting composite system, HC0. This can be attributed to the compatibilizing effect of maleic anhydride leading to the weakening of strong intermolecular hydrogen bonding in HDPE (Avalos et al. 2017).

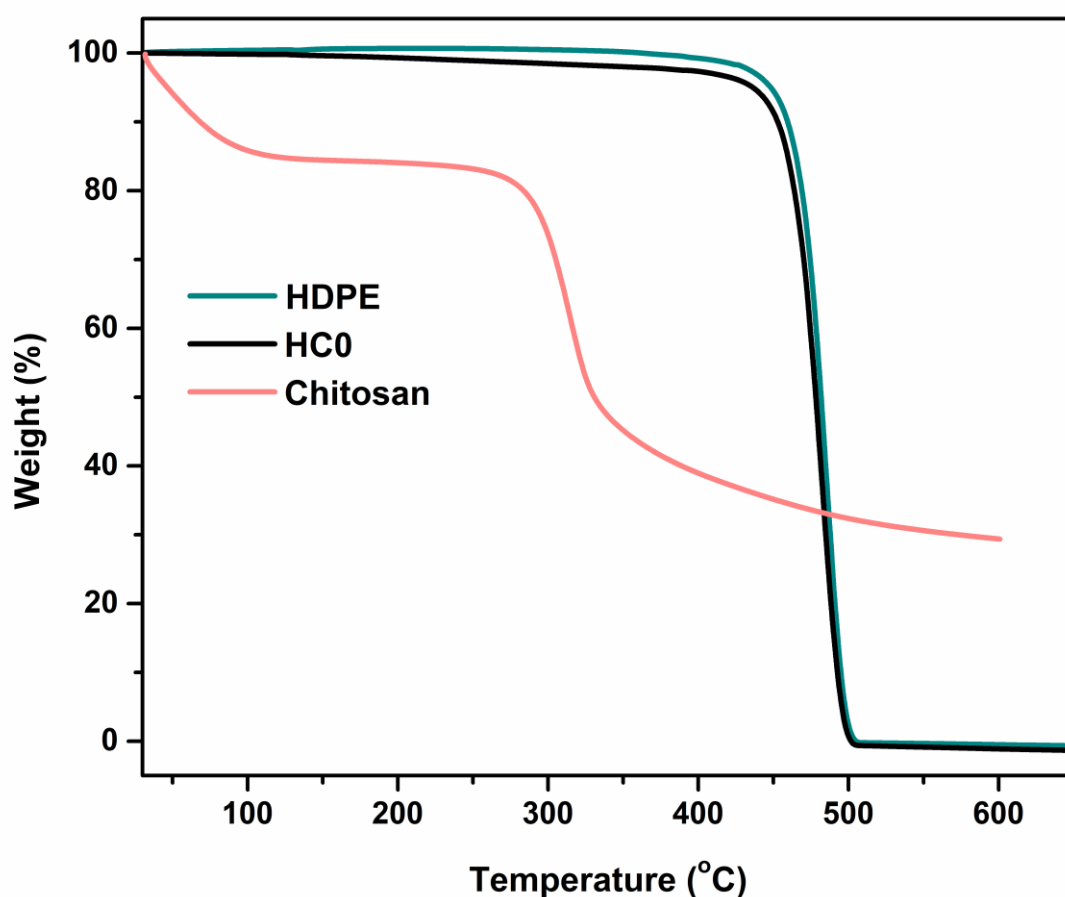


Figure 5.1 TGA of HDPE, HC0 and chitosan

Natural polymers have high thermal degradation rate than synthetic polymers, as observed from the TGA of chitosan. The thermal degradation of chitosan shows a three-step process: (a) nearly at 100 °C (b) 200 – 300 °C; and (c) > 400 °C, corresponding to the evaporation of trapped moisture, dehydration of the monomer units, depolymerization and decomposition of chitosan molecules (Sunilkumar et al. 2012).

The thermal behavior provides an understanding about the applications, compatibility and processing temperature of a material. The thermal degradation properties of HC composite series are shown in Figure 5.2.

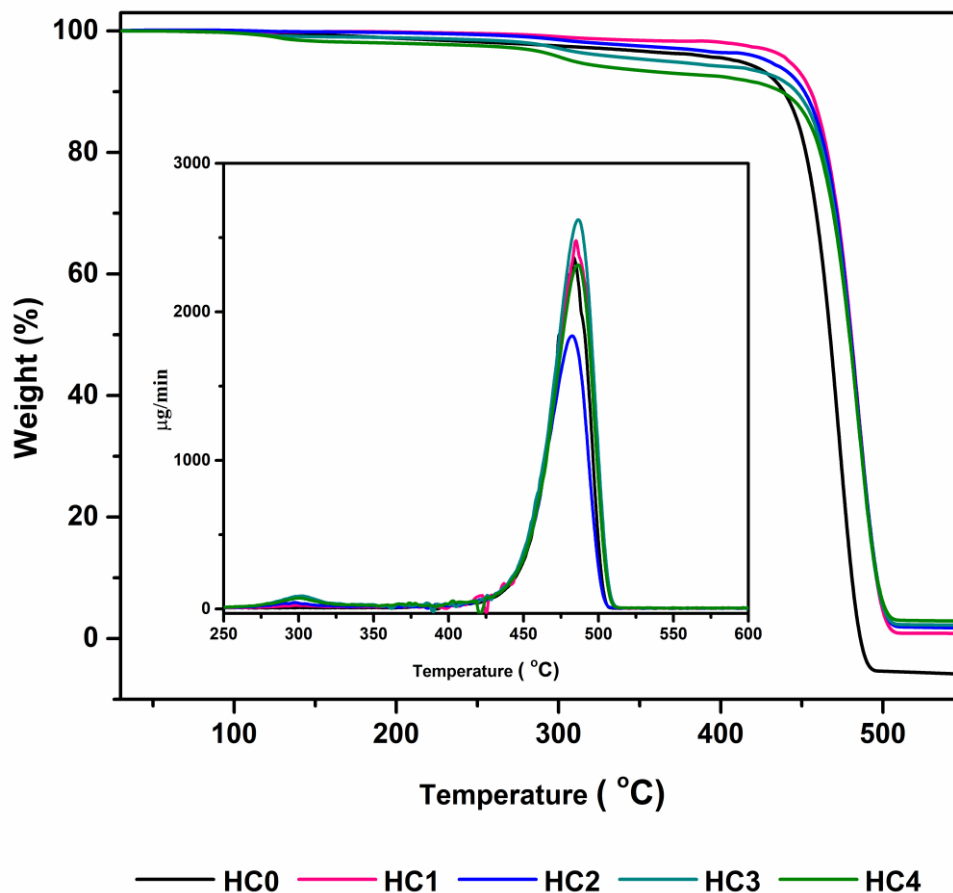


Figure 5.2 TGA and DTG (inset) analysis of HC composite series

The thermal degradation of HC composite series showed a similar trend in decomposition behavior to HC0 as seen from the graphs. The weight (%) vs change in temperature of the HC composite series remains unchanged till 350 °C. Also a two-stage degradation step is prominent in HC composite series which starts from: (a) 270 – 370 °C, a minor degradation resulting in dehydration of the monomer units of chitosan; and (b) 420 – 506 °C, a rapid single major degradation of the saturated and unsaturated groups of the remaining composite material. HC1 shows degradation stage in the range of 420 – 510 °C. At lower concentration of chitosan, maximum

interactions occurs with compatibilized HDPE chains. These interactions along with the unreacted HDPE polymer chains results in a stiff system that leads to a shift in degradation temperature to 484 °C for HC1 composite system. Furthermore, the degradation temperature of HC2 showed a slight shift to 482 °C. HC3 and HC4 shows an early commencement of thermal degradation, which can be ascribed to the low miscibility observed in the system due to the formation of agglomeration beyond the optimum concentration. The probability of formation of agglomeration could also contribute to the low thermal stability of the systems. Overall, the presence of chitosan has increased the thermal stability of compatibilized HDPE, which is similar to the study conducted by Koffi *et al* (Koffi et al. 2021).

5.2.1.2 Thermogravimetric analysis of HP composite series

Figure 5.3. present the TGA and DTG (inset) analysis of HC0, HC2, HP1 and HP2.

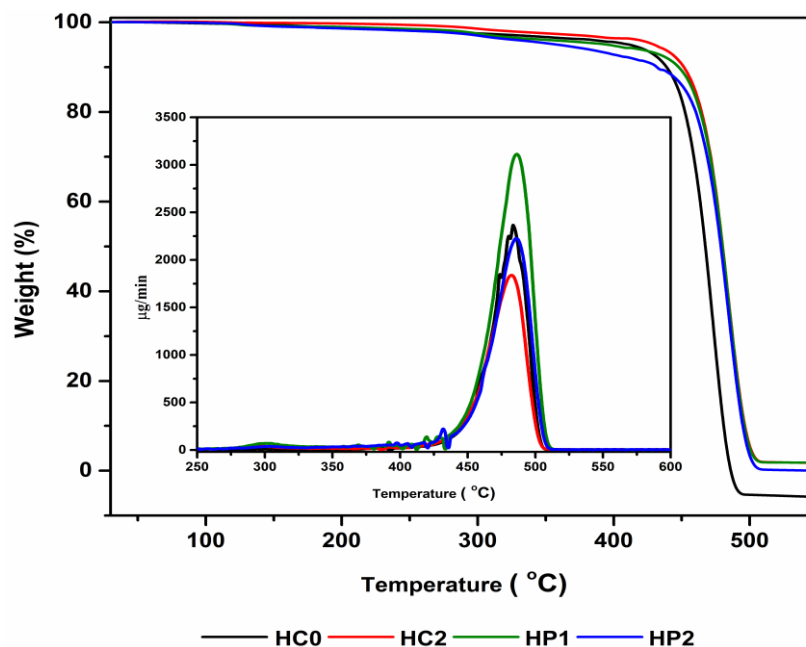


Figure 5.3 TGA and DTG (inset) analysis of HP composite series

As observed from the graphs, the initial stage in degradation temperature of HP composite series are lowered with the addition of palm oil as plasticizer. The

segmental mobility attained in the system and the weakening of strong polymer chains has resulted in this slight decrease. The presence of long chains of palm oil in the system could be another reason for the earlier degradation of HP1 and HP2 (Surender et al. 2015). The DTG analysis also shows a single shoulder peak which further supports the TGA analysis.

5.2.1.3 Activation energy analysis of HC composite series and HP composite series

The TGA images of HC and HP composite series shows same degradation trends, indicating similar pyrolysis behavior for the composites. These indicate the similarity of chemical bond formation and interactions observed in the final molecular structure of composite. The DTG analysis also shows a single peak for all composite series. The kinetic degradation of the composites studied using Coats Redfern model provides data about the activation energy and degradation mechanism of the systems. The activation energy values of HC and HP composite series are given in Table 5.1.

The activation energy of HC0 is obtained at 324 kJmol^{-1} which is higher than the values obtained for pure HDPE at 248 kJmol^{-1} as reported by Aboulkas *et al* (Aboulkas et al. 2008). HC2 shows the highest activation energy value (348 kJmol^{-1}) among the HC composite series. This can be ascribed to the good interfacial stability and homogeneity of filler dispersion in the composite matrix. The restricted mobility of the chains at higher temperature provides better thermal stability. When varying concentration of palm oil is added, a slight increase in activation energy is observed. On adding 5 wt% palm oil, the activation energy is increased to 348.2 kJmol^{-1} indicating enhanced interaction and better homogeneity that results in good thermal stability.

5.2.1.4 Thermogravimetric analysis of HA composite series

Thermal studies play a foremost role in designing a bio-composite as it needs to be employed in sterilization process before being applied to normal body temperature conditions (Fouad et al. 2013). The thermal degradation of HA composite series are shown in Figure 5.4.

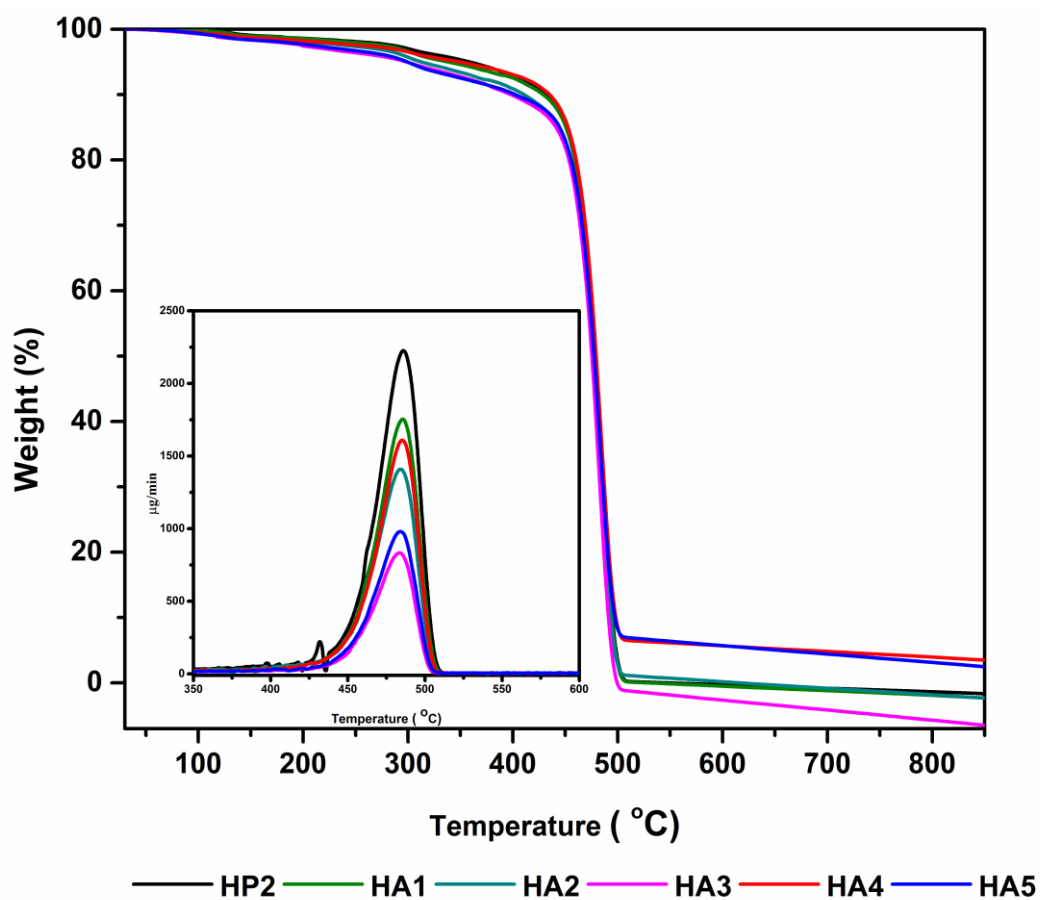


Figure 5.4 TGA and DTG (inset) analysis of HA composite series

The thermogram and degradation behavior of HA composite series are comparable to the HC composite series as discussed in Section 5.2.1. Besides, the one step degradation of HC0 (between 400-600 °C) occurring due to the thermolytic rupture of the macromolecular polymer units, the presence of hydroxyapatite and chitosan changed the degradation behavior of the ternary composite. The degradation stages of

HA composite series are observed at three main stages, viz.: (a) 90 - 160 °C, loss of adsorbed water; (b) 230 – 420 °C, degradation of the chitosan groups and; (c) 420 - 520°C, degradation of the polymer system (Shakir et al. 2014 b). Beyond 520 °C, the weight loss is constant in all hydroxyapatite added samples. This suggests an increase in stability for the ternary composite system presumably due to the interaction of all the three components in the composite system. Also, the degradation analyses indicate that the inorganic component has not undergone any phase change throughout the thermal analysis. With increasing concentrations of hydroxyapatite, a variation in decomposition temperature is also noted. For HA1 the decomposition temperature is obtained at 485 °C, owing to the good compatibility of hydroxyapatite with the reactive groups of chitosan and the decomposition of the strong bonds of HDPE. The final stage degradation of the remaining composites decreased and then started increasing with the addition of 8 wt% of hydroxyapatite.

The second stage of degradation described between 230 and 420 °C is negligible in HA4 system, depicting the unavailability of reactive group of chitosan. This indicates the miscibility of chitosan and hydroxyapatite in HA4 composite system. The possible reason for the shift in maximum degradation temperature of HA4 to 485 °C maybe attributed to the formation of a highly heat resistant composite with strong interface compatibility as observed from the DTG graphs. The thermogram of HA5 shows that higher concentration of hydroxyapatite beyond the optimum concentration can result in reduced filler-matrix interaction resulting in the formation of agglomeration, which further affects the stability of the system.

5.2.1.5 Thermogravimetric analysis of HAW composite series

Figure 5.5. demonstrates the effect of palm oil as plasticizer in HA4 and HA5 composite systems.

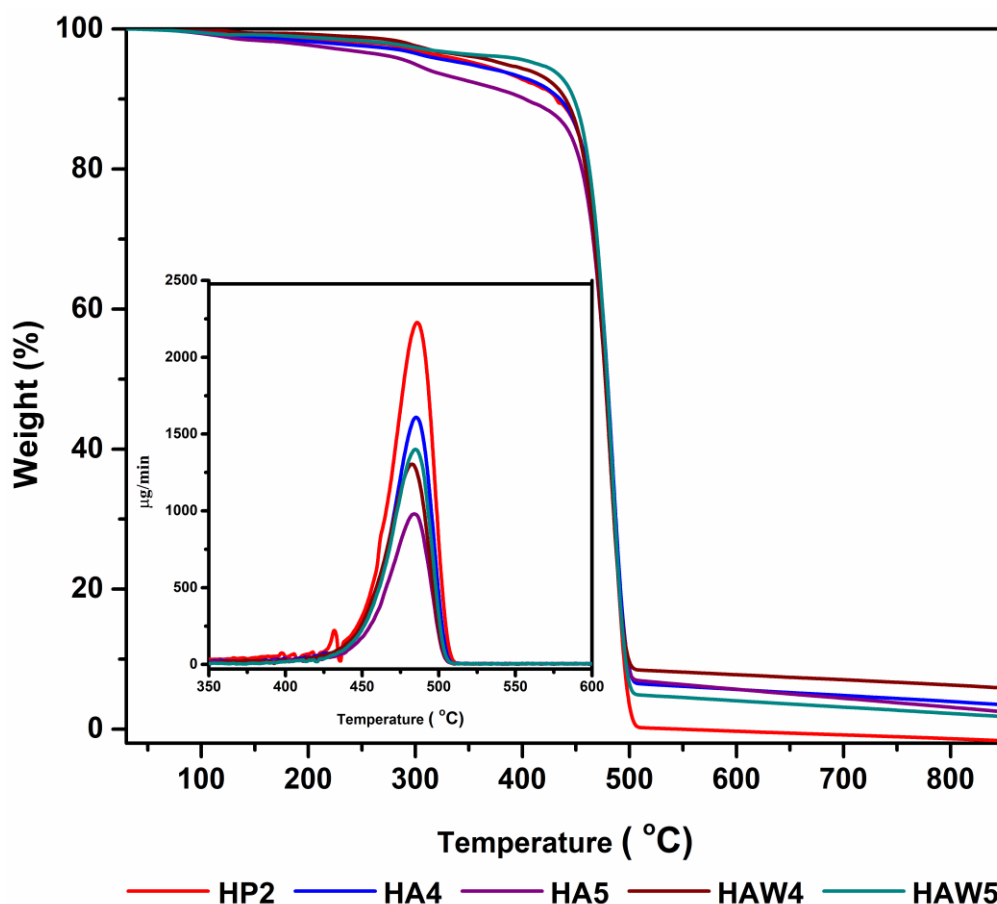


Figure 5.5 TGA and DTG (inset) analysis of HAW composite series

It is evident from the thermogram that the decomposition regions of plasticized composites and un-plasticized composites follow a regular pattern. A minor degradation peak observed around 200 °C and a major degradation peak around 400 °C was obtained for the un-plasticized composites of HA4 and HA5. The suppression of earlier degradation for HAW4 and HAW5 can be attributed to the difficulty in disassembling the polymer chains of HDPE in the polymer matrix. The absence of palm oil has also suppressed the unfolding of polymer chains, by reducing the interactions in the system. This results in larger number of unreacted side chains

which can be evaluated from the height of the DTG curves (Yu et al. 2020, Avalos et al. 2017). When palm oil was added, the segmental mobility of the polymer chain is increased resulting in improved chain relaxation in the system resulting in more interaction of filler with the matrix system. However, the thermal stability of the plasticized composites was maintained, forming a thermally resistant system. The hydroxyapatite component present in the ternary system protects the composite from earlier degradation due to the enhanced miscibility formed in the system (Dai et al. 2010).

5.2.1.6 Activation energy analysis of HA composite series and HAW composite series

The thermal stability of HA composite series and HAW composite series has been determined from the activation energy by applying Coats–Redfern’s method in which all the composites were assumed to undergo a single step thermal degradation process. Coats-Redfern Model follows a 0.5 order reaction rate. The values obtained from this model were closer to model free methods that makes it superior to other models (Kim et al. 2004). The activation energy calculated from the plots of $\ln[-\ln(1-\alpha)]/T$ vs $1/T$ are given in Table 5.2. The activation energy of HA composite series and HAW composite series were lower than HP2 composite system till HA3. But, higher activation energy of 333.2 kJmol^{-1} has been obtained for HA4 composite system, which is higher than the value of 330 kJmol^{-1} reported by Albano *et al* (Albano et al. 2010). The further addition of hydroxyapatite to 10 wt% has caused a reduction of activation energy to 226 kJmol^{-1} which can be attributed to the agglomeration formed in the system beyond the optimum concentration. The morphology of the system also helped in understanding the thermal stability of HA composite series. As observed from the SEM images from Figure 3.13, the addition of hydroxyapatite to palm oil

plasticized composites results in the formation of small clusters, rather than interacting with chitosan. At elevated temperatures, the decomposition of these clusters occurs, through “nucleation and nucleus growth” that finally leads to the breakage of bonds. As the concentration of hydroxyapatite is increased, the formation of these clusters are fewer, making space for more interaction with chitosan and compatibilized HDPE. Hence, the bonding becomes stronger, and higher activation energy is obtained for HA4. The thermal stability in HAW composite series is further decreased, due to the ineffective interaction between chitosan and hydroxyapatite with compatibilized HDPE.

Table 5.2 Activation energy analysis of HA composite series and HAW composite series

Sample	E_a (kJmol⁻¹)	R
HP2	348.2	0.9998
HA1	331.11	0.9948
HA2	308.4	0.9961
HA3	292.07	0.9632
HA4	333.2	0.9907
HA5	226.3	0.9714
HAW4	330.8	0.9875
HAW5	296.1	0.9915

5.2.2 Dynamic mechanical analysis (DMA)

The viscoelastic characteristics of HC composite series and HA composite series were analyzed by DMA studies. This technique has been widely used to measure the solid-

state rheological properties of viscoelastic materials as a function of frequency and temperature.

5.2.2.1 Dynamic mechanical analysis of HC and HP composite series

The effect of varying concentration of chitosan on the viscoelastic properties of HC composite series and HP composite series over the temperature range of -135°C to 110°C is shown in Figure 5.6 (a) and Figure 5.6 (b). The storage modulus is decreased in all composites as the temperature shifts to higher range.

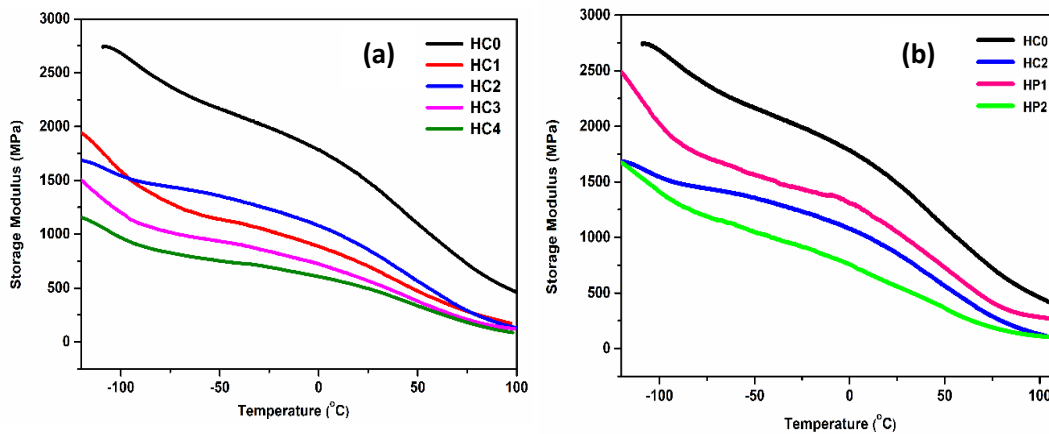


Figure 5.6 Storage modulus of (a) HC composite series and (b) HP composite series

As observed, the storage modulus of HC composite series are lower than HC0. The presence of short groups of maleic anhydride and methylene group of HDPE in the amorphous region leads to α relaxation resulting in higher storage modulus of HC0. The addition of chitosan to HC0 has imparted chain mobility as well as interactions in the system causing the movement of short segments of polymer chains. This has resulted in low storage modulus for HC composite series. An initial decrease in storage modulus for HC2 in the range of -135°C to -90°C as compared to HC1 can be ascribed to the pseudo - lubricating effect of chitosan. With increase in

temperature, HC2 shows higher storage modulus than the remaining HC composite systems. The higher values can be attributed to the strong interaction of chitosan with compatibilized HDPE resulting in a stiffer system (Sewda et al. 2013, Yadav et al. 2014). When varying concentration of palm oil is added to HC2 system, a slight variation in storage modulus is observed. Palm oil can provide toughening of a composite by allowing the polymer chains to undergo improved segmental interactions. When higher concentration of palm oil is added, a further softening of the system occurs thereby improving the flexibility of the side chains. The movement of the long chains of palm oil reduces the strong inter-chain bonds between the polymer molecules. This results in low storage modulus for higher concentration of palm oil. At higher temperature, the degradation of compatibilizing agent occurs thereby enhancing the interlayer slippage of polymer chains. As a result the value of storage modulus is found to decrease for all the composite systems with higher than 5 wt% chitosan loading (Xie et al. 2014).

The loss modulus, E'' of HC composite series and HP composite series are given in Figure 5.7. HC0 and HC composite series show two loss peaks in the regions of -135 to -100 °C and 0 to 100 °C corresponding to γ and α transitions respectively. The absence of β transition peak in the region of -100 to 0 °C indicates the absence of amorphous phase in the prepared composites. A small hump in HC4 in the β transition region indicates the formation of amorphous phase in the interfacial region between amorphous/crystalline regions. On approaching higher temperature range in the α transition region, peak broadening is observed in all composites which is due to the interaction between the filler and the matrix. These results are further supported by the crystallinity studies obtained from XRD analysis (Sewda et al. 2013).

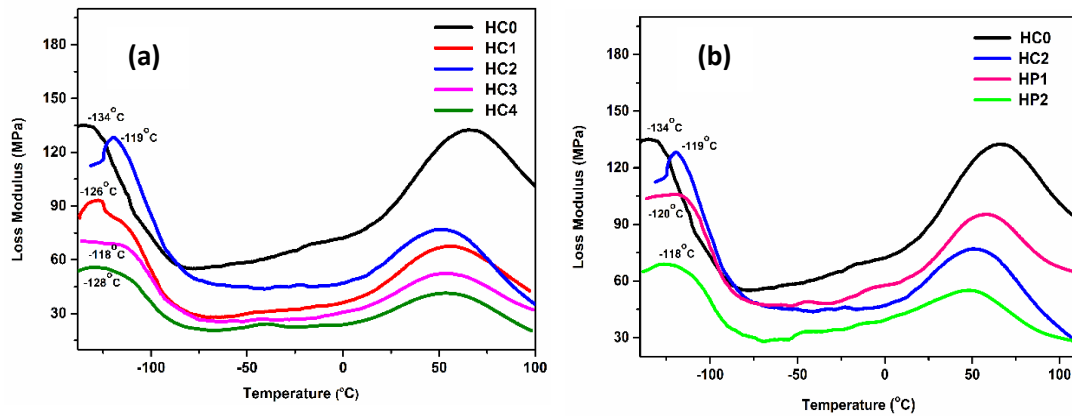


Figure 5.7 Loss modulus of (a) HC composite series and (b) HP composite series

HP2 having a higher concentration of palm oil shows a broader peak which can be ascribed to the plasticizing effect, that enables the easier movement of side chains which helps in energy dissipation. The glass transition temperature (T_g), obtained from loss modulus data provides information related to the molecular motion of the material under study. The highest peak of loss modulus is considered as T_g since it is the temperature at which the maximum energy dissipation is observed. HC0 is observed with a T_g at $-134\text{ }^\circ\text{C}$. HC2 exhibits higher value of T_g at $-119\text{ }^\circ\text{C}$ among HC composite series, indicating the limited movement of segments in the amorphous phase. Moreover, the miscibility of chitosan with compatibilised HDPE has restricted the movement of polymer chains. When palm oil is added, the T_g of HP1 and HP2 has changed to $-120\text{ }^\circ\text{C}$ and $-118\text{ }^\circ\text{C}$ respectively. With the increase in concentration of palm oil, the mobility of polymer chain segments has increased in the interfacial region. This reduced the glass transition temperature of HP2 (Bashir 2021).

The variation of damping parameter, $\tan \delta$ for HC composite series and HP composite series with change in temperature is given in Figure 5.8 (a) and Figure 5.8 (b) respectively. The damping parameter of HC composite series are higher than HC0 and

is caused by the increased segmental mobility in the amorphous phase leading to the interaction of chitosan with HDPE (Leite et al. 2010).

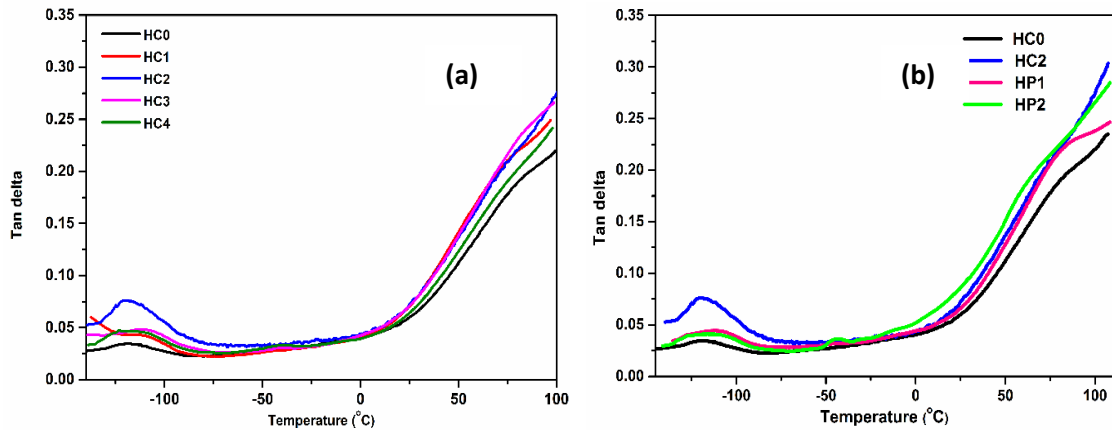


Figure 5.8 Tan delta of (a) HC composite series and (b) HP composite series

A reduction in peak value with increase in concentration of chitosan can be related to the higher rubbery storage modulus of the composites rather than the interaction between the filler and the matrix. This property is relevant for designing more robust polymer composites for specific applications (Bashir 2021). Higher the peak value of $\tan \delta$ in the region, greater is the extent of interaction between compatibilized HDPE and chitosan, leading to decreased molecular mobility of the system (Sewda et al. 2013). The interaction of the carbonyl moiety of maleic anhydride with the reactive groups of chitosan has improved crosslinking, which in turn improved the stiffness of the system, as indicated from the peak height (Yadav et al. 2014). The peak broadening with increase in chitosan concentration is due to (a) increased amorphization of HDPE matrix beyond the optimized concentration of chitosan thereby restricting the movement of polymer chains; and b) decrease in energy absorption caused by the presence of chitosan as filler (Gowman et al. 2018). The peak height for HC2 shows that more chain segments have undergone thermal

movement creating an internal friction, and has resulted in high loss peak value as discussed earlier. This has resulted in homogeneous filler dispersion owing to lesser filler - filler interactions in the system.

5.2.2.2 Dynamic mechanical analysis of HA composite series and HAW composite series

The viscoelastic behavior at a low frequency of 1 Hz has physiological significance in bone-implant materials (Lamarra et al. 2018). The interphase behavior of HA composite series and the effect of palm oil as plasticizer on its viscoelastic properties of the selected systems are explained below. The storage modulus of the HA composite series and HAW composite series over a temperature range from -135 to 110 °C are shown in Figure 5.9 (a) and Figure 5.9 (b). The storage modulus of all HA composites series decreased with increasing temperature as seen previously in the HC composite series.

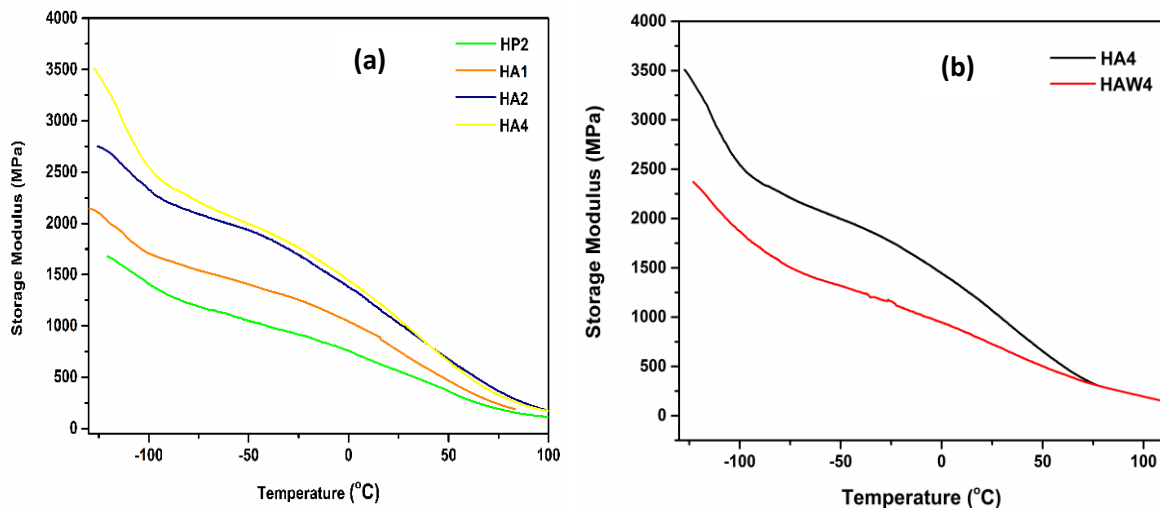


Figure 5.9 Storage modulus of (a) HA composite series and (b) HAW composite series

The addition of hydroxyapatite to HP2 has produced a pronounced effect on the storage modulus, which is mainly due to the decrease in free holes formed in the system. The E' values of HA4 were slightly higher than HP2 as well as the remaining HA composite series under study. This is attributed to the stiffness achieved by the interaction of hydroxyapatite with compatibilized HDPE and chitosan. The effect of palm oil on HAW4 was compared with HA4. Palm oil acts on the amorphous region of polyethylene matrix and has improved the viscoelastic properties of the polymer matrix. This impeded the crosslinking of HDPE chains with hydroxyapatite and chitosan resulting in the formation of rigid regions in the system (Alothman et al. 2014). During the initial mixing process of the composites, the shrinkage of HDPE polymer matrix around the hydroxyapatite particles occurred that has resulted in the increased stiffness of the HA composite series at lower temperatures (Wang et al. 1998). The viscoelastic measurements at higher temperature caused the stiffness of HAW4 to decrease due to the increased thermal movement of side chains of the HDPE polymer matrix. In addition to that, the energy could be absorbed by the surface of the agglomerates formed in the system or by the hydroxyapatite particles trapped in the free holes in the composites. This can also result in a comparable storage modulus of HAW4 with HA4 (Y. Zhang et al. 2007).

The maximum heat dissipation per unit deformation is expressed in terms of loss modulus values (E'') of HA composite series and HAW composite series are studied from Figure 5.10 (a) and Figure 5.10 (b).

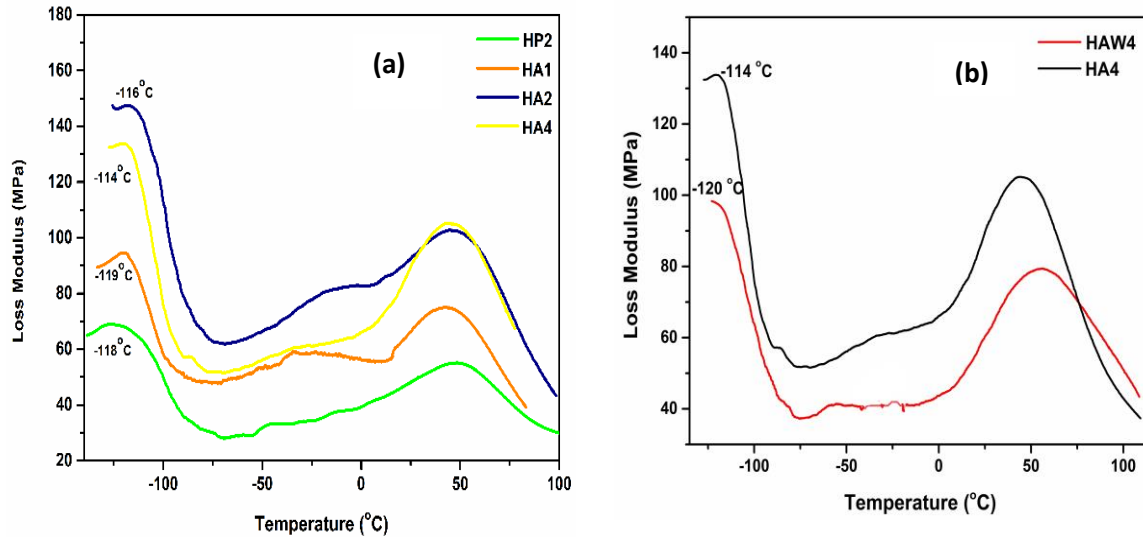


Figure 5.10 Loss modulus of (a) HA composite series and (b) HAW composite series

From the figures, β relaxation in the range of -100 to 0 °C was observed in HA1 and HA2. This can be related to the mechanical restraints formed in the system hindering the crystallization process. Due to this, the interfacial distance between crystalline and amorphous phase increases causing the formation of free holes. But it is negligible/absent for HP2 and HA4, indicating the homogeneity attained by the composites. Another important observation is that HAW4 show β relaxation. This further explains the significance of palm oil in segmental mobility and its role in enhancing the interaction between the matrix and filler. Palm oil facilitated the formation of a strong interface through crosslinking and hydrogen bonding. A peak broadening was observed for the plasticized system when compared with its un-plasticized systems. This can be attributed to the larger rotational freedom in the system due to the segmental mobility provided by the plasticizer. With the addition of hydroxyapatite, the peak broadening is reduced indicating the less viscous nature of the system.

The presence of increasing concentration of hydroxyapatite has reduced the damping of HA composite series and HAW composite series composites as observed from Figure 5.11(a) and Figure 5.11 (b) respectively. The toughness of a material is closely related to the magnitude of $\tan \delta$. High $\tan \delta$ values indicate increased relaxation occurring from the amorphous region of polyethylene side chains caused by the presence of chitosan, and hydroxyapatite. When increasing concentration of hydroxyapatite is added to HP2, the system becomes rigid and it impedes the movement of polymer chains (Q. Zhang et al. 2017). This reduces the damping of composite system. Initially, HA4 shows a reduction in sharpness and peak height, as the dispersion in the crystalline region hinder segmental mobility in the amorphous region. This promotes the capacity to absorb mechanical energy, resulting in higher mechanical strength (Sanyang et al. 2015, Sattar and Patnaik 2020). For HAW4, the melted polymer gets adsorbed on the surface of fillers restricting their molecular movement and changing the orientation of chain segments (Y. Zhang et al. 2007). This increases the rigidity of HAW4 and causes high damping energy.

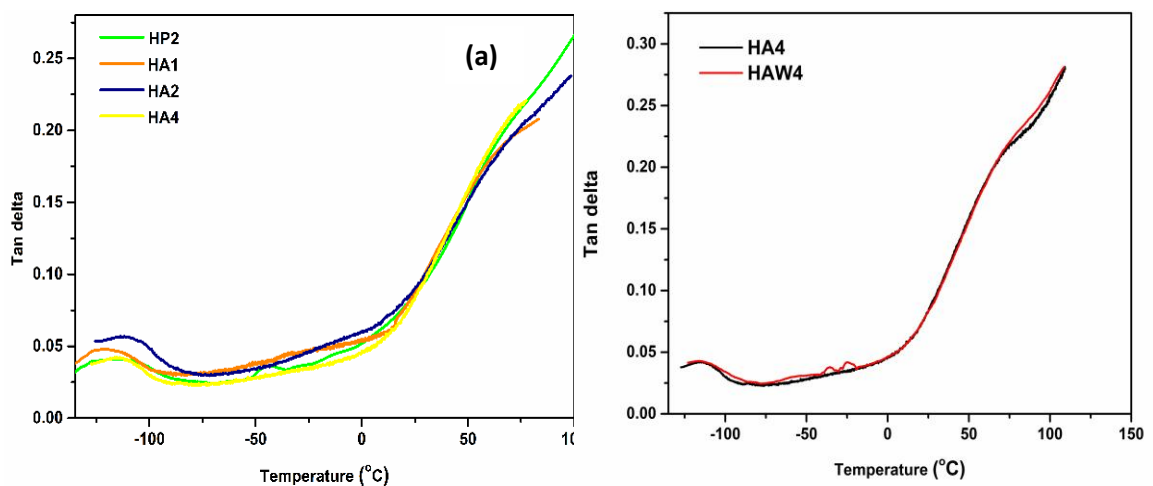


Figure 5.11 Tan delta of (a) HA composite series and (b) HAW composite series

This page is intentionally left blank

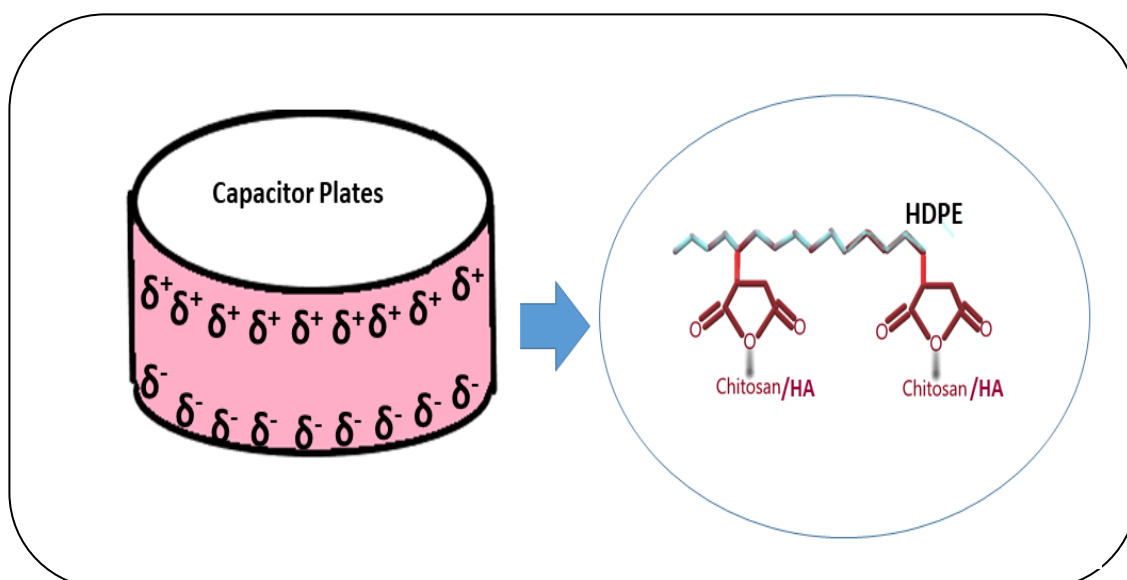
Chapter 6

Electrical Properties of High density polyethylene / Chitosan Composites and High density polyethylene / Chitosan / Hydroxyapatite Composites

Summary

The dielectric properties of HC composite series and HA composite series were studied. The dielectric constant, dielectric loss and ac conductivity of the prepared composites were evaluated. The optimised HA composite system – HA4 exhibited a dielectric constant similar to the dielectric constant of natural bone. The presence of polar groups and free holes in the composite provided enhanced conductivity. The miscibility of chitosan and hydroxyapatite in HDPE polymer matrix were analyzed using broadband dielectric spectroscopic analysis. The electrical properties helped to understand the efficiency of the prepared composites for bio-compatibility studies.

Graphical Abstract



6.1 Introduction

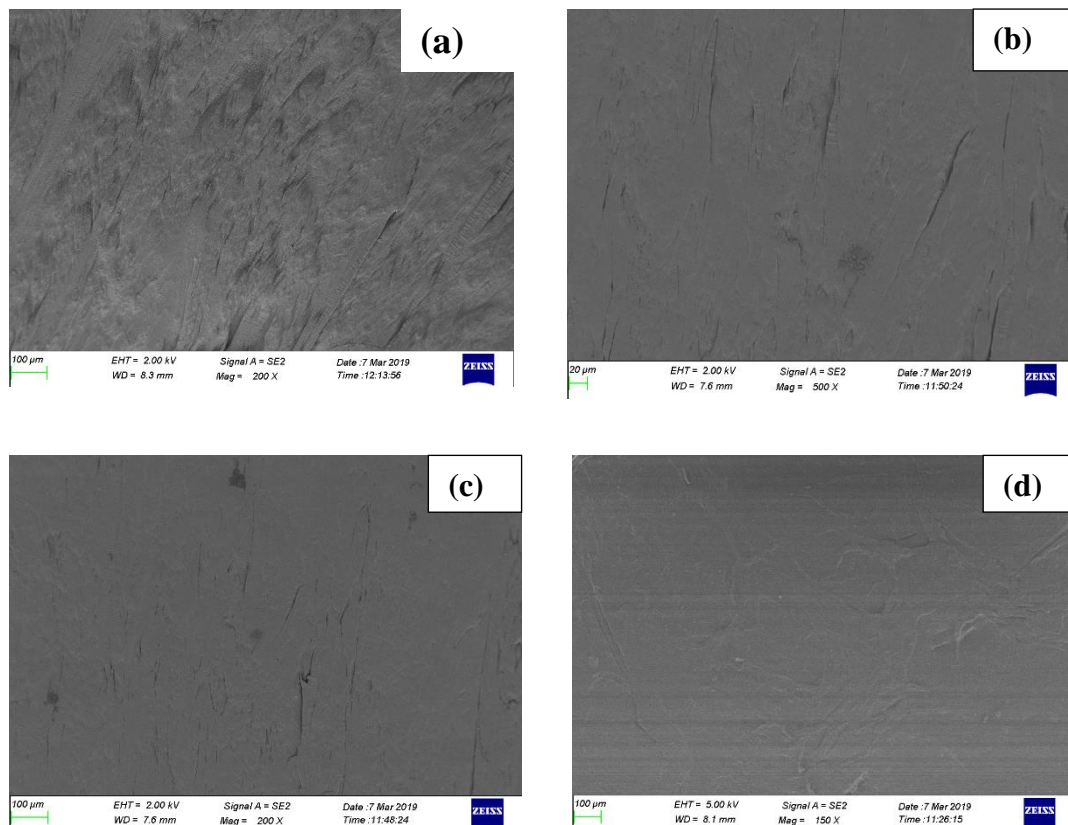
A bio-material with appropriate electrical properties makes it more compatible with the surrounding tissues and cells. The electrical properties of biological systems plays an influential role in understanding the response of bone to external stimulus like stress, repair and regeneration of bone fracture through cell signaling. Among the electrical properties dielectric constant (ϵ_r) helps in establishing the utility of the composite material in bio applications. Initially the electrical properties of bio-materials were utilized for drug delivery applications (Das et al. 2021). Recently, the electrical studies have been directed to understand the absorption of proteins leading to bone healing applications. When a material with low dielectric constant is combined with a material having high dielectric constant, an increase in energy storing capacity has been noted (Liu and Zhai 2014, Romero 2003). Hydroxyapatite having a dielectric constant at 5 -15 at 1 MHz, when combined with $\text{Ba}_{0.5}\text{Sr}_{0.5}\text{TiO}_3$ generates a material with medium ϵ_r . The studies also report that the presence of crosslinking also affects the dielectric properties of the composites. The radiofrequency regime between $10^6 - 10^9$ Hz has been chosen for clinical applications as it helps to understand the delayed unions and non-unions of bone fractures before *in-vivo* applications (Goldstein et al. 2010, Amin et al. 2018). The dielectric constant value in the range of 3 – 65 has been reported to accelerate bone fracture healing. For highly critical bone forming process, a time of three months is required when providing electric field which is obviously a lesser time for normal bone healing process. But the presence of electrically active materials, accelerate the healing process. An electrical stimulation in conjunction with an electrically active material can activate polarization. This is usually observed in materials composing of ceramic

particles and reactive groups. The electrical field in such materials are retained and hence can be used *in-vivo* applications even though the external field is removed (Goldstein et al. 2010). The current chapter presents the electrical properties of the bio-composites to study its efficiency in cell proliferation studies.

6.2 Results and Discussion

6.2.1 Surface study of HC composite series and HA composite series –Scanning electron microscope (SEM)

Figure 6.1 shows the surface SEM images of HC composite series and HA composite series under investigation. The composites exhibit a smooth surface which enables better dielectric interface contact and précised measurements over the wide frequency range.



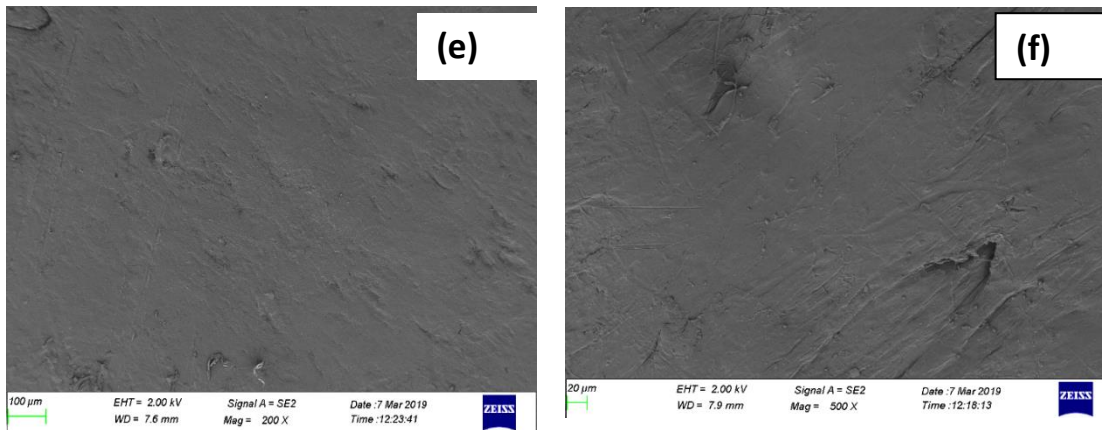


Figure 6.1 SEM images of the surfaces of (a) HC0, (b) HC2, (c) HC4, (d) HP2, (e) HA3 and (f) HA4

6.2.2 Dielectric properties of HC composite series

Dielectric constant of a material is related to its ability to gets polarized in the presence of an applied electric field. Improved miscibility between the filler and matrix, orientation of the components in the composite, free hole volume, electronic, atomic and orientation polarization contributes to the electrical properties of the composites (Sunilkumar et al. 2014). Figure 6.2. shows the effect of varying frequency on the dielectric constant of HC composite series. A highest dielectric constant value of 21 for HC0 can be ascribed to the unsaturated centers formed due to the compatibilization of HDPE with maleic anhydride (Varghese et al. 2015). The effective interaction of the amine /hydroxyl group of chitosan with maleic anhydride has resulted in high dielectric constant of 8 at 10^6 Hz for HC2 composite system among the HC composite series under study. A lag in dielectric constant is observed for all composite system in the lower frequency regime which can be attributed to the orientation polarization formed in the system as the polar groups in the composites

requires more time to get aligned to reach an equilibrium static field value (Sunilkumar et al. 2014). However, higher filler concentration lead to agglomeration in the system as observed by low dielectric constant values directing to the formation of unequal charge distribution at the interface that are not free to move, causing low permittivity (Rahman et al. 2018).

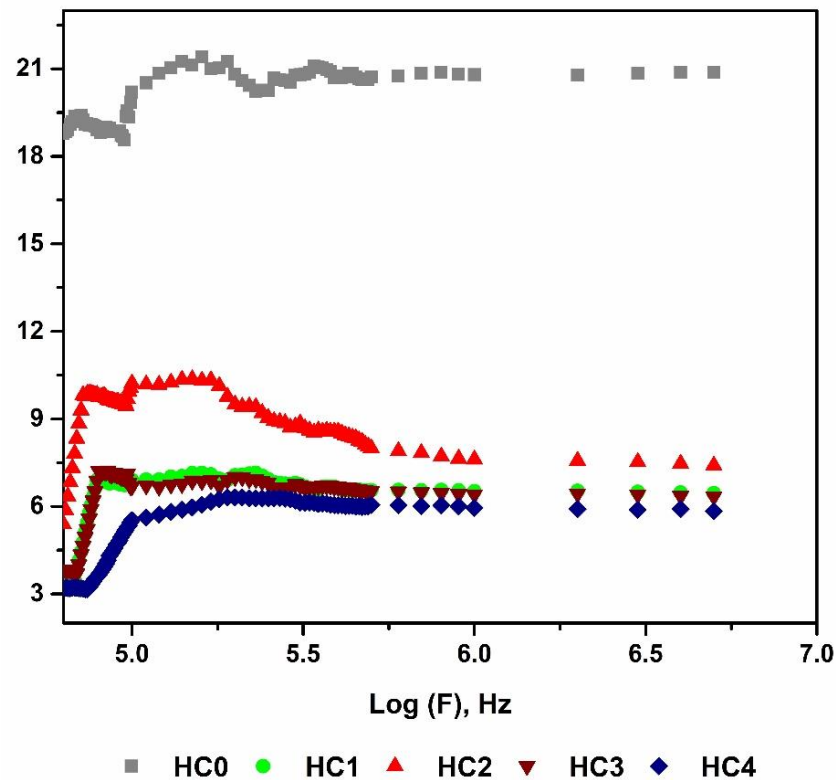


Figure 6.2 Dielectric constant of HC composite series

The inability of polarization process in a molecule, to follow the rate of change of the applied electric field results in the dielectric loss of the material. This arises due to the time taken by the dipoles to return to its original random orientation associated with energy absorption and dissipation of heat (Khouaja et al. 2021). The variation of dielectric loss ($\tan \delta$) in the radiofrequency range for HC composite series are shown in Figure 6.3. The $\tan \delta$ value is gradually increasing and a broad relaxation curve is observed around 10^5 Hz for all composites. Broad peaks in dielectric loss curves are

seen in all HC composite series arising due to the rotational behavior of polarized dipole in solid or liquid apart from that of the gaseous state. The low dielectric constant of HC2 can be attributed to the good integrity formed at the interfaces, which are efficient to produce an insulating barrier by suppressing the current loss. With higher concentration of chitosan, filler – filler interaction predominates which contributes to the heterogeneity in the system (Sun et al. 2014, Khouaja et al. 2021).

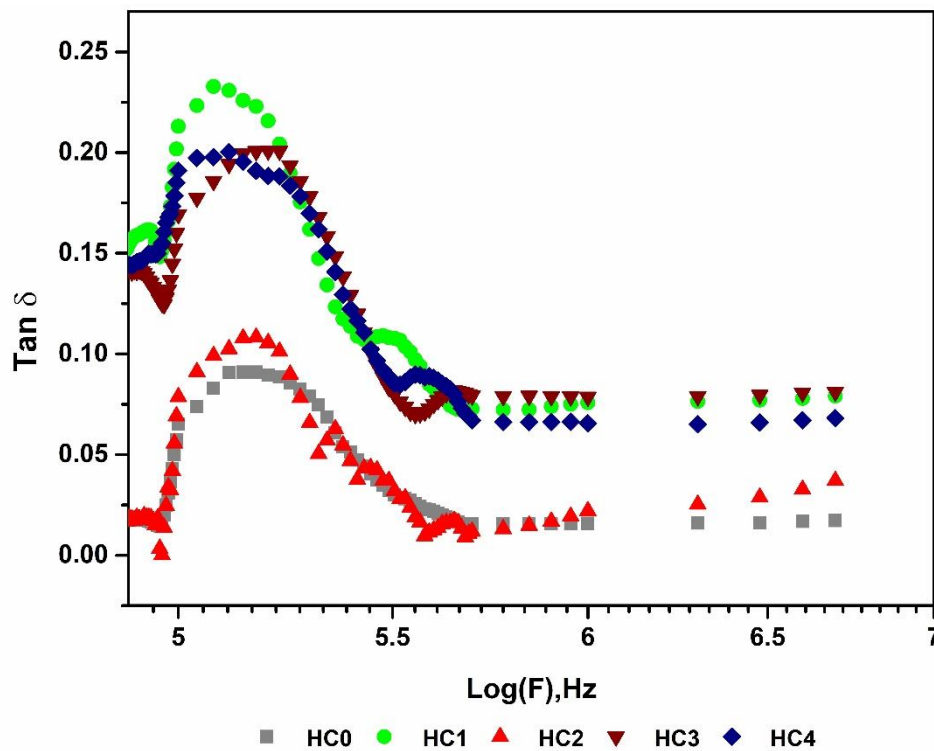


Figure 6.3 Tan δ of HC composite series

ac conductivity (σ_{ac}) has a significant effect on the dielectric properties of the material as it depends upon the homogeneous filler dispersion in the system. Figure 6.4 shows the variations in σ_{ac} conductivity values with frequency for HC composite series. The ac conductivity values remain constant at low frequency regions but is found to increase rapidly at high frequency regions indicating a transformation from frequency independent dc conductivity to frequency dependent ac conductivity as observed in previous studies (Pradhan and Tripathy 2013). This dc plateau is an evidence of

formation of conducting path in these materials, which signifies some relaxation processes occurring in the composites. The high ac conductivity for HC2 shows efficient interaction of the polar groups of chitosan with compatibilised HDPE hence providing a continuous network. When the concentration of chitosan increases, the filler-matrix interaction reduces, leading to the non-homogeneous distribution in the composite.

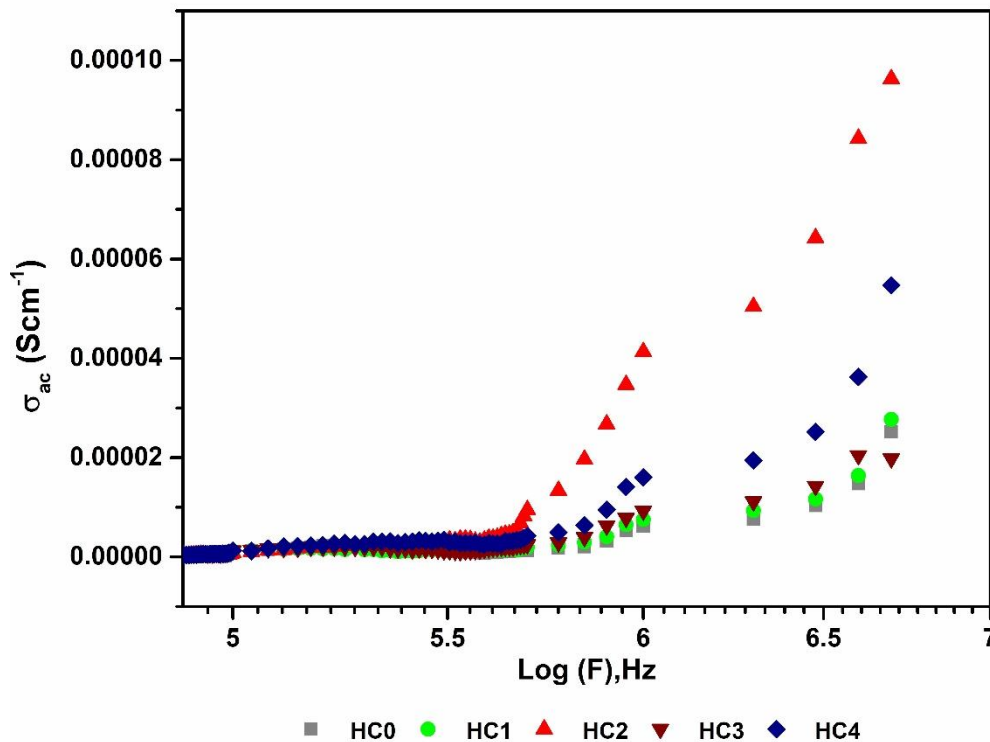


Figure 6.4 ac conductivity of HC composite series

6.2.3 Dielectric properties of HP composite series

Figure 6.5 shows the dielectric constant as a function of frequency for varying concentration of palm oil as plasticizer in HC2 composite system. The high dielectric constant for HP1 and HP2 is due to the polarization introduced in the composite system by the olefinic group of palm oil, which itself acts a good dielectric material (Shinoj et al. 2011). The delocalization of charge carriers increases, with the addition of palm oil owing to the improved segmental mobility in the system (Pradhan et al.

2008). The improved interactions in the highly crosslinked system increases its ability to hold energy.

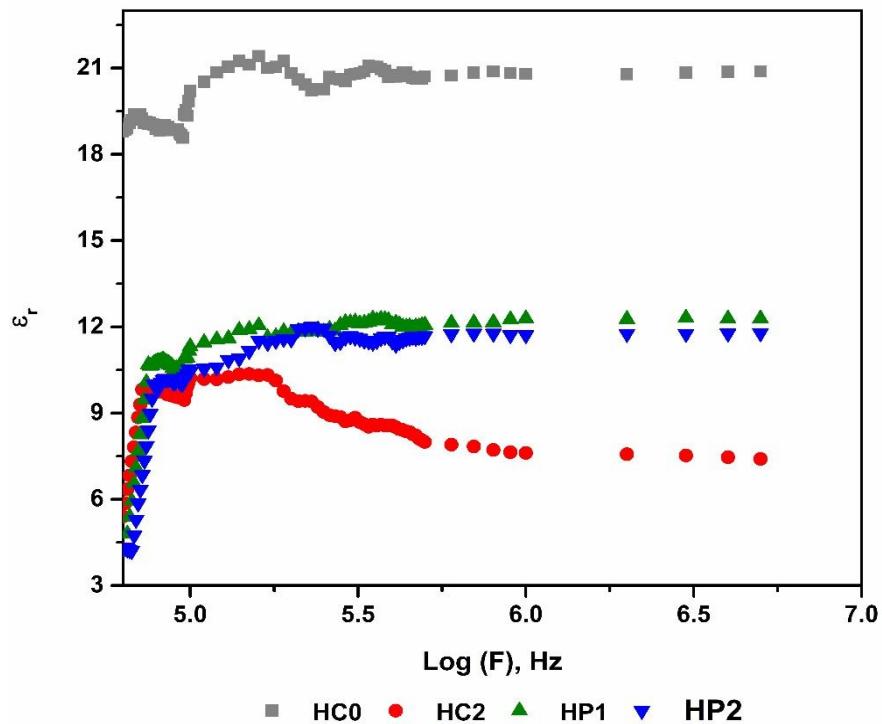


Figure 6.5 Dielectric constant of HP composite series

Tan δ expresses the amount of electromagnetic energy converted into heat. The Tan δ of HP composite series with varying frequency are shown in Figure 6.6. The high dielectric loss of plasticized samples can be associated with the relaxation phenomena arising due to the glass transition of the amorphous phase of the polymer (Sander et al. 2012). As the concentration of plasticizer increases, space-charge polarization is decreased due to the in-homogeneity formed in the composite system. The increase in fractional free hole volume obtained for plasticized samples also cause increased heat dissipation in the system.

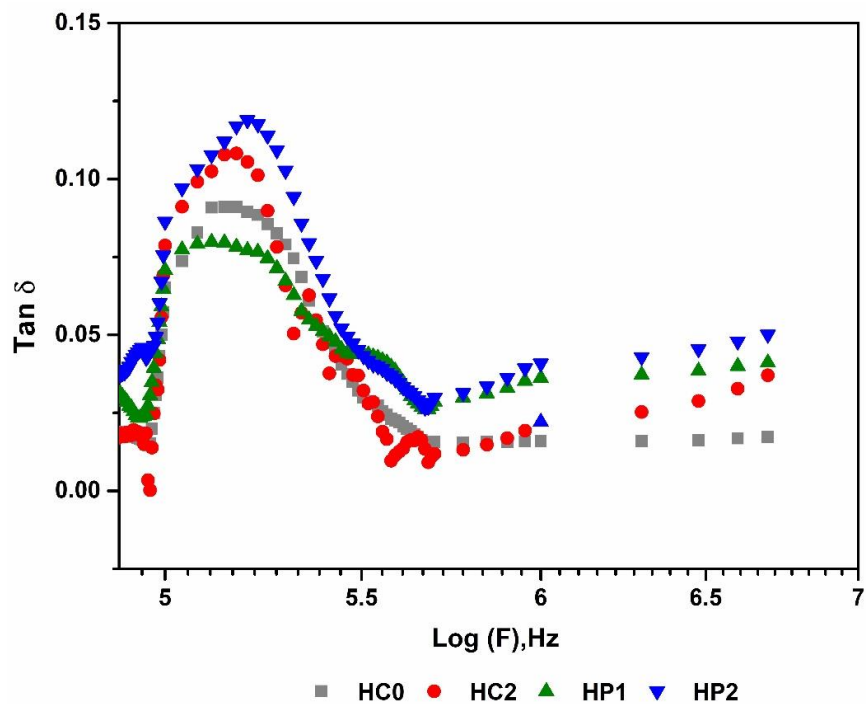


Figure 6.6 Tan δ of HP composite series

The ac conductivity measurement as a function of frequency of HP composite series is shown in Figure 6.7. Similar transformations observed in HC composite series have been found in the plasticized composites as well.

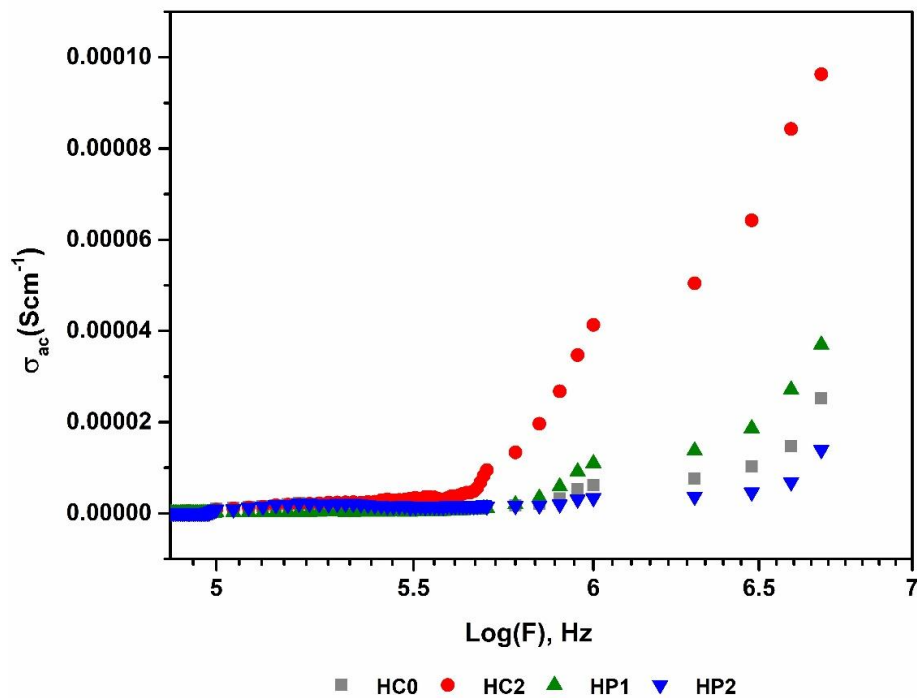


Figure 6.7 ac conductivity of HP composite series

As observed from the graphs, σ_{ac} is seen decreased with increase in concentration of palm oil. On addition of plasticizer to HC2, the amorphous content of the composite increases. Due to the relaxation of polymer chains, an increased interaction of chitosan with compatibilized HDPE increases causing a reduction in mobility of electric charges.

6.2.4 Dielectric properties of HA and HAW composite series

The electronic, atomic and orientation polarization of a system contributes to the overall dielectric property of a material. Free volume parameters, presence of polar groups, size of the groups that form and surface morphology of the system contributes to the dielectric properties of the material. Dielectric properties of bio based materials are required for applications in sensors and bone implant materials. The dielectric constants as a function of varying frequency for HA and HAW composite series are shown in Figure 6.8.

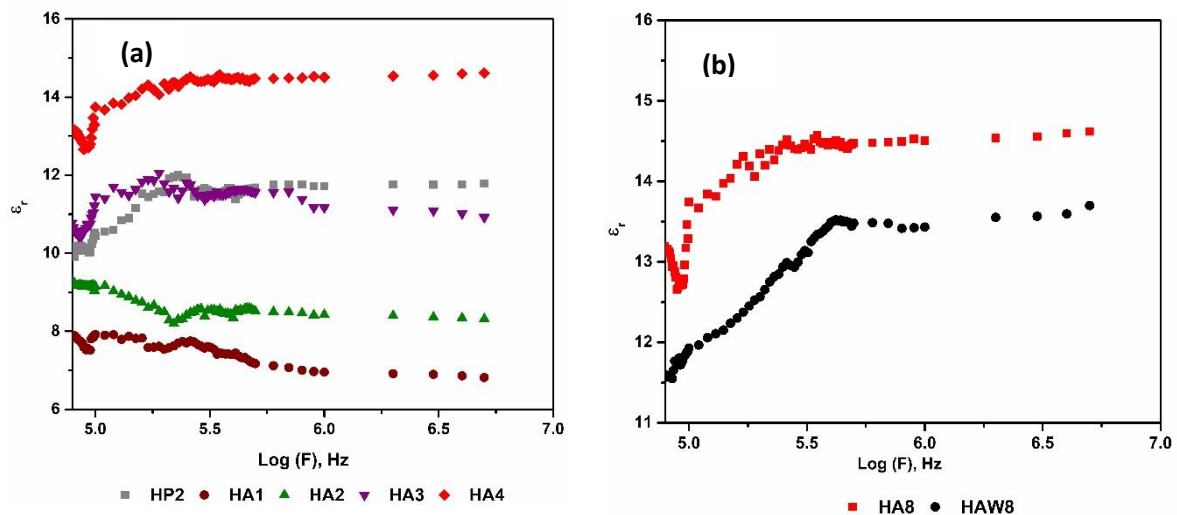


Figure 6.8 Dielectric constant of (a) HA composite series and (b) HP composite series

A lag in dielectric constant is observed for all composites in the low frequency

region because of the orientation polarization formed in the system. The presence of polar groups in the composites require more time to get aligned to reach an equilibrium static field value (Sunilkumar et al. 2014). HA4 shows a dielectric constant at 14.5 when compared with other composite systems. The effective interaction of hydroxyapatite with chitosan has produced sufficient crosslinking resulting in reduction in free hole volume in the composite. This results in the formation of few dipoles and ionic carriers available in the outer layer, which are not free to move, causing low permittivity at higher filler loading (Ramkumar et al. 2019). At lower concentration of hydroxyapatite, the miscibility of the system is lower leading to low dielectric constant. Similarly, HAW4 also exhibits low dielectric constant than HA4, which can be attributed to the decrease in crystallinity in the system due to decrease in interaction between the filler and matrix.

The dissipation constant with increasing frequency at room temperature for HA and HAW composite series are shown in Figure 6.9.

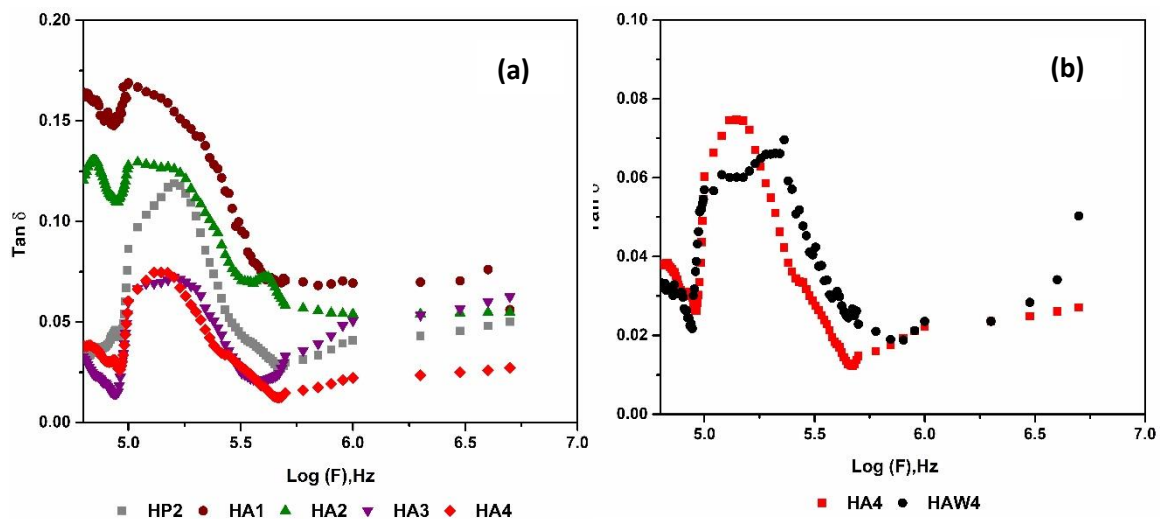


Figure 6.9 Dielectric loss of (a) HA composite series and (b) HAW composite series

At lower frequency, a slight decrease in loss factor is observed followed by an increase at higher frequency owing to the space charge polarization formed in the

system (Sunilkumar et al. 2014). At higher filler loading, the inter-particle distance between chitosan and hydroxyapatite decreases and causes an increase in interaction within the system. This enhances the crosslinking that results in low dielectric loss for the HA4 composite system. Furthermore, a shift in peak observed for HAW4 composite system can be attributed to the reduction in relaxation time. At this frequency region, the dipoles take time to follow the applied electric field and get less time to orient themselves in the direction of electric field (Khouaja et al. 2021). The ac conductivity depends on the dielectric nature of the sample and helps in understanding the charge transport mechanism present in the composites. The ac conductivity of HA and HAW composite series as a function of varying frequency is shown in Figure 6.10.

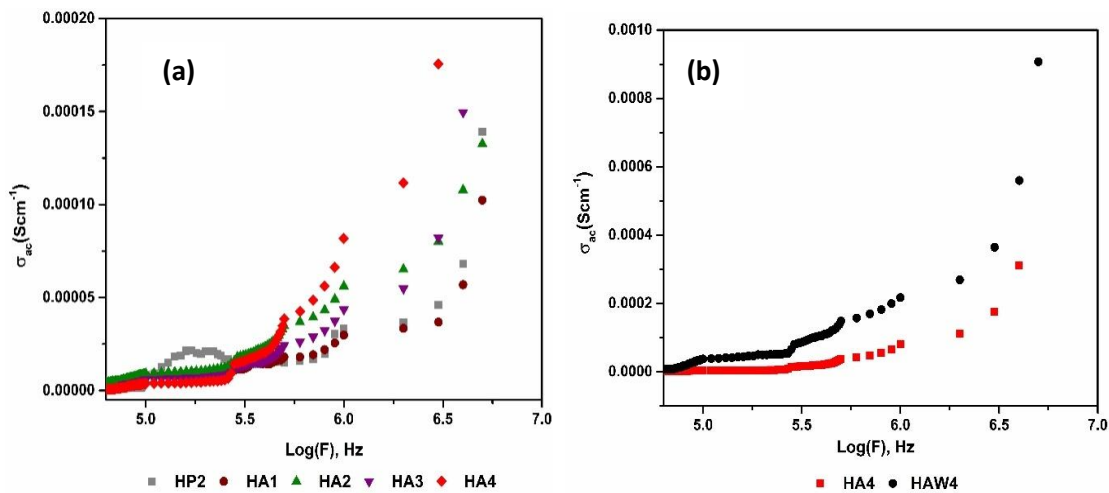


Figure 6.10 ac conductivity of (a) HA composite series and (b) HAW composite series

In the low-frequency region, σ_{ac} is almost constant but at high frequency region, the ac conductivity is seen increased. This can be attributed to the transformation of frequency independent dc conductivity to frequency dependent ac conductivity. As the concentration of hydroxyapatite increases, there is an increase in the polar groups, thereby increasing its conductive nature. This causes dipolar and interfacial

polarization that contributes to the conductivity of the system. Moreover, palm oil as plasticizer can alter the segmental mobility, thereby causing a rise in the conduction process at higher frequency. The ac conductivity of HAW4 is found to be lower than HA4, which can be attributed to the availability of polar groups in the system, indicating lesser interaction of hydroxyapatite and chitosan (Khouaja et al. 2021).

6.2.5 Broadband dielectric spectroscopic analysis of HA composite series

The dielectric measurements of HA composite series were carried out over wide frequency range. As all the samples have ion transport characteristics, their dc conductivity due to hopping of ions masked the structural relaxation, the analysis of dielectric data is meaningless as shown in Figure 6.11.

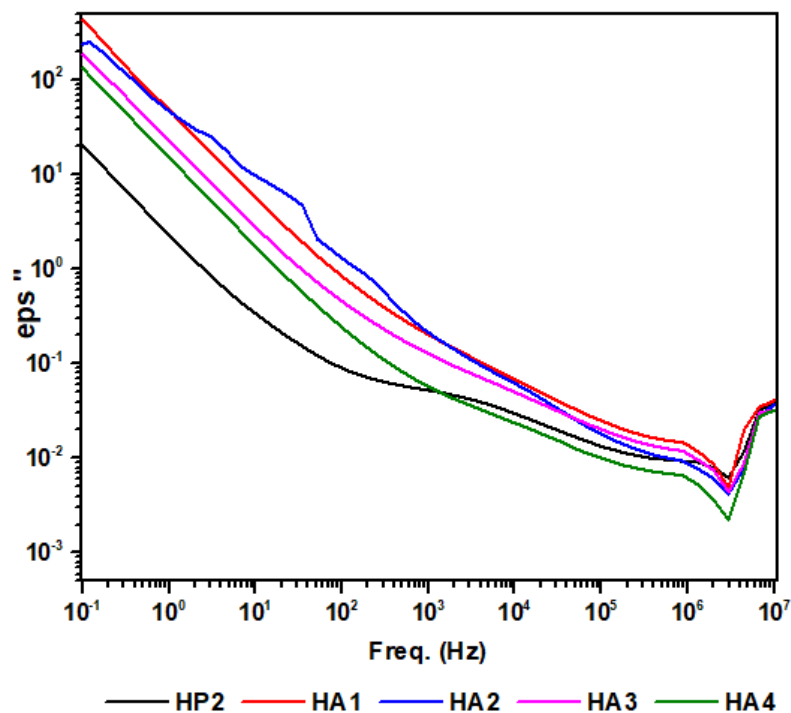


Figure 6.11 Frequency dependence of ϵ'' imaginary part of dielectric constant of HA composite series

The orientation of permanent dipoles occurs at higher frequency whereas chain segmental motion and electrode polarisation occurs at lower frequency. This

contributes to the dielectric polarisation of the composite system. High ϵ'' is observed for HA composite series having lower concentration of hydroxyapatite, which can be ascribed to the increase in free charges arising due to the presence of polar groups present in the system. It can also be observed that low ϵ'' value is obtained for binary composite system, HP2 attributing to the minimum availability of polar groups in the system. HA4 also shows lower ϵ'' value among the ternary composite system, due to the minimum number of polar groups present in the system owing to the interaction of phosphate group of hydroxyapatite with the reactive functional groups of chitosan. The increase in ϵ'' at higher frequency can be related to the electrode polarisation and interfacial polarisation in the system.

Hence, considering the charges as independent variables, the conductivity relaxation effects were analyzed in terms of electric modulus (M) which is the sum of imaginary part of electric modulus (M'') and real part of electric modulus (M'). Figure 6.12 depicts the imaginary parts of complex electrical modulus $M^*(\omega, T)$. It is observed that HP2 has two relaxations; additional to the conductivity a relaxation due to hopping of ions in HP2 a secondary relaxation at higher frequency range is observed due to the movement of side chains in the polymer composite system.

Interestingly, the ac conductivity relaxations in HA1 and HA2 is found to shift towards higher frequency region, this may be due to the presence of hydroxyapatite in HA1 and HA2 samples owing to the formation of dipoles due to the presence of polar groups in the system and formation of larger number of free holes that may increase the degree of freedom. Further addition of hydroxyapatite in HA2 and HA3 caused accumulation of more unreactive groups in the system due to the ineffective interaction of hydroxyapatite with chitosan and resulted a peak shift towards lower frequency region. Palm oil as plasticizer has improved the segmental mobility, which

in turn increased the miscibility of the system forming a homogeneous stable ternary system as observed in HA4 composite system.

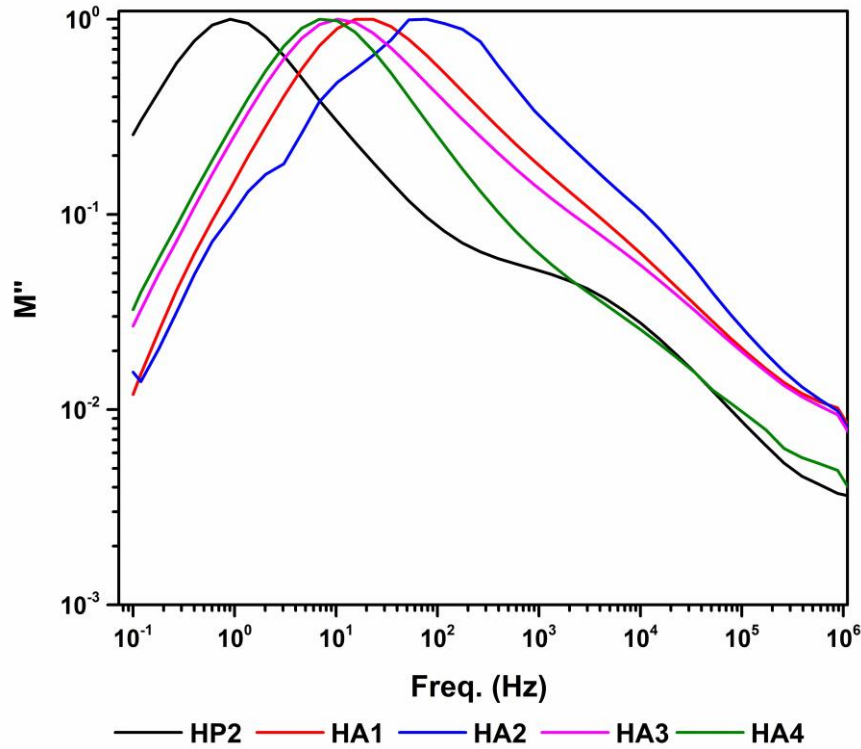


Figure 6.12 Frequency dependence of M'' imaginary part of electric modulus of HC composite series and HA composite series

A deep insight into the charge transport in HA composite series were obtained from BDS measurements. The ac conductivity (σ') of HA composite series were shown in Figure 6.13. All the spectra have a frequency - independent plateau in the low frequency region corresponding to the dc electrical conductivity followed by a frequency – dependent exponential region in the higher frequency side. The region of dc conductivity plateau is higher and extends to higher frequency for hydroxyapatite added composite systems. The high ac conductivity in HA2 composite system is due to the polymer chain segmental movement due to the ineffective interaction in the composite system. This leads to the formation of more unbound charges in the

system. The strong interaction between the PO_4^{3-} groups of hydroxyapatite with the reactive functional groups (hydroxyl and amino groups) of chitosan has caused a reduction in the formation of dipoles causing low sig' for HA4 composite system. Overall, an inter-connective conductive path has been formed that controls the dc conductivity in the material. The dielectric data shows secondary relaxation at higher frequency range (Jinitha et al. 2020).

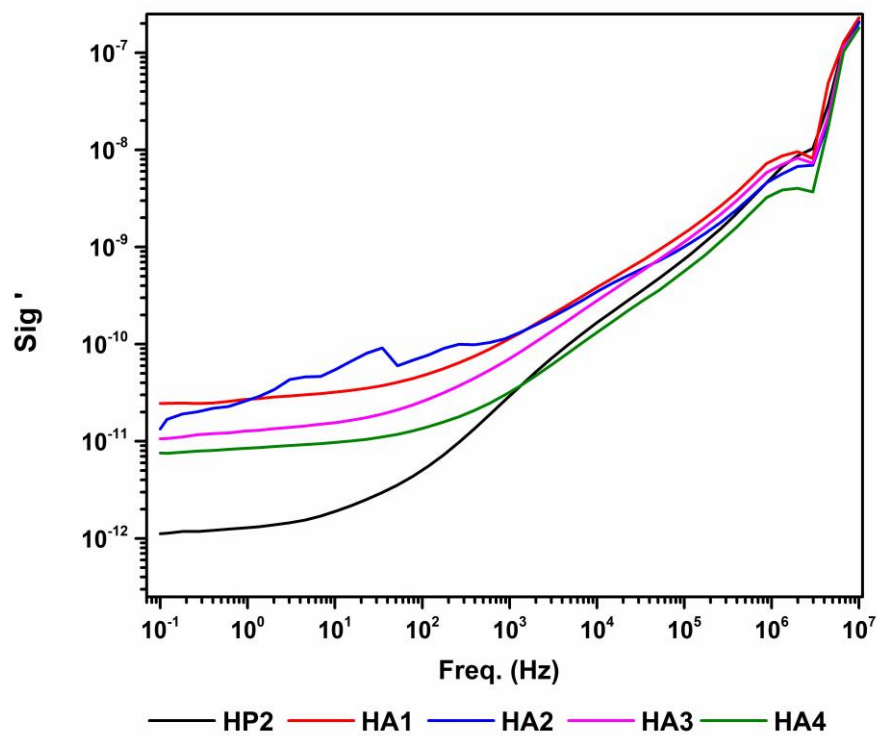


Figure 6.13 Frequency dependence of ac conductivity of HA composite series

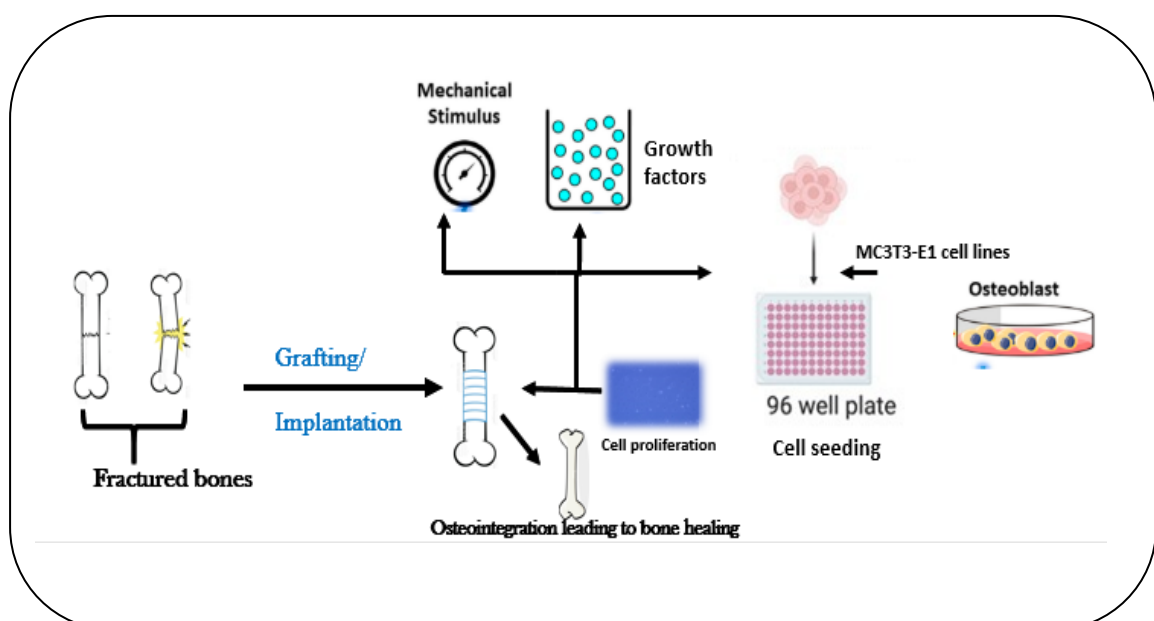
Chapter 7

Biodegradable and Biocompatibility Studies of High Density Polyethylene / Chitosan Composites and High Density Polyethylene / Chitosan / Hydroxyapatite Composites

Summary

The biodegradable and biocompatibility analysis of HDPE / Chitosan composites and HDPE / Chitosan / Hydroxyapatite composites were studied. The biodegradability of the composites was analyzed using water sorption analysis and soil burial tests. The mechanical strength of the samples after the soil burial test was evaluated. The surface wettability of the composites was carried out using contact angle measurements. The biocompatibility of the system was further studied using MC3T3-E1 cell lines. The prepared composites showed enhanced cell proliferation making the system a potential bone implant material.

Graphical Abstract



7.1 Introduction

Bone implants fulfill the healing procedure of bone fragments, initiate bone cell growth and provide mechanical support to the damaged portion. To initiate the cell response, the topography, surface roughness, sorption properties, surface wettability and cell compatibility needed to be understood in detail. Various steps in a cell–material interaction involves: a) cell contact b) cell attachment and c) cell adhesion. The interactions between HDPE and the fillers - hydroxyapatite and chitosan have a profound effect on the microstructural properties of the system, which in turn affect the surface wettability and cell proliferation in the system. Surface wettability reflects the extent of cell adhesion on the surface of the implant material (Setzer et al. 2009). Sorption studies help to understand the extent of miscibility in the system. The higher the sorption rate of the system more is the degradation rate and swelling attained by the system. Sorption provides the conditions for the degradation process and paves the path for the microorganisms to reach the composite system. The presence of plasticizers and compatibilizers has affected the degradation rate as well as the sorption rate (Sarifuddin et al. 2013). Palm oil as plasticizer has increased the segmental mobility, hence relaxing the polymer chains in the composite by enhancing the interaction between the reactive groups of the filler and the matrix. Beyond the optimum concentration of the filler, the particles undergo agglomeration or fill up the pores and affect the biodegradation rate to a great extent. The biocompatibility of the composite surface is influenced by the hydrophilicity of the surfaces, as they are more favorable for bone growth. Hence, the contact angle measurements have a huge impact on the cell proliferation of the prepared composites.

The current chapter studies the biodegradability of HC composite series and HA composite series through sorption tests and soil burial analysis. Furthermore, the mechanical studies of the composites after soil burial analysis were analyzed and compared. The water contact angle measurements of the developed composites were analyzed and correlated with the cell proliferation measurements using MC3T3-E1 cell lines.

7.2 Results and Discussion

7.2.1 Water sorption studies

7.2.1.1 Water sorption studies of HC composite series and HP composite series

The % water sorption for HC composite series and HP2 are given in Figure 7.1.

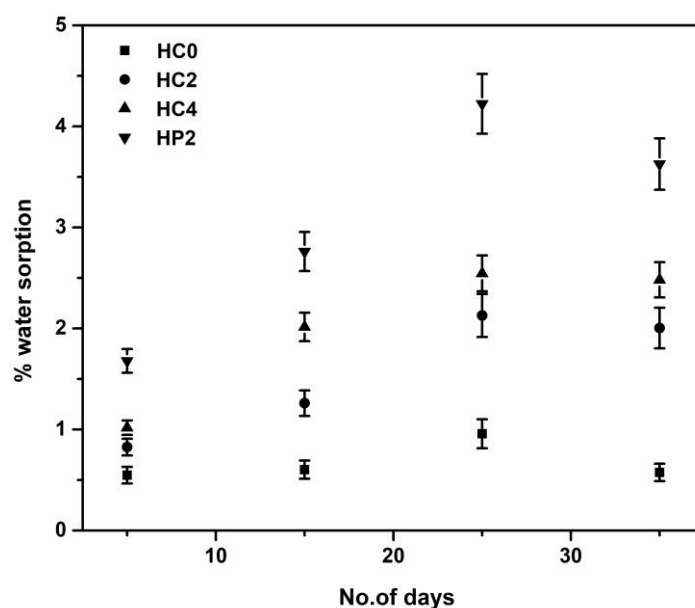


Figure 7.1 Water sorption studies of HC composite series and HP2

The water uptake capacity of the prepared films is calculated using Equation 17 in Chapter 2. Initially, a sharp uptake of water is observed in all cases and the % water sorption is slowly decreasing with the increase in the number of days. It was observed

that the sorption rate of chitosan-added samples is higher than HC0. For HC composite series, HC2 has the lowest water sorption ability. This can be attributed to the lesser availability of the reactive functional groups, arising due to the improved interaction between chitosan and compatibilized HDPE. The high interaction between the reactive groups of chitosan and compatibilized HDPE in HC2 was further supported by the high dielectric constant and low dissipation constant mentioned in Chapter 6. When palm oil is added to HC2, % water sorption is further increased with the increase in concentration of palm oil. As a result, the segmental mobility within the composite increases, providing more free space within it resulting in more water uptake (Sanyang et al. 2015). This in turn allows the matrix to adsorb more water promoting water clustering at successively higher hydration levels (Muhammad et al. 2016).

7.2.1.2 Water sorption studies of HA composite series

Water absorption curves of HA composite series are illustrated in Figure 7.2. in which the % water sorption is plotted against the number of days taken for study. The effect of chitosan and hydroxyapatite in compatibilized HDPE at room temperature is studied here. It is evident from the graphs that the presence of chitosan has increased the water sorption rate. But the presence of ceramic phase has significantly reduced the % water sorption rate as observed in the previous studies. A decrease in sorption value is observed with decrease in filler concentration from 10 wt % HA to 2 wt% HA. When water is absorbed at a higher rate, the polymer chains can undergo a relaxation process such that the probability of elution of unreacted monomer chains trapped in the composite matrix becomes easier (Ghazi et al. 2021). This can contribute to the degradation of the composite system over time.

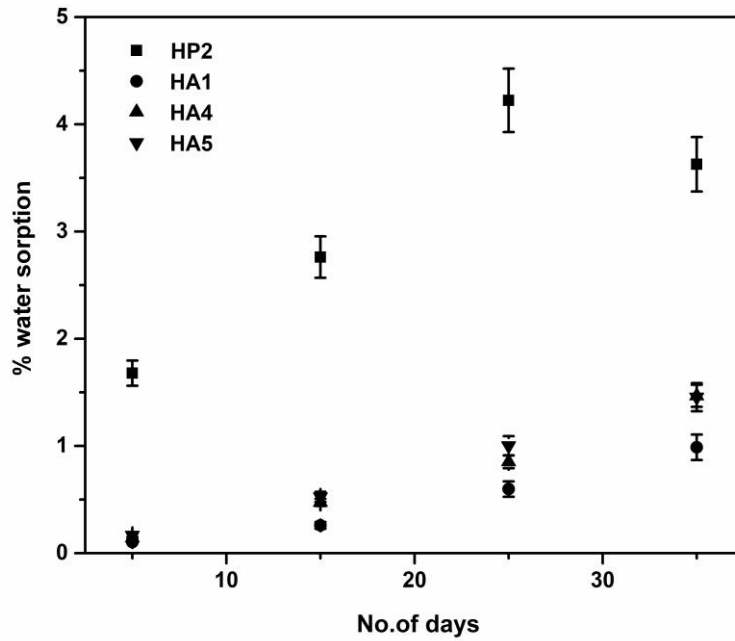


Figure 7.2 Water sorption studies of HA composite series

7.2.1.3 Water sorption studies of HAW composite series

The water sorption properties of plasticized HA4 and HA5 with its un-plasticized samples are shown in Figure 7.3.

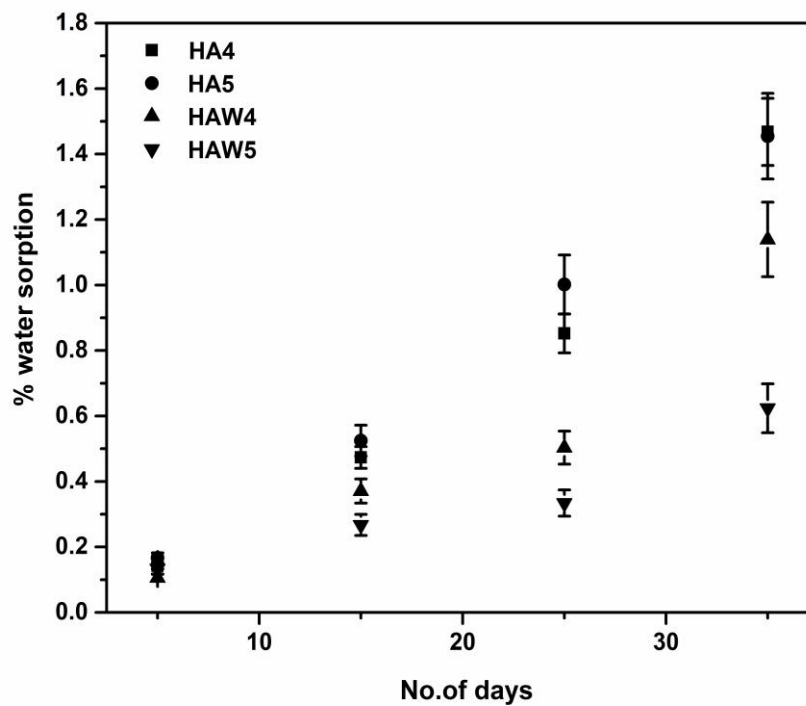


Figure 7.3 Water sorption studies of HAW composite series

The studies revealed that un-plasticized hydroxyapatite composites exhibit lower sorption rate when compared with HA4 and HA5. As observed in all composite series, the composites show a sharper uptake of water in the initial days. The palm oil in the composite systems - HA4 and HA5, has increased the segmental mobility as well as the space between the polymer chain enabling more absorption of water. HA5 having higher concentration of hydroxyapatite, has formed more micro-cracks and voids in the system as observed from impact studies, leading to more water sorption than HA4. But in the absence of palm oil, the hydroxyapatite is adhered to the melt mixed polyethylene / Chitosan system forming small cavities with smooth surfaces. This interface between the matrix phase and filler phase allows the water to reach the chitosan domains where it gets absorbed by the unreactive chitosan domains (Correlo et al. 2007).

7.2.2 Soil burial tests

Soil burial test enables to know the degradation behavior of a system when introduced to a decomposition system consisting of compost. The degradation of a composite depends upon the nature of the filler, matrix, plasticizer, miscibility between the components and the water uptake capacity of the composite systems.

7.2.2.1 Soil burial analysis of HC composite series

The soil burial analysis of HC composite series and HP composite series are shown in Figure 7.4. Highest % weight loss is observed for the chitosan incorporated systems incorporated with and without palm oil.

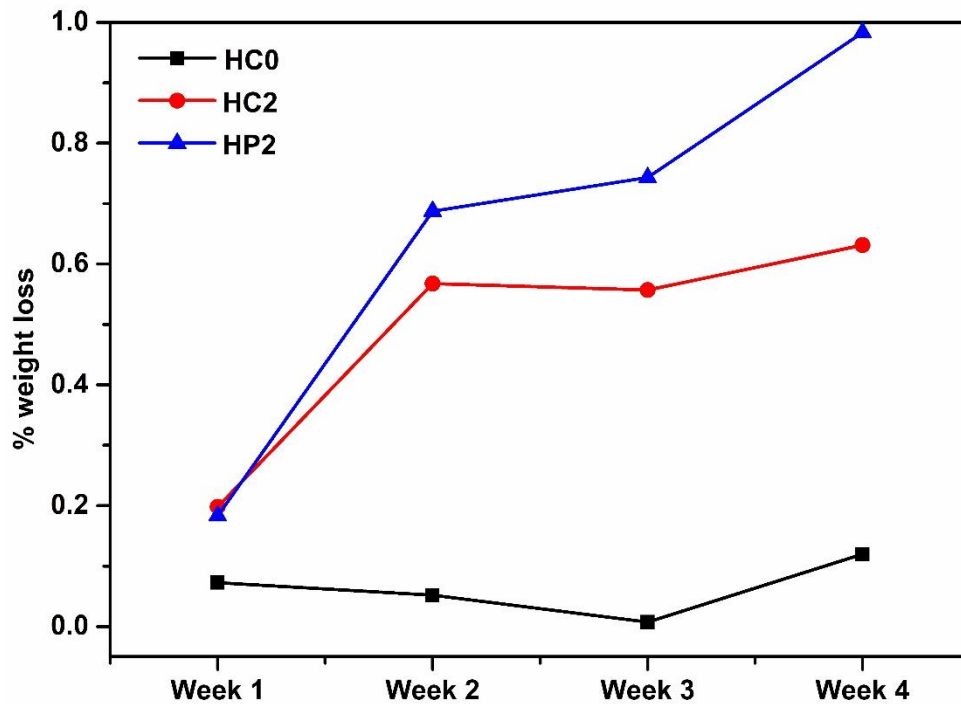


Figure 7.4 Soil burial analysis of HC0, HC2 and HP2 (*The solid lines shown to understand the degradation rate*)

The de-colouration observed for the composites after soil burial analysis are an indication of the microbial attack on the system as observed in Figure 7.5. HC0 has been noted with the lowest weight loss, which is due to the inert nature of maleic anhydride compatibilised HDPE (Rzayev 2011). The polymer matrix is not susceptible to microbial attack so that it gets more time to degrade than the corresponding chitosan incorporated composites. The weight loss for all the composites gives an indication of potential of biodegradability of the composites in the soil due to the presence of the bio-filler in the composite (Varyan et al. 2022). Absorption of moisture from the soil during the burial and the action of micro-organisms leads to the consumption of reactive groups in the system resulting in weight loss.

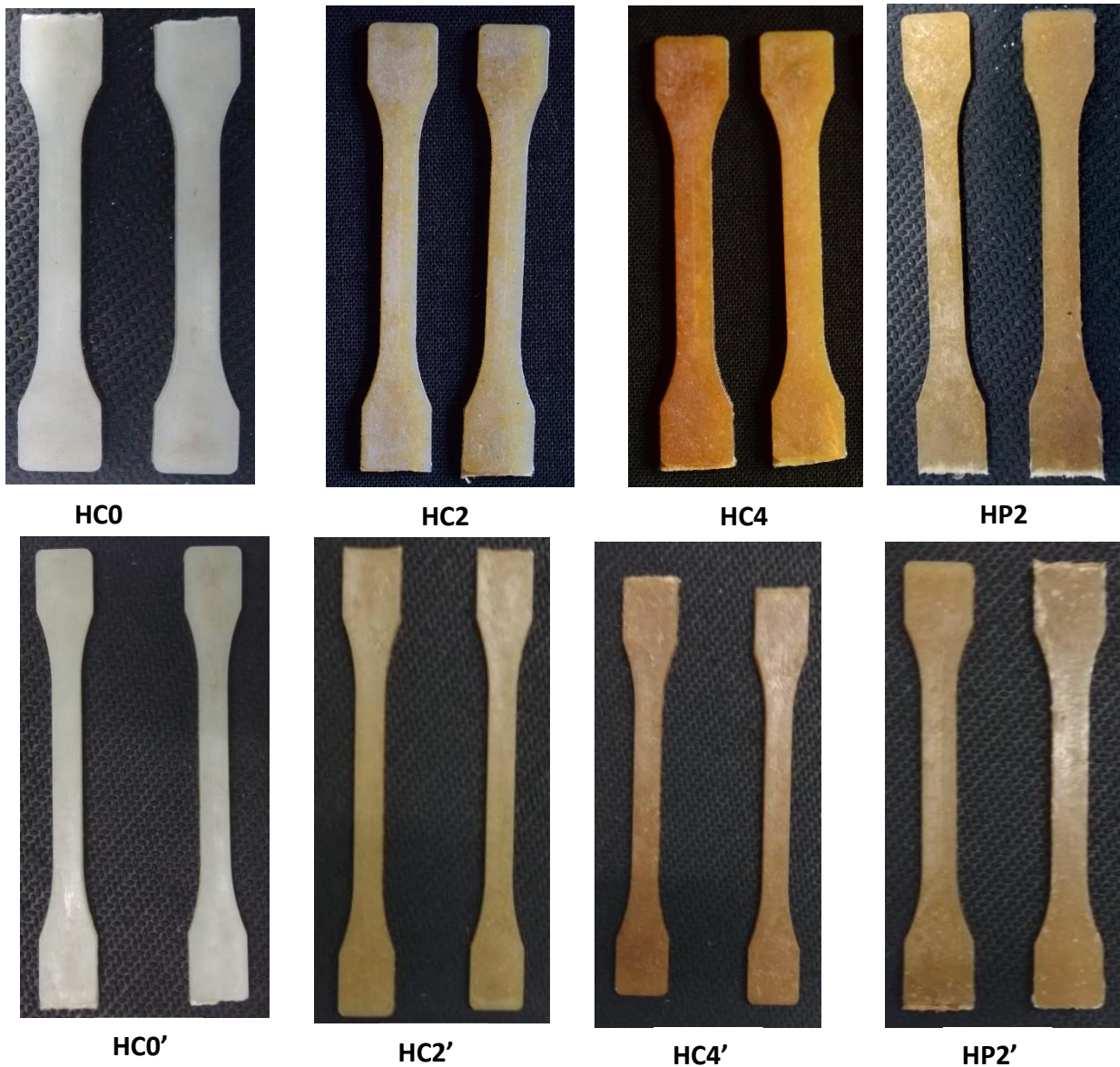


Figure 7.5 Images of composites before degradation (HC0, HC2, HC4 and HP2) and after 30 days of degradation (HC0', HC2', HC4' and HP2')

Higher the % water sorption exhibited by the composite, easier for the microbes to reach the composite system. Although, complete degradation of the composite is not achieved in 35 days, a significant reduction in the weight of the composite systems has been noted. The presence of hydrophilic filler, chitosan, has also triggered the degradation process, as it can act as a nutrient source for microbial growth. As reported in various works, the degradation process of a synthetic polymer- bio-filler is

usually initiated by the destruction of the bio-component. It occurs through the formation of crack propagation, followed by the formation of free radicals on the surface of the material. Hence, more the presence of unreactive chitosan and free holes in the composite more is the degradation (Kusumastuti et al. 2020).

7.2.2.2 Soil burial analysis of HA composite series and HAW composite series

The weight loss analysis of HA composite series and HAW composite series is depicted in Figure 7.6. All the composites in soil degraded rapidly in the first 7 days.

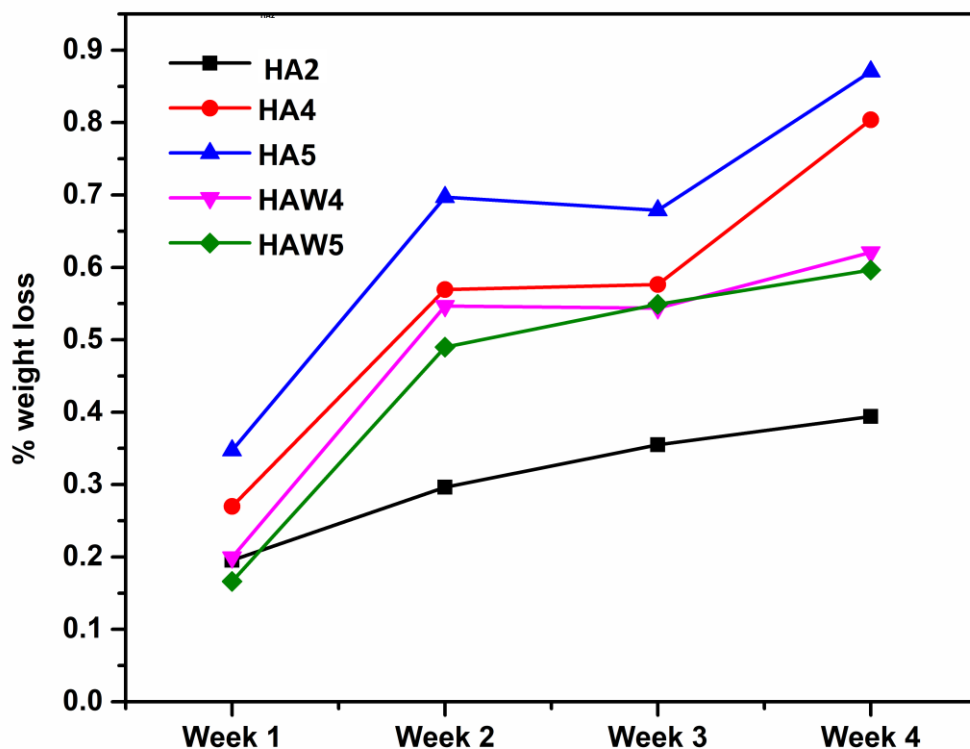


Figure 7.6 Soil burial analysis of HA composite systems and HAW composite systems

As observed from the graphs, all the samples show a rapid weight loss in the initial 7 days. This rapid degradation was due to the composting process, which occurred in two main stages: an active composting stage and a curing period. In the first stage, the

temperature rose and remained elevated as long as there was available oxygen, which resulted in strong microbial activity. In the second stage, the temperature decreased but the composite continued to compost at a slower rate (Chamas et al. 2020).

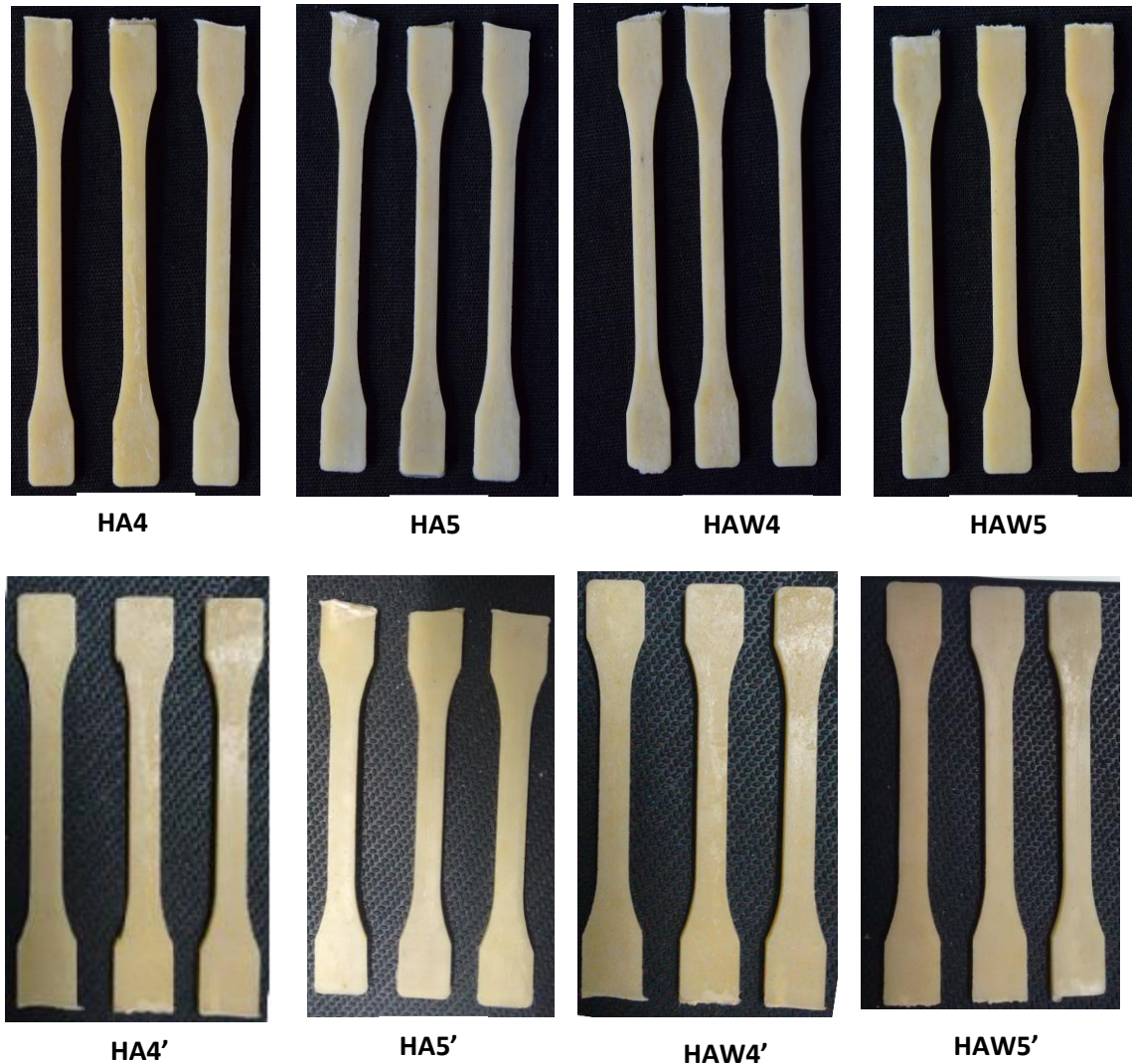


Figure 7.7 Images of composites before degradation (HA4, HA5, HAW4 and HAW5) and after 30 days of degradation (HA4', HA5', HAW4' and HAW5')

The highest biodegradability is observed for HA5 which showed a weight loss of up to 0.87% in a burial time of 4 weeks. The lowest weight loss is observed for HA4 and HA2. The minimum concentration of hydroxyapatite in HA2 has been one reason for the lowest weight loss for the system. The better interaction between the filler and matrix has caused HA4 degradation to become slower (Cheah et al. 2019). The de-

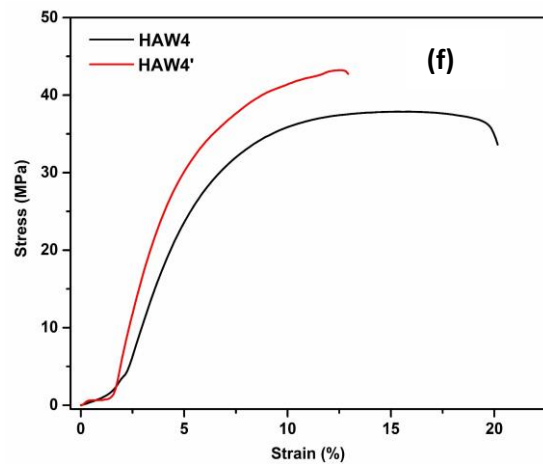
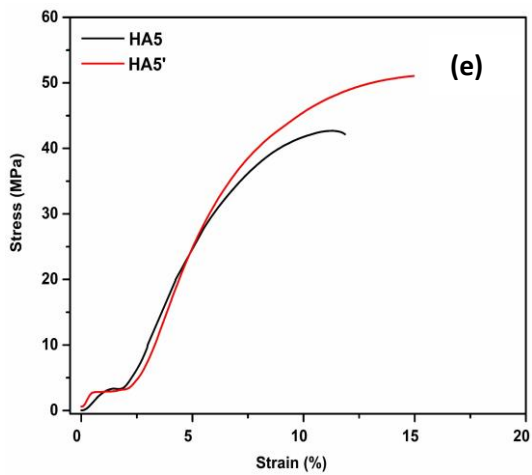
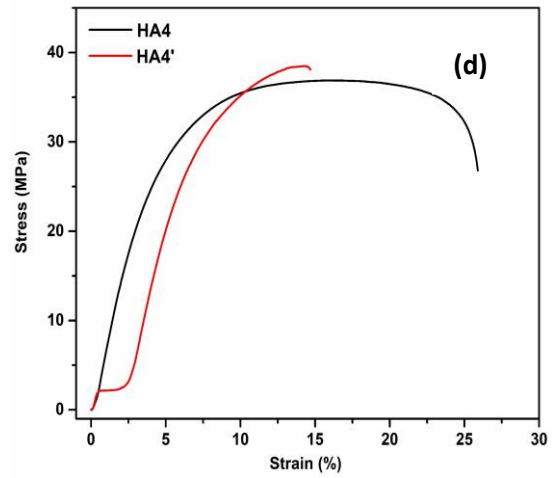
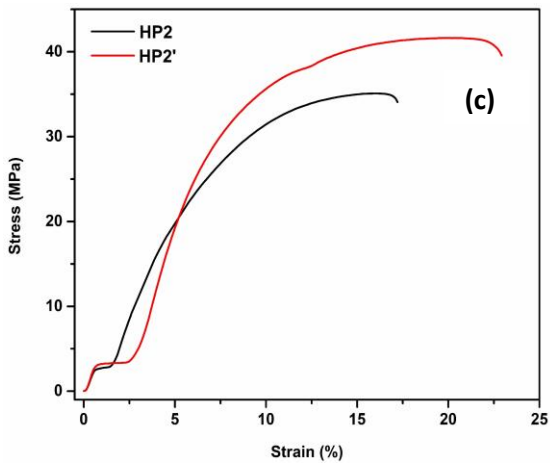
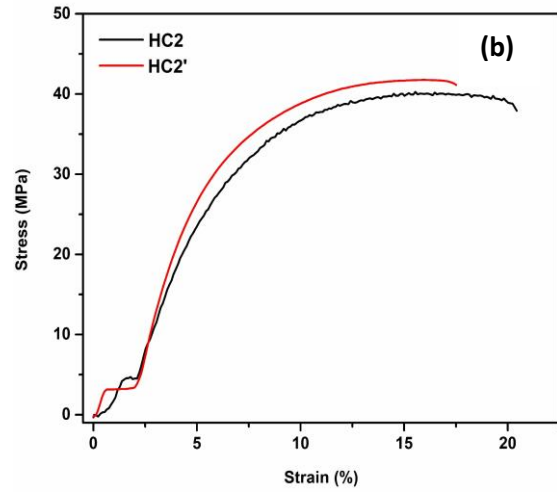
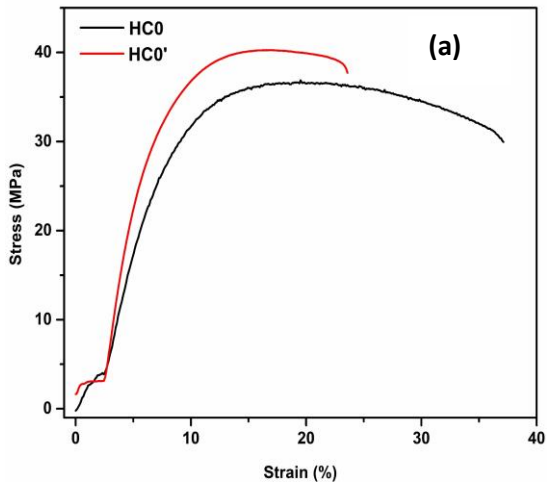
coloration obtained for the HA and HAW composite series are shown in Figure 7.7. The presence of palm oil has improved the segmental mobility and adhesion between compatibilized HDPE with chitosan and hydroxyapatite making it less susceptible for microbial attack. The moisture absorbing characteristics and interfacial bonding effect of chitosan along with the poor miscibility of filler in the matrix in the absence of plasticizer present in the system can be cited as the main reason for the reduced weight loss in the non-plasticized hydroxyapatite composite (Haq et al. 2016).

7.2.2.3 Mechanical strength analysis of HC, HP and HA composite series – before and after soil burial analysis

The effect of biodegradability on the mechanical properties of composites gives an insight into the structural properties as well as bio-compatibility of the system. Various factors such as molecular weight, sterilization techniques, orientation and interaction of filler with the matrix, orientation of crystalline and amorphous chains, processing conditions, pH of the soil, temperature, humidity and measuring techniques contributes to the mechanical strength of the system after soil burial analysis (Hersztek and Kopeć 2019). HDPE is a semi-crystalline polymer, consisting of amorphous phase and crystalline regions. The strength and rigidity of a system can be studied from the crystalline regions of the composite, whereas elastic properties and flexibility can be characterized from the amorphous regions of the system (Sarmah and Rout 2020). The crystallinity as well as the amorphous nature of the composites can be identified from the stress-strain analysis of the composites after soil burial analysis.

The stress-strain analysis curves of HC, HP and HA composite series before and after soil burial study are shown in Figure 7.8. For all composite systems, a reduction in

weight was followed by an increase in tensile strength and a decrease in elongation at break as observed from the reports.



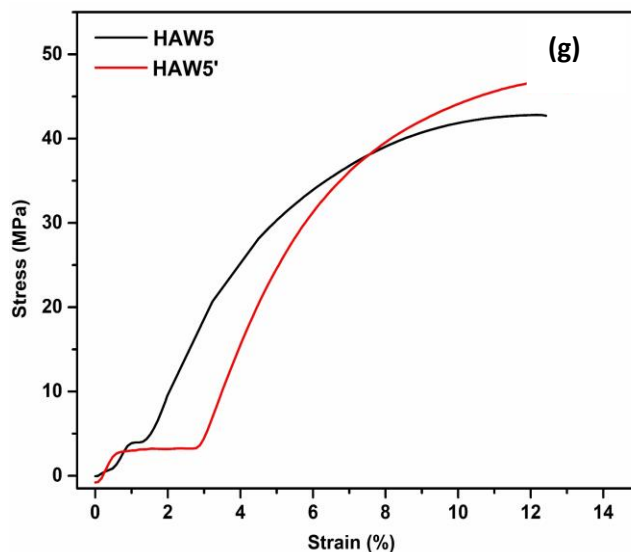


Figure 7.8 The stress-strain analysis of the composite systems (a) HC0, (b) HC2, (c) HP2, (d) HA4, (e) HA5, (f) HAW4 and (g) HAW5 before and after 30 days of soil burial analysis

*HC0', HC2', HP2', HA4', HA5', HAW4' and HAW5' indicates the samples after soil burial analysis

The increase in tensile strength observed in all composites after soil burial analysis can be attributed to the variation in crystallinity achieved by the system. During the degradation process, microbial attack is prominent in the amorphous region than the crystalline region. In HC0, the presence of maleic anhydride has increased the crystallinity of the system. During the soil burial process, the microbes consume the amorphous regions and an increase in tensile strength with reduced elongation at break is observed due to its crystalline regions (Sarmah and Rout 2020). The presence of 5 wt% of chitosan in HC2, has been optimized due to the homogeneous distribution of filler in the matrix and good mechanical strength as obtained in Chapter 3 (Figure 3.1). But after soil burial analysis, the tensile strength and elongation at break is maintained due to the improved miscibility and crystallinity achieved by the system.

With the addition of 5 wt% of palm oil in HC2 composite system, the tensile strength is increased with increase in elongation at break. This is because, after the consumption of amorphous regions, the short chains of the polymer untangles, creating more space to move. Due to this, the elongation of the polymer chains occurs with increase in crystallinity. But the presence of hydroxyapatite further increases the crystallinity of the system and creates a reduction in elongation at break unlike HP2. This is due to the presence of more stiff crystallite particles that cannot elongate unlike the amorphous chains (Gleadall 2015). As the microbes consume the amorphous region of the composite in a faster rate, the crystalline region remains unaffected and the stiffer crystalline region cannot elongate like the amorphous chains. The presence of crystalline region makes the system having high tensile strength and lower elongation at break as observed in HA4. At the same time HA4, was able to retain its mechanical strength even after the soil burial analysis due to its enhanced miscibility and crystallinity achieved during the mixing process. With higher concentration of hydroxyapatite in HA5 composite system, the formation of agglomerates is higher causing an increase in the amorphous content in the system. In such cases, the weight loss is higher with increased mechanical strength. For HAW4 and HAW5, the entanglement of polymer chains after the soil burial analysis provides an increase in mechanical properties of the system. After the degradation of the amorphous regions, the microbes start consuming the crystalline regions causing an increase in the proportion of larger crystals. Moreover, after causing a reduction in the basic properties of the materials, the polymer units are converted to monomer units, which is further converted to CO₂ and water (Ghatge et al. 2020). Hence, the biodegradation studies have a positive impact on portraying HDPE / Chitosan / Hydroxyapatite polymer composites as a potential bone-implant material.

7.2.3 Contact angle analysis of the optimized High density polyethylene / Chitosan / Hydroxyapatite Polymer composites

The hydrophilicity of a material is an important factor that determines the cell – biomaterial interaction. The hydrophilicity of a polymer depends upon the surface roughness, aggregation of filler in the matrix, pH etc. In general, the material with contact angle below 100 is generally expressed in terms of its hydrophilicity. The hydrophilicity of the optimized films has been analyzed by measuring the contact angle values of water droplets. High contact angle relates to lower hydrophilicity of the system. Neat HDPE and chitosan generally have a contact value of 101° and 83° respectively. It was noted that highly hydrophilic surfaces have negative impact on the cell-implant material.

It has been observed that the contact angle values of the composites are lying in the range of 50° and 85° making them appropriate for protein adsorption and cell adhesion. The hydrophilic value of compatibilized HDPE, HC0 can be attributed to the presence of reactive anhydride groups on HDPE. When chitosan is added, the hydrophilicity of the composite is reduced to 81.7°, which can be related to the surface morphology of the system. The surface alterations at the microscale as well as the less availability of functional group of chitosan in the system due to the interaction between the filler and the matrix has also caused to the formation of low contact angle values for HC plasticized composite series. (Tamburaci et al. 2019, Kubies et al. 2010, Carrasco-Guigón et al. 2017, Sivaselvi and Ghosh 2017).

Table 7.1 Contact angle values of High density polyethylene / Chitosan / Hydroxyapatite composites

Sl. No	Sample Code	Contact angle
1	HC0	78.9 ± 2
2	HC2	81.7± 1
3	HP2	77.9± 1
4	HA4	80.8± 0.5
5	HAW4	81.9±0.5

On exposing to polar liquid like water, the hydrophilic groups in the composite can interact with the polar groups of the liquid making the surface more wettable. The water contact angle value of neat chitosan film is $83.6 \pm 2.0^\circ$ as reported (Lewandowska 2015). HC2 and HP2 has a water contact angle value of 81.7° and 77.9° indicating more hydrophilic properties to HC2 and HP2 composite system. When 8 wt% of hydroxyapatite is added, the water contact angle value is further changed to 80.8° . This can be ascribed to the more crystalline nature attained by the composite upon the addition of hydroxyapatite that further restricts the spreading of water on the film surface. HAW4 is showing more hydrophobic nature, which can be attributed to the increased roughness attained by the composite (Allothman et al. 2014). Hence, the plasticized composites are more hydrophilic than the un-plasticized systems as shown in Figure 7.9.

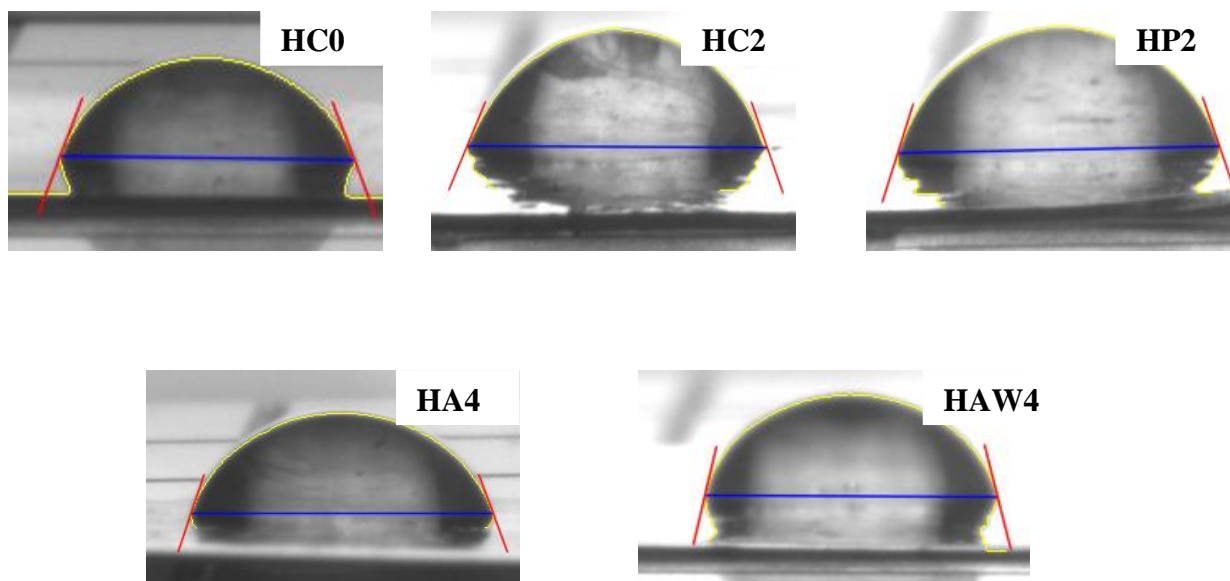


Figure 7.9 Contact angle measurements of the High density polyethylene / Chitosan / Hydroxyapatite polymer composites

7.2.4 Cell Proliferation analysis of the optimized High density polyethylene / Chitosan / Hydroxyapatite Polymer composites

The in-vitro cell behavior on the composites has been evaluated using MC3T3-E1 cells. The proliferative efficacy on the test composites has been measured by MTT assay after 24 h of exposure to the test materials. The percentage proliferation of the cells was calculated with respect to the untreated cell control, as shown in Table 7.2. The cell growth level on plasticized HC2 and HA4 was significantly higher than HC0. This enhancement may be due to the presence of nano-hydroxyapatite in the composites which boosted the osteoblastic phenotype to be effectively proliferated. The cell proliferation was observed to be very low in HC2 and also in un-plasticized HDPE/Chitosan/Hydroxyapatite composite system. The presence of palm oil in HP2 and HA4 certainly increased the crosslinking and interaction between the components in the composite system. The relative decreased cell proliferation in HC2 and in

HAW4 composite system can be attributed to the surface roughness of the composites.

Table 7.2 The cell proliferative efficacy of the test composites on mouse pre-osteoblast MC3T3-E1 cells. Values are represented as relative mean % \pm SD (n=3)

Sl. No	Sample	Cell Proliferation
1	HC0	118.13 \pm 3.03
2	HC2	104.53 \pm 3.03
3	HP2	142.67 \pm 3.61
4	HA4	125.87 \pm 5.33
5	HAW4	115.20 \pm 2.12

Increased surface roughness can retard cell proliferation, as reported by several studies. Grit-blasting and hydrophobic character of the diamond films was found to be responsible for the decrease in cell proliferation of hFOB human osteoblastic cell line (Heinrich et al. 1997). Increase in the surface roughness decreased the cell proliferation and migration of MG63 osteoblast-like cells via decreased expression of angiogenic and osteogenic markers (Andrukhov et al. 2016). The composites possessed mechanical properties similar to the natural bone and promoted cell proliferation. Use of chitosan phosphate in polymeric matrix ensured the uniform distribution of the particles along with particle-polymer interfacial interactions and promoted proliferation of L929 mouse fibroblasts (Pramanik et al. 2009). Higher mechanical strength of the polymer composites provides significant support for enhanced shelf-life in the *in vivo* scenario for biomedical and tissue regenerative applications. Biomaterials with compressive and elastic strength are known to be comparable to the host tissue promoting structural integrity in clinical applications

(Riches et al. 2017). Enhancement of the mechanical strength remains a challenge in bone tissue engineering (Venkatesan and Kim 2010). The prepared polymeric composites displayed increased mechanical strength indicating its promising future utilization in biomedical applications. The cell proliferation and cell distribution were assessed via phase-contrast microscopy as shown in Figure 7.10.

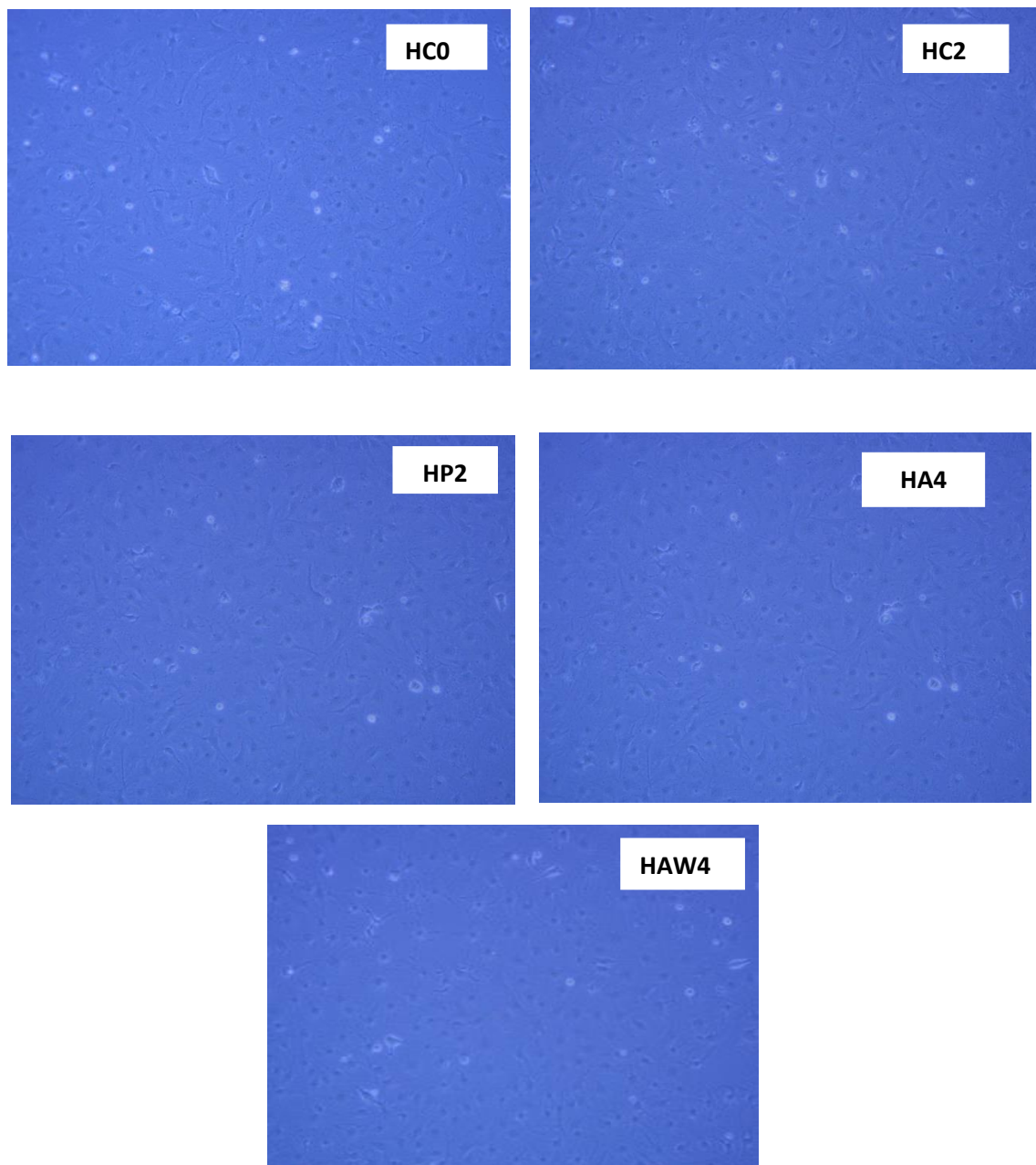


Figure 7.10 Fluorescence images of (a) HC0, (b) HC2, (c) HP2, (d) HA4 and (e) HAW4

It is also noted that the highly proliferated pre-osteoblasts had small globules of mineral deposits on them together with cellular attachments. As observed, the palm oil added samples enhanced cell proliferation. Cell density was found to be highest in HP1 followed by HA4, HC0, HAW4 and HC2 respectively. Compared to the untreated control cells, the cells adhered to the polymeric composite films displayed higher proliferation, as indicated by the compact distribution of the cells. All the tested composites showed good cyto-compatibility on osteoblasts and hence can be promising for biomedical applications after further pre-clinical and clinical validation.

CONCLUSIONS

The increased research on bio-based composites for bone-tissue engineering has led to the development of HDPE / Chitosan / Hydroxyapatite Polymer composites with the aim of improving the physical, microstructural and bio-based properties of the currently available bone replacement materials. Two sets of composites –binary composites (HDPE / Chitosan) and ternary composites (HDPE / Chitosan / Hydroxyapatite) has been developed. The effect of palm oil on the plasticized and unplasticized systems were also compared and analysed. Palm oil as plasticizer has been added to improve the segmental mobility of the system and has also played a role in the formation of pores in the system. The major conclusions derived from the Results and Discussions are given below:

Mechanical strength has been considered as one of the major parameters for designing HDPE / Chitosan / Hydroxyapatite bio-composites for bone tissue engineering applications. The prepared composites have been optimized, based on their ability to hold an external impact force. Among the binary composites systems, HC2 has been optimized due to its ability to hold impact energy, arising from the homogeneous distribution of chitosan in HC0. With the addition of varying concentrations of palm oil to this system, the optimized HP2 has resulted in similar impact strength to HC2. But, a slight reduction in tensile strength has been noted in palm oil plasticized samples when compared with the unplasticized samples, due to the interaction of the oleic acid component of palm oil with the additives added during the preparation process. Furthermore, the segmental mobility achieved during the addition of palm oil has improved the interaction of filler with the matrix. When the increasing concentration of hydroxyapatite was added to HP2, the interaction between hydroxyapatite and chitosan was increased notably. An increase in 67 % of tensile strength was noted for the HA4 composite system than the reported composite systems and currently available commercial bone implants.

The tensile strength data obtained from experimental methods were compared and correlated using computational modelling data. The closeness of theoretical data with experimental data showed the increasing isotropic nature of the composites. The theoretical predictions showed 85% accuracy for the composites prepared. The closeness of composites to isotropic nature was also predicted through Finite Element Analysis. The SEM images of the tensile fractured surface also showed a slight wave-like morphology similar to HC0, showing the ductile nature of the composites. This was confirmed through the elongation at break observed from the stress-strain graphs, arising due to the enhanced crosslinking in the composites. Table 1 shows the mechanical properties of the optimized composites.

Table 1 Mechanical properties of the optimized composites: HC2, HP2 and HA4

Mechanical properties	HC2	HP2	HA4
Impact strength (kJ/m²)	105 ± 2	102 ± 2	115.1 ± 3
Tensile strength (MPa)	40.3 ± 0.1	35.1 ± 0.90	36.9 ± 0.30
Young's Modulus (GPa)	0.585 ± 0.03	0.549 ± 0.03	0.739 ± 0.03

The microstructural properties of HDPE / Chitosan binary composites and HDPE / Chitosan / Hydroxyapatite ternary composites include the interaction between fillers and matrix, crystallinity, extend of free holes formed due to crosslinking, and phase formation are discussed using Fourier Transform Infrared spectroscopy, X-ray diffractometry, and Positron annihilation lifetime spectroscopy. The FTIR studies show the interaction of maleic anhydride with HDPE from the peaks obtained at Table 2. The segmental mobility arising from the chain relaxation with the addition of palm oil has improved the crosslinking and interactions in the composite system. Peak shift, peak broadening, and variation in the peak intensity as observed from the FTIR-ATR spectra of the prepared composites. The characteristics peak of the

individual components were retained in the spectra and confirms the contribution of the properties of HDPE, chitosan, and hydroxyapatite in the formation of the final system.

Table 2 Characteristics FTIR-ATR peaks of HDPE / Chitosan / Hydroxyapatite composites

Sl.No	Peaks noted(cm^{-1})	Peaks assigned
1.	1712 and 1748 cm^{-1}	Symmetric stretching of cyclic anhydride
2.	1129 cm^{-1}	C-O-C stretching of chitosan
3.	1050, 571 and 576 cm^{-1}	PO_4^{3-} symmetric stretching band and OH in-plane bending of HPO_4

The XRD analysis also shows no new phase formations during the processing of the composite systems. A slight reduction in crystallinity has been obtained with the addition of chitosan. But, with the addition of palm oil, the alignment of the polymer chains is improved owing to a homogeneous distribution of filler in the matrix. The addition of highly crystalline hydroxyapatite has further improved the crystallinity of the optimized system as shown in Table 3. A higher concentration of filler promoted the formation of agglomerates, which has been observed as peak broadening in the XRD spectra.

Table 3 % crystallinity of HDPE / Chitosan / Hydroxyapatite composites

Sample	HC2	HP2	HA4
% crystallinity	35.7	41.3	86.2

The effect of concentration and interaction of filler in the matrix decides the formation of free holes in the system. HC2 shows a reduction in o-Ps lifetime (τ_3) and o-Ps intensity (I_3). The addition of palm oil has also reduced the free-hole formation by 20 \AA^3 as compared with HC0. Further addition of hydroxyapatite has reduced the fractional free holes formed in the system, indicating the formation of a large number of free holes with reduced pore size. This is an

indication of the formation of a system with high crosslink density leading to increased mechanical properties. Higher the concentration of hydroxyapatite in the system beyond the optimum concentration of HA4, the particles tend to accumulate in the pores formed leading to the formation of agglomerates.

The thermal analysis (Thermogravimetric analysis (TGA) and Dynamic mechanical analysis (DMA)) of HDPE / Chitosan and HDPE / Chitosan / Hydroxyapatite composites were studied for estimating the thermal stability and viscoelastic properties of the system. The decrease of degradation temperature of HC0 to 350 °C indicates the compatibilization of maleic anhydride in HDPE. The addition of varying concentrations of chitosan as filler in HDPE / Chitosan systems has caused a shift in degradation temperature to 482 °C. The improved miscibility of chitosan with compatibilized HDPE has helped in forming a highly stable system. The preparation of the hybrid system employing hydroxyapatite and chitosan in HC0 also increased the thermal stability of the system as observed from the degradation temperature of HA4 at 480 °C due to the formation of a highly homogeneous system formed as a result of increased crosslinking. The addition of palm oil also showed a similar trend in the pyrolysis process which shows the similarity in the formation of chemical bonds and interactions. The thermal stability of the composites was obtained from the activation energy analysis analyzed from Coats Redfern Model. The high activation energy for the HA4 hybrid system shows the formation of a high heat resistant material formed due to the improved interfacial interaction.

Table 4 Activation energy analysis of HDPE / Chitosan / Hydroxyapatite composites

Sample	HC2	HP2	HA4
Activation Energy (kJ/mol)	348	348.2	333.2

The viscoelastic properties of the composites with varying temperatures have helped in studying the storage modulus (E'), loss modulus (E''), and damping parameter ($\tan \delta$). The

high storage modulus for the HC2 system is observed due to the formation of a highly stiffer composite due to the high miscibility achieved by the system. More homogeneous mixing is also noted for HC2 composite as studied from the loss modulus graph.

The glass transition temperature (T_g) calculated from the loss modulus (E'') curves provided information regarding the molecular motion of the composites. Moreover, the absence of β – relaxation peak in the region of -100 to 0 °C for the optimized composites shows the uniform and homogeneous mixing achieved by the systems. Palm oil has facilitated the formation of strong interfacial interaction between the filler and matrix, due to the segmental mobility of the system. The action of palm oil on the amorphous region of the HDPE matrix has further improved bonding and interaction in the system. The crystalline phase as well as the high crosslinking of the composite has provided a mechanically stable system that can withstand the external load.

Table 5 Glass transition temperature of HDPE / Chitosan / Hydroxyapatite composites

Sample	HC2	HP2	HA4
Glass transition temperature (T_g)	-119 °C	-118 °C	-114 °C

The electrical properties of bio-composites provided information regarding the conductivity of the system, homogeneity, and interfacial interaction between filler and matrix. Among the binary composite systems, HC2 exhibited a high dielectric showing indicating its ability to get polarised in the presence of an external electric field. At higher concentration of chitosan, the formation of agglomeration is prominent, leading to unequal charge distribution at the interface. This causes a low dielectric constant for HC3 and HC4 composites. Moreover, the low dielectric loss for HC2 shows the integrity at the interface that makes it efficient to form an insulating barrier. The homogeneous dispersion of chitosan in HDPE has enhanced the conductivity at the surface. The presence of hydroxyapatite HDPE / Chitosan composites has

improved the dielectric constant due to the polar nature of the filler. A high dielectric constant and ac conductivity is noted for HA4, due to the presence of polarised groups and uniformity of the system. The palm oil plasticized samples show high dielectric loss since it improves the segmental mobility and provides more space to act on the amorphous region of the system. This causes an increase in the fractional free hole volume of the composites and produces a high dielectric loss. The presence of polarised groups in the composite makes it a suitable candidate for bone tissue engineering applications.

Table 6 Dielectric constant of HDPE / Chitosan / Hydroxyapatite composites

Sample	HC2	HP2	HA4
Dielectric constant (ϵ_r)	8	11	14.5

The biodegradability of the prepared binary and ternary bio-composites was analyzed using water sorption and soil burial analysis. Among HDPE / Chitosan composites HC2 showed the lowest water sorption ability owing to the lesser availability of the reactive functional groups in the composites, indicating the miscibility of chitosan with HDPE. Palm oil as plasticizer has improved the segmental mobility of the polymer chains through the formation of a large number of free holes in the system. As a result, the water sorption is increased in HP2 composite system when compared with the unplasticized HDPE / Chitosan composite series. Moreover, the presence of hydroxyapatite has caused a reduction in the % water sorption due to the lesser number of reactive groups as well as the reduction in free hole volume formation. The water sorption behaviour is also reflected in the soil burial analysis. The binary composites showed a higher degradation rate than the ternary systems due to the presence of hydrophilic natural polymer chitosan. Higher degradation behaviour is exhibited by the HP2 system, due to the presence of chitosan along with the free holes formed in the system. The water gets absorbed in the free holes in the composite and can help in the elution of the unreactive

monomer units causing an initiation in biodegradation. The microorganisms can easily degrade the amorphous regions of the composites and the agglomerates by causing a reduction in weight loss. The crystalline regions of the system are maintained during the initial stage of degradation and high mechanical strength is maintained by the composites even after a degradation period of 35 days. The biocompatibility of the composites was studied by correlating the water contact angle measurements and cell proliferation analysis. The optimized composites show water contact angle values in the range of 77° to 81° indicating a hydrophilic surface suitable for cell proliferation. The cytotoxicity studies were conducted using MTT assay by employing MC3T3-E1 cell lines. The palm oil plasticized composites were highly hydrophilic and higher cell proliferation was noticed for HC2 and HA4 composite systems. The porosity of the systems as well as the presence of bio-based materials – chitosan and hydroxyapatite in HDPE has resulted in a biomaterial with improved mechanical strength has been developed as potential bone implant materials.

This page is intentionally left blank

RECOMMENDATIONS

- Environmental concerns arising from food packaging materials have been influencing the development of bio-degradable packaging materials instead of petrochemical-based materials. The influence of natural polymers such as chitosan as fillers in synthetic polymers as potential biodegradable material is widely reported due to its anti-microbial properties and good shelf life. Hence, the developed HDPE / Chitosan (HC) composite series can be analysed and compared for their anti-microbial, permeation, and shelf life properties as potential food packaging materials.
- Impact strength analysis and compression strength analysis are important mechanical properties for load-bearing applications. So, the computational simulation using Finite Element Analysis (FEA) employing ANSYS software can be used for predicting the potential of HC composite series and HA composite series for bone-tissue engineering applications.
- Theoretical modelling studies help to analyse the efficiency of the experimental results obtained. Moreover, theoretical predictions from experimental data provide a better understanding of the stability of prepared composites. Besides, the activation energy analysis using the Coats Redfern Model, a comparison of the model fitting methods and model-free methods can be studied on HC composite series and HA composite series, to get a deep understanding of the kinetics of the system. Furthermore, computational simulations can also be performed on the thermal properties of the system for getting information about the stability of the system.
- The *in-vivo* studies are very essential for more relevant and reliable results for the prepared HC and HA composite series as bone-implant materials. Hence, these studies can be conducted further as it helps in the rapid development and improvement of the existing bone implant materials with HDPE / Chitosan / Hydroxyapatite composite systems. A comparison

of the currently available commercial bone implant materials with the prepared HDPE / Chitosan / Hydroxyapatite composite systems can be done to understand the healing and cell-proliferative efficacy.

➤ Reports show that polyethylenes are easily degraded by micro-organisms such as *Streptomyces badius*, *S. setonii*, and *S. viridosporous*. So, the degradation behaviour of the prepared HC and HA composite series can be evaluated in detail with the action of micro-organisms with the thermo-oxidation process. This provides an insight into the anti-microbial and degradation behaviour of the prepared composites.

➤ Reports show that derivatives of chitosan and hydroxyapatite show good cell proliferation and cytotoxic properties. Hence, binary and ternary composite systems comprising the derivatives of chitosan and hydroxyapatite can be prepared and compared with the newly developed HDPE / Chitosan / Hydroxyapatite polymer composites

REFERENCES

- Aboulkas, A., and El Harfi, K. (2008). Study of the Kinetics and Mechanisms of Thermal Decomposition of Moroccan Tarfaya Oil Shale and Its Kerogen. *Oil shale*, 25(4), 426-443.
- Agboola, O., Fayomi, O.S., Sadiku, R.E., Ayoola, A.A., Mokrani, T., Mbuli, B.S., Popoola, A.P.I. and Perry, G. (2021). Evaluation of chitosan/sisal fiber/polyethylene membranes. *Mater. Today: Proc.* 43(2), 832-837.
- Ahn, Y., Jeon, J. H., Baek, C. S., Yu, Y. H., Thenepalli, T., Ahn, J. W., & Han, C. (2016). Synthesis and Non-Isothermal Crystallization Behaviors of Maleic Anhydride onto High Density Polyethylene. *J. Korean Ceram. Soc.*, 53(1), 24-33.
- Albano, C., Cataño, L., Perera, R., Karam, A., and González, G. (2010). Thermodegradative and morphological behavior of composites of HDPE with surface-treated hydroxyapatite. *Polym. Bull.*, 64(1), 67-79.
- Albertsson, A. C. and Hakkarainen, M. (2004). Environmental degradation of polyethylene. *Long term properties of polyolefins*, 177-200. Advances in Polymer Science book series (POLYMER, volume 169)
- Alhijazi, M., Zeeshan, Q., Qin, Z., Safaei, B., and Asmael, M. (2020). Finite element analysis of natural fibers composites: a review. *Nanotechnol. Rev.*, 9(1), 853-875.
- Ali, A., Zahid, N., Manickam, S., Siddiqui, Y., Alderson, P. G. and Maqbool, M. (2014). Induction of lignin and pathogenesis related proteins in dragon fruit plants in response to submicron chitosan dispersions. *Crop Prot.*, 63, 83-88.
- Ali, M.S., Al-Shukri, A.A., Maghami, M.R. and Gomes, C. (2021). Nano and bio-composites and their applications: A review. In *IOP Conference Series: Materials Science and Engineering*. 1067(1), 012093.
- Ali, S.F.A., Elsad, R.A. and Mansour, S.A., 2021. Enhancing the dielectric properties of compatibilized high-density polyethylene/calcium carbonate nanocomposites using high-density polyethylene-g-maleic anhydride. *Polym. Bull.*, 78(3), pp.1393-1405.
- Allothman, O.Y., Fouad, H., Al-Zahrani, S.M., Eshra, A., Al Rez, M.F. and Ansari, S.G. (2014). Thermal, creep-recovery and viscoelastic behavior of high density polyethylene/hydroxyapatite nano particles for bone substitutes: effects of gamma radiation. *Biomed. Eng. Online*, 13(1), 1-15.
- Amin, B., Elahi, M. A., Shahzad, A., Porter, E. and OHalloran, M. A. A review of the dielectric properties of the bone for low frequency medical technologies.. *Biomed. Phys. Eng. Express* 5, 2 (2019).
- Anbinder, P., Macchi, C., Amalvy, J., and Somoza, A. (2016). A microstructural study of acrylic-modified chitosan by means of PALS and SAXS. *Defect Diffus. Forum*, 373, 265-268). Trans Tech Publications Ltd.
- Andrukhov, O., Huber, R., Shi, B., Berner, S., Rausch-Fan, X., Moritz, A., Spencer, N.D. and Schedle, A. (2016). Proliferation, behavior, and differentiation of osteoblasts on surfaces of different microroughness. *Dent. Mater.*, 32(11), pp.1374-1384.
- Arda, B., Bal, A., and Acar, I. (2017). Characterization of the thermal oxidative degradation kinetics of thermoplastics. *Instrum Sci Technol*, 45(5), 558-576.

Arizmendi-Morquecho, A., Chávez-Valdez, A., Navarro, C.H. and Moreno, K.J., 2013. Performance evaluation of chitosan/hydroxyapatite composite coating on ultrahigh molecular weight polyethylene. *Polym. Test.*, 32(1), pp.32-37.

Avalos, S.A., Hakkarainen, M., and Odelius, K. (2017). Superiorly plasticized PVC/PBSA blends through crotonic and acrylic acid functionalization of PVC. *Polymers*, 9(3), 84.

Baatti, A., Erchiqui, F., Godard, F., Bussi eres, D., and B ebin, P. (2020). DMA analysis, thermal study and morphology of polymethylsilsesquioxane nanoparticles-reinforced HDPE nanocomposite. *J. Therm. Anal. Calorim.*, 139(2), 789-797.

Badji, A. M., Ndiaye, D., Diallo, A. K., Kebe, N., & Verney, V. (2016). The effect of poly-ethylene-co-glycidyl methacrylate efficiency and clay platelets on thermal and rheological properties of wood polyethylene composites. *Adv. Chem. Eng. Sci.* 6(4), 436-455.

Bagga, C.S., Jung, S. B., and Bae, H.W. (2014). WO2014152113A2

Bahrani, M., Abenajar, J., and Mart inez, M.  . (2020). Recent progress in hybrid biocomposites: Mechanical properties, water absorption, and flame retardancy. *Materials*, 13(22), 5145.

Balakrishnan, H., Husin, M.R., Wahit, M.U. and Abdul Kadir, M.R. (2013). Maleated high density polyethylene compatibilized high density polyethylene/hydroxyapatite composites for biomedical applications: properties and characterization. *Polym Plast Technol Eng*, 52(8), 774-782.

Banerjee, S., and Sankar, B. V. (2014). Mechanical properties of hybrid composites using finite element method based micromechanics. *Compos B Eng*, 58, 318-327.

Bashir, M. A. (2021). Use of dynamic mechanical analysis (DMA) for characterizing interfacial interactions in filled polymers. *Solids*, 2(1), 108-120.

Bauer, H., Bauer, G., Dingeldein E., and Wahlig, H. (1994). U.S. Patent No: US5338772A

Behzad, M., Tajvidi, M., and Robert H. Falk. (2004). Dynamic mechanical analysis of compatibilizer effect on the mechanical properties of wood flour-High-density polyethylene composites. *Int. J. Eng.*, 17(1), 95-104.

Benabid, F. Z., Kharchi, N., Zouai, F., Mourad, A. H. I., & Benachour, D. (2019). Impact of co-mixing technique and surface modification of ZnO nanoparticles using stearic acid on their dispersion into HDPE to produce HDPE/ZnO nanocomposites. *Polym. Polym. Compos.*, 27(7), 389-399.

Bergquist, P., Zhu, Y., Jones, A.A. and Inglefield, P.T. (1999). Plasticization and antiplasticization in polycarbonates: the role of diluent motion. *Macromolecules*, 32(23), 7925-7931.

Bin Rusayyis, M. A., Schiraldi, D. A., and Maia, J. (2018). Property/morphology relationships in SEBS-compatibilized HDPE/poly (phenylene ether) blends. *Macromolecules*, 51(16), 6513-6523.

Bonardd, S., Robles, E., Barandiaran, I., Sald as, C., Leiva,  ., and Kortaberria, G. (2018). Biocomposites with increased dielectric constant based on chitosan and nitrile-modified cellulose nanocrystals. *Carbohydr. Polym.*, 199, 20-30.

Bonfield, W., Bowman, J.A., and Gryn pas, M. D. (1991). U.K. Patent No: US5017627A

Bonfield, W., Gryn pas, M. D. and Bowman, J. A. (1984). U.K. Patent No: GB2085461B.

Brodland, G. W. (2015). How computational models can help unlock biological systems. In *Seminars in cell & developmental biology*, 47, 62-73. Academic Press.

Cai, X., Tong, H., Shen, X., Chen, W., Yan, J., & Hu, J. (2009). Preparation and characterization of homogeneous chitosan-poly(lactic acid)/hydroxyapatite nanocomposite for bone tissue engineering and evaluation of its mechanical properties. *Acta Biomater.*, 5(7), 2693-2703.

Carrasco-Guig on, F.J., Rodr guez-F elix, D.E., Castillo-Ortega, M.M., Santacruz-Ortega, H.C., Burruel-Ibarra, S.E., Encinas-Encinas, J.C., Plascencia-Jatomea, M., Herrera-Franco, P.J. and Madera-Santana,

- T.J. (2017). Preparation and characterization of extruded composites based on polypropylene and chitosan compatibilized with polypropylene-graft-maleic anhydride. *Materials*, 10(2), 105.
- Cato, T. L., Jessica, D. and Muhammed, A. (1998). U.S. Patent No: US5766618A
- Cecen, V., Seki, Y., Sarikanat, M., & Tavman, I. H. (2008). FTIR and SEM analysis of polyester-and epoxy-based composites manufactured by VARTM process. *J. Appl. Polym. Sci.*, 108(4), 2163-2170.
- Chamas, A., Moon, H., Zheng, J., Qiu, Y., Tabassum, T., Jang, J.H., Abu-Omar, M., Scott, S.L. and Suh, S., 2020. Degradation rates of plastics in the environment. *ACS Sustain. Chem. Eng.*, 8(9), pp.3494-3511.
- Charles, J. (2009). Qualitative analysis of high density polyethylene using FTIR spectroscopy. *Asian J. Chem.*, 21(6), 4477.
- Cheah, S.C. and Ab Wahab, M. K. (2019, December). Morphology and biodegradability of microcrystalline cellulose/chitosan films. In *IOP Conference Series: Materials Science and Engineering* (Vol. 701, No. 1, p. 012053). IOP Publishing.
- Cheng, Y., Morovvati, M.R., Huang, M., Shahali, M., Saber-Samandari, S., Angili, S.N., Nejad, M.G., Shakibaie, M. and Toghraie, D. (2021). A multilayer biomimetic chitosan-gelatin-fluorohydroxyapatite cartilage scaffold using for regenerative medicine application. *J. Mater. Res. Technol.*, 14, 1761-1777.
- Cleetus, C., Thomas, S., and Varghese, S. (2013). Synthesis of petroleum-based fuel from waste plastics and performance analysis in a CI engine. *J. Energy*, 2013.
- Cole, J. and Timothy, S. (2007). US7211266B2
- Cooper, I. (2007). Plastics and chemical migration into food. *Chemical migration and food contact materials*, 228-250.
- Cooper, K., Chen, C.C. and Scopelianos, A. (1997). US5679723A
- Correlo, V. M., Pinho, E. D., Pashkuleva, I., Bhattacharya, M., Neves, N. M., and Reis, R. L. (2007). Water absorption and degradation characteristics of chitosan-based polyesters and hydroxyapatite composites. *Macromol. Biosci.*, 7(3), 354-363.
- Crespo, J. E., Sanchez, L., Garcia, D., & Lopez, J. (2008). Study of the mechanical and morphological properties of plasticized PVC composites containing rice husk fillers. *J. Reinf. Plast. Compos.*, 27(3), 229-243.
- Crowley, J., and Vijaya, B. (2008). Dynamic Constitutive behavior of UHMWPE-HAP Nanocomposites. In *Proc. of the XIth Int. Congress and Exposition*. Orlando.
- Dai, X., Shang, Q., Jia, Q., Li, S., & Xiu, Y. (2010). Preparation and properties of HDPE/CaCO₃/OMMT ternary nanocomposite. *Polym. Eng. Sci.*, 50(5), 894-899.
- Daniel, M., Frank, R. and Tobias, W. (2021). US11103620B2
- Daramola, O.O., Taiwo, A.S., Oladele, I.O., Olajide, J.L., Adeleke, S.A., Adewuyi, B.O. and Sadiku, E.R. (2021). Mechanical properties of high density polyethylene matrix composites reinforced with chitosan particles. *Mater. Today: Proc.*, 38, 682-687.
- Das, A., and Pamu, D. (2019). A comprehensive review on electrical properties of hydroxyapatite based ceramic composites. *Mater. Sci. Eng. C*, 101, 539-563.
- Das, A., Dobbidi, P., Bhardwaj, A., Saxena, V., and Pandey, L. M. (2021). Microstructural, electrical and biological activity in Ca₁₀(PO₄)₆(OH)₂-Ba_{0.5}Sr_{0.5}TiO₃ ceramic composites designed for tissue engineering applications. *Sci. Rep.*, 11(1), 1-14.
- Daunzu, Sandorakauru, B., Anītazikikāni, and Mofusen. (2014). JP2014506506A
- David, C. G., and Srinivas K. (2011). EP2542187B1

Deshpande, S. and Munoli, A. (2010). Long-term results of high-density porous polyethylene implants in facial skeletal augmentation: An Indian perspective, *Indian J Plast Surg*, 43(01), 034-039.

Di Maro, M., Faga, M.G., Malucelli, G., Mussano, F.D., Genova, T., Morsi, R.E., Hamdy, A. and Duraccio, D. (2020). Influence of chitosan on the mechanical and biological properties of HDPE for biomedical applications. *Polym. Test.*, 91, 106610.

Dorozhkin, S.V. (2011). Biocomposites and hybrid biomaterials based on calcium orthophosphates. *Biomatter*, 1(1), 3-56.

Dreghici, D. B., Butoi, B., Predoi, D., Iconaru, S. L., Stoican, O., & Groza, A. (2020). Chitosan–Hydroxyapatite Composite Layers Generated in Radio Frequency Magnetron Sputtering Discharge: From Plasma to Structural and Morphological Analysis of Layers. *Polymers*, 12(12), 3065.

Duarte, M. L., Ferreira, M. C., Marvao, M. R., & Rocha, J. (2002). An optimised method to determine the degree of acetylation of chitin and chitosan by FTIR spectroscopy. *International Journal of Biological Macromolecules*, 31(1-3), 1-8.

Elieh-Ali-Komi, D. and Hamblin, M. R. (2016). Chitin and Chitosan: Production and Application of Versatile Biomedical Nanomaterials, *Int J Adv Res*, 4(3), 411–427.

Essabir, H., Boujmal, R., Bensalah, M. O., Rodrigue, D., & Bouhfid, R. (2016). Mechanical and thermal properties of hybrid composites: Oil-palm fiber/clay reinforced high density polyethylene. *Mech. Mater*, 98, 36-43.

Faria, E. A., and Prado, A. G. (2007). Kinetic studies of the thermal degradation of cellulose acetate/niobium and chitosan/niobium composites. *React Funct Polym*, 67(7), 655-661.

Fathima, P. E., Panda, S. K., Ashraf, P. M., Varghese, T. O., and Bindu, J. (2018). Polylactic acid/chitosan films for packaging of Indian white prawn (*Fenneropenaeus indicus*). *Int. J. Biol. Macromol*, 117, 1002-1010.

Forsyth, M., Meakin, P., MacFarlane, D. R., and Hill, A. J. (1995). Positron annihilation lifetime spectroscopy as a probe of free volume in plasticized solid polymer electrolytes. *Electrochim. Acta*, 40(13-14), 2349-2351.

Fouad, H., Elleithy, R. and Alothman, O.Y. (2013). Thermo-mechanical, wear and fracture behavior of high-density polyethylene/hydroxyapatite nano composite for biomedical applications: effect of accelerated ageing. *J Mater Sci Technol*, 29(6), 573-581.

García, E., Louvier-Hernández, J. F., Cervantes-Vallejo, F. J., Flores-Martínez, M., Hernández, R., Alcaraz-Caracheo, L. A., & Hernández-Navarro, C. (2021). Mechanical, dynamic and tribological characterization of HDPE/peanut shell composites. *Polym. Test.*, 98, 107075.

Ghatge, S., Yang, Y., Ahn, J. H., and Hur, H. G. (2020). Biodegradation of polyethylene: a brief review. *Appl. Biol. Chem.*, 63(1), 1-14.

Ghazi, I. F., Oleiwi, J. K., Salih, S. I., and Mutar, M. A. (2021). Water Sorption and Solubility of Light-Cured Dental Composites Prepared from Two Different Types of Matrix Monomers. In *IOP Conference Series: Materials Science and Engineering* (Vol. 1094, No. 1, p. 012169). IOP Publishing.

Gleadall, A. (2015). Mechanical properties of biodegradable polymers for medical applications. In *Modelling degradation of bioresorbable polymeric medical devices* (pp. 163-199). Woodhead Publishing.

Global Tissue Engineering Market Report 2021: Market to Reach \$26.8 Billion by 2027 - U.S. Market is Estimated at \$3.3 Billion, While China is Forecast to Grow at 13.1% CAGR - ResearchAndMarkets.com, May 17, 2021 07:33 AM Eastern Daylight Time

Goldstein, C., Sprague, S., and Petrisor, B. A. (2010). Electrical stimulation for fracture healing: current evidence. *J. Orthop. Trauma*, 24, S62-S65.

- Gowman, A., Wang, T., Rodriguez-Uribe, A., Mohanty, A. K., and Misra, M. (2018). Bio-poly (butylene succinate) and its composites with grape pomace: Mechanical performance and thermal properties. *ACS omega*, 3(11), 15205-15216.
- Han, X., Chen, T., Zhao, Y., Gao, J., Sang, Y., Xiong, H., & Chen, Z. (2021). Relationship between the Microstructure and Performance of Graphene/Polyethylene Composites Investigated by Positron Annihilation Lifetime Spectroscopy. *Nanomaterials*, 11(11), 2990.
- Haq, M. A., Jafri, F. A., and Hasnain, A. (2016). Effects of plasticizers on sorption and optical properties of gum cordia based edible film. *J. Food Sci. Technol.* 53(6), 2606-2613.
- Haraguchi K. (2014) Biocomposites. In: Kobayashi S., Müllen K. (eds) Encyclopedia of Polymeric Nanomaterials. Springer, Berlin, Heidelberg. https://doi.org/10.1007/978-3-642-36199-9_316-1
- Hebbar, V., Ravikumar, H. B., Nandimath, M., Masti, S., Munirathnamma, L. M., Naik, J., and Bhajantri, R. F. (2019). Conductivity and free volume studies on bismuth sulfide/PVA: polypyrrole nanocomposites. *Indian J. Phys.*, 93(2), 147-158.
- Heidari, F., Bahrololoom, M. E., Vashae, D., & Tayebi, L. (2015). In situ preparation of iron oxide nanoparticles in natural hydroxyapatite/chitosan matrix for bone tissue engineering application. *Ceramics International*, 41(2), 3094-3100.
- Heinrich, G., Grögler, T., Rosiwal, S. M., and Singer, R. F. (1997). CVD diamond coated titanium alloys for biomedical and aerospace applications. *Surf. Coat. Technol.*, 94, 514-520.
- Huang, H. X., and Zhang, J. J. (2009). Effects of filler–filler and polymer–filler interactions on rheological and mechanical properties of HDPE–wood composites. *J. Appl. Polym. Sci.*, 111(6), 2806-2812.
- Islam, A., Yasin, T., Rafiq, M. A., Shah, T. H., Sabir, A., Khan, S. M., & Jamil, T. (2015). In-situ crosslinked nanofiber mats of chitosan/poly (vinyl alcohol) blend: Fabrication, characterization and MTT assay with cancerous bone cells. *Fibers Polym.*, 16(9), 1853-1860.
- Jaggi, H. S., Kumar, Y., Satapathy, B. K., Ray, A. R., & Patnaik, A. (2012). Analytical interpretations of structural and mechanical response of high density polyethylene/hydroxyapatite bio-composites. *Mater. Des. (1980-2015)*, 36, 757-766.
- Jankovič, L., Végős, K., Šiffalovič, P., Šauša, O., Čaplovič, L., Čaplovičová, M., Medlín, R., Uhlík, P. and Nógellová, Z. (2016). XRD, SAXS, and PALS investigations of three different polymers reinforced with tetraoctylammonium exchanged montmorillonite. *Int. J. Polym. Anal. Char.* 21(6), 524-536.
- Jinitha, T. V., Safna Hussan, K. P., Mohamed Shahin, T., and Purushothaman, E. (2020). The interplay between the fragility and mechanical properties of styrene–butadiene rubber composites with unmodified and modified sago seed shell powder. *J. Appl. Polym. Sci.*, 137(39), 49180.
- Johnson, J.R., Marx, J.G. and Johnson, W.D. (2001) US6296667B1
- Joshi, M., Butola, B.S., Simon, G. and Kukaleva, N. (2006). Rheological and viscoelastic behavior of HDPE/octamethyl-POSS nanocomposites. *Macromolecules*, 39(5), 1839-1849.
- Kalambettu, A.B., Rajangam, P. and Dharmalingam, S., 2012. The effect of chlorotrimethylsilane on bonding of nano hydroxyapatite with a chitosan–polyacrylamide matrix. *Carbohydr. Res.*, 352, 143-150.
- Kalia, S., Kaith, B. S., and Kaur, I. (2009). Pretreatments of natural fibers and their application as reinforcing material in polymer composites—a review. *Polym Eng Sci*, 49(7), 1253-1272.
- Kasaai, M. R., Arul, J., & Charlet, G. (2000). Intrinsic viscosity–molecular weight relationship for chitosan. *Journal of Polymer Science Part B: Polymer Physics*, 38(19), 2591-2598.

- Khorasani, M., Janbaz, P. and Rayati, F. (2018). Maxillofacial reconstruction with Medpor porous polyethylene implant: a case series study. *J Korean Assoc Oral Maxillofac Surg*, 44(3), 128-135.
- Khouaja, A., Koubaa, A., and Daly, H. B. (2021). Dielectric properties and thermal stability of cellulose high-density polyethylene bio-based composites. *Ind. Crops Prod*, 171, 113928.
- Kim, H.J., Lee, K.J., Seo, Y., Kwak, S. and Koh, S.K. (2001). HDPE surface functionalization by low-energy ion-beam irradiation under a reactive O₂ environment and its effect on the HDPE/nylon 66 blend. *Macromolecules*, 34(8), 2546-2558.
- Kim, H.L., Jung, G.Y., Yoon, J.H., Han, J.S., Park, Y.J., Kim, D.G., Zhang, M. and Kim, D.J. (2015). Preparation and characterization of nano-sized hydroxyapatite/alginate/chitosan composite scaffolds for bone tissue engineering. *Mater. Sci. Eng. C*, 54, 20-25.
- Kim, S. H., Lim, B. K., Sun, F., Koh, K., Ryu, S. C., Kim, H. S., & Lee, J. (2009). Preparation of high flexible composite film of hydroxyapatite and chitosan. *Polymer Bulletin*, 62(1), 111-118.
- Kim, S., Jang, E. S., Shin, D. H., and Lee, K. H. (2004). Using peak properties of a DTG curve to estimate the kinetic parameters of the pyrolysis reaction: application to high density polyethylene. *Polym. Degrad. Stab.*, 85(2), 799-805.
- Kleczevska, J., Bielinski, D.M., Dryzek, E. and Piatkowska, A. (2010). Application of positron annihilation lifetime spectroscopy in studies of dental composites based on dimethacrylate resins. *Modern polymeric materials for environmental application*, 4(1), 143-150.
- Koffi, A., Mijiyawa, F., Koffi, D., Erchiqui, F., and Toubal, L. (2021). Mechanical Properties, Wettability and Thermal Degradation of HDPE/Birch Fiber Composite. *Polymers*, 13(9), 1459.
- Kong, L., Gao, Y., Cao, W., Gong, Y., Zhao, N., & Zhang, X. (2005). Preparation and characterization of nano-hydroxyapatite/chitosan composite scaffolds. *J Biomed Mater Res A*, 75(2), 275-282.
- Kubies, D., L. Himmlová, T. Riedel, E. Chánová, K. Balík, M. Douderova, J. Bártová, and V. J. P. R. Pesakova. "The interaction of osteoblasts with bone-implant materials: 1. The effect of physicochemical surface properties of implant materials." *Physiol. Res.* 60, no. 1 (2011): 95.
- Kurek, M., Ščetar, M., Voilley, A., Galić, K. and Debeaufort, F. (2012). Barrier properties of chitosan coated polyethylene. *J. Membr. Sci.*, 403, 162-168.
- Kusuktham, B., and Teeranachaideekul, P. (2014). Mechanical properties of high density polyethylene/modified calcium silicate composites. *Silicon*, 6(3), 179-189.
- Kusumastuti, Y., Putri, N. R. E., Timotius, D., and Syabani, M. W. (2020). Effect of chitosan addition on the properties of low-density polyethylene blend as potential bioplastic. *Heliyon*, 6(11), e05280.
- Lamarra, J., Damonte, L., Rivero, S., & Pinotti, A. (2018). Structural insight into chitosan supports functionalized with nanoparticles. *Adv. Mater. Sci. Eng.* 2018.
- Langer, R. S., and Vacanti, J. P. (1999). Tissue engineering: the challenges ahead. *Sci. Am.*, 280(4), 86-89.
- Leatherbury, N.C., Kieswetter, K., Slivka, M.A. and Niederauer, G. (1998). WO1998024483A2
- Leite, J. L., Salmoria, G. V., Paggi, R. A., Ahrens, C. H., & Pouzada, A. S. (2010). A study on morphological properties of laser sintered functionally graded blends of amorphous thermoplastics, *Int. J. Mater. Prod. Technol.*, 39(1-2), 205-221.
- Leong, S. T., Yusof, Y., & Tan, C. F. (2015). An experimental and numerical investigation of tensile properties of stone wool fiber reinforced polymer composites. *Adv. Mater. Lett.*, 6(10), 888-894.
- Lewandowska, K. (2015). Characterization of chitosan composites with synthetic polymers and inorganic additives. *Int. J. Biol. Macromol.*, 81, 159-164.

- Li, C., and Suzuki, K. (2009). Kinetic analyses of biomass tar pyrolysis using the distributed activation energy model by TG/DTA technique. *J. Therm. Anal. Calorim.*, 98(1), 261-266.
- Li, X., Nan, K., Shi, S. and Chen, H. (2012). Preparation and characterization of nano-hydroxyapatite/chitosan cross-linking composite membrane intended for tissue engineering. *Int. J. Biol. Macromol.*, 50(1), 43-49.
- Li, Y., Liu, T., Zheng, J. and Xu, X. (2013). Glutaraldehyde-crosslinked chitosan/hydroxyapatite bone repair scaffold and its application as drug carrier for icariin. *J. Appl. Polym. Sci.*, 130(3), 1539-1547.
- Liang, J., Wang, R., and Chen, R. (2019). The impact of cross-linking mode on the physical and antimicrobial properties of a chitosan/bacterial cellulose composite. *Polymers*, 11(3), 491.
- Lima, P.S., Troccoli, R., Wellen, R.M., Rojo, L., Lopez-Manchado, M.A., Fook, M.V. and Silva, S.M. (2019). HDPE/chitosan composites modified with PE-g-MA. thermal, morphological and antibacterial analysis. *Polymers*, 11(10), 1559.
- Lin, B., Du, Y., Li, Y., Liang, X., Wang, X., Deng, W., Wang, X., Li, L. and Kennedy, J.F. (2010). The effect of moist heat treatment on the characteristic of starch-based composite materials coating with chitosan. *Carbohydr. Polym.*, 81(3), 554-559.
- Liu, S., and Zhai, J. (2015). Improving the dielectric constant and energy density of poly (vinylidene fluoride) composites induced by surface-modified SrTiO₃ nanofibers by polyvinylpyrrolidone. *J. Mater. Chem. A*, 3(4), 1511-1517.
- Liu, X., Wang, T., Chow, L. C., Yang, M., and Mitchell, J. W. (2014). Effects of inorganic fillers on the thermal and mechanical properties of poly (lactic acid). *Int. J. Polym. Sci.*, <https://doi.org/10.1155/2014/827028>
- Loganathan, S., Valapa, R. B., Mishra, R. K., Pugazhenti, G., and Thomas, S. (2017). Thermogravimetric analysis for characterization of nanomaterials. In *Thermal and Rheological Measurement Techniques for Nanomaterials Characterization* (pp. 67-108). Elsevier.
- Mantia, F.P. and Morreale, M. (2011). Green materials: a brief review. *Mater Part A*, 42, 579-588.
- Mierzwa-Hersztek, M., Gondek, K., and Kopeć, M. (2019). Degradation of polyethylene and biocomponent-derived polymer materials: an overview. *J. Polym. Environ.*, 27(3), 600-611.
- Mir, S., Yasin, T., Halley, P.J., Siddiqi, H.M. and Nicholson, T. (2011). Thermal, rheological, mechanical and morphological behavior of HDPE/chitosan blend. *Carbohydr. Polym.*, 83(2), 414-421.
- Mohamed, K.R., Beherei, H.H. and El-Rashidy, Z.M. (2014). In vitro study of nano-hydroxyapatite/chitosan-gelatin composites for bio-applications. *J. Adv. Res*, 5(2), 201-208.
- Mohammed, L., Ansari, M.N., Pua, G., Jawaid, M. and Islam, M.S. (2015). A review on natural fiber reinforced polymer composite and its applications. *Int. J. Polym. Sci.*, <https://doi.org/10.1155/2015/243947>
- Morais, J. A. D., Gadioli, R., and De Paoli, M. A. (2016). Curaua fiber reinforced high-density polyethylene composites: effect of impact modifier and fiber loading. *Polímeros*, 26, 115-122.
- Morsy, R., Elsayed, M., Krause-Rehberg, R., Dlubek, G. and Elnimr, T. (2010). Positron annihilation spectroscopic study of hydrothermally synthesized fine nanoporous hydroxyapatite agglomerates. *J. Eur. Ceram. Soc.*, 30(9), 1897-1901.
- Müller, K., Bugnicourt, E., Latorre, M., Jorda, M., Echegoyen Sanz, Y., Lagaron, J.M., Miesbauer, O., Bianchin, A., Hankin, S., Böhlz, U. and Pérez, G., 2017. Review on the processing and properties of polymer nanocomposites and nanocoatings and their applications in the packaging, automotive and solar energy fields. *Nanomaterials*, 7(4), 74.

Nagalakshmaiah, M., Afrin, S., Malladi, R.P., Elkoun, S., Robert, M., Ansari, M.A., Svedberg, A. and Karim, Z., 2019. Biocomposites: Present trends and challenges for the future. In *Green Composites for Automotive Applications* (pp. 197-215). Woodhead Publishing.

Nagavally, R. R. (2017). Composite materials-history, types, fabrication techniques, advantages, and applications. *Int J Mech Prod Eng*, 5(9), 82-87.

Naqvi, S.R., Tariq, R., Hameed, Z., Ali, I., Naqvi, M., Chen, W.H., Ceylan, S., Rashid, H., Ahmad, J., Taqvi, S.A. and Shahbaz, M. (2019). Pyrolysis of high ash sewage sludge: Kinetics and thermodynamic analysis using Coats-Redfern method. *Renew. Energy*, 131, pp.854-860.

Neto, J. S., de Queiroz, H. F., Aguiar, R. A., and Banea, M. D. (2021). A Review on the Thermal Characterisation of Natural and Hybrid Fiber Composites. *Polymers*, 13(24), 4425.

Nikola, S., Jambrekočić, V., Šernek, M. and Medved, S. (2019). Influence of natural fillers on thermal and mechanical properties and surface morphology of cellulose acetate-based biocomposites. *Int. J. Polym. Sci.*, <https://doi.org/10.1155/2019/1065024>.

Ong, K. L., Yun, B. M., and White, J. B. (2015). New biomaterials for orthopedic implants. *Orthop. Res. Rev.*, 7, 107-130.

Pagès, P. (2005). Characterization of polymer materials using FT-IR and DSC techniques. *Universidade da Coruña*.

Pai, S., Kini, S. M., Selvaraj, R., and Pugazhendhi, A. (2020). A review on the synthesis of hydroxyapatite, its composites and adsorptive removal of pollutants from wastewater. *J. Water Process. Eng.*, 38, 101574.

Pal, A. K., and Katiyar, V. (2016). Nanoamphiphilic chitosan dispersed poly (lactic acid) bionanocomposite films with improved thermal, mechanical, and gas barrier properties. *Biomacromolecules*, 17(8), 2603-2618.

Park, S.J. and Seo, M.K., 2011. Element and processing. In *Interface science and technology* (Vol. 18, pp. 431-499). Elsevier.

Pech-Canul, M.I., and Valdez, S. (2015). Updating the Definition and Concepts in the Field of Composite Materials. *Contributed Papers from Materials Science and Technology (MS&T)*, 337-345.

Peter, X.M. and Ruiyun Z. (2001). US6281257B1

Polson, A.M., Swanbom, D.D., Dunn, R.L., Cox, C.P., Norton, R.L., Lowe, B.K. and Peterson, K.S. (2000). US6071530A

Pradhan, D.K. and Tripathy, S.N. (2013). Effect of plasticizer concentration on microstructural and dielectric properties of polymer composite electrolyte. *Advances Chem Sci.* 2, 114-21.

Pradhan, D.K., Choudhary, R.N. and Samantaray, B.K. (2008). Studies of dielectric relaxation and AC conductivity behavior of plasticized polymer nanocomposite electrolytes. *Int J Electrochem Sci*, 3(5), 597-608.

Pramanik, N., Mishra, D., Banerjee, I., Maiti, T. K., Bhargava, P., and Pramanik, P. (2009). Chemical synthesis, characterization, and biocompatibility study of hydroxyapatite/chitosan phosphate nanocomposite for bone tissue engineering applications. *Int. J. Biomater.*, 2009.

Pryde, R. F. (1990). Thermal analysis for characterising composite materials. *Mater. Des.*, 11(1), 44.

Pundhir, N., Pathak, H., and Zafar, S. (2021). Crashworthiness performance of HDPE-kenaf and HDPE-CNT composite structures. *Adv. Mater. Process. Technol.*, 1-19. doi: 10.1080/2374068X.2021.1927644

Queiroz, M. F., Teodosio Melo, K. R., Sabry, D. A., Sasaki, G. L., & Rocha, H. A. O. (2014). Does the use of chitosan contribute to oxalate kidney stone formation?. *Mar. Drugs*, 13(1), 141-158.

- Quiroz-Castillo, J.M., Rodríguez-Félix, D.E., Grijalva-Monteverde, H., del Castillo-Castro, T., Plascencia-Jatomea, M., Rodríguez-Félix, F. and Herrera-Franco, P.J. (2014). Preparation of extruded polyethylene/chitosan blends compatibilized with polyethylene-graft-maleic anhydride. *Carbohydr. Polym.*, *101*, 1094-1100.
- Rahman, P.M., Mujeeb, V.A., Muraleedharan, K. and Thomas, S.K. (2018). Chitosan/nano ZnO composite films: enhanced mechanical, antimicrobial and dielectric properties. *Arab. J. Chem.*, *11*(1), 120-127.
- Ramkumar, R. and Pugazhendhi, S.C. (2019). Investigation on the Electrothermal Properties of Nanocomposite HDPE. *J Nanomater* 1-9.
- Ranjan, R., Kumar, A., Kumar, S. and Badiyani, K. (2015). Role of high density porous polyethylene (HDPE) Implants in correction of maxillofacial defects and deformity: a review. *Int J Prev Clin Dent Res*, *2*(2), 71-75.
- Ratnam, C.T., Min, A.M., Chuah, T.G., Suraya, A.R., Choong, T.S. and Hasamuddin, W.W. (2006). Physical properties of polyethylene modified with crude palm oil. *Polym Plast Technol Eng*, *45*(8), 917-922.
- Reichert, C.L., Bugnicourt, E., Coltelli, M.B., Cinelli, P., Lazzeri, A., Canesi, I., Braca, F., Martínez, B.M., Alonso, R., Agostinis, L., and Verstichel, S., (2020). Bio-based packaging: Materials, modifications, industrial applications and sustainability. *Polymers*, *12*(7), 1558.
- Riedel, U., 2012. Biocomposites: Long natural fiber-reinforced biopolymers.
- Rinaudo, M. (2006). Chitin and chitosan: Properties and applications. *Prog. Polym. Sci.*, *31*(7), 603-632.
- Rodríguez-Sánchez, A. E., Vega-Rios, A., Flores-Gallardo, S. G., Zaragoza-Contreras, E. A., and Mendoza-Duarte, M. E. (2019). Numerical analysis of wood-high-density polyethylene composites: A hyperelastic approach. *J. Compos. Mater*, *53*(1), 73-82.
- Romero, Edwar. *Powering biomedical devices*. Academic Press, 2013.
- Rzayev, Z. M. (2011). Graft copolymers of maleic anhydride and its isostructural analogues: High performance engineering materials. *Int. Rev.Chem. Eng.*, *3*(2011) 153-215
- Sailaja, G.S., Velayudhan, S., Sunny, M.C., Sreenivasan, K., Varma, H.K. and Ramesh, P. (2003). Hydroxyapatite filled chitosan-polyacrylic acid polyelectrolyte complexes. *J. Mater. Sci.* *38*(17), 3653-3662.
- Saleh, M., Al-Hajri, Z., Popelka, A. and Javaid Zaidi, S. (2020). Preparation and characterization of alumina HDPE composites. *Materials*, *13*(1), 250.
- Sander, M.M., Nicolau, A., Guzzato, R. and Samios, D. (2012). Plasticiser effect of oleic acid polyester on polyethylene and polypropylene. *Polym. Test.*, *31*(8),1077-82.
- Sanyang, M. L., Sapuan, S. M., Jawaid, M., Ishak, M. R., & Sahari, J. (2015). Effect of plasticizer type and concentration on dynamic mechanical properties of sugar palm starch-based films. *Int. J. Polym. Anal. Char*, *20*(7), 627-636.
- Sarifuddin, N., Ismail, H., & Ahmad, Z. (2013). Studies of properties and characteristics of low-density polyethylene/thermoplastic sago starch-reinforced kenaf core fiber composites. *J. Thermoplast. Compos. Mater.*, *28*(4), 445-460.
- Sarmah, P., and Rout, J. (2020). Role of algae and cyanobacteria in bioremediation: prospects in polyethylene biodegradation. In *Advances in cyanobacterial biology*, 333-349, Academic Press.
- Sattar, M. A., and Patnaik, A. (2020). Role of Interface Structure and Chain Dynamics on the Diverging Glass Transition Behavior of SSBR-SiO₂-PIL Elastomers. *ACS omega*, *5*(33), 21191-21202.

- Setzer, B., Bächle, M., Metzger, M. C., and Kohal, R. J. (2009). The gene-expression and phenotypic response of hFOB 1.19 osteoblasts to surface-modified titanium and zirconia. *Biomaterials*, 30(6), 979-990.
- Sewda, K. and Maiti, S.N. (2013). Dynamic mechanical properties of high density polyethylene and teak wood flour composites. *Polym. Bull.*, 70(10), 2657-2674.
- Seymour, A. B., Harold L. R., William, E. R., Seymour, B. (1972). US3662405A.
- Shakir, M., Jolly, R., Khan, M. S., e Iram, N., and Khan, H. M. (2015 b). Nano-hydroxyapatite/chitosan–starch nanocomposite as a novel bone construct: Synthesis and in vitro studies. *Int. J. Biol. Macromol.*, 80, 282-292.
- Shakir, M., Jolly, R., Khan, M.S., Iram, N.E., Sharma, T.K. and Al-Resayes, S.I. (2015a). Synthesis and characterization of a nano-hydroxyapatite/chitosan/polyethylene glycol nanocomposite for bone tissue engineering. *Polym. Adv. Technol.*, 26(1), 41-48.
- Shaojin, J., Zhicheng, Z., Yangmei, F., Huiming, W., Xianfeng, Z. and Rongdian, H. (2002). Study of the size and numerical concentration of the free volume of carbon filled HDPE composites by the positron annihilation method. *Eur. Polym. J.*, 38(12), 2433-2439.
- Sharma, A. K., and Gupta, S. (2020). Microwave processing of biomaterials for orthopedic implants: Challenges and possibilities. *JOM*, 72(3), 1211-1228.
- Sharma, P., Bhanot, V. K., Singh, D., Undal, H. S., and Sharma, M. (2013). Research work on fiber glass wool reinforced and epoxy matrix composite material. *Int. J. of Mech. Eng. & Robotics Res.*, 2(2), 106-124.
- Sheik, S., Sheik, S., Nairy, R., Nagaraja, G.K., Prabhu, A., Rekha, P.D. and Prashantha, K. (2018). Study on the morphological and biocompatible properties of chitosan grafted silk fibre reinforced PVA films for tissue engineering applications. *Int. J. Biol. Macromol.*, 116, 45-53.
- Sherwani, S. F. K., Zainudin, E. S., Sapuan, S. M., Leman, Z., & Khalina, A. (2021). Physical, Mechanical, and Morphological Properties of Treated Sugar Palm/Glass Reinforced Poly (Lactic Acid) Hybrid Composites. *Polymers*, 13(21), 3620.
- Shimamoto, T., Oka, T., Adachi, M., Hyon, S.H., Nakayama, K. and Kaito, K. (1995). US5431652A
- Shinoj, S., Visvanathan, R., Panigrahi, S. and Kochubabu, M. Oil palm fiber (OPF) and its composites: A review. (2011). *Ind Crops Prod*, 33(1), 7-22.
- Singh, A.A., Afrin, S. and Karim, Z., 2017. Green composites: Versatile material for future. In *Green biocomposites* (pp. 29-44). Springer, Cham.
- Sivaselvi, K., and Ghosh, P. (2017). Characterization of modified Chitosan thin film. *Mater. Today: Proc.*, 4(2), 442-451.
- Sousa, R.A., Reis, R.L., Cunha, A.M. and Bevis, M.J. (2003). Coupling of HDPE/hydroxyapatite composites by silane-based methodologies. *J. Mater. Sci.: Mater. Med.* 14(6), 475-487
- Sreekumar, P. A., Leblanc, N., & Saiter, J. M. (2013). Effect of glycerol on the properties of 100% biodegradable thermoplastic based on wheat flour. *J Polym Environ*, 21(2), 388-394.
- Sun, D., Zhou, Z., Chen, G.X. and Li. Q. (2014). Regulated dielectric loss of polymer composites from coating carbon nanotubes with a cross-linked silsesquioxane shell through free-radical polymerization. *ACS Appl Mater*, 6(21):18635-18643.
- Sunilkumar, M., Francis, T., Thachil, E.T. and Sujith, A. (2012). Low density polyethylene–chitosan composites: A study based on biodegradation. *Chem. Eng. Sci.*, 204, 114-124.
- Sunilkumar, M., Gafoor, A.A., Anas, A., Haseena, A.P. and Sujith, A. (2014). Dielectric properties: A gateway to antibacterial assay—A case study of low-density polyethylene/chitosan composite films. *Polym. J.*, 46(7), 422-429.

- Surender, R., Mahendran, A. R., Wuzella, G., and Vijayakumar, C. T. (2016). Synthesis, characterization and degradation behavior of thermoplastic polyurethane from hydroxylated hemp seed oil. *J. Therm. Anal. Calorim.*, 123(1), 525-533.
- Tajau, R., Rohani, R., Alias, M.S., Mudri, N.H., Abdul Halim, K.A., Harun, M.H., Mat Isa, N., Che Ismail, R., Muhammad Faisal, S., Talib, M. and Rawi Mohamed Zin, M. (2021). Emergence of polymeric material utilising sustainable radiation curable palm oil-based products for advanced technology applications. *Polymers*, 13(11), 1865.
- Takashi, A., Yamato, Y., Shimada, N., and Asai, H. (2017). WO2018117266A1.
- Tamburaci, S., Cecen, B., Ustun, O., Ergur, B.U., Havtcioglu, H. and Tihminlioglu, F. (2019). Production and characterization of a novel bilayer nanocomposite scaffold composed of chitosan/Si-nHap and zein/POSS structures for osteochondral tissue regeneration. *ACS Appl. Bio Mater.*, 2(4), 1440-1455.
- Teng, S. H., Lee, E. J., Yoon, B. H., Shin, D. S., Kim, H. E., & Oh, J. S. (2009). Chitosan/nanohydroxyapatite composite membranes via dynamic filtration for guided bone regeneration. *J Biomed Mater Res A*, 88(3), 569-580.
- Thein-Han, W. W., and Misra, R. D. K. (2009). Three-dimensional chitosan-nanohydroxyapatite composite scaffolds for bone tissue engineering. *JOM*, 61(9), 41-44.
- Timothy, J. N. S., Hendry, J., Pugh, S.M. and Smith, R. (2003) WO2003026714A1.
- Tong, J. Y., Royan, N. R. R., Ng, Y. C., Ab Ghani, M. H., & Ahmad, S. (2014). Study of the mechanical and morphology properties of recycled HDPE composite using rice husk filler. *Adv. Mater. Sci. Eng.*, 2014.
- Tripathi, G., Gough, J.E., Dinda, A. and Basu, B. (2013). In vitro cytotoxicity and in vivo osseointegration properties of compression-molded HDPE-HA-Al₂O₃ hybrid biocomposites. *J Biomed Mater Res A*, 101(6), 1539-1549.
- Turnbull, G., Clarke, J., Picard, F., Riches, P., Jia, L., Han, F., Li, B. and Shu, W., 2018. 3D bioactive composite scaffolds for bone tissue engineering. *Bioact. Mater.* 3: 278–314.
- Varghese, J., Nair, D.R., Mohanan, P. and Sebastian, M.T. (2015). Dielectric, thermal and mechanical properties of zirconium silicate reinforced high density polyethylene composites for antenna applications. *Phys Chem Chem Phys*, 17(22):14943-14950.
- Varyan, I., Kolesnikova, N., Xu, H., Tyubaeva, P., and Popov, A. (2022). Biodegradability of Polyolefin-Based Compositions: Effect of Natural Rubber. *Polymers*, 14(3), 530.
- Venkatesan, J., and Kim, S. K. (2010). Chitosan composites for bone tissue engineering—an overview. *Mar. Drugs*, 8(8), 2252-2266.
- Wang, H. M., Chen, Z., Wang, P. F., and Wang, S. J. (2009). The Influence of acrylic acid groups on the microstructure of HDPE/PS/clay system studied by positron annihilation. *Mater. Sci. Forum*, 607, 88-90. Trans Tech Publications Ltd
- Wang, M., Joseph, R. and Bonfield, W. (1998). Hydroxyapatite-polyethylene composites for bone substitution: effects of ceramic particle size and morphology. *Biomaterials*, 19(24), 2357-2366.
- Wang, Z., and Hu, Q. (2010). Preparation and properties of three-dimensional hydroxyapatite/chitosan nanocomposite rods. *Biomed. Mater.*, 5(4), 045007.
- Wang, Z., Peng, Y., Zhang, L., Zhao, Y., Vyzhimov, R., Tan, T., and Fong, H. (2016). Investigation of palm oil as green plasticizer on the processing and mechanical properties of ethylene propylene diene monomer rubber. *Ind. Eng. Chem. Res.*, 55(10), 2784-2789.

Wu, A., Jia, L., Yu, W., Zhu, F., Liu, F., Wang, Y., Lu, G., Qin, S., Gao, D., Wang, H. and Wu, X. (2021). Preparation and Finite Element Analysis of Fly Ash/HDPE Composites for Large Diameter Bellows. *Polymers*, 13(23), 4204.

Wu, Z., Huang, X., Li, Y. C., Xiao, H., and Wang, X. (2018). Novel chitosan films with laponite immobilized Ag nanoparticles for active food packaging. *Carbohydr. Polym.*, 199, 210-218.

Xie, Z., Chen, Y., Wang, C., Liu, Y., Chu, F. and Jin, L. (2014). Effects of bio-based plasticizers on mechanical and thermal properties of PVC/wood flour composites. *BioResources*, 9(4), 7389-7402.

Yadav, M., Rhee, K.Y., Park, S.J. and Hui, D. (2014). Mechanical properties of Fe₃O₄/GO/chitosan composites. *Compos. B. Eng.*, 66, 89-96.

Yu, X., Yao, S., Chen, C., Wang, J., Li, Y., Wang, Y., Khademhosseini, A., Wan, J. and Wu, Q. (2020). Preparation of Poly (ether-ether-ketone)/Nanohydroxyapatite Composites with Improved Mechanical Performance and Biointerfacial Affinity. *ACS omega*, 5(45), 29398-29406.

Zaleski, R., Maciejewska, M., & Puzio, M. (2015). Mechanical stability of porous copolymers by positron annihilation lifetime spectroscopy. *J. Phys. Chem. C* 119(21), 11636-11645.

Zaydouri, A. and Grivet, M. (2009). The effect of electron irradiation on high-density polyethylene: Positron annihilation lifetime spectroscopy, differential scanning calorimetry and X-ray scattering studies. *Radiat. Phys. Chem.*, 78(9), 770-775.

Zeng, M., Xiao, H., Zhang, X., Sun, X., Qi, C. and Wang, B. (2011). A novel chitosan/polyvinyl pyrrolidone (CS/PVP) three-dimensional composite and its mechanism of strength improvement. *J. Macromol. Sci.*, 50(7), 1413-1422.

Zhang, Q., Cai, H., Ren, X., Kong, L., Liu, J. and Jiang, X. (2017). The dynamic mechanical analysis of highly filled rice husk biochar/high-density polyethylene composites. *Polymers*, 9(11), 628.

Zhang, Y., Hao, L., Savalani, M. M., Harris, R. A., and Tanner, K. E. (2008). Characterization and dynamic mechanical analysis of selective laser sintered hydroxyapatite-filled polymeric composites. *J Biomed Mater Res A*, 86(3), 607-616.

Zulkifli, W. N. F. M. (2017). Bioplasticiser and palm oil. *Palm Oil Dev*, 67, 16-19.

https://www.reportlinker.com/p06033135/?utm_source=GNW (10/01/2022)

15 European Bioplastic Conference, Bioplastics market development update 2020

List of Publications based on PhD Research Work

1. **Meril Shelly**, Raghavendra M, Ashwini Prabhu, H.B.Ravikumar, Meril Mathew, Tania Francis, Improved mechanical and microstructural performance of high density polyethylene chitosan-hydroxyapatite composites as potential bone implant materials, 19, *Materials Today Sustainability*, November 2022. <https://doi.org/10.1016/j.mtsust.2022.100186>
2. **Meril Shelly**, M. Raghavendra, H. B. Ravikumar and Tania Francis, Structural and free-hole volume characterization of high-density polyethylene/chitosan composites plasticized with palm oil, *Polymer Engineering and Science*, 61(2), 2021, 3060-3068. <https://doi.org/10.1002/pen.25818>
3. **Meril Shelly.**, Meril Mathew., Pradyumnan, P.P. and Tania Francis, Dielectric and thermal stability studies on high density polyethylene–Chitosan composites plasticized with palm oil, *Materials Today:Proceedings*, 46(7), 2021, 2742-2746. <https://doi.org/10.1016/j.matpr.2021.02.479>
4. **Meril Shelly**, Meril Mathew and Tania Francis, HDPE-Chitosan composites as potential bone composite materials Full Paper: ISBN No:978-93-5279-203-0 Page No. 301-304,2018.
5. Annie Stephy, **Meril Shelly**, Meril Mathew and Tania Francis, XRD and FESEM characterization of size controlled nanohydroxyapatite synthesized by wet precipitation technique. Full Paper : ISSN-2348-3369, Page No. 382-390

Book Chapter:

1. Neethumol Varghese, Tania Francis, **Meril Shelly** and Ajalesh B. Nair (2021). Nanocomposites of polymer matrices: Nanoscale processing. Sabu Thomas and Preetha Balakrishnan (Eds), in *Nanoscale Processing*, (pp. 383-406). Elsevier. <https://doi.org/10.1016/B978-0-12-820569-3.00014-1>

Bio-data

Name : MERIL SHELLY

Date of Birth : 28-11-1991

Permanent Address: Kuruvachira (House)
Kuppayakode (P.O.)
Kodencherry (via)
Calicut, Kerala -673008

Email: merilshelly28@gmail.com

Contact No: 9446161431, 6238003675

Academic Qualifications:

- **MSc:** Chemistry, Vimala College, Thrissur (University of Calicut)
- **BSc :** Chemistry, St.Joseph's College (Autonomous), Devagiri, (University of Calicut)

Academic Projects:

M.Sc Project- "Synthesis of mesoporous carbon aerogels through gel drying at ambient conditions for application as EDLC electrode" carried out from C-MET Thrissur under the supervision of Dr. N .C. Pramanik, Scientist-E,C-MET Thrissur and Ms. Priyanka , Asst. Professor Vimala College Thrissur.

B.Sc Project- "A study of variation of solubility of oxalic acid in water in the presence of various ammonium electrolytes" carried out from Chemistry Dept. St.Joseph's College (Autonomous), Devagiri under the supervision of Prof. Varkey Pattani, Department of Chemistry, St.Joseph's College (Autonomous), Devagiri, Kozhikode.

Work Experience:

- **Junior Project Fellow** in KSCSTE-SRS funded project entitled: " Preparation and Characterization of HDPE/nano-chitosan/nano-hydroxyapatite biocomposites" from 2016-2019
- **Teaching Experience:** 1 year (Tharananellur Arts and Science College, Irinjalakuda, Thrissur and Christ College (Autonomous), Irinjalakuda, Thrissur).

International/National/State Level Conferences

1. Attended in IP Awareness/Training program on National Intellectual property Awareness Mission organized by Intellectual Property Office, India on July 12, 2022
2. Meril Shelly, International Conference on Emerging Trends in Mechanical and Materials Engineering-2021" (ICEMME-2021) organized by Dept of Mechanical Engineering, Christ College of Engineering, Irinjalakuda, 13-15 July 2021.
3. Meril Shelly, Meril Mathew, Tania Francis, International Conference in advances in polymer chemistry (APT 21), CUSAT, May 2021.
4. Meril Shelly, Raghavendra M, Ravikumar HB, Tania Francis, International online conference on Macromolecules (ICM 2020), MG University and Gdansk University of Technology, Chemical Faculty, Poland (13-15 November, 2020), (**Second Best Poster Award**)
5. Meril Shelly, Meril Mathew, Pradyumnan P P, Tania Francis, 2nd International Conference on Smart and Sustainable developments in Materials, Manufacturing and Energy Engineering, NMAM Institute of Technology, Nitte, Karnataka, December 2020.
6. Meril Shelly, Meril Mathew, Tania Francis, An international virtue conference in chemistry, A webinar on progress and polymer in chemical sciences (PPCS2020), Christ University, Bangalore, February 2020.
7. Meril Shelly, Meril Mathew, Tania Francis, (Oral Presentation) Second International Conference on Processing and Characterization of Materials (ICPCM-2019), NIT Rourkela, December 2019.
8. Meril Shelly, participated in the International Conference on Frontiers of Material Science (FOMS-19), St.Joseph's College (Autonomous), Devagiri, Kozhikode, December 2019.
9. Meril Shelly, Meril Mathew, Tania Francis, International Conference on Sustainable Globalization, Kochi, January 11-13, 2018.

10. Meril Shelly, Annie Stephy, Dona P G, Tania Francis, International Conference on Emerging Frontiers in Chemical Sciences, September 23-25, Farook College, Kozhikode, 2017.
11. Annie Stephy, Meril Shelly, Meril Mathew, Tania Francis, MESMAC Conferences on “Existence and Expression: Science, Philosophy and Art” MES Mampad, Malappuram, February 2017.
12. Annie Stephy, Meril Shelly, Tania Francis, participated in the International Conference on Emerging Frontiers in Chemical Sciences, Dept. of Chemistry, Farook College (Autonomous), Kozhikode, September 23-25, 2017.
13. Meril Shelly, Meril Mathew, Tania Francis, Frontiers in chemical sciences (FCS 2020), University of Calicut, January 29-31, 2020.
14. Meril Shelly, Meril Mathew, Tania Francis, (Contributory Lecture) in National conference on materials chemistry, NCMC- '19, St.Joseph's College (Autonomous), Devagiri, Kozhikode, December 9-10, 2020.
15. Meril Shelly, Meril Mathew, Tania Francis, Participated in the National Conference on Biopolymers and Green composites (BPGC), Centre for biopolymer science and technology (CBPST)- A unit of CIPET, Kochi, January 14-15, 2019.
16. Meril Shelly, Meril Mathew, Tania Francis, National Conference on Emerging Frontiers of Chemical Sciences (EFCS), Farook College, Calicut, November 23- 24, 2018.
17. Meril Shelly, Meril Mathew, Tania Francis, presented a paper in the National Conference on Current Trends in Polymer Science, Department of Polymer Science and Rubber Technology, CUSAT, February 9, 2018.
18. Meril Shelly, Annie Stephy, Tania Francis , presented a paper in the National Conference on Biopolymers and Green Composites BPGC 2017- 5 th in series, Centre for biopolymer science and technology (CBPST)- A unit of CIPET, Kochi, December 15-16, 2017, (**Second Best Poster Award**).
19. Meril Shelly, Meril Mathew, Tania Francis, 32nd Kerala Science Congress (KSC), Organized by KSCSTE and KFRI at Yuvakshetra institute of management, Mundoor, January 25-27,2020.

20. Meril Shelly, Meril Mathew, Tania Francis, 31st Kerala Science Congress (KSC), Organized by KSCSTE and JNTBGRI at Fatima Mata National College, Kollam, February 2-3,2019, (**Best Poster Award**).
21. Meril Shelly, Meril Mathew, Tania Francis, 30th Kerala Science Congress, Govt. Brennen College, Kannur, January 28-30, 2018.
22. Annie Stephy, Meril Shelly, Tania Francis, participated in Seminar on National Seminar on “Frontiers in Chemistry”, University of Calicut, March 2017.
23. Meril Shelly, has participated in the one day seminar on Graphene and Beyond, at Regional Science Centre and Planetarium, Kozhikode, February 2017.